frontiers | Research Topics

Crash prevention and protection challenges for all road users

Edited by
Yong Han, Koji Mizuno, Robert Thomson and Bingbing Nie

Published in
Frontiers in Future Transportation

ISSN 1664-8714
ISBN 978-2-83252-190-8
DOI 10.3389/978-2-83252-190-8

About Frontiers

Frontiers is more than just an open access publisher of scholarly articles: it is a pioneering approach to the world of academia, radically improving the way scholarly research is managed. The grand vision of Frontiers is a world where all people have an equal opportunity to seek, share and generate knowledge. Frontiers provides immediate and permanent online open access to all its publications, but this alone is not enough to realize our grand goals.

Frontiers journal series

The Frontiers journal series is a multi-tier and interdisciplinary set of open-access, online journals, promising a paradigm shift from the current review, selection and dissemination processes in academic publishing. All Frontiers journals are driven by researchers for researchers; therefore, they constitute a service to the scholarly community. At the same time, the *Frontiers journal series* operates on a revolutionary invention, the tiered publishing system, initially addressing specific communities of scholars, and gradually climbing up to broader public understanding, thus serving the interests of the lay society, too.

Dedication to quality

Each Frontiers article is a landmark of the highest quality, thanks to genuinely collaborative interactions between authors and review editors, who include some of the world's best academicians. Research must be certified by peers before entering a stream of knowledge that may eventually reach the public - and shape society; therefore, Frontiers only applies the most rigorous and unbiased reviews. Frontiers revolutionizes research publishing by freely delivering the most outstanding research, evaluated with no bias from both the academic and social point of view. By applying the most advanced information technologies, Frontiers is catapulting scholarly publishing into a new generation.

What are Frontiers Research Topics?

Frontiers Research Topics are very popular trademarks of the *Frontiers journals series*: they are collections of at least ten articles, all centered on a particular subject. With their unique mix of varied contributions from Original Research to Review Articles, Frontiers Research Topics unify the most influential researchers, the latest key findings and historical advances in a hot research area.

Find out more on how to host your own Frontiers Research Topic or contribute to one as an author by contacting the Frontiers editorial office: frontiersin.org/about/contact

Crash prevention and protection challenges for all road users

Topic editors

Yong Han — Xiamen University of Technology, China
Koji Mizuno — Nagoya University, Japan
Robert Thomson — Chalmers University of Technology, Sweden
Bingbing Nie — Tsinghua University, China

Citation

Han, Y., Mizuno, K., Thomson, R., Nie, B., eds. (2023). *Crash prevention and protection challenges for all road users*. Lausanne: Frontiers Media SA.
doi: 10.3389/978-2-83252-190-8

Table of contents

frontiers in Future Transportation

ORIGINAL RESEARCH
published: 03 November 2021
doi: 10.3389/ffutr.2021.760640

A Decade Long Slowdown in Road Crashes and Inherent Consequences Predicted for South Africa

*Dimakatso Machetele and Kowiyou Yessoufou**

Department of Geography, Environmental Management and Energy Studies, University of Johannesburg, APK campus, Johannesburg, South Africa

Globally, there are 1.35 million road fatalities every year, which are estimated to cost governments approximately US$ 518 billion, making road fatalities the eighth leading cause of death across all age groups and the leading cause of death of children and young adults. In South Africa, despite tremendous governmental efforts to curb the soaring trajectory of road crashes, the annual number of road fatalities has increased by 26% in recent years. By fitting a structural equation model (SEM) and a GARCH Model (Generalized Auto-Regressive Conditional Heteroskedasticity) to analyze and predict future trend of road crashes (number of road crashes, number of casualties, number of fatal crashes and number of persons killed) in South Africa, we propose and test a complex metamodel that integrates multiple causality relationships. We show an increasing trend of road crashes over time, a trend that is predictable by number of vehicles in the country, the population of the country and the total distance travelled by vehicles. We further show that death rate linked to road crashes is on average 23.14 deaths per 100,000 persons. Finally, in the next decade, the number of road crashes is predicted to be roughly constant at 617,253 crashes but can reach 1,896,667 crashes in the worst-case scenario. The number of casualties was also predicted to be roughly constant at 93,531 over time, although this number may reach 661,531 in the worst-case scenario. However, although the number of fatal crashes may decrease in the next decade, it is forecasted to reach 11,241 within the next 10 years with the worse scenario estimated at 19,034 within the same period. At the same time, the number of persons killed in fatal crashes is also predicted to be roughly constant at 14,739 but may also reach 172,784 in the worse scenario. Overall, the present study reveals perhaps the positive effects of government initiatives to curb road crashes and their consequences; we call for more stronger actions for a drastic reduction in road accident events in South Africa.

Keywords: road crashes, fatalities, casualties, persons killed in road crashes, GARCH model, South Africa

OPEN ACCESS

Edited by:
Bingbing Nie,
Tsinghua University, China

Reviewed by:
Wesley Kumfer,
University of North Carolina at Chapel Hill, United States
Jie Wang,
Changsha University of Science and Technology, China

****Correspondence:***
Kowiyou Yessoufou
kowiyouy@uj.ac.za

Specialty section:
This article was submitted to Transport Safety, a section of the journal Frontiers in Future Transportation

Received: *18 August 2021*
Accepted: *24 September 2021*
Published: *03 November 2021*

Citation:
Machetele D and Yessoufou K (2021) A Decade Long Slowdown in Road Crashes and Inherent Consequences Predicted for South Africa. Front. Future Transp. 2:760640. doi: 10.3389/ffutr.2021.760640

INTRODUCTION

Road crashes can be defined as events on the road that involve the collision of either two or more vehicles, or a vehicle and a vulnerable road user (cyclists or pedestrian), or a vehicle and a fixed object, e.g., bridge (RTMC, 2008). According to the leading road safety agency in South Africa, road crashes are classified into four categories of severity, namely: fatal crashes, major crashes, minor crashes, and damage-only crashes (RTMC, 2017). Fatal crashes result to death of one person or more; such

crashes may result in serious and light injuries (RTMC, 2008). Major crashes are defined as crashes in which one person or more people are seriously injured (RTMC, 2017). Minor crashes are crashes in which one or more persons are slightly injured (RTMC, 2017) whereas damage-only crashes are crashes in which no one has been injured or killed but vehicles or property may be damaged (RTMC, 2008).

Globally, there are 1.35 million road fatalities every year, which are estimated to cost approximately US$ 518 billion to governments (WHO, 2018). Existing statistics indicate that more than 90% of road crashes are fatal in both low- and middle-income countries, and these fatal crashes often involve more than 50% of unregistered vehicles (WHO, 2009). The Global Status Report on Road Safety reported road fatalities to be the eighth leading cause of death across all age groups (Donaldson et al., 2009) and are now the leading cause of death of children and young adults aged 5–29 years (RTMC, 2019).

In response to these crashes, several initiatives have been taken by different governments across the world; however, the frequency of road crashes remains on the rise with unacceptable consequences (Benlagha and Charfeddine, 2020). For example, existing statistics indicate that more than 90% of road crashes are fatal especially in developing countries, and these fatal crashes often involve more than 50% of unregistered vehicles (WHO, 2009). The increasing ownership of vehicles is one of the major contributory factors to the rise of road fatalities and injuries in developing countries (Nantulya and Reich, 2002).

In South Africa and in the past few years, an increasing trend of road fatalities has been observed (RTMC, 2018), although the country made strides in reducing road fatalities since their peak in 2006 (ITF, 2018). The annual number of road fatalities increased every year between 2013 and 2016 (RTMC, 2017) and, between 1990 and 2017, they increased by 26% (ITF, 2018). The high number of road crashes and their associated consequences have a significant negative impact on the socioeconomic development of all South Africans (Labuschange et al., 2017). Impacts are measured in terms of loss of lives, grief and suffering as well as the heavy financial burden of road crashes on the country's economy (Verster and Fourie, 2018). The primary underlying factors of road crashes in South Africa have been identified (Verster and Fourie, 2018). These factors are linked to vehicle (7.8%), environment and road (12%) as well as human (80%) (Verster and Fourie, 2018). In 2017 alone, the factor "vehicle" contributed 3% to road crashes in the country; environmental and road conditions 5% and human factors were responsible for 91% of road crashes (RTMC, 2018). However, still in the South African context, we still have limited understanding of the complexity of road accident events as several potential mediators of road crashes are generally not factored in the analysis of road crashes in the country. In the present study, a more complex approach is employed to analyse potential causality relationships between several variables linked to road accident events.

In the face of this alarming road accident statistics in South Africa, existing studies on road safety in the country focus mainly on identifying contributory factors, e.g., human, vehicle, and environmental factors, to road crashes (e.g., Verster and Fourie, 2018). Whilst other studies indicated that road accident events may be more complex than thought (e.g., Eboli and Mazzulla, 2007), we have limited understanding of this complexity in South Africa, owing to the simplistic approach we generally take in analysing road accident events.

The present study proposes and tests a more comprehensive metamodel (**Figure 1**) formulated by integrating multiple causality relationships among variables previously linked to road crashes. In the proposed theoretical metamodel, road crashes are represented by four main response variables, including total number of crashes (road crashes), total number of casualties, number of fatal crashes and number of persons killed each year. Our first prediction is that the total number of crashes would have a cascading effect on the other three main variables such that, as the total number of crashes increases over time, so too would the total number of casualties, number of fatal crashes and number of persons killed in a cascading manner.

In addition, the metamodel includes six predictor variables. These include total number of vehicles in the country at a given year, number of registered vehicles, number of unroadworthy and unlicensed vehicles, number of driver's license issued, the population of the country and the distance travelled by vehicles each year. Our prediction is that, as the total number of vehicles in the country increases over time, this would increase the likelihood of more crashes, which, as indicated above, would have a cascading effect on the total number of casualties, number of fatal crashes and number of persons killed (positive relationship; **Figure 1**). Similar to the total number of vehicles, we also predict that, if the number of unroadworthy and unlicensed vehicles increases over time, this would also increase the total number of crashes. This is grounded on the assumption that, not only the drivers of unroadworthy and unlicensed vehicles are more likely to not have a driver's license, but their unroadworthy vehicles are more likely in a defective state conducive for road crashes. To illustrate this, Verster and Fourie (2018) reported that 7.8% of road crashes in South Africa are linked to vehicles, and in 2017 alone, the factor "vehicle" contributed 3% to road crashes in the country (RTMC, 2018). Again, an increase number of unroadworthy unregistered vehicles would thus increase the risk of more road crashes, which would have a cascading effect on the total number of casualties, number of fatal crashes and number of persons killed over time. Furthermore, we predict the increase in human population would also result in the increase in road crashes and thus the increase in total number of casualties, number of fatal crashes and number of persons killed. The rationale of this prediction is that when the population increases, the number of vehicle owners would increase such that more vehicles (both registered and unregistered) would be on the road, thus increasing the risk of road crashes. Also, when more vehicles are on the road, the total distance travelled by vehicles would increase, and this would reduce the quality and strength of the vehicles over time, and thus increasing the risk of road crashes.

As opposed to the positive relationships predicted above, we predict that the number of registered vehicles as well as the number of issued drivers' license would cause a reduction in the

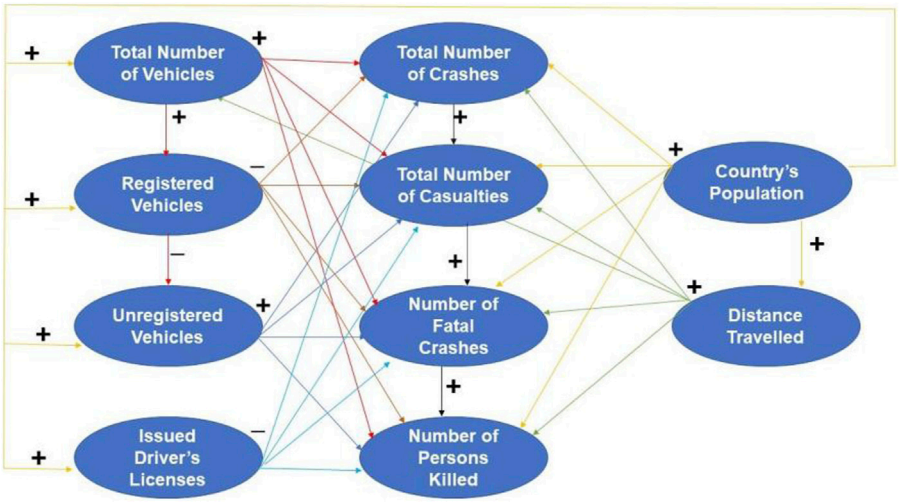

FIGURE 1 | Proposed theoretical metamodel to explain road accident events in South Africa.

number of road crashes, the total number of casualties, number of fatal crashes and number of persons killed. This is grounded in the assumption that the drivers of registered vehicles are more likely to have a driver license, and in theory, a licenced driver is relatively less likely to cause road crashes than non-licenced drivers. This leads to our last assumption, which predicts that the more driver's licenses issued, the less likely the risk of more road crashes than the other way around. All these hypotheses/assumptions are graphically represented in **Figure 1**, which represents the metamodel proposed and tested to explain the complexity of road accident events in South Africa.

The aim of the study is to explain the complexity of road crashes in South Africa. The following objectives are set for the study: 1) to elucidate the temporal trends of road crashes and related consequences (number of crashes, causalities, fatal crashes, and deaths) in South Africa, 2) to propose and test a model to explain the complexity of road crashes in South Africa, 3) to predict future trends of road crashes and related consequences (number of crashes, casualties, fatal crashes, and road fatalities) in South Africa.

MATERIALS AND METHODS

Study Area

The study site is South Africa, a country located right at the southern tip of the African continent (Tibane et al., 2016). South Africa stretches from 22°S to 35°S in latitude and 17°E to 33°E in longitude (Tibane et al., 2016). The country is bordered by Namibia, Zimbabwe, Mozambique, and Botswana (Thompson et al., 2019). The Atlantic Ocean and the Indian Ocean are the two coastlines found in the southwest and southeast direction, respectively. In 2019, the mid-year population was estimated at 58,78 million and approximately 51,2% (30 million) of the population is female (Stats SA, 2019).

South Africa is ranked 10th in the world in term of the volume of road network estimated at 750,000 km (Tibane et al., 2016). The South African National Road Agency (SANRAL) is responsible for 21 403 km of the national road network (Tibane et al., 2016). Out of the 21,403 km, 18 283 km (85%) are non-toll roads and 3,120 km (15%) are toll roads (DoT, 2002). SANRAL's role is to provide effective strategic road infrastructure to assist with the development, accessibility, and finance towards the proclaimed national roads (Tibane et al., 2016). The country's toll-road network consists of approximately 19% (3,120 km) of the national grid and SANRAL manages 1,832 km of these toll roads (DoT, 2002). In 2017, the number of registered vehicles in South Africa were 12.2 million, and the number of un-roadworthy and unlicensed vehicles had increased from 1.0 million vehicles in 2016 to 1.1 million vehicles in 2017 (RTMC, 2018). The Gauteng province accounted for approximately 40% of the registered vehicle population in the country (RTMC, 2018).

Data Collection

Various Variables for Which Data Were Collected

The variables for which data were collected are defined as follows:

- "Total number of vehicles" is the total sum of the number of registered vehicles and both the number of unroadworthy and unlicensed vehicles.
- "Number of registered vehicles" is the number of (motorised and towed) vehicles registered on the National Traffic Information System (NaTIS) (RTMC, 2018).
- "Unregistered vehicles" are vehicles which are not registered under the licensing department. The owners of unregistered vehicles might have failed to renew the vehicles' licenses or failed to submit the vehicles for compulsory annual roadworthy tests within a certain period (RTMC, 2008).
- "The total distance travelled" variable is defined as the total distance travelled by vehicles on the road each year

measured as million vehicle kilometres (mvk) (RTMC, 2018).

- "Drivers licenses issued" is the annual total number of issued driving licenses obtained by drivers after they have passed their driver's license test (RTMC, 2019).
- "Estimated population of South Africa" is the estimate number of all residents of South Africa in a particular year (mid-year point) and based on the latest information (Stats SA, 2017).
- "Total number of crashes" is the number of road crashes (fatal, major, or minor crashes) that occurred in each year (RTMC, 2018).
- "Fatal crashes" are crashes that result to death of one person or more people in a road accident (RTMC, 2018).
- "Number of casualties" is the number of people that have been injured and/or killed in a crash (RTMC, 2019).
- "Fatalities" is defined as person or people that are killed during or immediately after a road accident, or death within 30 days after the accident has occurred as a direct result of the road accident (RTMC, 2019).

Sources of Data Analysed in This Study

Data analysed in the present study are retrieved from various sources. These sources include the Government's online campaign database known as *Arrive Alive* (www.arrivealive.co.za), various reports of the Road Traffic Management Corporation (RTMC, 2006; RTMC, 2007; RTMC, 2011; RTMC, 2012; RTMC, 2013; RTMC, 2014; RTMC, 2015; RTMC, 2016; RTMC, 2017; RTMC, 2018) as well as reports from *Statistics SA* (Stats SA, 1995; Stats SA, 2008; Stats SA, 2009; Stats SA, 2010; Stats SA, 2011; Stats SA, 2012; Stats SA, 2013; Stats SA, 2014; Stats SA, 2015; Stats SA, 2016; Stats SA, 2017). Data from *Arrive Alive* (period of 1935–2000) was obtained by email request. The data from the RTMC (period of 1935–2017) was obtained from the corporation's website; and the data from *Statistics SA* (period of 1936–2017) was retrieved from their website as well as by email request.

How were Data Collected by Various Sources?

Arrive Alive is the South African government's campaign to promote road safety and public awareness. They make use of data from both the RTMC and Stats SA and compile their reports for public use or research. The RTMC is the leading agency on road safety and management (RTMC, 2018). They collect their data from the South African Police Service (SAPS), Provisional Traffic Authorities and the Metropolitan Municipalities through Accident Report and Quick Response forms (RTMC, 2015). The Accident Report forms are used to capture data for all road accident types (injuries and damages) while the Quick Response forms are used to record fatal road crashes and are captured by RTMC. Furthermore, the RTMC makes use of other data sources such as the Culpable Homicide Crash: Observation Report (CHoCOR) form, CAS Analyst Report, National Traffic Information System (NaTIS), Statistics South Africa (Stats SA) (RTMC, 2018). The limitation to the methodology the RTMC used to collect their data is that road traffic information on their reports are mainly based on fatal crashes only (RTMC, 2018). While reporting and capturing road accident, data sometimes are duplicated (RTMC, 2013). The process of verifying the data is a lengthy process, which involves comparing the initial data that was received from various police stations at the time of the crash with that received from the central SAPS database (RTMC, 2013). Another limitation is that the consolidated inputs from provinces may not be received on time during the period of data collection for the specific report (RTMC, 2013). There is still a need for the leading road traffic agency to conduct in-depth research to collect scientific based facts to complement their administrative data (RTMC, 2018).

Statistics South Africa (Stats SA) is the national statistical service of South Africa (Stats SA, 2019). For their mid-year population estimates of South Africa, they make use of the cohort-component method (Stats SA, 2007). In the cohort-component methodology, a base population is estimated that is consistent with the known demographic characteristics of the country (Stats SA, 2017). The mid-year population estimates are produced by making use of the Spectrum model developed by the Future Group alongside with UNAIDS, WHO and UNICEF (Stats SA, 2013). In 2011, Stats SA made use of census for population estimate. Census is a procedure used to collect basic information on the population and housing statistics of a country for socioeconomic development, creation, and the implementation of policies (Stats SA, 2012). South Africa has conducted three Censuses (1996, 2001 and 2011) (Stats SA, 2012). In addition, Stats SA follows the standards of the International Monetary Fund's (IMF) Special Data Dissemination Standard (SDDS) to publish the mid-year population estimates annually (Stas SA, 2007). The limitation with the methodology Stats SA applies to collect data on the mid-year population estimates for South Africa is that the estimates may change as new data becomes available (Stats SA, 2017). The population estimates are accompanied by a series of revised estimates from the period of 2002–2017 (Stats SA, 2017).

Data Analysis

All analyses were done in R Development Core Team (2017), and R script used is provided as supplemental information.

Despite the efforts deployed to consult as many sources as possible, there are still some missing values in the dataset. Traditionally, prior to analysis, most statistical packages use listwise deletion to remove entire rows that have missing values; this practice leads to the loss of information sometimes critical for the understanding of the research question at hand or the hypothesis to be tested. To retrieve the information encapsulated in missing values in order to generate a comprehensive dataset, missing values have been imputed. This imputation was done as implemented in the R package *Amelia* (Honaker et al., 2011). Five different imputations were done concurrently on different computers and then combined in a single dataset. The means of those five imputed data were used for the analysis. The complete dataset is presented in **Supplementary Table S1**. In addition, during the analysis, because variables are not in the same scale (e.g., population in million vs. fatal crashes in hundred), variables were first re-scaled as follows: scaled variable = (observed-mean)/standard deviation.

To test the adequacy of the proposed metamodel to explain the complexity of road crashes in South Africa, a structural equation

model (SEM) was fitted to the imputed data collected. Structural equation modelling (SEM) is a multivariate and powerful technique used to test and evaluate multivariate causal relationships (Fan, 2016). The benefits of an SEM is that various causal relationships can be defined and tested simultaneously in one SEM. Each of the relationships or paths in the SEM was translated into GLM models (Generalized Linear Model) with appropriate error structure, depending on the nature of the response variable.

In the present study, four main response variables were defined. These variables include total number of crashes, total number of casualties, number of fatal crashes and number of persons killed. These variables are all "count data", meaning that the appropriate link function to specify in model fitting is "negative binomial" (O'Hara and Kotze 2010), given that count data should not be log-transformed (O'Hara and Kotze 2010). Six explanatory variables were defined: total number of vehicles, number of registered vehicles, number of unroadworthy and unlicensed vehicles, number of issued drivers' licenses, population of the country and vehicle distance travelled. Since most of the response variables in the metamodel are "count data" except the variable "distance travelled", the negative binomial GLM was fitted. GLM model with quasi-poison error family was appropriate to model "count data" but to avoid overdispersion the negative binomial GLM was better fitted as demonstrated by O'Hara and Kotze (2010). The GLM model was fitted to model the variable "distance travelled" rather by specifying the Gaussian family of error. All the GLM models were then combined in SEM which was fitted as implemented in the R library *piecewiseSEM* (Lefcheck, 2016). The adequacy of the metamodel was tested based on its overall Goodness-of-fit (C value) and the p value. C values are an indicator of whether an SEM is good enough to explain the data. To tell if an SEM is good enough, the lower the C value the better. Another key parameter of the goodness-of-fit is the p-value of the test of goodness-of-fit. The p-value here tests whether the proposed SEM is different from the best fit to the data at hand. If $p < 0.05$, this means that the proposed SEM is significantly different from the best fit and therefore should be rejected; if $p > 0.05$, this means that the SEM is no different from the best fit to the data and therefore can be used to explain the data (Schermelleh-Engel et al., 2003; Lefcheck 2016).

Prior to all these analyses, multicollinearity among predicting variables are first tested. Unlike in simple regressions, there is no straightforward way to deal with the problem of multicollinearity in SEM. Some authors even argue that multicollinearity is not an issue in SEM (e.g., Maruyama 1998; Malhotra et al., 1999; Verbeke and Bagozzi 2000). This is based on the ground that "if highly correlated variables can be regarded as indicators of a common underlying construct, multicollinearity problems can be avoided" (Grewal et al., 2004). Other authors argued that multicollinearity is a source of unreliable estimates of SEM parameters (e.g., Jagpal 1982; Grapentine 2000; Tarka 2018). There is no doubt that multicollinearity poses a problem in parameter estimates but the problem is particularly complex with SEM for the simple reason that, in SEM, an independent variable in one of the models that form the SEM can be a response variable in another model within the same SEM and *vice versa*.

In the present study, the following is how the multicollinearity problem was dealt with. For each of the models in the SEM, the variance inflation factor (VIF) was calculated in R and predicting variables with VIF > 5 (rules of thumb) were considered as highly collinear. Then, using the stepwise selection techniques, collinear variables were removed from the model starting from the variable with the highest VIF. After removing a collinear variable, the model is rerun, and the goodness-of-fit and p values calculated. This stepwise selection was repeated until the model is made up of only variables with VIF < 5. This process was followed for all the nine models that form the SEM. At the end, the SEM was reconstructed using only models with non-collinear variables and then was rerun. The AIC value for this SEM is: AIC = 1,788.486. The global goodness-of-fit for this SEM in which no model contains collinear variables is as follow: Fisher's C = 1,718.486 with p-value = 0 on 56 degrees of freedom. For any SEM, $p > 0.05$ means the SEM is of a good fit for the data while $p < 0.05$ means that the SEM departs significantly from the data analysed (Lefcheck 2016). In the present case, $p = 0$, meaning that the SEM with only non-collinear variables could not be used to explain the data.

In that case, we started bringing back (into each of the models in the SEM) each of the variables initially removed from the model because of collinearity. In this case, only missing variables that show significant relationships with each response variable in the SEM were brought back into the model, but this was done using one missing variable at a time (stepwise process). Each time, the goodness-of-fit and p value were calculated. It is only when all significant variables were brought back into the SEM that an SEM with $p > 0.05$ was found, indicating that a suitable SEM to explain the data is found.

Furthermore, the R^2 for each of the models in the SEM was calculated in scenario 1 where only non-collinear variables were included, and in scenario 2 where the final SEM is constructed with all previously missing but significant variables. This is summarized in **Supplementary Table S2**. In this table, R^2 values do not change substantially in SEM with collinear variables in comparison with SEM without collinear variables, except for variable "driver licence". This means that, although missing variables share similar information with other variables in each of the models in the SEM (that is why they are collinear), they also bear unique or complementary information (that is why it is only when they are added to the SEM that an SEM with $p > 0.05$ is found). These findings support our inclusion of all significant missing variables into the SEM.

The future of road accident in the country was predicted by fitting the Generalized Autoregressive Conditional Heteroskedasticity (GARCH) to the time-series data collected (**Supplementary Table S1**). GARCH model was selected to account for the expected high volatility of the variance in the time-series data of road accident (Bollerslev, 1986). The key assumption behind GARCH model is that variance is volatile or is not constant over time in a time series dataset. To test that this assumption is met, the Dickey-Fuller test (Fuller 1976) was run to test the null hypothesis that a unit root is present in an autoregressive model of each of the time series data, and that the process is thus not stationary (non-constant variance over time). The results confirm the null hypothesis, i.e., $p > 0.05$ for each response variable (fatal crashes, $p = 0.20$; persons killed, $p = 0.09$;

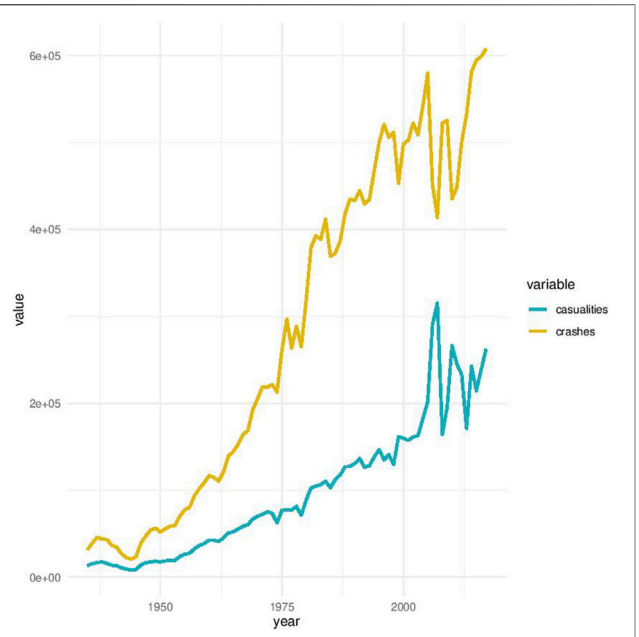

FIGURE 2 | Trends in number of crashes (road crashes) and casualties over the period 1935–2017 covered in this study.

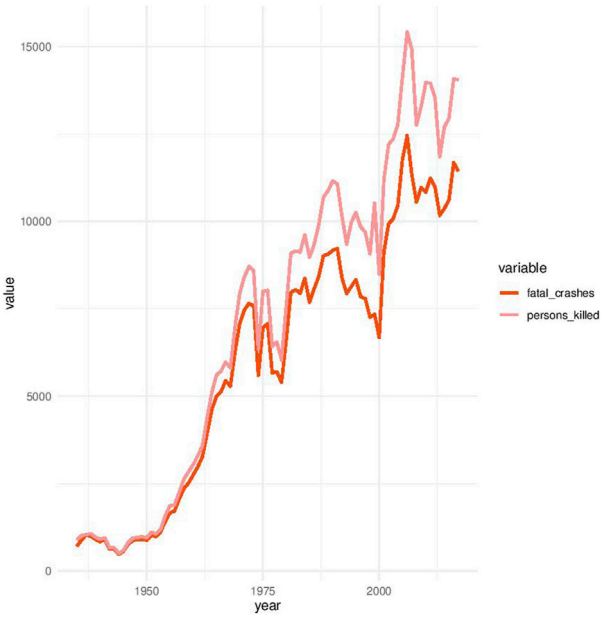

FIGURE 3 | Trends in number of fatal crashes and number of persons killed over the period 1935–2017 covered in this study.

casualties, $p = 0.51$ and crashes, $p = 0.99$), thus justifying the use of GARCH in this study. GARCH model was fitted as implemented in the R library *rugarch* (Ghalanos, 2020). Different variances of GARCH models were fitted depending on the starting time intervals for the modelling. The best GARCH model was selected using Akaike Information Criteria (AIC). This model was used to forecast future of road crashes in the next 10 years. Predicted values for each variable are presented in **Supplementary Tables S3–S6**.

RESULTS

Temporal Trends of Road Crashes and Related Consequences

The data analysed include missing values for some of the variables; these missing values represent 20% of all values across all variables, i.e., 80% of all values are present in the dataset (**Supplementary Figure S1**). For further analysis, the missing values have been imputed such that the findings reported below are based on a complete dataset (i.e., without missing values). The descriptive statistics of all data are summarized in **Supplementary Table S7**. The analysis shows that the number of crashes increases steadily over time since 1935 but exhibits important variations from the year 2000 (**Figure 2**). A similar trend is found for the number of casualties, and interestingly, there are always less casualties than crashes (**Figure 2**): roughly 32% of crashes on average results in casualties (**Supplementary Table S1**).

Some of these crashes are fatal, and as can be expected from the patterns in **Figure 3**, the number of fatal crashes and the number of persons killed in fatal crashes increase too over time with a sharp increase from the year 2000. Unfortunately, there

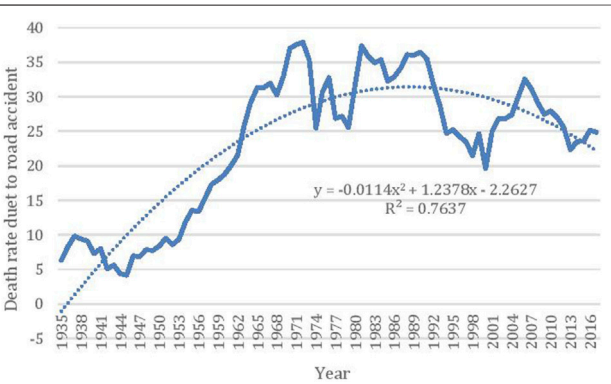

FIGURE 4 | Trends in the death rate due to road accident. Death rate is estimated over 100,000 people.

have always been more deaths (persons killed) than the number of fatal crashes (**Figure 3**) such that, on average, the number of persons killed represents 1.15 times the number of fatal crashes and 0.03 times the total annual number of road crashes (**Supplementary Table S1**).

The death rate follows a polynomial shape (**Figure 4**) whose trend line follows the equation: $y = -0.0114x^2+1.2378x-2.2627$ ($R^2 = 0.76$) with y = death rate and x = year. This trend can be broken down into four noticeable periods (**Figure 4**): between 1935 and 1938, the death rate per 100,000 people increased from 6 to 9.5; from 1938 to 1945, there is a decrease from 9.5 to 4.18; the 1945–1972 period witnessed an exponential increase from 4.18 to 37.88 deaths per 100,000 people; this sharp increase has been slowing down since 1972 until 2017 where it decreased from

TABLE 1 | Coefficients of the structural equation model fit to the dataset analysed in the present study.

Responses	Predictors	Estimates	Standard error	Df	*p*-values	R2
Crashes	Number of vehicles	−0.32	0.06	76	<0.001	1
	Registered vehicles	1.76	0.12	76	<0.001	
	Unregistered vehicles	0.14	0.04	76	0.003	
	Number of driver's licence issued	0.05	0.07	76	0.44	
	Country population	−0.88	0.13	76	<0.001	
	Total distance travelled by vehicles	0.02	0.01	76	0.12	
Casualties	Number of vehicles	−0.02	0.11	75	0.80	1
	Registered vehicles	1.44	0.34	75	0.0001	
	Unregistered vehicles	−0.10	0.07	75	0.14	
	Number of driver's licence issued	−0.06	0.10	75	0.52	
	Country population	−0.42	0.23	75	0.08	
	Total distance travelled by vehicles	−0.04	0.02	75	0.03	
	Number of crashes	0.04	0.16	75	0.76	
Fatal crashes	Number of vehicles	−0.79	0.09	75	<0.001	1
	Registered vehicles	3.73	0.23	75	<0.001	
	Unregistered vehicles	0.22	0.06	75	0.0008	
	Number of driver's licence issued	−0.11	0.09	75	0.22	
	Country population	−3.04	0.18	75	<0.001	
	Total distance travelled by vehicles	0.20	0.02	75	<0.001	
	Number of casualties	−0.11	0.10	75	0.29	
Persons killed	Number of vehicles	0.20	0.06		0.001	1
	Number of crashes	−0.14	0.06	73	0.04	
	Number of casualties	0.32	0.04	73	<0.001	
	Registered vehicles	−0.31	0.26	73	0.23	
	Unregistered vehicles	−0.10	0.03	73	0.003	
	Number of driver's licence issued	−0.07	0.04	73	0.07	
	Country population	0.36	0.19	73	0.06	
	Total distance travelled by vehicles	0.03	0.01	73	0.009	
	Number of fatal crashes	0.80	0.05	73	<0.001	
Number of vehicles	Country population	−0.18	0.10	81	0.08	0.06
Registered vehicles	Country population	1.01	0.01	80	<0.001	1
	Number of vehicles	0.13	0.01	80	<0.001	
Unregistered vehicles	Country population	1.17	0.20	79	<0.001	0.98
	Registered vehicles	−0.74	0.20	79	0.0004	
	Number of vehicles	1.07	0.03	79	<0.001	
Number of driver's licence issued	Country population	1.60	0.11	78	<0.001	1
	Unregistered vehicles	0.39	0.05	78	<0.001	
	Registered vehicles	−1.47	0.10	78	<0.001	
	Number of vehicles	0.81	0.06	78	<0.001	
Total distance travelled by vehicles	Country population	−1.17	0.96	77	0.22	0.92
	Unregistered vehicles	−1.30	0.31	77	0.0001	
	Number of driver's licence issued	1.06	0.50	77	0.03	
	Number of vehicles	−0.26	0.49	77	0.59	
	Registered vehicles	2.27	0.88	77	0.01	

37.88 to 24.85 and reached the lowest rate of 19.60 in the year 2000 (**Figure 4**). These trends result in an average death rate of 23.14 deaths per 100,000 people.

Understand the Complexity of Road Crashes in South Africa

Structural Equation Model of Road Crashes

The metamodel represented in **Figure 1** was tested. The following parameters of the metamodel suggest that the metamodel is suitable to explain the complexity of the mechanism driving road crashes: Fisher's C = 3.895 with *p*-value = 0.143 on 2 degrees of freedom.

The coefficients of each of the models in the metamodel are summarized in **Table 1**. This Table shows that the number of crashes could significantly be explained by total number of vehicles ($\beta = -0.32 \pm 0.06$, $p < 0.001$), number of registered vehicles ($\beta = 1.76 \pm 0.12$, $p < 0.001$), number of unregistered vehicles ($\beta = 0.14 \pm 0.04$, $p = 0.003$) and the population of the country ($\beta = -0.88 \pm 0.13$, $p < 0.001$). As opposed to expectation, the number of driver licences issued, and total distance travelled by vehicles do not correlate significantly with number of crashes ($p > 0.05$).

Furthermore, the analysis reveals that the number of casualties could be linked significantly to number of registered vehicles ($\beta = 1.44 \pm 0.0.34$, $p < 0.001$) and total distance travelled by vehicles ($\beta = -0.04 \pm 0.02$, $p = 0.03$). None of the other variables tested correlates significantly with number of casualties ($p > 0.05$).

As of the number of fatal crashes, the analysis reveals that the total number of vehicles ($\beta = -0.79 \pm 0.09$, $p < 0.001$), number of registered ($\beta = 3.73 \pm 0.23$, $p < 0.001$) and unregistered vehicles

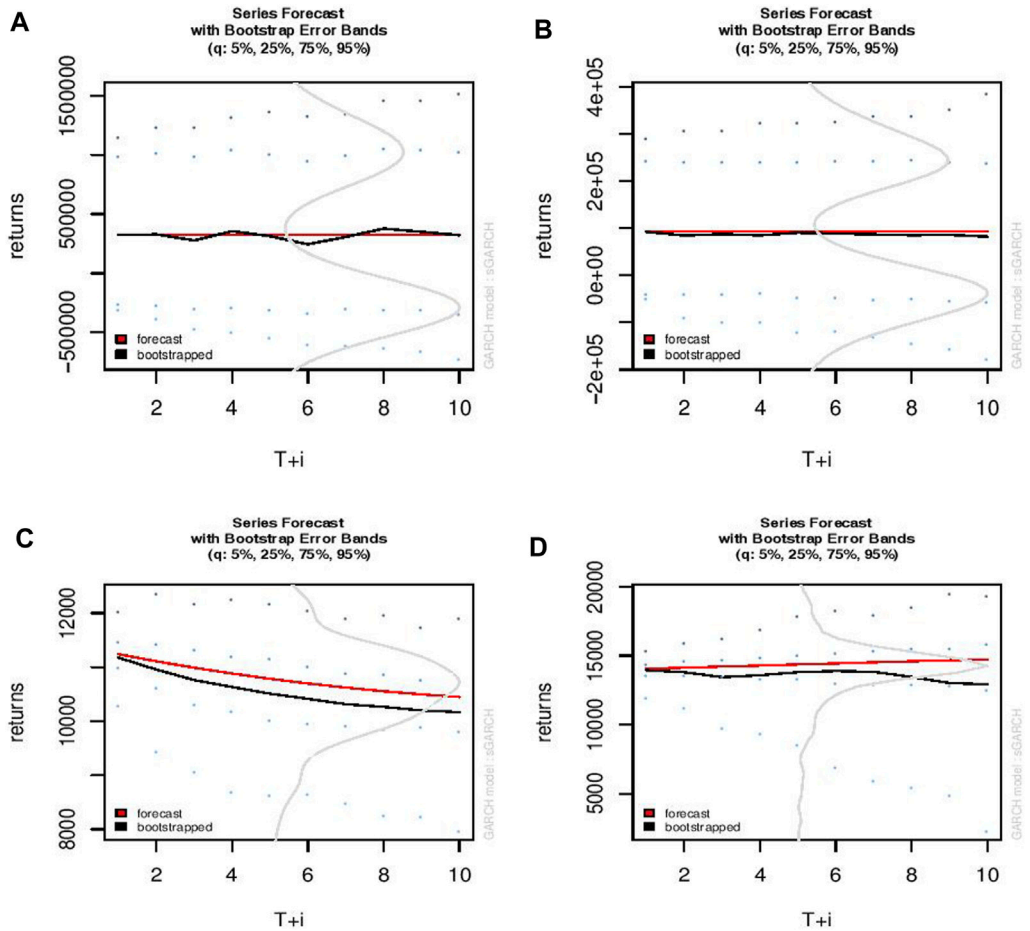

FIGURE 5 | Prediction of the trends of road crashes and its consequences for the next 10 years in South Africa using GARCH model. **(A)** = number of crashes (road crashes), **(B)** = number of casualties, **(C)** = number of fatal crashes and **(D)** = number of persons killed.

(β = 0.22 ± 0.06, $p < 0.001$), the population of the country (β = -3.04 ± 0.18, $p < 0.001$) and the total distance travelled by vehicles (β = 0.20 ± 0.02, $p < 0.001$) correlate significantly with the number of fatal crashes. However, the number of casualties and again the number of driver licence do not seem to determine the number of fatal crashes ($p > 0.05$).

Finally, the findings of the SEM analysis reveal that the total number of vehicles (β = 0.20 ± 0.06, p = 0.0017), number of unregistered vehicles (β = −0.10 ± 0.03, p = 0.003), number of crashes (β = −0.14 ± 0.06, p = 0.04), number of casualties (β = 0.32 ± 0.04, $p < 0.001$), distance travelled (β = 0.03 ± 0.01, p = 0.009) and obviously the number fatal crashes (β = 0.80 ± 0.05, $p < 0.001$) are significant determinant of the number of persons killed in road crashes (Table 4.1).

Expected Trends of Road Crashes for the Future

Using the GARCH model, the future of road crashes was predicted. The number of crashes or crashes is predicted to be roughly constant over time at 617,253 crashes for the next 10 years, with the worse scenario suggesting that this number may reach 1,896,667 (**Figure 5A**). The number of casualties was also predicted to be roughly constant at 93,531 over time although this number may reach 661,531 in the worst-case scenario (**Figure 5B**). However, although the number of fatal crashes may decrease over time, it is forecasted to reach 11,241 fatal crashes within the next 10 years with the worse scenario estimated at 19,034 within the same period (**Figure 5C**). Finally, the number of persons killed is also predicted to be roughly constant at 14,739 but may also reach 172,784 in the worse scenario (**Figure 5D**).

DISCUSSION

Temporal Trajectory of Road Crashes in South Africa

Over the 82 years (1935–2017) period covered in this study, the findings reveal an increasing trend in number of reported road crashes, casualties, fatal crashes, and deaths. The study also reveals that, unfortunately, 32% of crashes lead to casualties, and when these are fatal, the ratio persons killed: fatal crashes

(referred to as accident severity rate in Verster and Fourie, 2018) is 1.15. In their recent study, Verster and Fourie (2018) estimated the severity rate at 1,2–1,3 between 2010 and 2015, a rate similar to what is revealed in the present study, although our present study covers a longer period of time than theirs. In any case, these findings suggest that, overall, in any fatal accident in South Africa, more than 1 person lose their lives. Verster and Fourie's (2018) further showed that the severity rate is not uniform within a week, with the highest severity rates (1.22–1.25) found for Mondays, Fridays, Saturdays, and Sundays (South African Department of Transport, 2015; Verster and Fourie, 2018).

However, the number of road crashes fluctuated more notably from the year 2000 onward, resulting into a sharp increase of fatal crashes and the number of persons killed from the year 2000. This corresponds to a post-apartheid era where vehicle ownership started increasing in the country, which may account for the sharp increase that we observed in fatal crashes and persons killed. Furthermore, this year 2000 corresponds to the period where 75% of road crashes recorded in South Africa were linked to drivers driving under the influence of alcohol (Ncube et al., 2016). In 2000, the cost of road traffic crashes in South Africa was estimated at R13.8 billion (US$2 billion) (Ministry of Transport, 2001). South Africa is the world leading country in drunk driving followed by Canada and the US (McCarhy, 2016). The number of drunk drivers has increased by four times since 1980. It is therefore not surprising that we observe the notable fluctuations of road accident occurrence as well as the increase in fatal crashes and number of persons killed from 2000 onward. Surprisingly, it is in the same year 2000 that the lowest death rate of 19.60 was observed. This implies that the increase in fatal crashes did not result in high death rate after correcting for population size.

Specifically, the death rate increased drastically from 6 death per 100,000 persons in 1935–37.88 deaths per 100,000 people in 1972 before it decreased gradually to 24.8. This trend or shape of reverse curve is seems to be a global trend as it is reported in several parts of the world, including Australia, Poland, China, etc. (Borsos et al., 2012; Al-Madani 2018; WHO, 2018). Efforts need to be continuously deployed to maintain this decreasing trend because, after a long period of safety improvement, the risky behaviours leading to the re-increase in the number of road crashes may occur again (Bąk et al., 2019) as predicted in the behavioural theory (Wilde, 1988).

The overall trend found in the present study is similar to the one reported, also for South Africa, by WHO (2009), WHO (2018), which identified four key points in the trajectory of death rate. They reported that, from 1972 to 1992, the death rate fluctuated within a window of 25–40 deaths/100,000 people. They also indicated that this rate decreased to 20 death/100,000 people from 1992 to 2002, and then increased again to 35 deaths/100,000 people from 2002 to 2007 before it decreases to 21 death/100,000 people from 2007 to 2013 and then a slight increase to the present day. The similarity between the WHO's trend and what is reported in the present study suggests that the data imputation done in the present study did not cause significant bias in the data analysed.

On average, the study reveals a death rate of 23.14 deaths per 100,000 people. This death rate is lower than that reported for low-income countries (27.5 deaths per 100,000 population) and for the African continent (26 deaths/100,000; WHO, 2018) but is similar to what is reported for Brazil in the last 10 years (WHO, 2018). However, it is three times the rate reported (8.3 deaths per 100,000 population) for developed world (WHO, 2018) and 4-times the 6 deaths/100,000 rate reported for Australia (Mooren et al., 2011). In this developed world, the death rate has been slowing down since the 1960s: 27% decrease in the US and 63% decline in Canada from 1975 to 1988 while an increase was noted in developing countries (an increase by 44% in Malaysia and 243% in China; Kopits and Cropper, 2003). Although we are losing globally 1,35 million people annually owing to road crashes, the youth (5–29 years old; WHO, 2019) is disproportionately the most affected. The consequences of these losses are significant: heavy deterioration of standard of living for family (Silcok, 2003), the loss of 1–2% of the gross national product of developing countries (Peden and Hyder, 2002). To South Africa, it costs 3.4% of its GDP (South African Department of Transport, 2016). This is unaffordable in a country where basic service delivery to community is still a problem, and therefore calls for vigorous actions. These actions may include enforcement of seat belt safety laws, enforcement of speed limits, and strict and unapologetic punishment for drunk driving.

The Proposed Metamodel for Road Crashes in South Africa and Future Trends

The parameters of the metamodel tested show that the metamodel in **Figure 1** is suitable to explain the complexity of the mechanism driving road crashes. As predicted in the theoretical framework in **Figure 1**, the number of crashes is indeed predicted by the total number of vehicles but contrary to prediction, the relationship is negative. This negative relationship means that the increase in the number of vehicles do not lead to the increase in the number of crashes but the later actually decreases. This may imply that, while the number of vehicles is increasing, these vehicles may be in majority good roadworthy cars driven by licenced and careful drivers such that this increase in the number of cars does not result in an increase in crashes. For the next 10 years, the GARCH model employed in this study predicted a roughly constant number of crashes or road crashes (617,253 crashes), but this number may triple, in the worst-case scenario, reaching 1,896,667. This calls for vigorous actions against the worst scenario.

Similarly, the results of this study show a negative relationship between the population of the country and the number of crashes. The initial expectation is that the increase in human population would also result in the increase in road crashes (Al-Reesi et al., 2013). The rationale for this is that when the population increases, the number of vehicle owners would increase such that more vehicles (both registered and unregistered) would be on the road, thus increasing the risk of road crashes. Also, when more vehicles are on the road, the distance travelled by vehicles would increase, and this would reduce the quality and strength of

the vehicles over time, and thus increasing the risk of road crashes. However, the total distance travelled by vehicles does not correlate significantly with number of crashes, discounting the importance of this variable. The finding reported in the present study matches what has been found for other countries, such as United Kingdom where, in the last 30-years, although the population size has grown by 15%, road fatalities have fallen by 68% (Department for Transport, 2015).

The counterintuitive finding of negative relationships between number of population and number of crashes could mean that the increase in population is followed by an increase in careful and licenced drivers. However, the part of the explanation linked to driver's licence is discounted by the finding that, as opposed to expectation, the number of driver licences issued does not correlate significantly with number of crashes, putting into question the contribution of driver's licences to good driving behaviour on the road. In Botswana, unlicensed drivers, or failure to produce a licence are found to correlate significantly to road fatalities (Mphela, 2011). Interestingly, matching the theoretical prediction, the number of crashes increases when the number of both registered and unregistered vehicles also increases. A potential explanation is that, irrespective of whether vehicles are registered or unregistered, too many vehicles on the road predisposes to an increase of the likelihood of crashes. Unregistered vehicles are likely to be unroadworthy and faulty; vehicle roadworthiness was reported as a major contributing factor to road crashes (Bayam et al., 2005; Verster and Fourie, 2018; WHO, 2018). Verster and Fourie (2018) reported that 7.8% of road crashes in South Africa are linked to vehicles, and in 2017 alone, the factor "vehicle" contributed 3% to road crashes in the country (RTMC, 2018).

Furthermore, as predicted for number of crashes, the expectation is also that the number of casualties would correlate positively and significantly with all six predictors analysed in the study. The findings in this study reveal that the number of casualties indeed correlate positively and significantly but with only the number of registered vehicles and negatively with total distance travelled by vehicles. The positive relationship is an indication that, as the number of registered vehicles increases, more vehicles are on the road, heightening the risk of crashes thus casualties. The negative relationship between casualties and distance travelled is unexpected and means that more vehicles on the road do not increase road casualties. Again, the GARCH model predict a roughly constant number of casualties for the next 10 years (93,531) but this may increase 6-fold in the worst-case scenario.

As expected, the analysis reveals that the total number of vehicles, number of registered and unregistered vehicles, the population of the country and the total distance travelled by vehicles correlate each significantly with the number of fatal crashes. However, the number of vehicles and the population of the country which were predicted to correlate positively with the number of fatal crashes show instead negative correlations. This is in contrast with the reports from other studies that reported the positive relationships predicted in the theoretical metamodel in the present study (Jacobs and Cutting, 1986; Aderamo, 2012). The contrasting findings in the present study mean that, as the total number of vehicles and the country's population size increase, the number of fatal crashes decreases.

On a global scale, Jacobs and Aeron-Thomas (2000) predicted the road fatalities to reach between 900,000 and 1.1 million in 2010 and between 1 million and 1.3 million in 2020. For the next 10 years, the GARCH model predicted a decreasing trend of the number of fatal crashes, but this number may reach 11,241–19,034 in South Africa. Again, the observed decrease in fatal crashes is unexpected and could imply that one or more key variables that decrease the number of fatal crashes while the total number of vehicles and population size are increasing are not taken into consideration in the proposed metamodel in the present study. An example of such variable could be road policy enforcement or improvement, improvement of drivers' consciousness or behaviour that may cause a decline in the frequency of fatal crashes (Shaw and McMartin, 1977; Farmer et al., 1997; Deffenbacher et al., 2002; Delen et al., 2006; Papantoniou et al., 2019; Sârbescu and Maracatu, 2019). Further variables, focused on the drivers' characteristics such as age, gender, driving experience, the roadway length (for different road grades), the economic development, and education level that are not considered in the present study may be important too as reported in previous studies (Bayam et al., 2005; Eboli and Mazulla 2007; Papantoniou et al., 2019; Papantoniou et al., 2018). Additional factors that may be linked to road crashes but not included in our model are alcohol, seat belts, speed, fatigue, and red-light running as potential behavioral variables (Wegman et al., 2013), while Vanderschuren et al. (2020) emphasized the importance of examining infrastructure effects or pedestrian fatality trends. Nevertheless, several studies called for road crashes to be regarded as more driven by a failure of a system and not just of a person (the driver) (Reason, 2000). In that system is a complex of interactive factors and an accident is the consequence of a failure of the interactions (Reason, 2000; Bayam et al., 2005; Eboli and Mazulla, 2007; Aderamo, 2012; Hassan and Abdel-Aty, 2013, Bergel-Hayat et al., 2013; Theofilatos, 2017; Lee, et al., 2018; Verster and Fourie 2018; Papantoniou et al., 2019; Papantoniou et al., 2018).

In the present study, six interactive factors/predictors are tested as linked to road crashes and their effects (casualties, fatal crashes, number of persons killed, etc.). Counterintuitively, the number of casualties and the number of driver licences do not correlate significantly with the number of fatal crashes. The lack of significant correlation between number of casualties and number of fatal crashes disproves the cascading effects initially predicted in **Figure 1**, implying that an increase in road casualties does not necessarily lead to an increase in road fatalities. Again, this could be linked to a potential improvement of drivers' consciousness or behaviour on the road. The lack of correlation between the number of drivers' licence issued and number of fatal crashes dismiss the initial prediction that an increase in number of licences issued should mirror an improvement of driving behaviour or experience (da Silva et al., 2014) and thus limit the number of crashes/crashes and all inherent consequences (e.g., fatalities). This finding may

not be that surprising given the corruption around driver's licence delivery (Arrive Alive, 2020).

Finally, as expected, the total number of vehicles correlate significantly and positively with the number of persons killed: more cars mean high risk of fatalities. One relationship not predicted in **Figure 1** is the positive significant correlation found between number of casualties and number of persons killed. In the predicted theoretical metamodel, it was suggested an indirect link between number of casualties and number of persons killed but mediated by number of fatal crashes. The analysis reveals instead a direct link between number of casualties and number of persons killed and reported above there is no significant link between number of casualties and number of fatal crashes. Overall, the finding here means that an increase in number of casualties may heighten the risk of more persons killed without necessarily increasing the number of fatal crashes. Similar positive and significant links were found between distance travelled on one hand and number of fatal crashes on the other with the number of persons killed. The link between distance travelled and number of persons killed were predicted in **Figure 1** and means that more cars on the road increases the likelihood of more persons killed in case of road crashes. The positive significant link between number of fatal crashes and number of persons killed goes without saying. Surprisingly, while the number of unregistered vehicles increases, the number of persons killed decreases and similar relationship is found for the link between total crashes and persons killed. As indicated above, there must have been important variables (e.g., improvement in road enforcement, drivers behaviours, etc.) that are not included in the metamodel tested in the present study and which are the basis for the counter-intuitive relationships found in the present study. A constant pattern is predicted for the next 10-years using the GARCH model but could fluctuate between 14,739 and 172,784. In the Mthatha area in South Africa, Meel (2008) predicted 57 road death/100,000; if this rate is generalized to the total population of the country, this would be equivalent to 34,200 road deaths annually, well contained within the 14,739–172,784 range identified in the present study. For Africa, Al-Madani (2018) predicted the number of crash death to range between 87 640 and 126 000 during the 2014–2025 period. Our model's predictions show the contribution of South Africa to the crash death predicted for the entire continent by Al-Madani (2018), and also reveal that the worst-case scenario (172 784 crash death) predicted for South Africa alone may even surpass the prediction for Africa. This calls for vigorous actions to avoid this scenario.

Based on the findings of the present study revealing significant correlations between vehicles and various road accident events, we recommend the following:

- Limit the usage of vehicles on the road. This can be done: by promoting a safe public transport system to reduce drastically the number of vehicles on the roads. This is based on our finding that the number of crashes correlate positively and significantly with the number of registered vehicles.
- Vehicles that are not registered should be impounded by traffic officers. This is based on our finding that the number of crashes correlates positively and significantly with the number of unregistered vehicles. We suggest that legal provisions must be made towards a harsh punishment of drivers of unregistered vehicles, e.g., jail time or heavy financial penalties.
- Reinforcing road traffic measures such as seat belt law enforcement, severe penalties for reckless and drunk drivers and speed control. This is based on our finding that the number of crashes correlates negatively with the country's population. The number of crashes decreases when country's population increases. This suggests that population growth and vehicle ownership do not increase at the same rate such that the increase in population may not lead to the increase in car ownership, and this, in conjunction with road traffic measures in place, may lead to the decrease in road crashes.
- Old vehicles must be removed from the road. This is based on our finding that "total distance travelled by vehicles" correlates positively and significantly with the "number of fatal crashes". This means that the Traffic Department must set a threshold for kilometrage above which vehicles must not be allowed on the road. This requires a scientific study to identify such threshold. However, this removal must not be done systematically since some old cars may still be roadworthy. We suggest that the decision to remove or not must be based on not only the mileage but also the roadworthiness of the car.
- Identifying and promoting measures that are working successfully in reducing the number of fatalities in road accident, e.g., promoting seat belt, strict check-up of roadworthiness, severe punishment of drunk drivers. This has to be done by the traffic department. This is grounded on our finding that the number of persons killed correlates negatively with the number of crashes. That the number of persons killed in road crashes decreases with more crashes is unexpected. The finding may imply that not all crashes are fatal but also measures could have been taken so that there are less and less death in most crashes. Government's Arrive Alive Road-Safety Campaign (https://www.arrivealive.co.za/) should be intensified. Emergency services should respond quicker to calls of road crashes in order to make it on time at an accident scene to save lives.

Potential Limitations of the Study

There are some debates around road accident data sources and their reliability (Joseph, 2013). A number of studies make use of two data sources (Benlagha and Charfeddine, 2020). The first data source includes police-recorded data (Manner and Wünsch-Ziegler, 2013; Feng et al., 2016; Lee et al., 2018). The second data source is insurance companies (Krishnan and Carnahan, 1985; Mills and Hambly, 2011). The debates emanate from the mismatch between both sources in term of data provided. For example, 1 out of 5 road deaths is reported by police in the Philippines (WHO, 1996). In Indonesia, police report 40% less

road deaths than insurance companies (Lu et al., 1999). Even in China, the Beijing Research Institute of Traffic Engineering (Liren, 1996) estimated that the actual number of people killed in road crashes was over 40% more than the number reported by the police. In term of reliability of data, several studies suggest that insurance companies are more reliable than police-recorded data, given that, not only they are always informed once an accident occurs (fatal accident or not), but also given the professional way (unlike government officials; Joseph 2013) they handle data collection (Cohen, 2005; and; González Dan et al., 2017).

Another limitation is that our model did not take into account the fact that vehicle design has changed significantly since 1935, as have occupant protection measures and vehicle speeds. There is no doubt that these changes have important impact on the trends of road crashes. With these improvements in design and occupant protection measures, the impact to expect in the future is reduction in road crashes and consequences. However, given that this is what our model predictions show, this perhaps implies that our models may have captured this future improvement in design and safety measures. In the present study, a multiple-source approach was used as presented in the Methodology to minimize the influence of potential inconsistency in data reported in various sources(World Health Organisation, 2011; WHO, 2013; WHO, 2015).

DATA AVAILABILITY STATEMENT

The original contributions presented in the study are included in the article/**Supplementary Material**, further inquiries can be directed to the corresponding author. All supplemental materials including the R script used can be found at: https://github.com/kowiyou/Kowiyou

AUTHOR CONTRIBUTIONS

Conceptualization, KY and DM; methodology, KY; software, KY; validation, KY; formal analysis, KY; investigation, KY; resources, DM; data curation, DM; writing—original draft preparation, KY; writing—review and editing, KY; visualization, KY; supervision, KY; project administration, DM and KY; funding acquisition, DM and KY. All authors have read and agreed to the published version of the manuscript.

FUNDING

This research was funded partially by the National Research Foundation (NRF) South Africa, grant number 112113 to KY. DM benefited from the same funding as registration fee for her MSc programme.

ACKNOWLEDGMENTS

We acknowledged all who contributed to make data available as well as the University of Johannesburg for logistics. We also thank two reviewers who provided valuable comments that improve the initial version of this manuscript.

SUPPLEMENTARY MATERIAL

The Supplementary Material for this article can be found online at: https://www.frontiersin.org/articles/10.3389/ffutr.2021.760640/full#supplementary-material

REFERENCES

Aderamo, A. J. (2012). Assessing the Trends in Road Traffic Accident Casualties on Nigerian Roads. *J. Soc. Sci.* 31, 19–25. doi:10.1080/09718923.2012.11893011

Al-Madani, H. M. N. (2018). Global Road Fatality Trends' Estimations Based on Country-wise Micro Level Data. *Accid. Anal. Prev.* 111, 297–310. doi:10.1016/j.aap.2017.11.035

Al-Reesi, H., Ganguly, S. S., Al-Adawi, S., Laflamme, L., Hasselberg, M., and Al-Maniri, A. (2013). Economic Growth, Motorization, and Road Traffic Injuries in the Sultanate of Oman, 1985-2009. *Traffic Inj. Prev.* 14, 322–328. doi:10.1080/15389588.2012.694088

Alive, Arrive. (2020). Corruption, Traffic Enforcement and Road Safety. Available at: https://www.arrivealive.mobi/corruption-traffic-enforcement-and-road-safety, (Accessed on September 02, 2020).

Bayam, E., Liebowitz, J., and Agresti, W. (2005). Older Drivers and Accidents: A Meta Analysis and Data Mining Application on Traffic Accident Data. *Expert Syst. Appl.* 29, 598–629. doi:10.1016/j.eswa.2005.04.025

Benlagha, N., and Charfeddine, L. (2020). Risk Factors of Road Accident Severity and the Development of a New System for Prevention: New Insights from China. *Accid. Anal. Prev.* 136, 105411–105415. doi:10.1016/j.aap.2019.105411

Bergel-Hayat, R., Debbarh, M., Antoniou, C., and Yannis, G. (2013). Explaining the Road Accident Risk: Weather Effects. *Accid. Anal. Prev.* 60, 456–465. doi:10.1016/j.aap.2013.03.006

Bollerslev, T. (1986). Generalized Autoregressive Conditional Heteroskedasticity. *J. Econom.* 31, 307–327. doi:10.1016/0304-4076(86)90063-1

Borsos, A., Koren, C. S., Ivan, J. N., and Ravishanker, N. "Long-term Safety Trends Related to Vehicle Ownership in 26 Countries", in Proceedings of the Paper presented at: Annual Meeting of the Transportation Research Board, Washington, DC, USA, January 22–26 .

Bąk, I., Cheba, K., and Szczecińka, B. (2019). The Statistical Analysis of Road Traffic in Cities of Poland. *Transportation Res. Proced.* 39, 14–23.

Cohen, A. (2005). Asymmetric Information and Learning: Evidence from the Automobile Insurance Market. *Rev. Econ. Stat.* 87, 197–207. doi:10.1162/0034653053970294

Deffenbacher, J. L., Lynch, R. S., Oetting, E. R., and Swaim, R. C. (2002). The Driving Anger Expression Inventory: A Measure of How People Express Their Anger on the Road. *Behav. Res. Ther.* 40, 717–737. doi:10.1016/s0005-7967(01)00063-8

Delen, D., Sharda, R., and Bessonov, M. (2006). Identifying Significant Predictors of Injury Severity in Traffic Accidents Using a Series of Artificial Neural Networks. *Accid. Anal. Prev.* 38, 434–444. doi:10.1016/j.aap.2005.06.024

Department for Transport (2015). Reported Road Casualties, Great Britain: 2015 Annual Report. Available at: https://assets.publishing.service.gov.uk/government/uploads/system/uploads/attachment_data/file/556406/rrcgb2015-02.pdf(Accessed on September 2, 2020).

Donaldson, L. H., Brooke, K., and Faux, S. G. (2009). Orthopaedic Trauma from Road Crashes: Is Enough Being Done? *Aust. Health Rev.* 33, 72–84. doi:10.1071/ah090072

Eboli, L., and Mazzulla, G. "A Structural Equation Model for Road Accident Analysis," in Proceedings of the 4th International SIIV Congress, Palermo, 12-14 September 2007 (Palermo, Italy: University of Calabria).

Fan, Y., Chen, J., Shirkey, G., John, R., Wu, S. R., Park, H., et al. (2016). Applications of Structural Equation Modeling (SEM) in Ecological Studies: An Updated Review. *Ecol. Process.* 5, 19. doi:10.1186/s13717-016-0063-3

Farmer, C. M., Braver, E. R., and Mitter, E. L. (1997). Two-Vehicle Side Impact Crashes: The Relationship of Vehicle and Crash Characteristics to Injury Severity. *Accid. Anal. Prev.* 29, 399–406. doi:10.1016/s0001-4575(97)00006-7

Feng, S., Li, Z., Ci, Y., and Zhang, G. (2016). Risk Factors Affecting Fatal Bus Accident Severity: Their Impact on Different Types of Bus Drivers. *Accid. Anal. Prev.* 86, 29–39. doi:10.1016/j.aap.2015.09.025

Fuller, W. A. (1976). *Introduction to Statistical Time Series*. New York: John Wiley & Sons. ISBN 0-471-28715-6.

Ghalanos, A. (2020). Package 'rugarch' Version 1.4-4. Available at https://bitbucket.org/alexiosg, (Accessed on September 16, 2020).

González Dan, J. R., Arnaldos, J., and Darbra, R. M. (2017). Introduction of the Human Factor in the Estimation of Accident Frequencies through Fuzzy Logic. *Saf. Sci.* 97, 134–143. doi:10.1016/j.ssci.2015.08.012

Grapentine, T. (2000). Path Analysis vs. Structural Equation Modeling. *Marketing Res.* 12 (3), 12–20.

Grewal, R., Cote, J. A., and Baumgartner, H. (2004). Multicollinearity and Measurement Error in Structural Equation Models: Implications for Theory Testing. *Marketing Sci.* 23, 519–529. doi:10.1287/mksc.1040.0070

Hassan, H. M., and Abdel-Aty, M. A. (2013). Predicting Reduced Visibility Related Crashes on Freeways Using Real-Time Traffic Flow Data. *J. Saf. Res.* 45, 29–36. doi:10.1016/j.jsr.2012.12.004

Honaker, J., King, G., and Blackwell, M. (2011). Amelia II: A Program for Missing Data. *J. Stat. Softw.* 45 (7), 1–47. doi:10.18637/jss.v045.i07

ITF (International Transport Forum) (2018). *Road Safety Annual Report 2018: South Africa*. East Jerusalem.

Jacobs, G., Aeron-Thomas, A., and Astrop, A. (2000). "Estimating Global Road Fatalities",. TRL Report 445.

Jacobs, G. D., and Cutting, C. A. (1986). Further Research on Accident Rates in Developing Countries. *Accid. Anal. Prev.* 18, 119–127. doi:10.1016/0001-4575(86)90056-4

Jagpal, H. S. (1982). Multicollinearity in Structural Equation Models with Unobservable Variables. *J. Marketing Res.* 19, 431–439. doi:10.1177/002224378201900405

Joseph, R. (2013). Who Are South Africa's Worst Drivers? the Truth Doesn't Lie in the Data. Africa Check. Available at: https://africacheck.org/2013/07/04/who-are-south-africas-worst-drivers-the-truthisnt-in-the-data/, (Accessed on January 12, 2018).

Kopits, E., and Cropper, M. (2003). *Traffic Fatalities and Economic Growth*. The World Bank, Policy Research Working Paper No. 3035 (Washington, DC: World Bank).

Krishnan, K. S., and Carnahan, J. V. (1985). Analysis of the Effect of Car Size on Accident Injury Probability Using Automobile Insurance Data. *Accid. Anal. Prev.* 17, 171–177. doi:10.1016/0001-4575(85)90019-3

Labuschange, F., De Beer, E., Roux, D., and Venter, K. "The Cost of Crashes in South Africa 2016", in Proceedings of the 36th Southern African Transport Conference (SATC 2017), Pretoria, South Africa, July 2017. Conference Partners.

Lee, J., Chae, J., Yoon, T., and Yang, H. (2018). Traffic Accident Severity Analysis with Rain-Related Factors Using Structural Equation Modeling - A Case Study of Seoul City. *Accid. Anal. Prev.* 112, 1–10. doi:10.1016/j.aap.2017.12.013

Lefcheck, J. S. (2016). PiecewiseSEM : Piecewise Structural Equation Modelling in R for Ecology, Evolution, and Systematics. *Methods Ecol. Evol.* 7, 573–579. doi:10.1111/2041-210x.12512

Liren, D. (1996). Viewing China Road Traffic Safety and the Counter Measures in Accordance with International Comparison, Proceedings of the Second Conference in Asian Road Safety, Beijing, 28-31 October 1996, Beijing: Beijing Research in Traffic Engineering.

Lu, T. H., Chou, M. C., and Lee, M. C. (1999). Regional Mortality from Motor Vehicle Traffic Injury: Relationships Among Place-Of-Occurrence, Place-Of-Death, and Place-Of-Residence. *Accid. Anal. Prev.* 32 (2000), 65–69. doi:10.1016/s0001-4575(99)00051-2

Malhotra, N. K., Peterson, M., and Kleiser, S. B. (1999). Marketing Research: A State-Of-The-Art Review and Directions for the Twenty-First Century. *J. Acad. Marketing Sci.* 27 (2), 160–183. doi:10.1177/0092070399272004

Manner, H., and Wünsch-Ziegler, L. (2013). Analyzing the Severity of Accidents on the German Autobahn. *Accid. Anal. Prev.* 57, 40–48. doi:10.1016/j.aap.2013.03.022

Maruyama, G. M. (1998). *Basics of Structural Equation Modeling*. Thousand Oaks, CA: Sage.

McCarthy, N. (2016). The Worst Countries in the World for Drunk Driving (Infographic). Available at: https://blogs-images.forbes.com/niallmccarthy/files/2016/08/20160709_Drunk_Driving.jpg(Accessed on August 11, 2016).

Meel, B. L. (2008). Fatal Road Traffic Crashes in the Mthatha Area of South Africa, 1993 – 2004. *South Afr. Med. J.* 98, 716–719.

Mills, B. N., Andrey, J., and Hambly, D. (2011). Analysis of Precipitation-Related Motor Vehicle Collision and Injury Risk Using Insurance and Police Record Information for Winnipeg, Canada. *J. Saf. Res.* 42, 383–390. doi:10.1016/j.jsr.2011.08.004

Ministry of Transport (2001). The Road to Safety 2001-2005: Building the Foundations of a Safe and Secure Road Traffic Environment in South Africa. Available at: http://www.transport.gov.za/projects/index.html(Accessed on June 12, 2006).

Mooren, L., Grzebieta, R., and Job, S. "Safe System – Comparisons of This Approach in Australia", in Proceedings of the Australasian College of Road Safety Conference, Melbourne, VIC, Australia, September 2011.

Mphela, T. (2011). The Impact of Traffic Law Enforcement on Road Accident Fatalities in Botswana. *J. Transport Supply Chain Management* 5, 264–277. doi:10.4102/jtscm.v5i1.77

Nantulya, V. M., and Reich, M. R. (2002). The Neglected Epidemic: Road Traffic Injuries in Developing Countries. *Br. Med. J.* 324, 1139–1141. doi:10.1136/bmj.324.7346.1139

Ncube Cheteni, P. P., and Sindiyandiya, K. (2016). Road Crashes Fatalities Trends and Safety Management in South Africa. *Probl. Perspect. Management* 14, 627–633.

O'Hara, R. B., and Kotze, D. J. (2010). Do Not Log-Transform Count Data. *Methods Ecol. Evol.* 1, 118–122.

Papantoniou, P., Antoniou, C., Yannis, G., and Pavlou, D. (2018). Which Factors Affect Accident Probability at Unexpected Incidents? A Structural Equation Model Approach. *J. Transportation Saf. Security* 11, 544–561. doi:10.1080/19439962.2018.1447523

Papantoniou, P., Yannis, G., and Christofa, E. (2019). Which Factors Lead to Driving Errors? A Structural Equation Model Analysis through a Driving Simulator Experiment. *IATSS Res.* 43, 44–50. doi:10.1016/j.iatssr.2018.09.003

Peden, M., and Hyder, A. A. (2002). Road Traffic Injuries Are a Global Public Health Problem. *Br. Med. J.* 324, 1153. doi:10.1136/bmj.324.7346.1153

R Core Team (2017). *R: A Language and Environment for Computing*.

Reason, J. (2000). Human Error: Models and Management. *Br. Med. J.* 320, 768–770. doi:10.1136/bmj.320.7237.768

RTMC (Road Traffic Management Corporation) (2008). *2007 Road Traffic Report on Number of Registered, Un-roadworthy and Un-licenced Vehicles, Driving Licences and PrDPs and Fatal Crashes and Fatalities*. Pretoria East: Road Traffic Management Corporation.

RTMC (Road Traffic Management Corporation) (2019). *Parow: Violence, Injury and Peace Research Unit SAMRC Alcohol and its Implications for Road Traffic Crashes in South Africa Phase A- Review*; Pretoria East: Road Traffic Management Corporation.

RTMC (Road Traffic Management Corporation) (2007). *Interim Road Traffic and Fatal Crash Report for the Year 2006*. Pretoria East: Road Traffic Management Corporation.

RTMC (Road Traffic Management Corporation) (2016). *Road Traffic Calendar Report 1 January- 31 December 2015*. Pretoria East: Road Traffic Management Corporation.

RTMC (Road Traffic Management Corporation) (2017). *Road Traffic Calendar Report 1 January-31 December 2016*. Pretoria East: Road Traffic Management Corporation.

RTMC (Road Traffic Management Corporation) (2013). *Road Traffic Calendar Report 31 December 2012*. Pretoria East: Road Traffic Management Corporation.

RTMC (Road Traffic Management Corporation) (2014). *Road Traffic Calendar Report 31 December 2013*. Pretoria East: Road Traffic Management Corporation.

RTMC (Road Traffic Management Corporation) (2015). *Road Traffic Calendar Report 31 December 2014*. Pretoria East: Road Traffic Management Corporation.

RTMC (Road Traffic Management Corporation) (2011). *Road Traffic Report 31 December 2010*. Pretoria East: Road Traffic Management Corporation.

RTMC (Road Traffic Management Corporation) (2018). *State of Road Safety Report: January-December 2017*. Pretoria: Department of Transport.

RTMC (Road Traffic Management Corporation) (2012). *Traffic Calendar Report 31 December 2011*. Pretoria East: Road Traffic Management Corporation.

RTMC (Road Traffic Management Corporation) (2006). *Year 2005 Traffic Report*. Pretoria East: Road Traffic Management Corporation.

Sârbescu, P., and Maricuțoiu, L. (2019). Are You a "bad Driver" All the Time? Insights from a Weekly Diary Study on Personality and Dangerous Driving Behavior. *J. Res. Personal.* 80, 30–37. doi:10.1016/j.jrp.2019.04.003

Schermelleh-Engel, K., Moosbrugger, H., and Müller, H. (2003). Evaluating the Fit of Structural Equation Models: Tests of Significance and Descriptive Goodness-Of-Fit Measures. *Methods Psychol. Res.* 8, 23–74.

Shaw, J. I., and McMartin, J. A. (1977). Personal and Situational Determinants of Attribution of Responsibility for an Accident. *Hum. Relations* 30, 95–107. doi:10.1177/001872677703000106

Silcok, B. R. (2003). *Guidelines for Estimating the Costs of Road Crashes in Developing Countries*. London: U.K. Department for International Development.

Silva, F. P. d., Santos, J. A., and Meireles, A. (2014). Road Accident: Driver Behaviour, Learning and Driving Task. *Proced. - Soc. Behav. Sci.* 162, 300–309. doi:10.1016/j.sbspro.2014.12.211

Stats SA (Statistics South Africa) (2012). *Census 2011*. Pretoria: Department of Statistics South Africa.

Stats SA (Statistics South Africa) (2007). *Mid-Year Population Estimates 2007*. Pretoria: Department of Statistics South Africa.

Stats SA (Statistics South Africa) (2008). *Mid-Year Population Estimates 2008*. Pretoria: Department of Statistics South Africa.

Stats SA (Statistics South Africa) (2010). *Mid-Year Population Estimates 2010*. Pretoria: Department of Statistics South Africa.

Stats SA (Statistics South Africa) (2013). *Mid-Year Population Estimates 2013*. Pretoria: Department of Statistics South Africa.

Stats SA (Statistics South Africa) (2014). *Mid-Year Population Estimates 2014*. Pretoria: Department of Statistics South Africa.

Stats SA (Statistics South Africa) (2015). *Mid-Year Population Estimates 2015*. Pretoria: Department of Statistics South Africa.

Stats SA (Statistics South Africa) (2017). *Mid-Year Population Estimates 2017*. Pretoria: Department of Statistics South Africa.

Stats SA (Statistics South Africa) (2019). *Mid-Year Population Estimates 2019*. Pretoria: Department of Statistics South Africa.

Stats SA (Statistics South Africa) (2009). *South African Statistics, 2009*. Pretoria: Department of Statistics South Africa.

Stats SA (Statistics South Africa) (1995). *Suid-Afrikaanse Statistieke- South African Statistics*. Pretoria: Department of Statistics South Africa.

Tarka, P. (2018). An Overview of Structural Equation Modeling: its Beginnings, Historical Development, Usefulness and Controversies in the Social Sciences. *Qual. Quant* 52, 313–354. doi:10.1007/s11135-017-0469-8

Theofilatos, A. (2017). Incorporating Real-Time Traffic and Weather Data to Explore Road Accident Likelihood and Severity in Urban Arterials. *J. Saf. Res.* 61, 9–21. doi:10.1016/j.jsr.2017.02.003

Thompson, L., Bundy, C., Lowe, C., Mabin, A., Vigne, R., and Gordon, D. (2019). South Africa. Available at: https://www.britannica.com/place/South-Africa(Accessed on September 15, 2019).

Tibane, E., Lentsoane, N., Honwane, M., and Kraamwinkel, J. (2016). *South Africa Yearbook 2015/2016*. Pretoria: Government Communications (GCIS).

Vanderschuren, M., Arendse, M., Lane-Visser, T., and Janmohammed, A. (2020). Combatting the Road Safety Burden in the Developing World: The Case of South Africa. *Transportation Res. Proced.* 48, 1174–1184. doi:10.1016/j.trpro.2020.08.141

Verbeke, W., and Bagozzi, R. P. (2000). Sales Call Anxiety: Exploring what it Means when Fear Rules a Sales Encounter. *J. Marketing* 64, 88–101. doi:10.1509/jmkg.64.3.88.18032

Verster, T., and Fourie, E. (2018). The Good, the Bad and the Ugly of South African Fatal Road Crashes. *South Afr. J. Sci.* 114, 63–69. doi:10.17159/sajs.2018/20170427

Wegman, F., Schermers, G., and van Schagen, I. (2013). *Towards a National Road Safety Strategy for South Africa*. The Netherlands: SWOV Institute for Road Safety Research, 65.

WHO (World Health Organisation) (2013). *Global Status Report on Road Safety 2013: Supporting a Decade of Action*. Geneva: The World Health Organization.

WHO (World Health Organisation) (2015). *Global Status Report on Road Safety 2015*. Geneva: The World Health Organisation.

WHO (World Health Organisation) (2018). *Global Status Report on Road Safety 2018*. Geneva: The World Health Organisation.

WHO (World Health Organisation) (2009). *Global Status Report on Road Safety: Time for Action*. Geneva: World Health Organisation.

WHO (World Health Organisation) (2019). Road Traffic Injuries. Available at: https://www.who.int/newsroom/fact-sheets/detail/road-traffic-injuries(Accessed on September 21, 2019).

Wilde, G. J. S. (1988). Risk Homeostasis Theory and Traffic Accidents: Propositions, Deductions and Discussion of Dissension in Recent Reactions. *Ergonomics* 31, 441–468. doi:10.1080/00140138808966691

World Health Organisation (WHO) (2011). Global Plan for the Decade of Action for Road Safety 2011-2020. Available at: https://www.who.int/roadsafety/decade_of_action/plan/plan_english.pdf?ua=1.

Conflict of Interest: The authors declare that the research was conducted in the absence of any commercial or financial relationships that could be construed as a potential conflict of interest.

frontiers | Frontiers in Future Transportation

ORIGINAL RESEARCH
published: 08 June 2022
doi: 10.3389/ffutr.2022.890117

Reducing Lumbar Spine Vertebra Fracture Risk With an Adaptive Seat Track Load Limiter

Martin Östling[1]*, *Christer Lundgren*[2], *Nils Lubbe*[1] and *Bengt Pipkorn*[1]

[1]Autoliv Research, Vårgårda, Sweden, [2]System and CAE Department, Autoliv Sweden, Vårgårda, Sweden

In future fully automated vehicles, sleeping or resting will be desirable during a drive. While a horizontal position currently appears infeasible, a relaxed seating position with a reclined seatback and an inclined seat pan which enables a safe, comfortable position for sleeping or resting is possible. However, the inclined seat pan increases the forces and moments acting on the lumbar spine of the occupant and thereby the risk of lumbar vertebra fractures in a frontal crash. An energy management system integrated into the longitudinal seat adjustment (a seat track load limiter: STLL) that can reduce this risk should be investigated. When evaluating the injury reduction potential of a new restraint system such as a STLL it is important to include variations in both occupant size and crash severity. Otherwise, there is a risk of sub-optimizing, that is, the restraint system is only working for a limited number of situations. The restraint systems addressing these variations are normally referred to as adaptive restraint systems. The first objective of the study is to develop an activation strategy (adaptive release time of the STLL) for different crash severities and occupant sizes, making full use of the available stroke distance without bottoming out the STLL. The second objective is to evaluate the potential of the adaptive STLL to reduce the risk of lumbar vertebra fractures by comparing it to 1) a fixed seat and 2) a passive version of the STLL. Simulated frontal impacts were performed with two male SAFER human body models (HBMs) as occupant surrogates: mid-sized (80 kg and 1.8 m) and large (130 kg and 1.9 m). Three crash pulse severity levels were evaluated: low (40 km/h), medium (50 km/h), and high (56 km/h) impact speeds. The fracture risk was evaluated for the five lumbar vertebrae (L1–L5) in three different seat conditions: 1) a seat fixed to the sled, 2) a passive STLL that moves when a given force is exceeded, and 3) an adaptive STLL which moves at a time that depends on the occupant mass and crash pulse severity. The risk for lumbar vertebra fracture increased with crash pulse severity, while HBM size had no effect on risk. For all conditions, the passive STLL reduced injury risks compared to the fixed seat, and the adaptive STLL reduced risk even further.

Keywords: adaptive restraint, automated vehicles, human body model, lumbar vertebra fracture, occupant restraint system, relaxed seating position, seat track load limiter

OPEN ACCESS

Edited by:
Yong Han,
Xiamen University of Technology, China

Reviewed by:
Qing Zhou,
Tsinghua University, China
Fang Wang,
Changsha University of Science and Technology, China

***Correspondence:**
Martin Östling
martin.ostling@autoliv.com

Specialty section:
This article was submitted to Transport Safety, a section of the journal Frontiers in Future Transportation

Received: *05 March 2022*
Accepted: *22 April 2022*
Published: *08 June 2022*

Citation:
Östling M, Lundgren C, Lubbe N and Pipkorn B (2022) Reducing Lumbar Spine Vertebra Fracture Risk With an Adaptive Seat Track Load Limiter. Front. Future Transp. 3:890117. doi: 10.3389/ffutr.2022.890117

1 INTRODUCTION

With the introduction of automated vehicles, the driver task will no longer be required, making it possible for the driver to engage in other tasks. Resting and sleeping are highly rated in surveys as desirable activities during a car ride (Koppel et al., 2019), particularly for longer trips (Östling and Larsson, 2019). When sleeping, a supine (horizontal, seatback fully reclined) position is preferred (Stanglmeier et al., 2020; Caballero-Bruno et al., 2021). However, the limited cabin space in most passenger cars prevents fully supine positions. Furthermore, current seatbelts are designed to load the strong parts of the occupant's body, traveling across the pelvis, over the shoulder, and across the chest, allowing a controlled forward motion during the crash (Adomeit and Heger, 1975; Adomeit, 1977). Any occupant position that is not upright, e.g., reclined or supine, compromises loading and control of the pelvis and chest, with submarining (the pelvis sliding under the lap belt, causing the lap belt to intrude into the soft abdomen) as a likely consequence (Dissanaike et al., 2008; McMurry et al., 2018; Boyle et al., 2019).

A relaxed position, with a reclined seatback and an inclined seat pan, is comfortable for sleeping (Stanglmeier et al., 2020). A relaxed position increases seatback inclination compared to what is commonly referred to as reclined position and is more challenging for occupant protection (Östling et al., 2021). However, during a frontal crash, the inclined seat pan provides most of the restraining force and control of the forward movement of the lower body, thereby reducing the risk of submarining and the dependence on the lap and shoulder seatbelt (Wiechel and Bolte 2006). This added restraining force is especially important, as the relaxed position requires a seat away from the instrument panel and thereby makes it infeasible to restrain the lower body in the traditional way with a knee bolster or knee airbag as proposed in earlier studies (Ji et al., 2017; Rawska et al., 2019; Tang et al., 2020; Rawska et al., 2021). However, a reclined position induces compression forces to the lumbar vertebrae because they are in line with the impact direction (Boyle et al., 2019). This increases the fracture risk, particularly for the first lumbar vertebra, L1 (Richardson et al., 2020). In addition to the L1 fractures, Richardson et al. (2020) also reported rib, sternum, and pelvis wing fractures from 50 km/h frontal sled tests with post mortem human subjects (PMHS) in reclined seating position.

To address the increased forces and moments acting on the lumbar vertebrae in the relaxed position (reclined seatback and inclined seat pan), Sengottu-Velavan and Huf (2018) incorporated an energy management system in the longitudinal seat adjustment in a concept seat (the system, a seat track load limiter, is hereafter referred to as a passive "STLL"). That passive STLL (the seat moves when a given force is exceeded) substantially reduced the lumbar spine compression force and flexion moment for different anthropomorphic test devices (ATDs). Östling et al. (2021) further improved the concept by making the STLL actively controlled (the seat was initially fixed to the vehicle and then released by activation of a pyrotechnical unit at a fixed pre-defined time). The active STLL further reduced the lumbar spine force in tests with a Test Device for Human Occupant Restraint 50th percentile male (THOR-50M). However, Östling et al. (2021) highlighted the need for an activation strategy that considers occupant's mass and crash severity, to avoid reaching the limit of the forward displacement of the seat track ("bottoming out"). The energy absorbing elements in the seat have also been shown to reduce the risk for whiplash injury in rear impacts (Luo and Zhou, 2010; Zhang and Zhou, 2016).

The effect of variation in the occupant's mass can be investigated with ATDs to some extent. They are available in three adult sizes, representing the heights and masses of a 5th percentile female, a 50th percentile male, and a 95th percentile male (Mertz et al., 1989). However, the sizes are based on US population measurements of height and mass from the 1970s (Schneider et al., 1983). More recent data have shown that the 50th and 95th male ATDs' masses corresponded to the 33rd and 81st percentiles, respectively, of the current US population (Reed and Rupp, 2013).

The intention of this investigation is to design robust restraint systems for a diverse population by covering 95% of the population in terms of occupant mass. Morphable FE HBMs can be designed to simulate the whole range of occupant anthropometry by parametric morphing (Hwang et al., 2016). The first objective of the study is to develop an activation strategy (adaptive release time of the STLL) for different crash severities and occupant sizes (enabled by parametric morphed HBMs), making full use of the available seat stroke distance without bottoming out the STLL. The second objective is to evaluate the potential of the adaptive STLL to reduce the risk of lumbar vertebra fractures by comparing it to 1) a fixed seat and 2) a passive version of the STLL.

2 MATERIALS AND METHODS

Finite element (LS-Dyna, R9.3.1 R140922, LSTC) frontal sled simulations were executed using three different crash pulse severities and two different anthropometries of the SAFER HBM v9 with a reclined seatback and inclined seat pan. The influence on lumbar vertebrae fracture risk was investigated for three seat track configurations: the seat fixed to the sled, a passive STLL, and an adaptive STLL. Unlike the passive STLL, which moves when a given force is exceeded, the adaptive STLL's release mechanism timing is dependent on an activation strategy that adapts to the occupant mass and the predicted crash severity.

2.1 Occupant Surrogates

The US National Health and Nutrition Examination Survey (NHANES) data from 2011–2014 (Fryar et al., 2016) was used to define a large 65-year-old occupant (95th percentile) who would challenge the STLL by reaching the limit of the forward displacement (bottoming out). Starting with the validated SAFER HBM v9 mid-sized male (80 kg and 1.8 m), parametric HBM morphing with statistical human shape target geometries from Hwang et al. (2016) generated an HBM matching the sex, age, stature, and mass of the large male anthropometry (130 kg and 1.9 m); see **Figure 1**.

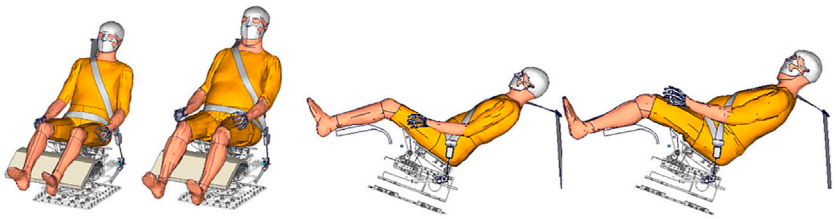

FIGURE 1 | SAFER HBM v9 positioned on the generic seat with seatbelt routed. Left: front views of a mid-sized male and a large male. Right: side views of a mid-sized male and a large male.

TABLE 1 | Cross-section area in mm^2 for L1–L5 for the two HBMs.

HBM	L1	L2	L3	L4	L5
Mid-sized male	1049	1142	1137	1140	1323
Large male	1366	1585	1558	1433	1450

The SAFER HBM v9 was originally developed from the Total Human Model for Safety (THUMS) v3 (Iwamoto et al., 2002), for the purpose of improving the understanding of impact response and injury mechanisms for car occupants. The SAFER HBM v9 has an updated rib cage (Iraeus and Pipkorn, 2019) and lumbar spine (Östh et al., 2020). Moreover, the SAFER HBM v9 has been validated to predict the kinematics and rib fracture risk of an upright seated occupant (Pipkorn et al., 2019) and the kinematics of a reclined seated occupant (Mroz et al., 2020). The parametric morphed versions of the SAFER HBM v9 include females and males of various anthropometries (including a large male), which were validated by means of PMHS tests in both frontal and lateral impact conditions (Larsson et al., 2021).

2.2 Risk of Lumbar Vertebrae Fracture

The risk of lumbar vertebra fractures was evaluated with the recently proposed injury risk function for combined compression flexion loading of the lumbar vertebra (Tushak et al., 2022) in the SAFER HBM v9. The injury risk function is based on censored force and moment failure data from three-vertebrae lumbar segments tested in combined compression flexion. 40 spine segments were tested. The injury risk function is based on a linear combination of stresses from the axial compression (force divided by cross-section area: CSA) and flexion moment (moment divided by $CSA^{3/2}$) expressed as the predictor variable, L (**Eq. 1**). The function also includes a weighting factor to account for the relative contributions of force and moment to failure (**Eq. 1**). The age (in years) is included as a covariate (**Eq. 2**).

$$L(t) = (1 - 0.11)\frac{F(t)}{CSA} + 0.11\frac{M(t)}{CSA^{3/2}}, \quad (1)$$

$$P(fracture|L, Age) = 1 - e^{-\left[\frac{L(t)}{e^{1.896-0.00874*Age}}\right]^{\frac{1}{0.201}}}. \quad (2)$$

In the HBM simulations, lumbar vertebra forces and moments were extracted in the L1–L5 vertebrae using cross-section force-moment measurements. The cross-sections were defined for each vertebra, including the cortical and trabecular bones of the vertebral body as well as the transverse and spinous processes (Mroz et al., 2020; Mroz et al., 2022). The cross-section areas were calculated for L1–L5 for both the mid-sized male and the large male; **Table 1**. The forces and moments from all five vertebrae as well as each vertebra cross-section area are used in **Eqs 1**, **2** to assess the risk of injury for each vertebra for 45- and 65-year-old occupants as it has been reported that the risk of lumbar vertebra fracture is age-dependent (Jakobsson et al., 2006; Bilston et al., 2011; Rao et al., 2014).

The risk of two or more fractured ribs (AIS2+) was calculated and evaluated, in order to ascertain whether there were any negative effects from the STLL on other body areas. The rib fracture risk was calculated using a strain-based probabilistic method based on peak strains in the cortical bone of each rib (Forman et al., 2012) and the Weibull smoothed injury risk function for 45- and 65-year-old occupants (Iraeus, 2015).

2.3 Restraint System and STLL

The investigation was carried out for belted HBMs seated in a relaxed position (seatback reclined to 60° and seat pan inclined to 35°) in a generic semi-rigid seat with a rigid seatback, and lower leg support, as described by Östling et al. (2021). The HBMs were restrained by a seat-integrated three-point seatbelt system comprising two 2 kN lap belt pretensioners (buckle and end-bracket) to avoid submarining (Östling et al., 2017; Richardson et al., 2020). In addition, the seatbelt system included a shoulder belt retractor with a 2 kN pretensioner and 4 kN load limiter and a crash locking tongue, preventing webbing slippage from the shoulder belt to the lap belt (or vice versa). The activation times of the pretensioners were as in the work by Östling et al. (2021), with the buckle pretensioner activated at 2 ms and the shoulder belt and end bracket pretensioners activated at 9 ms. The STLL force levels were also provided by Östling et al. (2021), who tuned the force levels of the active (30 ms release time) and passive STLLs in order to achieve 0.2–0.25 m seat stroke distance in a 50 km/h crash pulse, using the THOR-50M in a generic seat weighing 130 kg. 0.25 m was chosen as the maximum stroke distance as this is approximately the adjustment range of drivers' seats in passenger cars (Bohlin et al., 1978).

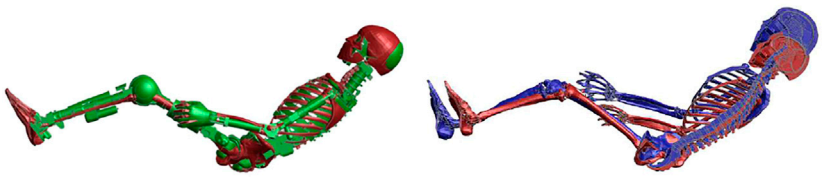

FIGURE 2 | Left: overlay of SAFER HBM v9 mid-sized male (red) and THOR-50M (green). Right: overlay of SAFER HBM v9 mid-sized male (red) and morphed large male (blue).

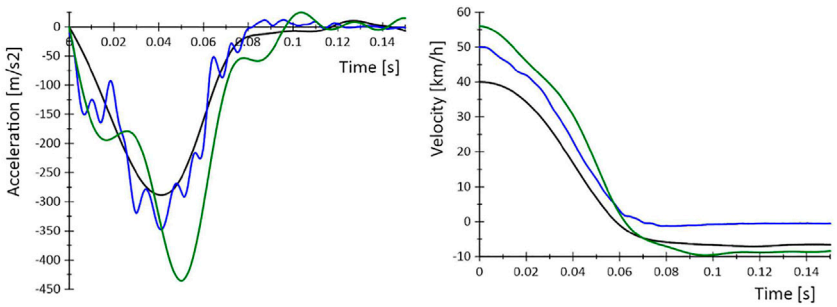

FIGURE 3 | Left: acceleration vs. time. Right: velocity vs. time. For both figures, the black curves represent the low-severity crash pulse (40 km/h), the blue curves represent the mid-severity crash pulse (50 km/h), and the green curves represent the high-severity crash pulse (56 km/h).

2.4 HBM Positioning

Using an in-house positioning tool, the SAFER HBM v9 was positioned to match the test position of the THOR-50M described by Östling et al. (2021). First, the SAFER HBM's H-point was positioned at the corresponding H-point of the THOR-50M (20 mm rearward and 20 mm downward compared to the THOR H-point). Second, the SAFER HBM v9 pelvis was rotated around the H-point to match the angle of the THOR-50M. Finally, the thorax, neck, head, arms, and legs were rotated to match the position of the THOR-50M; see **Figure 2**. The large male HBM's H-point was positioned according to the H-point of the mid-sized male HBM. Then the pelvis was rotated around the H-point to match the pelvis shape, with a focus on the notch angle, the angle created by a line that connects the anterior superior iliac spine (ASIS) and the anterior inferior iliac spine (AIIS) measured to the horizontal axis (Moreau et al., 2021). Care was taken with the ASIS and AIIS area because it is an important support area for the lap belt and provides a good overall overlay of the pelvis. The thorax, neck, head, arms, and legs were adjusted to line up with the mid-size male; see **Figure 2**. The final positions of the HBMs, seated in the relaxed position on a generic seat with the belts routed, are shown in **Figure 1**.

2.5 Crash Pulses

Three full frontal crash pulses, varying in severity, were used in the analysis, see **Figure 3**. An HBM simulation of a 50 km/h crash pulse (mid-severity), also used by Östling et al. (2021), was compared to the results from the sled test result with THOR-50M. The high-severity crash pulse at 56 km/h (Dobberstein et al., 2021; Höschele et al., 2021) challenged the seat track load limiter, potentially provoking bottoming out in combination with the HBM of a large male. A low-severity crash pulse at 40 km/h (Dobberstein et al., 2021; Höschele et al., 2021) represented a crash velocity at which the majority of occupants get injured (Forman and McMurry, 2018). Injury risk reduction at the low-severity crash pulse has a large effect on the overall number of injuries.

2.6 Simulations

In the first stage, the simulation model was validated by means of mechanical sled tests performed in the set-up used by Östling et al. (2021); see **Supplementary Appendix SA**. The mass of the generic seat used in the tests was 130 kg. The mass of a production seat with a seat-integrated seatbelt was replicated by reducing the seated mass to 70 kg (Östling et al., 2021). The force-displacement characterization used by Östling et al. (2021) (both the passive and the adaptive STLL force levels) was adjusted to reach the same stroke distance for the new seat mass. The adaptive STLL force-displacement characteristics started at 19.6 kN at 0.012 m and increased progressively to 31.6 kN at a forward displacement of 0.25 m, while the passive STLL started at 20.6 kN at 0.012 m and reached 35.1 kN at 0.25 m; see **Figure 4**.

In a second stage, the simulations of the adaptive STLL were performed starting with a 30 ms release time (used by Östling et al., 2021), for all HBM and crash pulse severity combinations. Depending on how the resulting seat stroke distance related to the maximum allowed distance (0.25 m), the release time was either decreased (as for the mid-sized male in the low-severity crash pulse), kept constant (for the mid-sized male in the mid-severity crash pulse), or increased (all other combinations). The decrease

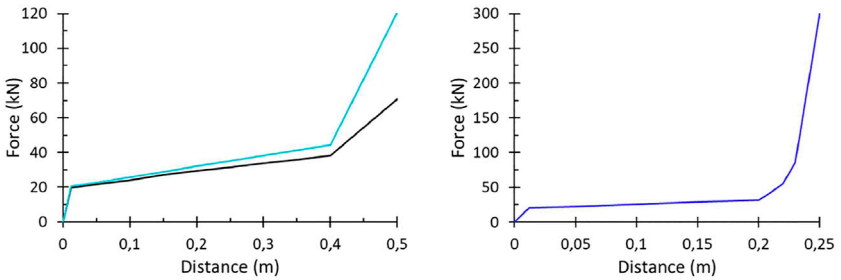

FIGURE 4 | Left: STLL force characteristics vs. displacement for adaptive (black) and passive without soft stop (light blue). Right: STLL force characteristics vs. displacement for passive with a soft stop limit the seat stroke to 0.25 m (dark blue).

and increase in release time were performed in 10 ms steps until the maximum seat stroke distance was reached. However, as crash severity estimation, needed in order to calculate the adaptive release time, assumed to be done in-crash, similar to current crash severity estimation used to activate dual-stage airbags (Takata Corporation, 2017), release time less than 20 ms was not allowed. If the resulting seat stroke distance was less than 0.22 m, a 5 ms increase in release time was simulated to complement the final 10 ms step. These simulations were performed to demonstrate the need for an adaptive release and to provide suitable release times to be used for risk calculations. The results are presented in **Section 3.2**. The risks for lumbar vertebra fracture and rib fracture were only calculated for the seat track distances that best met the 0.25 m seat stroke requirement.

In a third stage, the simulations of the passive STLL were performed for all HBMs and crash pulse severity combinations using the force defined by Östling et al. (2021). As with the simulations with a 30 ms release time for the adaptive STLL, many of the simulations exceeded the 0.25 m seat stroke distance. A "soft stop" was therefore implemented at the passive STLL to limit the seat stroke to 0.25 m: starting at 0.2 m, the STLL force ramps up to 55 kN at 0.22 m, 86 kN at 0.23 m, and 300 kN at 0.25 m; see **Figure 4**. Additional simulations were then performed with the soft stop. These simulations were performed to demonstrate the need for a soft stop in addition to the force-displacement characteristics proposed by Östling et al., 2021. The results are presented in **Section 3.3**. Similar to the adaptive STLL, the risks for lumbar vertebra fracture and rib fracture were only calculated for seat track distances less than 0.25 m.

The three simulation steps: validation, adaptive STLL, and passive STLL are visualized in a flow chart in **Supplementary Appendix SB**.

3 RESULTS

3.1 HBM Kinematic Response

The crash kinematics followed the same overall pattern at the three crash severities for both HBMs. The seatbelt pretensioners held the HBM against the seat pan and seatback. The pelvis started to translate forward where it compressed the seat pan springs and started to load the lap belt but the angled seat pan prevented the pelvis from translating forward notably. Submarining did not occur in any of the simulations. The longest pelvis displacement occurred for the high-severity crash pulse with the fixed seat: 163 and 234 mm in the *x*-direction for the mid-size male and large male, respectively. The torso was effectively restrained by the shoulder belt which prevented any larger forward displacement. The longest torso displacements, measured at the first thoracic vertebra (T1), were observed with the fixed seat and the high-severity crash pulse: 331 mm and 325 in the *x*-direction for the mid-size male and large male, respectively. The initial relaxed position of the upper body prevented upward forward rotation of the torso; however, the head rotated forward (under flexion moment) until it touched the chest. The legs and feet moved forward more than the pelvis when the knee joints straightened. The crash kinematics are exemplified in **Figure 5**, showing the mid-sized male in the fixed seat in 20 m increments after the high-severity crash pulse (at 0 m).

3.2 Release Times of the Adaptive STLL

Seat stroke distance and peak force in the adaptive STLL for all simulations are presented in **Table 2**. The simulations with 30 m release times resulted in excessive seat stroke distances: 0.37, 0.30, 0.35, and 0.48 m (for the mid-sized male with the high-severity crash pulse and the large male with the low-, mid-, and high-severity crash pulses, respectively). On the other hand, the seat stroke distance was too short for the mid-sized male in the low-severity crash pulse (0.2 m). After adjusting the release times to fulfill the 0.25 m requirement, they were all in the interval of 20–60 m. As the crash severity increased, the release times for both HBMs increased. The release times that best met the 0.25 m seat stroke requirement are highlighted by an underlined release time value in **Table 2**. The injury risk was calculated for these underlined cases only.

3.3 Passive STLL With and Without Soft Stop

For all simulations with the passive STLL, the seat strokes and peak forces (with and without the soft stop) are presented in **Table 3**. The simulations without the soft stop resulted in too

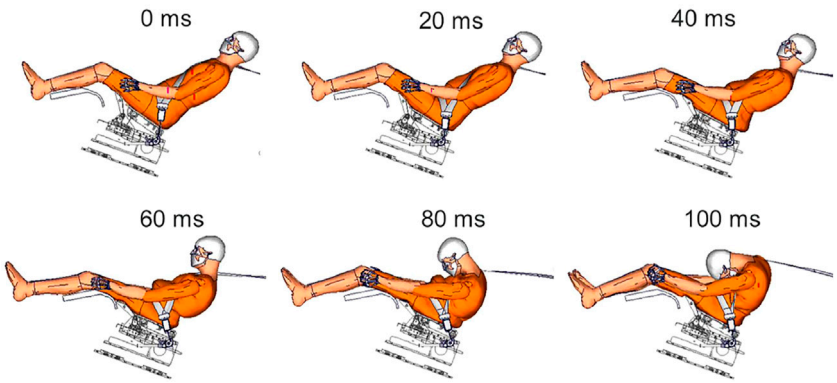

FIGURE 5 | Kinematic responses for mid-sized males in high-severity crash pulse in 20 ms increments, starting at 0 ms and ending at 100 ms.

TABLE 2 | Release time and corresponding seat stroke distance and peak force in the STLL for the adaptive STLL simulations.

Case	Crash pulse severity	HBM size	Release time (ms)	Seat stroke distance (m)	Peak force STLL (kN)
1	Low	Mid-sized male	30	0.20	29.4
2	Low	Mid-sized male	20	0.21	30.0
3	Low	Large male	30	0.30	33.7
4	Low	Large male	40	0.27	32.3
5	Low	Large male	45	0.24	31.1
6	Low	Large male	50	0.21	29.7
7	Mid	Mid-sized male	30	0.24	31.3
8	Mid	Large male	30	0.35	36.1
9	Mid	Large male	40	0.30	33.7
10	Mid	Large male	45	0.26	32.0
11	Mid	Large male	50	0.21	30.2
12	High	Mid-sized male	30	0.37	36.9
13	High	Mid-sized male	40	0.33	35.1
14	High	Mid-sized male	50	0.24	31.2
15	High	Large male	30	0.48	63.6
16	High	Large male	50	0.38	37.1
17	High	Large male	60	0.25	31.5

TABLE 3 | Seat stroke distance and peak force in the STLL for in the passive STLL simulations with and without soft stop.

Case	Crash pulse severity	HBM size	Soft stop	Seat stroke distance (mm)	Peak force STLL (kN)
1	Low	Mid-sized male	No	0.19	31.2
2	Low	Mid-sized male	Yes	0.19	31.1
3	Low	Large male	No	0.27	36.6
4	Low	Large male	Yes	0.23	84.5
5	Mid	Mid-sized male	No	0.23	34.1
6	Mid	Mid-sized male	Yes	0.22	56.1
7	Mid	Large male	No	0.33	40.0
8	Mid	Large male	Yes	0.24	169.7
9	High	Mid-sized male	No	0.34	40.8
10	High	Mid-sized male	Yes	0.24	196
11	High	Large male	No	0.44	76.7
12	High	Large male	Yes	0.25	275.6

long seat stroke distances: 0.34 m for the mid-sized male in the high-severity crash pulse, and 0.33 m, and 0.44 m for the large male in mid and high-severity crash pulse, respectively. After implementing the soft stop starting at 0.22 m, all seat stroke distances met the 0.25 m requirement. The injury risk was only calculated for simulation with the soft stop.

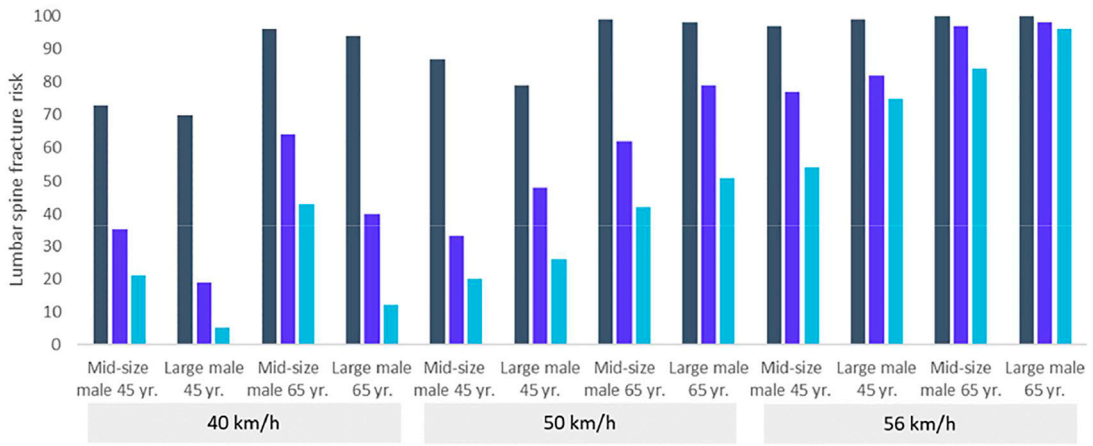

FIGURE 6 | Lumbar vertebra fracture risk calculated according to **Eqs 1**, **2** for the three crash pulse severity levels, the two HBM sizes, and the two ages. The black columns represent the fixed seat, the dark blue the passive STLL with a soft stop, and the light blue the adaptive STLL.

3.4 Lumbar Vertebra Fracture Risk

The maximum lumbar vertebra fracture risks for the two HBMs in the three crash pulse severity levels (calculated according to **Eqs 1**, **2**) are presented in **Figure 6**. For all the scenarios, the highest risk was seen for L1. The corresponding L1 compression forces and flexion moment are in **Supplementary Appendix Figures SD1, SD2**. The fracture risk was similar for the two HBMs and increased with age and crash pulse severity. While the passive STLL with a soft stop and the adaptive STLL both reduced the fracture risk for all scenarios, the adaptive STLL had the lowest risk. However, for the high-severity crash pulse, the risk of lumbar fractures is never below 50%.

The risk of two or more fractured ribs (AIS2+) was calculated using the injury risk curves for 45- and 65-year-old occupants (Iraeus, 2015) for both the mid-sized male and the large male in the three crash pulse severities; results are in **Supplementary Appendix Tables SC1–SC3**. The rib fracture risk increased with age and crash pulse severity; while risk was substantially reduced in simulations with both versions of the STLL, the adaptive STLL produced the lowest risk.

4 DISCUSSION

Each combination of HBM size and crash severity level required an individual release time to avoid bottoming out the STLL, while using the available stroke distance. Moreover, it was shown that the STLL with an adaptive release time achieved lower lumbar vertebra fracture and rib fracture risks than the passive STLL—for every combination.

The simulations with the SAFER HBM v9 of a mid-sized male in the relaxed position supported the test results with THOR-50M (Östling et al., 2021), both indicating a reduced risk of lumbar spine vertebra fracture using the STLL. A more severe crash pulse and/or the heavier HBM demonstrated the need for an adaptive release time to guarantee a seat stroke distance of less than 0.25 m. However, the SAFER HBM showed a substantial reduction in risk for thorax injury (risk of rib fractures) with the mid-severity crash pulse (50 km/h) using the STLL. In contrast, the tests with THOR-50M indicated an increased risk of thorax injury, when measured as the maximum of the resultant value from the four infra-red telescoping rods for the assessment of chest compression (IR-TRACCs): Rmax or a slight decrease when measured as the maximum longitudinal value from the four IR-TRACS: Xmax for the STLL (Östling et al., 2021). This difference supported the statement of Östling et al. (2021): "We believed HBMs with human-like design and use of rib strain as an indicator of risk of rib fracture, are likely to be more biofidelic than chest deflection to evaluate a potential increase or decrease in risk of rib fractures in reclined and relaxed positions".

With the HBM in the relaxed position in the fixed seat, the lumbar vertebra fracture risk is already high with the low-severity crash pulse (73% and 96% for the 45-year and 65-year-old mid-sized males, respectively). Although the adaptive STLL reduces the risk substantially, by reducing both the components of the injury risk predictor, compression force, and flexion moment (see **Supplementary Appendix Figures SD1, SD2**), it fails to reduce the injury risk below 25% for the 65-year-old mid-sized male at any crash severity level. Furthermore, with the high-severity crash pulse, the risk is above 50% for all HBMs. To put this percentage in perspective, a 25% risk of sustaining an AIS3+ injury is often used as a threshold value for assessing acceptable crashworthiness using ATDs (Craig et al., 2020), and a major compression burst fracture of the lumbar vertebra is defined as an AIS3 injury (AAAM, 2015). The reason for the adaptive STLL's inability to reduce the risk of injury in the high-severity crash pulse is the relatively late release time required to keep the seat stroke distance below 0.25 m (the release times were 50 ms for the large male with the 50 km/h crash pulse and the mid-sized male with the 56 km/h crash pulse, and 60 ms for the large male with the 56 km/h crash

pulse). At these times, the maximum forces in the lumbar vertebrae have just about been reached; see **Supplementary Appendix Figure SD1**. The STLL force levels were initially designed for the THOR-50M with a 50 km/h crash pulse (Östling et al., 2021). Designing the STLL force level for the large male with the high-severity crash pulse instead would enable an earlier release time and a concomitant lower risk of lumbar vertebra fracture. However, the consequence of a higher STLL force level is higher injury risks in the low- and mid-severity crash pulses. Clearly, any optimization targeting equal risks, i.e., the same probability of injury in various conditions, has its downsides. While most car crashes occur at a relatively low speed (20 km/h) with low injury risk, the majority of injuries occur at approximately 40 km/h (Forman and McMurry, 2018). As a result, risk reductions at 40 km/h are estimated to result in the largest absolute number of injuries prevented. With this statistic in mind, the force level used in this study is recommended. Another way to reduce the risk of sustaining injury in high-severity crash pulses without increasing it in low- and mid-severity crash pulses is to implement either longer seat stroke distances or dual force levels for the STLL. Both these ideas enable earlier release times for the high-severity crash pulse.

To enable individual release times (calculated with an activation strategy), classifications of the crash severity and occupant's mass are needed. To predict and classify crash severity, an in-crash algorithm similar to the one used to select single- or dual-stage activation of the driver airbag might be feasible, as the earliest time for activation is similar—around 20 m after first contact (Takata Corporation, 2017). To detect and classify the occupant mass, an onboarding occupant monitoring system is needed. This investigation included two different HBM sizes; however, a future monitoring system might have the capacity to detect finer mass differences between occupants with a concomitant ability to calculate new release times.

To improve the activation strategy further, information about the seat position (i.e., available stroke distance given any initial seat position) and potential activation of frontal airbags could be included. In addition, the crash pulses with a lateral component, like a frontal oblique crash, should also be analyzed to evaluate whether the STLL is negatively affected: the lateral force might prevent the seat from moving along the track. More research and development are needed to explore the full potential of the system.

The equations to calculate lumbar vertebrae fracture risk are based on the linear combination of stresses from the axial compression (force/cross-section area) and flexion moment (moment/cross-section area$^{3/2}$) with a weighting factor of 0.11. This means that the calculated risk comes mainly from the compression force, which increases with body mass and crash pulse severity. However, because the force is divided by the vertebrae cross-section area, which is larger for the large male, the risk is actually higher for the mid-size male. (This difference is not seen in the high-severity crash pulse results, due to the late release time required to avoid bottoming out the STLL for the large male). An obese mid-size male or female appears to be the most challenging anthropometry (e.g., relatively heavy body mass and relatively small vertebral cross-section).

Alternative risk functions addressing lumbar vertebra fractures have been proposed by Stemper et al. (2018) and Ortiz-Paparoni et al. (2021). The former's was based on compression forces at the lumbar spine measured in drop tower tests, from 23 PMHS lumbar specimens. The flexion moment was found to have some (albeit small) influence on the fracture risk, so it was included in the risk function proposed by Tushak et al. (2021). Ortiz-Paparoni et al. (2021) carried out a combined analysis from tests with 75 PMHS lumbar spines. Based on the test results, they developed an injury risk function using a combined metric. The intercept value for the flexion moment was higher than the moment at fracture that Tushak et al. (2021) obtained in lumbar spine testing and therefore the risk function proposed by Tushak et al. (2021) was considered more appropriate for the study.

Parameterized morphing of HBMs enabled us to use statistical data to generate HBM versions of different anthropometries. However, the individual variation of humans is large, and we have only evaluated one (average) version each of the mid-sized and the large males. Furthermore, as noted, the vertebral cross-section area has a large effect on the risk of lumbar vertebra fracture. A 10% increase or decrease for a 1000 mm^2 cross-section area with 4500 N lumbar vertebrae compression force and 100 Nm flexion moment changes the risk by approximately 30%. Moreover, parametric morphing is based on the geometrical data and does not include any variation in the material properties. SAFER HBM v9 is currently not validated for predicting lumbar vertebra fractures, although a future version validated for predicting lumbar forces, moments, and vertebra fracture risk is under development.

The adaptive STLL effectively reduces the risk of lumbar vertebra fracture but it should be considered alongside alternative solutions. One other solution is to actively re-position the occupant in an upright position before the impact by means of electric drives in the seat. Such a solution, which would require accurate pre-crash sensing and relatively fast movement of the occupant, might be feasible in the future. However, before this solution is implemented, it must be determined that the fast movements themselves do not cause any harm to the occupant—and, further, that all possible crash scenarios are within the pre-crash sensors' operational design domain, so they can be detected and classified correctly.

In conclusion, an adaptive STLL, accommodating variations in HBM mass and frontal crash pulse severity, was shown to be beneficial, efficiently reducing the risk of lumbar and chest injuries for occupants seated in a relaxed position. However, more research is needed to reduce the injury risk in the high-severity crash pulse, enabled the activation strategy by developing an occupant monitoring system, and evaluated the strategy's robustness in other types of crashes (e.g., oblique frontal crashes).

DATA AVAILABILITY STATEMENT

The datasets presented in this article are not readily available because the dataset belongs to Autoliv Development AB. The requests to access the datasets should be directed to martin.ostling@autoliv.com.

AUTHOR CONTRIBUTIONS

MÖ and CL conceptualized the study and undertook the analysis. CL built and validated the simulation model, executed all simulations, and extracted all the results. MÖ planned and led the drafting of the manuscript in conjunction with NL and BP. All the authors were involved in interpreting the findings and drafting the manuscript.

FUNDING

The work has received fundings from two sources: The work was partly carried out as part of the EU project SAFE-UP which has received funding from the European Union's Horizon 2020 research and innovation programme under Grant Agreement 861570. The work was partly carried out in the project 2020-02943 Car Passenger Safety–To the Next Level, which has received funding from FFI (Strategic Vehicle Research and Innovation), Vinnova (Sweden's Innovation Agency), the Swedish Transport Administration, the Swedish Energy Agency, and the Swedish vehicle industry.

ACKNOWLEDGMENTS

The authors would like to thank Karl-Johan Larsson at Autoliv Research for executing the parametrized morphing of the SAFER HBM v9 to the anthropometry of a large 65-year-old male and for providing fundamentally important feedback and discussions on how to use and extract results from the SAFER HBM. Furthermore, the authors would like to thank Kristina Mayberry for language revisions.

SUPPLEMENTARY MATERIAL

The Supplementary Material for this article can be found online at: https://www.frontiersin.org/articles/10.3389/ffutr.2022.890117/full#supplementary-material

REFERENCES

Adomeit, D. (1977). Evaluation Methods for the Biomechanical Quality of Restraint Systems during Frontal Impact. *SAE Technical Paper 770936*. doi:10.4271/770936

Adomeit, D., and Heger, A. (1975). Motion Sequence Criteria and Design Proposals for Restraint Devices in Order to Avoid Unfavourable Biomechanics Conditions and Submarining. *SAE Technical Paper 751146*. doi:10.4271/751146

Association for the Advancement of Automotive Medicine (AAAM) (2015). *The Abbreviated Injury Scale*. Chicago, IL: Association for the Advancement of Automotive Medicine 35 E Wacker Drive Ste

Bilston, L. E., Clarke, E. C., and Brown, J. (2011). Spinal Injury in Car Crashes: Crash Factors and the Effects of Occupant Age. *Inj. Prev.* 17 (4), 228–232. doi:10.1136/ip.2010.028324

Bohlin, N., Hallen, A., Runberger, S., and AAsberg, A. (1978). Safety and Comfort - Factors in Volvo Occupant Compartment Packaging. *SAE Tech.* doi:10.4271/780135

Boyle, K. J., Reed, M. P., Zaseck, L. W., and Hu, J. (2019). "A Human Modelling Study on Occupant Kinematics in Highly Reclined Seats during Frontal Crashes," in Proceedings of IRCOBI conference. Florence, Italy, September 11–13, 2019.

Caballero-Bruno, I., Töpfer, D., Wohllebe, T., and Hernández-Castellano, P. M. (2021). Novel Car Seat Posture Assessment through Comfort and User Experience. *Proceeding Comf. Congr.* 2021.

Craig, M., Parent, D., Lee, E., Rudd, R., Takhounts, E., and Hasija, V. (2020). *Injury Criteria for the THOR 50th Male ATD*. Available at: https://lindseyresearch.com/wp-content/uploads/2021/10/NHTSA-2020-0032-0005-Injury-Criteria-for-the-THOR-50th-Male-ATD.pdf (Accessed February 17, 2022).

Dissanaike, S., Kaufman, R., Mack, C. D., Mock, C., and Bulger, E. (2008). The Effect of Reclined Seats on Mortality in Motor Vehicle Collisions. *J. Trauma Inj. Infect. Crit. Care March* 64, 614–619. doi:10.1097/TA.0b013e318164d071

Dobberstein, J., Schmidt, D., Östling, M., Bálint, A., Lindman, M., and Höschele, P. (2021). Final Results on Detailed Crash Configurations from Collisions Expected to Remain for Automated Vehicles. *OSCCAR Proj. Deliv.* 3, 2021. Available at: https://www.osccarproject.eu/.

Forman, J. L., Kent, R. W., Mroz, K., Pipkorn, B., Bostrom, O., and Segui-Gomez, M. (2012). Predicting Rib Fracture Risk with Whole-Body Finite Element Models: Development and Preliminary Evaluation of a Probabilistic Analytical Framework. *Ann. Adv. Automot. Med.* 56, 109–124.

Forman, J. L., and McMurry, T. L. (2018). Nonlinear Models of Injury Risk and Implications in Intervention Targeting for Thoracic Injury Mitigation. *Traffic Inj. Prev.* 19, S103–S108. doi:10.1080/15389588.2018.1528356

Fryar, C. D., Gu, Q., Ogden, C. L., and Flegal, K. M. (2016). Anthropometric Reference Data for Children and Adults: United States, 2011-2014. National Center for Health Statistics. *Vital Health Stat.* 3 (39), 9–15.

Höschele, P., Smit, S., Tomasch, E., Östling, M., Mroz, K., and Klug, C. (2021). *Generic Crash Pulses Representative for Future Accident Scenarios of Highly Automated Vehicles, SAE International Journal of Transportation Safety, Special Issue on Occupant Protection & Crashworthiness for ADS-Equipped Vehicles*. doi:10.3217/datacite.2400t-cxv49

Hwang, E., Hu, J., Chen, C., Klein, K. F., Miller, C. S., Reed, M. P., et al. (2016). Development, Evaluation, and Sensitivity Analysis of Parametric Finite Element Whole-Body Human Models in Side Impacts. *Stapp Car Crash J.* 60 (November), 473–508. doi:10.4271/2016-22-0014

Iraeus, J., and Pipkorn, B. (2019). "Development and Validation of a Generic Finite Element Ribcage to Be Used for Strain Based Fracture Prediction," in Proceedings of the IRCOBI Conference, Florence, Italy, September 11–13, 2019.

Iraeus, J. (20152015). "Stochastic Finite Element Simulations of Real Life Frontal Crashes: With Emphasis on Chest Injury Mechanisms in Near-Side Oblique Loading Conditions," (Sweden: Faculty of Medicine, Department of Surgical and Perioperative Sciences, Surgery, Umeå University). PhD Thesis.

Iwamoto, M., Kisanuki, Y., Watanabe, I., Furusu, K., Miki, K., and Hasegawa, J. (2002). "Development of a Finite Element Model of the Total Human Model for Safety (THUMS) and Application to Injury Reconstruction," in Proceedings of IRCOBI Conference, Munich, Germany, 2002-9-18 to 2002-9-20.

Jakobsson, L., Bergman, T., and Johansson, L. (2006). "Identifying Thoracic and Lumbar Spinal Injuries in Car Accidents," In Proceedings of IRCOBI Conference on Biomechanics of Impacts, Madrid, September 20–22, 2006.

Ji, P., Huang, Y., and Zhou, Q. (2017). Mechanisms of Using Knee Bolster to Control Kinematical Motion of Occupant in Reclined Posture for Lowering Injury Risk. *Int. J. Crashworthiness* 22 (4), 415–424. doi:10.1080/13588265.2016.1275430

Koppel, S., Jiménez Octavio, J., Bohman, K., Logan, D., Raphael, W., Quintana Jimenez, L., et al. (2019). Seating Configuration and Position Preferences in Fully Automated Vehicles. *Traffic Inj. Prev.* 20, S103–S10. doi:10.1080/15389588.2019.1625336

Larsson, K.-J., Pipkorn, B., Iraeus, J., Forman, J., and Hu, J. (2021). Evaluation of a Diverse Population of Morphed Human Body Models for Prediction of Vehicle Occupant Crash Kinematics. *Comput. Methods Biomechanics Biomed. Eng.*, 1–31. doi:10.1080/10255842.2021.2003790

Luo, M., and Zhou, Q. (2010). A Vehicle Seat Design Concept for Reducing Whiplash Injury Risk in Low-Speed Rear Impact. *Int. J. Crashworthiness* 15 (3), 293–311. doi:10.1080/13588260903335282

McMurry, T. L., Poplin, G. S., Shaw, G., and Panzer, M. B. (2018). Crash Safety Concerns for Out-Of-Position Occupant Postures: A Look toward Safety in Highly Automated Vehicles. *Traffic Inj. Prev.* 19 (6), 582–587. doi:10.1080/15389588.2018.1458306

Mertz, H., Irwin, A., Melvin, J., Stalnaker, R., and Beebe, M. (1989). *Size, Weight and Biomechanical Impact Response Requirements for Adult Size Small Female and Large Male Dummies*. Detroit, MI: SAE International Congress and Exposition.

Moreau, D., Donlon, J. P., Richardson, R., and Gepner, B. (2021). "A Methodology to Replicate Lap Belt Loading Conditions from a Sled Impact Test in a Non-impact Dynamic Environment on Whole-Body Postmortem Human Subjects," in Proceedings of IRCOBI Conference, September 8–10, 2021.

Mroz, K., Östling, M., Klug, C., Höschele, P., and Lubbe, N. (2022). Supplementing Future Occupant Safety Assessments with Critical Intersection Crashes Selected Using the SAFER Human Body Model. *SAE Int. J. Trans. Saf.* 2021.

Mroz, K., Östling, M., Richardson, R., Kerrigan, J., Forman, J., Gepner, B., et al. (2020). "Effect of Seat and Seat Belt Characteristics on the Lumbar Spine and Pelvis Loading of the SAFER Human Body Model in Reclined Postures," in Proceedings of the IRCOBI Conference, Munich, Germany.

Ortiz-Paparoni, M., Op 't Eynde, J., Kait, J., Bigler, B., Shridharani, J., Schmidt, A., et al. (2021). The Human Lumbar Spine during High-Rate under Seat Loading: A Combined Metric Injury Criteria. *Ann. Biomed. Eng.* 49 (11), 3018–3030. doi:10.1007/s10439-021-02823-x

Östh, J., Bohman, K., and Jakobsson, L. (2020). "Evaluation of Kinematics and Restraint Interaction when Repositioning a Driver from a Reclined to Upright Position Prior to Frontal Impact Using Active Human Body Model Simulations," in Proceedings of the IRCOBI Conference, Munich, Germany.

Östling, M., and Larsson, A. (2019). "Occupant Activities and Sitting Positions in Automated Vehicles in China and Sweden," in Proceedings of Conference for the Enhancement of Safety Vehicles (ESV), 2019, Eindhoven, Netherlands, June 10–13, 2019.

Östling, M., Lundgren, C., Lubbe, N., Huf, A., Wernicke, P., and Pipkorn, B. (2021). "The Influence of a Seat Track Load Limiter on Lumbar Spine Compression Forces in Relaxed, Reclined, and Upright Seating Positions: A Sled Test Study Using THOR-50M," in Proceedings of the IRCOBI Conference, September 8–10, 2021.

Östling, M., Sunnevång, C., Svensson, C., and Kock, H. O. (2017). *Potential Future Seating Positions and the Impact on Injury Risks in a Learning Intelligent Vehicle (LIV)*. Berlin, Germany: VDI-Tagung Fahrzeugsicherheit.

Pipkorn, B., Iraeus, J., Björklund, M., Bunketorp, O., and Jakobsson, L. (2019). "Multi-Scale Validation of a Rib Fracture Prediction Method for Human Body Models," in Proceedings of the IRCOBI Conference, 2019, Florence, Italy, September 11–13, 2019.

Rao, R. D., Berry, C. A., Yoganandan, N., and Agarwal, A. (2014). Occupant and Crash Characteristics in Thoracic and Lumbar Spine Injuries Resulting from Motor Vehicle Collisions. *Spine J.* 14 (10), 2355–2365. doi:10.1016/j.spinee.2014.01.038

Rawska, K., Gepner, B., and Kerrigan, J. R. (2021). Effect of Various Restraint Configurations on Submarining Occurrence across Varied Seat Configurations in Autonomous Driving System Environment. *Traffic Inj. Prev.* 22, S128–S133. doi:10.1080/15389588.2021.1939872

Rawska, K., Gepner, B., Kulkarni, S., Chastain, K., Zhu, J., Richardson, R., et al. (2019). Submarining Sensitivity across Varied Anthropometry in an Autonomous Driving System Environment. *Traffic Inj. Prev.* 20, S123–S127. doi:10.1080/15389588.2019.1655734

Reed, M. P., and Rupp, J. D. (2013). An Anthropometric Comparison of Current ATDs with the U.S. Adult Population. *Traffic Inj. Prev.* 14 (7), 703–705. doi:10.1080/15389588.2012.752819

Richardson, R., Donlon, J. P., Jayathirtha, M., Forman, J. L., Shaw, G., Gepner, B., et al. (2020). Kinematic and Injury Response of Reclined PMHS in Frontal Impacts. *Stapp Car Crash J.* 64, 83–153. doi:10.4271/2020-22-0004

Schneider, L. W., Robbins, D. H., Pflug, M. A., and Snyder, R. G. (1983). *Development of Anthropometrically Based Design Specifications for an Advanced Adult Anthropomorphic Dummy Family Report No: UMTRI-83-53-1*. Corporate Author: University of Michigan, Ann Arbor: Transportation Research Institute

Sengottu Velavan, S., and Huf, A. (2018). "Development of Occupant Restraint Systems for Future Seating Positions in Fully or Semi Autonomous Vehicles," in Proceedings of FISITA World Automotive Congress, 2018, Chennai, India, October 2–5, 2018.

Stanglmeier, M. J., Paternoster, F. K., Paternoster, S., Bichler, R. J., Wagner, P. O., and Schwirtz, A. (2020). Automated Driving: A Biomechanical Approach for Sleeping Positions. *Appl. Ergon.* 86, 103103. doi:10.1016/j.apergo.2020.103103

Stemper, B. D., Chirvi, S., Doan, N., Baisden, J. L., Maiman, D. J., Curry, W. H., et al. (2018). Biomechanical Tolerance of Whole Lumbar Spines in Straightened Posture Subjected to Axial Acceleration. *J. Orthop. Res.* 36 (6), 1747–1756. doi:10.1002/jor.23826

Takata Corporation (2017). *Advanced Adaptive Restraint Systems. Report No. DOT HS 812 432*. Washington, DC: National Highway Traffic Safety Administration.

Tang, L., Zheng, J., and Zhou, Q. (2020). Investigation of Risk Factors Affecting Injuries in Reclining Seat under Frontal Impact. *Int. J. Veh. Saf.* 11. doi:10.1504/ijvs.2020.109277

Tushak, S. K., Gepner, B. D., Forman, J. L., Hallman, J. J., Pipkorn, B., and Kerrigan, J. R. (2022). *Human Lumbar Spine Injury Risk in High-Rate Combined Compression and Flexion Loading in Press* (Online ahead of print).

Wiechel, J., and Bolte, J. (2006). *Response of Reclined Post Mortem Human Subjects to Frontal Impact*. SAE Technical Paper 2006-01-0674 2006. United State: SAE International. doi:10.4271/2006-01-0674

Zhang, X., and Zhou, Q. (2016). An Energy-Absorbing Sliding Seat for Reducing Neck Injury Risks in Rear Impact-Analysis for Prototype Built. *Traffic Inj. Prev.* 17 (3), 313–319. doi:10.1080/15389588.2015.1064908

Conflict of Interest: The authors are employed at Autoliv in Vårgårda, Sweden. Autoliv (www.autoliv.com) is a company that develops, manufactures, and sells protective safety systems to car manufacturers (among other products). Results from this study may impact how Autoliv choose to develop their products.

Publisher's Note: All claims expressed in this article are solely those of the authors and do not necessarily represent those of their affiliated organizations, or those of the publisher, the editors, and the reviewers. Any product that may be evaluated in this article, or claim that may be made by its manufacturer, is not guaranteed or endorsed by the publisher.

frontiers | Frontiers in Future Transportation

ORIGINAL RESEARCH
published: 22 June 2022
doi: 10.3389/ffutr.2022.913887

Tram to Pedestrian Collisions—Priorities and Potentials

Christian Lackner[1], Philipp Heinzl[1], Maria C. Rizzi[2], Christoph Leo[3], Martin Schachner[3], Petr Pokorny[4], Peter Klager[1], David Buetzer[5], Rune Elvik[4], Astrid Linder[2,6] and Corina Klug[3]*

[1]System Engineering, Siemens Mobility Austria GmbH, Vienna, Austria, [2]Swedish National Road and Transport Research Institute, VTI, Linköping, Sweden, [3]Vehicle Safety Institute, Graz University of Technology, Graz, Austria, [4]Institute of Transport Economics, TØI, Oslo, Norway, [5]Accident Research and Prevention, AXA, Winterthur, Switzerland, [6]Vehicle Safety Division, Department of Mechanics and Maritime Science, Chalmers University, Gothenburg, Sweden

OPEN ACCESS

Edited by:
Yong Han, Xiamen University of Technology, China

Reviewed by:
Guibing Li, Hunan University of Science and Technology, China
George Yannis, National Technical University of Athens, Greece

***Correspondence:**
Christian Lackner
lackner.christian@siemens.com

Specialty section:
This article was submitted to Transport Safety, a section of the journal Frontiers in Future Transportation

Received: *06 April 2022*
Accepted: *11 May 2022*
Published: *22 June 2022*

Citation:
Lackner C, Heinzl P, Rizzi MC, Leo C, Schachner M, Pokorny P, Klager P, Buetzer D, Elvik R, Linder A and Klug C (2022) Tram to Pedestrian Collisions—Priorities and Potentials. Front. Future Transp. 3:913887. doi: 10.3389/ffutr.2022.913887

To improve mobility in cities in line with environmental goals, in urban traffic, trams represent an increasingly important means of transport. Due to the close interaction with other road users, this makes collisions with trams fairly frequent. This study has investigated accidents between trams and vulnerable road users resulting in personal injury, aimed at identifying priorities for simulating collisions between trams and pedestrians to assess passive safety measures. Tram accident data collection established throughout Europe from multiple sources and with varying degree of details, have been combined and analysed. These analyses comprise risk assessments per km-driven and general tram accident partner and site type evaluations, with more detailed analyses on accident site distance to the closest tram stop and injured body regions, respectively. In total, 7,535 tram-pedestrian accident resulting in 8,802 pedestrian injuries, collected in the year 2000–2021, was analysed. Accident risk ranges from 0.934 accidents per number of tram (million) km-driven, for slight injuries to 0.063 for fatal injuries. Pedestrians represent a large proportion of tram accident collision partners, especially for severe and fatal accidents. In accidents between trams and pedestrians, 3% of reported injuries are fatal, 23% severe and 74% minor. Generally, low-speed accidents close to tram stops often leading to minor injuries were observed to be of significant importance (<20m to the GPS location of a stop). Analysis of accidents was done bases on gender of the pedestrian showing overall similar involvements in accident with slight difference for various age groups and sites. Regardless of injury severity, the most frequently injured body region in accidents involving a tram is the head. Likewise, injuries sustained to the thorax, especially for higher injury severities are of high relevance, followed by injuries to the lower extremities. Based on this study, recommendations for developing reasonable tram-pedestrian accident scenarios for virtual testing can be derived for further optimisation of pedestrian safety of trams.

Keywords: Tram, public transport, pedestrian, injury severity, accident, injuries

INTRODUCTION

Trams as an integral part of (sub) urban mass public transport services are of significant importance in many cities around the world. While the reopening of tramway lines has been concentrated to western Europe (such as France, Spain, Sweden, and the United Kingdom), in Germany and eastern Europe, the existing systems continue to be expanded and modernised (MVG, 2009). The renaissance of trams goes hand in hand with efforts to improve mobility, accessibility and reduce environmental issues in urban areas (Guerrieri, 2018).

Currently, trams run in 204 cities in Europe with a continuously increasing tram network length by almost 4% (420 km) in Europe between 2015 and 2018 (UIC: International union of Railways, 2009). Obviously, increased number of trams in the cities means that the interaction between trams and other road users are more frequent than ever. Thus, ensuring safety and mitigating tram related accidents is a major concern in the design, operation and development of tram systems (Naznin et al, 2016a), which requires reliable data and first-rate safety knowledge. Current knowledge is almost entirely based on analyses of reported accident data (Naznin et al., 2017), which shortcomings are well-known, such as lack of information on human related accident contributory factors (Naznin et al., 2017) and a high level of underreporting, especially for less severe accidents (Budzynski et al., 2019b). However, despite these limitations, data on accidents are crucial for understanding the safety trends and recognising several accident risk factors.

Accident Data

In 2015, only one country (France) in Europe had a specific tram accident database on a national scale (COST, 2015) while such database did not exist on the European level. Some countries, such as Germany or Switzerland, included tram accidents in their national road traffic accidents databases, operated by police. Typically, on a city level, tram operators collect tram accident data, which are often publicly available, i.e., in form of annual reports, and therefore the level of detail is deficient.

Budzynski et al. (2019a) have categorised tram accidents into four groups: 1) involving a single tram, 2) involving other trams, 3) involving other road users, and 4) others, i.e., accidents between cars and pedestrians near tram stops. In our study, we have focussed on accidents involving other road users, more specifically pedestrians, as they present a particular challenge due to their vulnerability in traffic (Guerrieri, 2018).

Overall accident risk data indicate that the tramway transportation systems are relatively safe when compared to other modes of transport (Guerrieri, 2018). However, injury severity for pedestrians is higher in tram-pedestrian accidents than in accidents with other motor vehicles. This particular higher injury risk has been documented in a number of studies, such as Hedelin et al., 2002; Margaritis, 2007; Naznin et al., 2016b; Chevalier et al., 2019, and Gaca and Franek, 2021.

Occurrence of Tram-Pedestrian Accidents

The conflicts with other users of public space, in relation to their behaviour and their perception of risk are recognised as the primary cause of tram accidents in the COST report TU 1,103 (COST, 2015). Human factors relate to the issues of risk perception, expectancy, inattention and risk behaviour. Lack of danger awareness by tram drivers, and inappropriate reactions of other road users played a major role in all fatal accidents analysed by Margaritis (2007). Castanier et al., 2012 demonstrated that road users have little awareness of accident risks with trams and young pedestrians in particular, perceive a lower risk for themselves than for others. According to Kruszyna and Rychlewski (2013), an approaching tram affects pedestrian behaviour in such way that they behave unsafely, such as violating a red light. A common accident type identified by Sagberg and Sætermo (1997) is pedestrians stepping into the street, often against a red light, without noticing an approaching tram. Furthermore, being under the influence of alcohol is an important factor, as intoxicated pedestrians were frequently identified as victims in tram-pedestrian accidents by Hedelin et al. (1996). The road safety campaign website "*Don't jump under my wheels*" that was launched in Prague (CZ) in 2020, describes that 25% of pedestrians involved in tram-pedestrian accidents in Prague (in period 2016–2019) were foreigners. It suggests that unfamiliarity with tram traffic by some foreigners (Prague has one of the most extensive tram networks in the world) might play a role in accident occurrence, as might very silent tram vehicles. Furthermore, pedestrian inattention (particularly looking at a mobile device) is mentioned as the most common contributory factor with regard to accidents in Prague (DPP–Prague Public Transit Company, 2020). although tram driver related accidents are important as well. Naweed and Rose (2015) revealed three major topics relating to causes of accidents from the point of view of tram drivers: situation awareness, time pressure, and organisational behaviour. Tram driver focus groups conducted by Naznin et al. (2017) identified factors such as pressure of keeping to the timetable, maintaining constant concentration, predicting other road users' behaviour, operational constraints of trams as well as fatigue from workload.

Infrastructure factors, especially tram stop design was found a key accident risk factor by Naznin et al. (2016a) and Sagberg and Sætermo (1997). In Melbourne, for instance, curbside stops have been identified as a major passenger safety concern (Currie and Shalaby, 2007). According to Budzynski et al. (2019a), the biggest risk is at tram stops forming part of pavements where pedestrians have to cross the road as the tram approaches the stop and when tram stops are at signalised junction exits. Design of road intersections plays a significant role, as well (Guirrieri, 2018).

Vehicle factors, such as low floor and older trams, were reported by Naznin et al. (2016b). Sagberg and Sætermo (1997) found that pedestrians are often crossing too close to the front of a stationary tram, that the driver is unable to notice them due to blind spots. Technical factors, i.e., failure of the tram door safety system and the braking system, and the deceleration performance of trams, which largely differs to other vehicles, (the braking efficiency of trams generally being lower compared to

buses, for instance), were also identified as an accident risk factor in the in-depth accident study by Margaritis (2007).

Severity of Tram-Pedestrian Accidents

The injuries sustained by a pedestrian being hit by a tram can go through several phases—initially from the impact of the tram, subsequently by falling onto the ground and lastly, potentially, being run over by the tram. The most serious injuries occur when pedestrians are run over (Hedelin et al., 1996). In general, the severity of tram-pedestrian accidents is primarily affected by vehicle related factors, especially by the mass difference between a tram and a human (a tram vehicle can weigh up to 50 tonnes) and ergonomics and stiffness of the vehicle's front (Hedelin et al., 1996; Grzebieta and Rechnitzer, 2000; Margaritis, 2007; COST, 2015; Gaca and Franek, 2021). A simulation study by Chevalier et al., 2019 on the effects on pedestrian injury by tram front-end shape, showed that the injury risk is more severe for the head than any other body region. Špirk et al. (2021) stated that the most prominent part of the tram front-end responsible for the level of head injury is the windshield. Margaritis (2007) discusses the function of the front under-run protection—he notes that it is more effective at low tram speeds. The injury severity is further affected by the secondary impact, i.e., the physical infrastructure or railway equipment, respectively, the pedestrian hits following the primary impact (Gaca and Franek, 2021). Human factors, such as age, might play a role as well, as exclusively elderly people were found to be involved in fatal tram accidents investigated by Currie et al., 2011.

The recently published Technical Recommendation 17,420 (Technical Committee CEN/TC, 2019) defines pedestrian tram front design safety requirements for the first time, mainly based on geometrical guidelines. Deeper knowledge of relevant tram-pedestrian accident parameters and advanced simulation methods will also lead to improved standardisation and tram designs in future.

Safety management requires the most recent and valid knowledge on accident risks, accident locations, characteristics of pedestrians involved, tram characteristics, etc. This study is contributing to safety management by answering the following research questions on a European level:

- What is the most relevant vulnerable group of road users in tram accidents?
- What is the accident risk for pedestrian to tram accidents?
- Accident locations for pedestrian to tram accidents, e.g., near tram stops?
- Which collision speeds can be observed in pedestrian to tram accidents?
- Which injuries can be observed in pedestrian to tram accidents, e.g., age and gender?

This study aims to derive representative boundary conditions for simulation scenarios to evaluate safety measures for vulnerable road user (VRU) protection of novel trams by answering these questions above. Priorities will be defined based on field data and the derived boundary conditions will be used as input for simulation scenarios. Within the simulations, the injury risk of baseline systems compared to enhanced ones can be compared and finally cost benefit analyses (CBA) can be performed to support decision-making on the introduction of new safety systems for trams.

MATERIALS AND METHODS

Accident Risk Analysis Data

Accident risk quantifies the level of safety relative to the amount of an exposure. The terms risk and exposure should be defined within the context of the issue studied (Hakkert and Braimaister, 2002). In this study, we consider the risk as the probability of pedestrian injury within km-driven by trams. Regardless its limitations (not capturing the respective pedestrian volumes) km-driven is chosen as exposure measure by a transport mode because of its common availability (Elvik, 2015). We have calculated such risk as the number of injured pedestrians in tram-pedestrian accidents (separately for fatal, severe, slight, fatal + severe and all injuries), divided by the amount of km-driven by trams in each respective period. Such calculations are easy to understand and interpret (Bjørnskau and Ingebrigtsen, 2015).

The accident data (annual number of fatally, severely and slightly injured pedestrians in tram-pedestrian accidents) and data on exposure (km-driven) were collected and will be referred to as "cases" throughout this study. The data span over the period 2014–2020, with minor timing differences but a minimum period of 4 years in each case. **Table 1** shows the data for all these cases - note that for Sweden, each case contains several cities.

The accident risk for each severity level was calculated separately for each case. To obtain the best estimates of the risks, data from all cases were counted and the best estimates were calculated as the total number of accidents for a specific severity level, divided by the total number of km-driven by each tram line. To obtain the upper and lower values at 95% confidence level for the best estimates, we have assumed that injuries and crashes are Poisson-distributed. The standard deviation is then equal to the square root of the number of accidents. A 95% confidence interval is obtained by multiplying the standard deviation by 1.96. The upper and lower 95% estimate of the number of crashes = number of accidents ± (1.96 * $\sqrt{}$the number of accidents).

Furthermore, the distribution of injury severity levels in tram-pedestrian accidents, was calculated separately for each case and together for all cases.

Accident Scenarios

To obtain an extensive picture, the analysis of tram accident scenarios was based on accident data of more than 260 public transport system operators, statistics institutes, ministries/ authorities, police, hospitals, rescue organisations, insurance companies and tramway manufacturers. Data sets from several countries including Austria, Germany, Sweden and Switzerland have been collected in a database, free of any personal data of the involved individuals. Furthermore, metadata from other European countries were collected, however due to their quantity and quality these were not considered in the overall evaluation. A full survey was carried out for Austria, Sweden and

TABLE 1 | Data for tram-pedestrian accident risk calculation.

Case	Data source		Time period	Injuries in tram−pedestrian accidents				Km-driven in the time period (million)
	Nr. of injuries	Km−driven		Total	Slight	Severe	Fatal	
Zurich (CH)	Police database (FEDRO, 2022)	(Verkehrsbetriebe Zürich, 2022)	2016–2019	94	65	26	3	69.57
Bern (CH)		SVB, (2022)		8	6	1	1	15.50
Basel (CH)		(Verkehrs-Betriebe, 2022)		24	16	8	0	25.16
Geneva (CHE)		Transports publics genevois, (2022)		18	8	7	3	21.17
Prague (CZ)	PT provider (DPP, 2020)	TSK Praha, (2022)	2015–2019	340	278	42	20	280.20
Berlin (DE)	Police d. BE 2019	Verkehrsverbund Berlin-Brandenburg, (2021)	2010–2017	284	115	146	23	167.68
Brandenburg an der Havel (DE)	Police d. BR a.d. H 2019	Verkehrsverbund Berlin-Brandenburg, (2021)		4	3	1	0	5.99
Karlsruhe (DE)	Police d. KA 2019	(Verkehrsbetriebe Karlsruhe, 2020)		185	109	68	8	68.80
Potsdam (DE)	Police d. P 2019	(Verkehrs-Betriebe, 2022)		36	10	25	1	46.08
Saarbrücken (DE)	Police d. SB 2019	Saarbrücken, (2018)		63	23	37	3	15.20
Vienna (AT)	Police d. (Statistik Austria, 2022)	Wiener Linien (2022)	2014–2020	470	348	113	9	161.60
Graz (AT)		Graz Holding (2022)		69	51	17	1	106.03
Innsbruck (AT)		Innsbrucker Verkehrsbetriebe, (2022)		16	12	4	0	72.80
Linz (AT)		Verkehrsverbund, (2022)		48	34	12	2	54.60
Gothenburg + Mölndal (SW)	Police and hospital d. (STRADA, 2022)	Göteborgs Stad, (2022)	2014–2020	94	55	37	2	103.30
			Total	1753	1,133	544	76	1213,68

Switzerland, as well as a partial survey for Germany. In total, the following statistics are based on 7,535 accidents with at least one tram involved during the period 2000 to 2021 and 8,802 injuries/fatalities sustained by persons in the above mentioned countries.

Tram Accident Data From Austria

Vienna's tram network, with a total length of 175.6 km (Wiener Wiener Linien, 2020), is one of the longest and the third busiest tram network in the world (UITP: International Association of Public Transport, 2019). By law in Austria, all accidents involving personal injury must be reported by the police (Bundesgesetzblatt, BGBI, 2017) and subsequently transmitted to the federal statistical office "STATISTIK AUSTRIA". Accident reports contain information on the accident type, participants, injury severities, as well as geographical location. Thus, a full statistical survey is made available, including for tram-pedestrian accidents. The relevance of the tram network, as well as the available accident data make Vienna a particularly interesting source for investigating tram-pedestrian accidents. During the period 2014–2020, 470 accidents were reported in Vienna, which have been further analysed in this paper, with respect to severity, type and site.

Tram Accident Data From Germany

The Federal Statistical Office, the German counterpart to Statistics Austria, only provides a statistical overview, which was only used to check whether the data otherwise obtained from Germany is representative. The Federal Statistical Office obtains the data from the police. In order to obtain individual data, the individual police headquarters of the federal states were contacted. The data collection procedure of each police station is similar, irrespective of federal state. However, the police headquarters only partially released the data, which meant that not all data sets met the requirements. Data from the police headquarters in Baden-Württemberg, Lower Saxony, Brandenburg West, Middle Franconia, Bavaria, Berlin and Saarland were made available. The data cover 31.4% of the total number of accidents and 16.5% of the network length in Germany (Federal Statistical Office of Germany, 2021). Thus, unlike the Austrian, Swedish and Swiss data, this is a partial survey. Trams are operated in over 50 German cities, with a total network length of over 3,100 km (UIC: International union of Railways, 2009).

Tram Accident Data From Sweden

The Swedish Traffic Accident Data Acquisition (STRADA) database holds information on road traffic accidents occurring on public roads in Sweden. The information regarding these accidents stem from two sources: the police and emergency hospital departments. As of 2016, all emergency hospital departments in Sweden are included, allowing hospital reported data to be deemed nationally representative (Swedish Government Offices, 1965; Mattsson and Ungerbäck, 2013). Hospital reports included in STRADA normally provide a number of parameters regarding accident circumstances, i.e., a brief description of the accident, accident type and location of the accident. Also included is personal information about the patient, e.g., age and gender, together with a full injury diagnosis classified according to the 2005 AIS scale (AAAM, 2005). For example, data from the police, include a description of the crash, information about involved vehicles and the road environment. The STRADA database is described in more detail in (Howard and Linder, 2014; Yamazaki, 2018).

In this study, all crashes between 1st January 2000 until 1st November 2021 involving a tram, resulting in personal injury reported by the police and/or emergency hospital department, were included (N = 1,552). As the specific focus of the present study is pedestrians, additional data of injuries were included from the 259 injured pedestrians reported by emergency hospital departments. Of these, detailed AIS 2005 codes were available for 176 injured pedestrians resulting in 896 individual injuries.

Tram Accident Data From Switzerland

The data from Switzerland were provided by the Federal Office of Transport. In contrast to the above mentioned data sources, these data come directly from the transport operators, who are obliged to report traffic accidents involving personal injury. As in the case of Austria and Sweden, these data are also a full statistical survey. Trams are operated in the cities of Basel, Bern, Geneva, Lausanne, Neuchâtel and Zurich (Verkehrsbetriebe Zürich, 2022).

Accident Location Analysis in the Austrian Database

In comparison to other national statistics (German, Swedish, Swiss), the Austrian data does not disclose whether a tram-pedestrian accident has occurred close to a tram stop. Furthermore, in-depth data recording the collision speeds of the trams is unavailable. To overcome this drawback, the distance between each documented accident to the nearest tram stop has been evaluated, by matching its geo location with the tram network.

A typical modern tram accelerates and decelerates, respectively, at approximately 1 m/s^2 in regular service (Peng et al., 2018). Assuming this speed the constant acceleration/deceleration from the stop to the accident location, the respective impact speed can be estimated for each accident. To avoid unrealistic high impact speeds at accident locations far away from a stop, speed limits for associated edges have been retrieved from the OSM tram network to cap the maximum speed.

To determine tram stop coordinates, data from Vienna's public transport provider "Wiener Linien" (BMDW, 2018a; BMDW, 2018b, Wiener Linien 2021) was used. The data contains geo information, as well as associated travel routes, which are dependent on time of day and public holidays amongst other factors. In total, 978 stops have been determined. Although a reconstruction of the tram network is possible in principle, a network of that kind would still lack detailed track information, i.e., curvatures or speed limits on a particular track section. In order to deal with this issue, data from OpenStreetMap (OSM), the largest Volunteered Geographic Information (VGI) project, was used additionally, please see **Figure 1**. OSM is continuously updated and extended and grants users free access to an editable map of the world (Corcoran et.al., 2013). Data can either be viewed online (openstreetmap.com), or downloaded through programming interfaces, such as OSMnx (Boeing, 2017), which was used for this study. For retrieving the OSM information, "Vienna, Austria" was selected as location and as an additional filter: "railway"~"tram|rail" was used. Although data quality is one of the main concerns (Barron et al., 2014, the quality which is quite accurate for many countries, depends on the maintainers in specific areas (Girres and Touya, 2010; Haklay, 2010), which for certain locations are also updated through federal funded projects (Hakley, 2014). According to the OSM wiki, the Vienna tram track network is almost complete (OSM Wiki, 2020). The extracted tram track network of Vienna consists of 4,721 nodes and 12,540 edges.

The retrieved tram stop locations have further been fused with the OSM tram track network. For each tram stop, a corresponding node or edge, respectively, has been determined in the graph by calculating the respective minimum Euclidean distance. The median distance is 0.14 m with 933 of 978 stops, being at a distance of less than 5 m between their respective retrieved tram stop location and the tram track according to OSM, which indicates a good correspondence between the location of the stops and the actual network. Further analysis shows that 933 stops have been used to determine distances between the accident sites and the closest stops. Similarly, distances between the accident locations and the tram track network have been retrieved. Here, a median distance of 1.76 m has been observed (90 percentile of 15.22 m and a 95 percentile of 23 m) between the accident location and the tram network. For the further analysis, 20 m has been used as a cut off to omit inaccurate mapping, which finally resulted in 442 of 470 evaluable accidents.

Data Analysis

Accident risk data has been collected for Austria, the Czech Republic, Sweden and Switzerland. Of these five countries, the largest tram networks in the following cities were studied: Graz, Innsbruck, Linz, Vienna, Prague, Gothenburg, Mölndal, Zurich, Bern, Basel, Geneva, totalling 1753 accidents recorded between; 2016 and 2019 (Czech Republic, Switzerland) and 2016 and 2020 (Austria, Sweden), as listed in **Table 1**.

A total of 7,535 accidents with reference to road use and severity were studied, which had occurred in the following four countries: Austria, Germany and Switzerland between 2010 and 2017 and in Sweden between 2000 and 2021. In the same countries and during the same period, a survey of injured persons by road use and severity was carried out, comprising a total of 8,802 injured persons.

The accident site analysis is based on data from Germany (2010–2017), Switzerland (2010–2017) and Sweden (2000–2021). In addition, data from accidents that had occurred in Vienna, Austria, between 2014 and 2020 were also used.

Data on age and gender of the injured pedestrians were analysed for Austria, Germany, Sweden and Switzerland. Again, data from Austria, Germany and Switzerland are from the time period 2010–2017, while data from Sweden was available for the period 2000 and 2021. Demographic data of Austria, Switzerland and Sweden stem from Eurostat (European Union, 2021), demographic data of observed regions in Germany of the federal statistical office of Germany (Federal Statistical Office of Germany, 2021).

For the detailed injury analysis, only data from Sweden was available (2000–2021), as detailed AIS codes have not been recorded in any of the other databases for tram accidents. The analysis of injuries is based on AIS 2005.

TABLE 2 | Risk estimates for each city.

City	Accident risk			
	Total	Slight	Severe	Fatal
Zurich	1,351	0.934	0.374	0.043
Bern	0.516	0.387	0.065	0.065
Basel	0.954	0.636	0.318	0.000
Geneva	0.850	0.378	0.331	0.142
Prague	1,213	0.992	0.150	0.071
Berlin	1,694	0.686	0.871	0.137
Brandenburg an der Havel	0.668	0.501	0.167	0.000
Karlsruhe	2,689	1,584	0.988	0.116
Potsdam	0.781	0.217	0.543	0.022
Saarbrücken	4,145	1,513	2,434	0.197
Wien	2,908	2,153	0.699	0.056
Graz	0.651	0.480	0.160	0.009
Innsbruck	0.220	0.165	0.055	0.000
Linz	0.879	0.623	0.220	0.037
Gothenburg + Mölndal	0.910	0.532	0.358	0.019

TABLE 3 | Total risk estimates.

Accident risk for	Estimate		
	Lower	Best	Upper
Fatal injury	0.049	0.063	0.077
Severe injury	0.411	0.448	0.486
Fatal + severe injury	0.473	0.513	0.553
Slight injury	0.879	0.934	0.988
Any injury	1,377	1,444	1,512

TABLE 4 | Severity distribution of pedestrian injuries in tram-pedestrian accidents.

Case	Fatal (%)	Severe (%)	Slight (%)
Zurich	3	28	69
Bern	13	13	75
Basel	0	33	67
Geneva	17	39	44
Prague	6	12	82
Berlin	8	51	40
Brandenburg an der Havel	0	25	75
Karlsruhe	4	37	59
Potsdam	3	69	28
Saarbrücken	5	59	37
Vienna	2	24	74
Graz	1	25	74
Innsbruck	0	25	75
Linz	4	25	71
Gothenburg + Mölndal	2	39	59

RESULTS

Accident Risk

The results for accident risks are provided in **Table 2** and **Table 3**. **Table 2** contains the risk values for each city, while **Table 3** provides lower, best and upper estimates of risks calculated from all cases together.

Regarding the severity distribution in tram-pedestrian accidents, the aggregated data from these cases show that 3% of reported injuries are fatal, 23% severe and 74% slight. There are obvious regional differences in the cases–see **Table 4**.

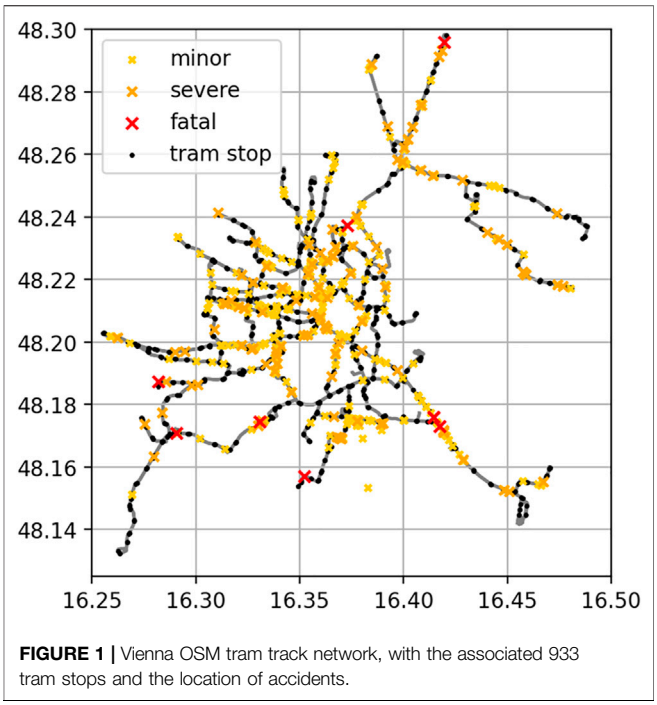

FIGURE 1 | Vienna OSM tram track network, with the associated 933 tram stops and the location of accidents.

Injured People Classified by Road Use and Severity

Most of the accidents analysed in this study led to minor injuries (80%), please see **Table 2** in the Appendix, followed by severe injuries (16%). With an absolute number of 123 fatal injuries, these account for only 1.4% of all accidents investigated in this study.

Figure 2 shows the distribution of injured people in tram accidents classified by severity and road use across Austria, Germany, Sweden and Switzerland. Road user fatalities occur most likely to pedestrians (70.1%) and cyclists (17%), who together represent the most vulnerable group (87.1%) of road users. Pedestrians generally form the largest group in the severity category "severe" (41.9%). Therefore, the design of pedestrian-friendly trams is highly relevant. Also of interest is the individual severity results for pedestrians across the considered countries, which tendencies are similar.

Injured People by Accident Site

Typical tram vs. pedestrian accident sites have been compared for Germany, Sweden and Switzerland, please see **Figure 3**. In Germany, accidents at crossings, junctions and roundabouts (23%) are commonly observed, yet there is also a large number of accidents not explicitly disclosing each respective site. Accidents at tram stops account for approximately 13% of all accidents in Germany, which in comparison to data from Sweden and Switzerland seems low. In Switzerland most of the

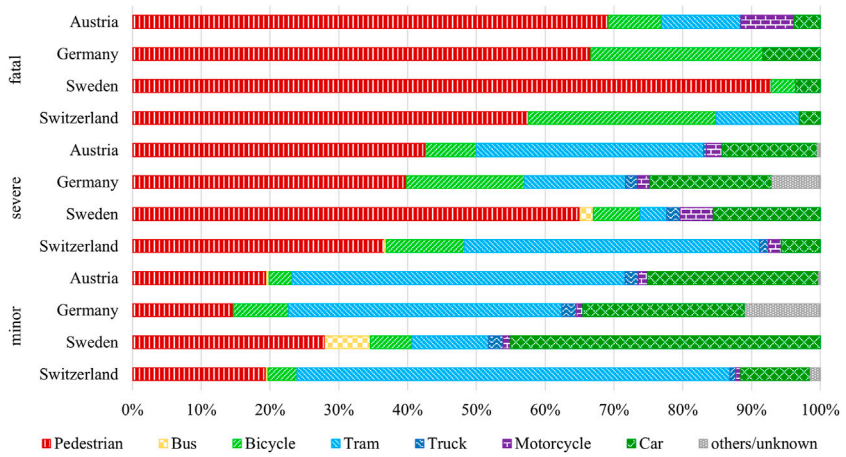

FIGURE 2 | Injured people classified by road use and severity (8,802 injured people).

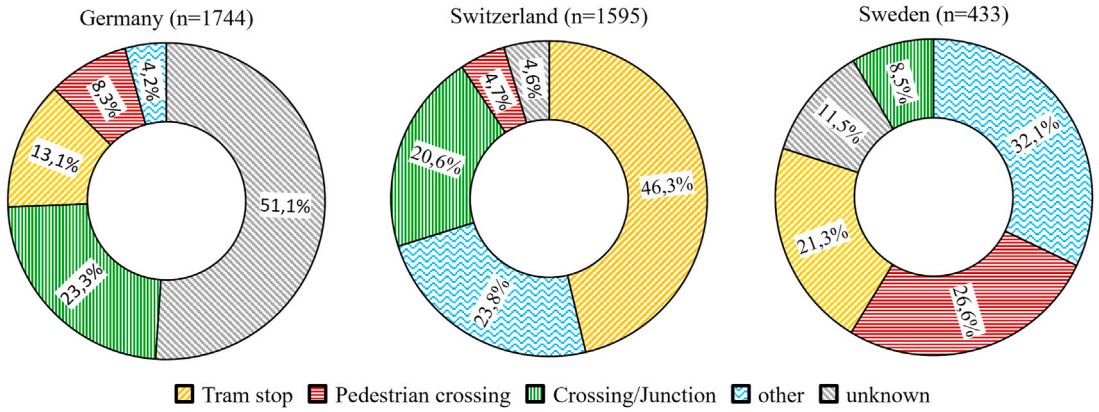

FIGURE 3 | Tram vs. Pedestrian Accidents by Site (3,772 accidents in total).

accidents happen at or near a tram stop (46.3%) which indicates relatively low tram impact speeds. Also in Sweden, accidents at tram stops are the third most common type of accident after accidents on pedestrian crossings. In the STRADA accident database, "pedestrian crossing" is a subcategory of all accidents in general, which is summarised in **Table 4** of the appendix. In the order of a quarter (26.6%) of the accidents involving a pedestrian and a tram in Sweden occur at a zebra crossing.

For Vienna, accident sites and types have been re-evaluated by incorporating distances between tram stops and accidents. Accidents which happened within a distance of 20 m of the accident location, were reclassified "tram stop" accidents, the detailed classification, i.e., pedestrian from right/left, has further been relaxed to match the categories of the other countries (please see **Supplementary Figure SI** of the Appendix).

The evaluation of the distances between tram stops and accidents in Vienna, revealed that accidents followed by minor injury occurred in a median of 30.30 m (95 percentile: 179.8, 97.5 percentile: 210.4) to a tram stop, seen in **Figure 4**. For severe accidents a median of 48.5 m (95 percentile: 207.69, 97.5 percentile: 229.16) has been observed, fatal accidents occurred in a median of 136.7 m (95 percentile: 306.7, 97.5 percentile: 327.4).

Tram vs. Pedestrian Accident Collision Speeds

The distribution for the resulting impact speeds for the investigated accident locations in Vienna is shown in **Figure 5**. The estimated median speed in the cases with minor injuries is 28 km/h and 36 km/h in the severe cases and 30 km/h for both together. The majority of fatal cases happened at a distance with more than 100 m to the next tram stop, where the speed limit was assumed as collision speed, leading to a median value of 50 km/h.

Injured People by Age and Gender

Figure 6 shows accident rates per age and gender group. To obtain representative accident incidences, the absolute

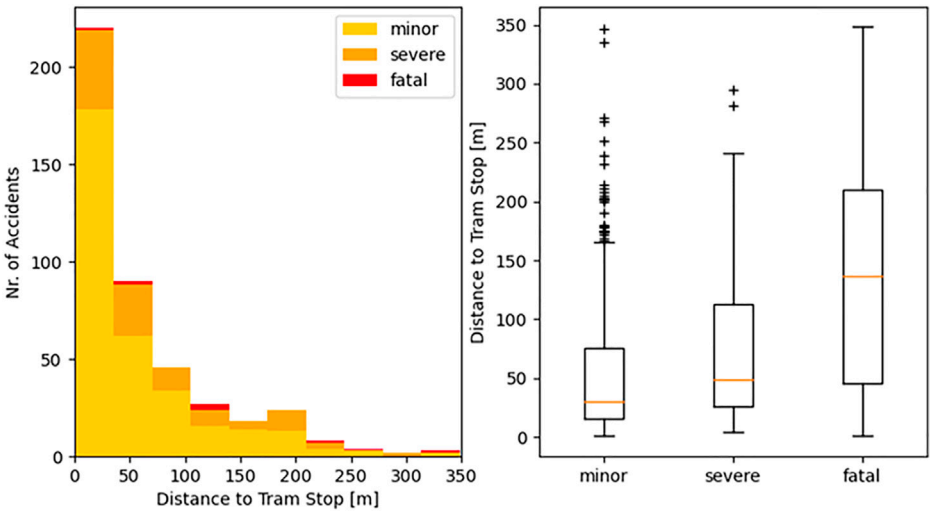

FIGURE 4 | Distance distribution between accident-tram stops in the city of Vienna (443 cases during the period 2014–2020), highlighted according to severity.

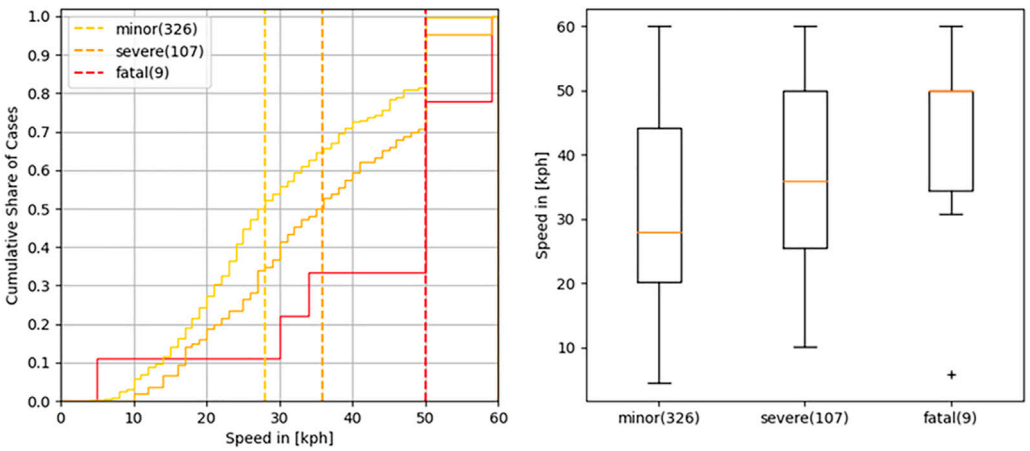

FIGURE 5 | Estimated distribution of tram collision speeds for pedestrian accidents in the city of Vienna (443 cases in the period 2014–2020), highlighted according to their severity.

accident figures have been divided by the respective number of inhabitants per country and age group. For absolute numbers please see **Supplementary Figure SH** in the Appendix. Overall, Austria has the highest incidence of tram-pedestrian accidents due to the significantly higher amount of vehicle kilometres travelled. In the Swiss data, the attribute "age" is often missing, therefore only the total number of accidents in Switzerland is shown in **Figure 6**. Most of the pedestrian accidents per 100,000 persons occur in the age range of 15–24. In Austria and Germany injured pedestrians aged 75 and older, represent the second largest group, whereas in Sweden older pedestrian are not as often involved in tram accidents. In general, the frequency of female and male pedestrians being involved in tram accidents, is similarly. Slight differences between different age-groups were identified for different genders. In Sweden and Germany, slightly more males than females were involved in accidents. In Austria, more accidents involving female pedestrians have been observed in the age groups 15–24 and older than 75, respectively, for Switzerland no further subdivision into age-groups are available.

Detailed Injury Analyses of Swedish Accident Data

Figure 7 shows the share of injuries according to different AIS body regions for AIS2+ and AIS3+ injuries, and as a function of gender, held on the Swedish accident database. For AIS2+ as well as AIS3+ injuries, no significant difference in the distribution of

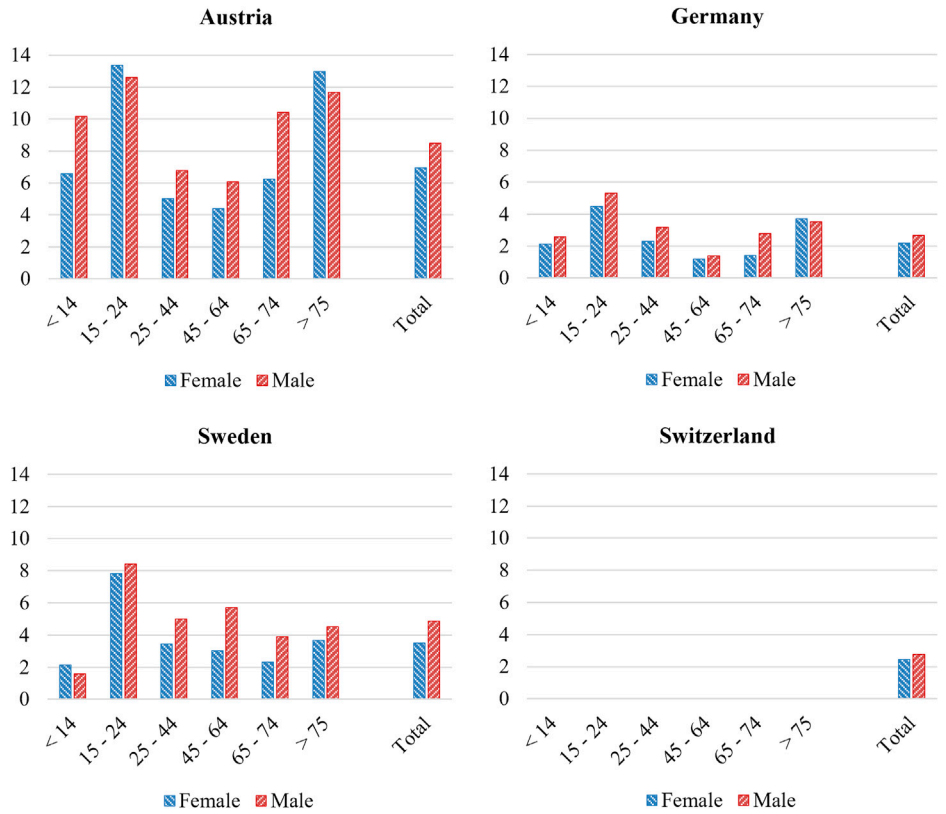

FIGURE 6 | Incidence of injured pedestrians classified by age and gender.

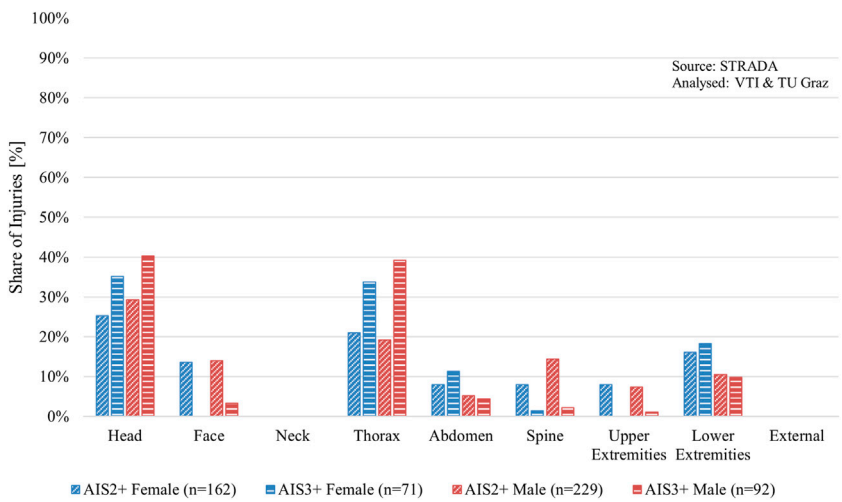

FIGURE 7 | Injured Body Regions as a function of gender and injury severity in Sweden.

injuries between females and males could be observed for all body regions. Regardless of injury severity, the most frequently injured body region in accidents involving a tram is the head. AIS2+ and AIS3+ are mainly represented by internal organ injuries, e.g., cerebrum, cerebellum and brain stem, and skeletal injuries, e.g., skull fractures, for both female and male pedestrians

(**Supplementary Appendix Figure SB**). Injuries sustained to the thorax, especially for higher injury severities (AIS3+), are highly relevant too. These thorax injuries are mainly represented by internal organ injuries, e.g., lung, heart, hemopneumothorax, pneumothorax, and skeletal injuries, e.g., rip fractures, regardless of injury severity and gender (**Supplementary Appendix Figure SD**). For AIS3+ injuries, in addition to the head and thorax, injuries to the lower extremities also play an essential role. These injuries are mainly represented by skeletal injuries, e.g., pelvic, femur and tibia fractures, for both females and males (**Supplementary Appendix Figure SH**). A detailed analysis as a function of anatomical structure, gender and injury severity for pedestrian to tram accidents in Sweden for the remaining body regions, can be found in the Appendix.

Supplementary Figure SA in the Appendix shows the share of injuries for different age groups with respect to AIS2+ and AIS3+ injuries, split in terms of gender based on the Swedish accident database. Regardless of injury severity, injuries are mainly sustained by pedestrians above 25 years, for both females and males. For the age group 50-60YO, females show significant lower odds of sustaining AIS2+ injuries (OR = 0.4, p-value < 0.05) than males. This is also the case for AIS3+ injuries (OR = 0.4, p-value < 0.05). On the other hand, for the age group 65 + YO, females show significantly higher odds of sustaining AIS2+ (OR = 4.8, p-value < 0.05) as well as AIS3+ (OR = 5.6, p-value < 0.05) injuries.

DISCUSSION

At 30%, pedestrians represent the largest group of vulnerable tram collision partners, please see **Supplementary Figure SK** of the appendix, especially for severe and fatal accidents. In contrast to car occupants, they are more vulnerable to severe injuries in accidents with trams. Therefore, accident prevention and mitigating measures addressing pedestrians should be of high priority for tram and infrastructure developers.

As expected, accident risk is the highest for slight injury which decreases as the injury severity increases. There are slight differences between the accident rates in each city under consideration in this study, which can be attributed to different local conditions (such as types of trams and stops used in each case city, degree of segregation, density of tram network, tram volumes, safety culture, etc.) When interpreting the results and considering their transferability to other cities or countries, we must be mindful of the potential effects of these local conditions.

A conclusive comparison of accident risks for other transport modes, such as personal cars, would require the knowledge of an adequate exposure measure. Cars are spending significant parts of their service life in rural areas and on motorways, while trams almost exclusively move in urban areas, being exposed to pedestrians (such as in city centres, in front of train stations, in pedestrian zones, etc.). Therefore, without an exposure measure, i.e., capturing the exposure of cars to pedestrians, such a comparison is not relevant and conducting such an analysis is also out of scope of this study.

Looking at the figures from the evaluated databases in this study, the most frequently mentioned type of accident location in Switzerland and Sweden is a tram stop. In many cases there is no defined accident location which presents a problem in estimating the impact speed in collisions between pedestrians and trams. Based on the data from Switzerland and the accident investigation in Vienna (Austria), one can only assume that a tram stop is one of the most common accident locations for pedestrians. Perhaps this is due to the source of the data, whereby the accidents in Germany stemming from the police, while the data in Switzerland stem from the Federal Statistical Office and the Swedish data from police reports and hospital databases.

The detailed analysis of tram-pedestrian accidents in Vienna shows that accidents, where minor injuries tend to occur closer to tram stops than accidents resulting in a severe or fatal outcome. This observation seems reasonable since reduced speeds can be expected in the vicinity of stopping areas, which should feasibly lead to reduced injury severity. The presented results certainly benefit from the quantification of the distance, compared to the estimations usually provided in accident reports. This benefit also becomes evident when comparing the different accident configurations in various countries. Thus, it appears difficult to achieve a uniform accident representation, which might also be explainable by the different assessment strategies in different countries.

Under certain circumstances the mapping of the OSM network data with the documented tram stops of the public transport provider "Wiener Linien" sometimes leads to a large distance to the tram network because the nearest stop, determined by the shortest Euclidean distance, is actually not on the actual driven tram route and therefore neglect these cases.

An impact speed distribution figure could be generated by taking various accident site to tram stop distances into account and applying a simplification for the acceleration/deceleration additionally capping the resulting speeds with an upper limit, retrieved from the OSM network. This showed that a tram-pedestrian accident most frequently occurs at impact speeds below 28 km/h for slightly injured and 36 km/h for severely injured pedestrians. However, the respective actual impact speed is always also influenced by the road layout (curve radius), prevailing surrounding traffic, priority rules and a possible emergency braking event before an accident. Compared to this, the average speed of trams in Vienna is approximately 15 km/h, according to official data (Wiener Wiener Linien, 2020) which might be due to the idle times at stops. A detailed analysis of the surrounding traffic and the influence due to emergency braking (Schachner et al., 2020) would be of additional value. The speeds represented in the current paper should be understand as worst-case prediction.

In the recently published Technical Recommendation (TR) 17,420 (Technical Committee CEN/TC, 2019), also 20 km/h are defined as relevant collision speed between trams and pedestrians. However, since according to **Figure 5**, higher speeds seem to be also relevant for severe and fatal accidents, we suggest assessing safety measures also for higher speeds. At 30 km/h, the majority of slight and sever accidents would be covered.

Regardless of injury severity, the most frequently injured body region in accidents involving a tram is the head. Injuries sustained to the thorax, especially for higher injury severities (AIS3+) are highly relevant too. In addition to AIS3+, injuries to the head and thorax, injuries to the lower extremities also play an essential role.

Injuries are mainly sustained by both male and female pedestrians above the age of 25 years, with no difference in the severity of the injury. For the age group 50-60YO females show significantly lower odds of sustaining AIS2+ injuries than males. This is also the case for AIS3+ injuries. On the other hand, for the age group 65 + YO, females show significantly higher odds of sustaining AIS2+ as well as AIS3+ injuries.

Strengths and Limitations

For the accident risk analysis, the strength of the study lies in the quality of data. Accident data from public transport (PT) providers (CZ), a combined police and hospital database (SWE) and utilised police databases (CHE, AUT) were collected. Although the data is very up-to-date it is still difficult to see whether design improvements in passive safety of trams are having an effect, because there are both old and new vehicles on the tracks due to the long life span of trams, i.e., vehicles older than 30 years are often still in service (Linien, 2022) and (GRAZ Holding, 2022), respectively.

A strength of the present study is that it was possible to combine and compare data cross-nationally. However, simultaneously as only a few parameters could be analysed, making this type of comparison also became a limitation. Although it has been possible to present an overall picture of accidents involving trams in this paper, only subsets of different data sets could be used to carry out detailed analyses, i.e., only Swedish data could be used to analyse injuries. Regrettably, a consistent dataset was not available for the whole dataset. As sample sizes were generally low, as much data as available for each individual research question were used. If only the datasets covering all research questions at once had been used, the resulting dataset would have been too small.

The main limitations include the small sample size of the cases and limited transferability of the results. Furthermore, the injury categories in different hospital databases may have been incorrectly classified in some cases. As the police reporting of accident severity do not necessarily describe the real injury severity, the injury data from emergency hospital departments in Sweden provided an important contribution. It has been possible to provide a comprehensive picture of tram accidents in Sweden, as (virtually) all available data held in STRADA could be included.

Another limitation of this study is that some accidents between pedestrians and trams have not been deemed as road traffic crashes as the traffic is rail-bound. However, questioning the results does not seem to be necessary since the proportion of injured pedestrians is similar across all countries.

In this study, several regional differences were observed. The results of the analysis are very much dependent on infrastructure, as well as the definition of a tram-stop, e.g. radius, etc. in the city under consideration. Infrastructure in Gothenburg, where most tram related accidents in Sweden are recorded, integrates the tram network firmly with the bus network on "ordinary" roads next to other motor traffic. This might be an explanation for the fact that only Sweden showed buses as collision partners for trams.

Additionally, for the analysis of the accident risk, we do not know the number of pedestrians and number of walked kilometres, therefore we have not been able to capture pedestrian activity in our risk calculations.

OUTLOOK

Current tram front design is more and more aligned with pedestrian safety and today's best practice in this respect is to follow the geometry-based tram front design guidelines of TR 17420 (CEN/TR 17420, 2019). However, analogous to automotive industry, computer simulations will also gain in importance in future tram-relevant standards and, when dealing with computer analyses, appropriate priorities must be set in the development of load cases or the evaluation of results, respectively. Based on the field data analysis presented here, the following recommendations can be made for simulations with Human Body Models (HBMs):

- Safety measures should also be assessed at higher speeds, i.e., up to 30 km/h
- Injury assessment should focus on head and thoracic injuries
- Both, female and male anthropometries should be taken into account in the assessment, taking also the elderly and children into account
- Simulations should be performed with varying impact locations around the vehicle width, as no limitations can be deduced based on available accident data

The predicted injury severities gathered from the simulations can be used as input for cost-benefit analyses (CBAs), to guide engineers and decision makers on future inventions and recommendations. Socio-economic costs and benefits of safety systems are therefore considered, providing insight to the costs of vehicle safety systems, the safety impacts (injuries and quality-of-life loss) and the associated monetary benefits and the socio-economic return (balance of benefits and costs). For such analysis, the crash risk is needed as an input parameter. We recommend using region-specific crash risks, as in the past trams were also designed and sold for specific cities. If a risk assumption on an overall European level is required, or if no regional accident risk is available, the "best estimates" in **Table 3** can be used as input for CBA.

CONCLUSION

Tram accidents involving VRUs are prevalent in urban areas across Europe. The overall average risk for tram pedestrian accidents per million tram kilometres travelled resulting in

minor, severe and fatal injuries, is 0.934, 0.448 and 0.063, respectively. The data analysis of accidents involving trams shows that pedestrians clearly account for the largest proportion of fatal injuries, directly followed by cyclists. The various countries in this study show differences in typical tram-pedestrian accident locations though tram stops generally tend to predominate. Regarding the age of pedestrians involved in tram accidents, the accident data show a significant peak for the age group 15–24, however the group older than 75 years also shows a strikingly high involvement. In terms of injured body regions, the head shows the highest rate of AIS2+ and AIS3+ injuries for both males and females.

The analysed data can be used to derive representative virtual testing scenarios, that can be used in the future for utilising the latest analysis techniques, like HBM simulations, to further optimise the pedestrian-safety of trams.

DATA AVAILABILITY STATEMENT

The original contributions presented in the study are included in the article/**Supplementary Material**, further inquiries can be directed to the corresponding author.

AUTHOR CONTRIBUTIONS

The main theme for this publication was developed and guided by CK. PK collected tram accident data across Europe. Particularly the Swedish data were collected and analysed by MR. Further accident data and the accident risk analysis are contributed by DB, PP, and RE. MS investigated the Vienna tram accidents in terms of location and impact speed. CLe contributed to the detailed injury analysis of tram accidents in Sweden. AL initiated and coordinated the project funding this study. CLa and PH collated and completed this study with additional evaluations and references. All authors have read and approved the final manuscript.

FUNDING

This study has been conducted within the VIRTUAL project that has received funding from the European Union Horizon 2020 Research and Innovation Programme under Grant Agreement No. 768960. The overall objective of VIRTUAL is to improve the safety of urban road users by providing procedures and open access tools to assess the benefit of novel safety systems. HBMs of both female and male users are being developed in this project and are now freely available on an open-source basis to facilitate analysis of vulnerable road users' interaction with public transport systems, e.g., trains, subways, trams, buses, for instance, in great detail.

SUPPLEMENTARY MATERIAL

The Supplementary Material for this article can be found online at: https://www.frontiersin.org/articles/10.3389/ffutr.2022.913887/full#supplementary-material

REFERENCES

AAAM (2005). *Abbreviated Injury Scale 2005*. Illinois: Des Plaines.

Barron, C., Neis, P., and Zipf, A. (2014). A Comprehensive Framework for Intrinsic OpenStreetMap Quality Analysis. *Trans. GIS* 18 (6), 877–895. doi:10.1111/tgis.12073

Bundesgesetzblatt, BGBI (2017). Bundesgesetz über die Statistik zu Straßenverkehrsunfällen mit Personenschaden (Straßenverkehrsunfallstatistik-Gesetz, StVUSt-G) StF. BGBl. I Nr. 7/2017

Bjørnskau, T., and Ingebrigtsen, R. (2015). Alternative Forståelser Av Risiko Og Eksponering. (Alternative Understanding of Risk and Exposure). TØI report 1449/2015. Available at: https://www.toi.no/getfile.php?mmfileid=41817.

BMDW (Bundesministerium für Digitalisierung und Witschaftsstandort) (2018a). *Open Data Austria*. Vienna: Datenauftritt Stadt Wien. Available at: https://data.wien.gv.at (Accessed January 28, 2022).

BMDW (Bundesministerium für Digitalisierung und Witschaftsstandort) (2018b). Open Data Austria: Katalog Wiener Linien Echtzeitdaten via Datendrehscheibe Wien. Available at: https://www.data.gv.at/katalog/dataset/wiener-linien-echtzeitdaten-via-datendrehscheibe-wien (Accessed January 28, 2022).

Boeing, G. (2017). OSMnx: New Methods for Acquiring, Constructing, Analyzing, and Visualizing Complex Street Networks. *Comput. Environ. Urban Syst.* 65, 126–139. doi:10.1016/j.compenvurbsys.2017.05.004

Basel Verkehrs-Betriebe, B. V. B (2022). Basler Verkehrsbund. Available at: https://www.bvb.ch/de/unternehmen/geschaeftsbericht/?j=2020 (Accessed February 17, 2022).

Budzyński, M., Szmagliński, J., Jamroz, K., Birr, K., Grulkowski, S., and Wachnicka, J. (2019a). Assessing Tram Infrastructure Safety Using the Example of the City of Gdańsk. *J. KONBiN* 49, 293–322. doi:10.2478/jok-2019-0060

Budzynski, M., Tubis, A., and Jamroz, K. (2019b). Identifying Selected Tram Transport Risks. *IOP Conf. Ser. Mater. Sci. Eng.* 603, 042053. doi:10.1088/1757-899X/603/4/042053

Castanier, C., Paran, F., and Delhomme, P. (2012). Risk of Crashing with a Tram: Perceptions of Pedestrians, Cyclists, and Motorists. *Transp. Res. Part F Traffic Psychol. Behav.* 15, 387–394. doi:10.1016/j.trf.2012.03.001

CEN/TR 17420 (2019). *Railway Applications – Vehicle End Design for Trams and Light Rail Vehicles with Respect to Pedestrian Safety*. Brussels: Technical Report.

Chevalier, M.-C., Brizard, D., and Beillas, P. (2019). Study of the Possible Relationships between Tramway Front-End Geometry and Pedestrian Injury Risk. *Traffic Inj. Prev.* 20, 107–113. doi:10.1080/15389588.2018.1536823

Corcoran, P., Mooney, P., and Bertolotto, M. (2013). Analysing the Growth of OpenStreetMap Networks. *Spat. Stat.* 3, 21–32. doi:10.1016/j.spasta.2013.01.002

COST (2015). Operation and Safety of Tramways in Interaction with Public Space. Available at: https://www.cerema.fr/system/files/documents/2019/04/tu1103_report_red.pdf (Accessed February 9, 2022).

Currie, G., and Shalaby, A. (2007). Success and Challenges in Modernizing Streetcar Systems: Experiences in Melbourne, Australia, and Toronto, Canada. *Transp. Res. Rec.* 2006, 31–39. doi:10.3141/2006-04

Currie, G., Tivendale, K., and Scott, R. (2011). Analysis and Mitigation of Safety Issues at Curbside Tram Stops. *Transp. Res. Rec.* 2219, 20–29. doi:10.3141/2219-03

DPP – Prague Public Transit Company (2020). Main Causes of Tram-Pedestrian Accidents. Available at: https://www.neskakejmipodkola.cz/#priciny (Accessed February 9, 2022).

Elvik, R. (2015). Some Implications of an Event-Based Definition of Exposure to the Risk of Road Accident. *Accid. Analysis Prev.* 76, 15–24. doi:10.1016/j.aap.2014.12.011

European Union (2021). Eurostat. Available at: ec.europa.eu/eurostat (Accessed November 11, 2021).

Federal Statistical Office of Germany (2021). DESTATIS. Available at: https://www-genesis.destatis.de/genesis/online (Accessed November 11, 2021).

Gaca, S., and Franek, L. (2021). Pedestrian Fatality Risk as a Function of Tram Impact Speed. *Open Eng.* 11, 1105–1113. doi:10.1515/eng-2021-0110

Girres, J.-F., and Touya, G. (2010). Quality Assessment of the French OpenStreetMap Dataset. *Trans. GIS* 14 (4), 435–459. doi:10.1111/j.1467-9671.2010.01203.x

Göteborgs Stad (2022). Göteborgs Stad. Available at: https://www4.goteborg.se/prod/intraservice/namndhandlingar/samrumportal.nsf (Accessed February 17, 2022).

Graz Holding (2022). FAQs zu den Graz Linien. Available at: https://www.holding-graz.at/de/mobilitaet/faq/(Accessed February 17, 2022).

Grzebieta, R. H., and Rechnitzer, G. (2000). *Tram Interface Crashworthiness. ICrash 2000 - International Crashworthiness Conference*. London: The Royal Aeronautical Society.

Guerrieri, M. (2018). Tramways in Urban Areas: An Overview on Safety at Road Intersections. *Urban Rail Transit* 4, 223–233. doi:10.1007/s40864-018-0093-5

Hakkert, A. S., and Braimaister, L. (2002). *The Uses of Exposure and Risk in Road Safety Studies*. Netherlands: SWOV Institute for Road Safety Research.

Haklay, M. (2010). How Good Is Volunteered Geographical Information? A Comparative Study of OpenStreetMap and Ordnance Survey Datasets. *Environ. Plann B Plann Des.* 37 (4), 682–703. doi:10.1068/b35097

Haklay, M. (2014). *Crowdsourced Geographic Information Use in Government*. London: World Bank Publications.

Hedelin, A., Björnstig, U., and Brismar, B. (1996). Trams-a Risk Factor for Pedestrians. *Accid. Analysis Prev.* 28, 733–738. doi:10.1016/s0001-4575(96)00048-6

Hedelin, A., Bunketorp, O., and Björnstig, U. (2002). Public Transport in Metropolitan Areas - a Danger for Unprotected Road Users. *Saf. Sci.* 40, 467–477. doi:10.1016/s0925-7535(01)00014-5

Howard, C., and Linder, A. (2014). *Review of Swedish Experiences Concerning Analysis of People Injured in Traffic accidentsVTI Notat 7A-2014*. Linköping: National Road and Transport Research Institute VTI.

Innsbrucker Verkehrsbetriebe (2022). Innsbrucker Verkehrsbetriebe und Stubaitalbahn GmbH. Available at: https://www.ivb.at/unternehmen/ueber-uns/(Accessed February 17, 2022).

Kruszyna, M., and Rychlewski, J. (2013). Influence of Approaching Tram on Behaviour of Pedestrians in Signalised Crosswalks in Poland. *Accid. Analysis Prev.* 55, 185–191. doi:10.1016/j.aap.2013.03.015

Margaritis, D. (2007). *Accident Analysis into the Primary and Secondary Safety of City Trams in the Netherlands*. Leiden: Association for European Transport and contributors. European Transport Conference.

Mattsson, K., and Ungerbäck, A. (2013). *Vägtrafikolyckor: Handledning Vid Rapportering*. Borlänge: Transportstyrelsen.

MVG (2009). The Modern Tram in Europe. Available at: http://www.reconnectingamerica.org/assets/Uploads/The-Modern-Tram-in-Europe.pdf (Accessed February 9, 2022).

Naweed, A., and Rose, J. (2015). "It's a Frightful Scenario": A Study of Tram Collisions on a Mixed-Traffic Environment in an Australian Metropolitan Setting*. *Procedia Manuf.* 3, 2706–2713. doi:10.1016/j.promfg.2015.07.666

Naznin, F., Currie, G., Logan, D., and Sarvi, M. (2016a). Safety Impacts Of Platform Tram Stops On Pedestrians In Mixed Traffic Operation: A Comparison Group Before–After Crash Study. *Accid. Analysis Prev.* 86, 1–8. doi:10.1016/j.aap.2015.10.007

Naznin, F., Currie, G., and Logan, D. (2016b). Exploring the Impacts of Factors Contributing to Tram-Involved Serious Injury Crashes on Melbourne Tram Routes. *Accid. Analysis Prev.* 94, 238–244. doi:10.1016/j.aap.2016.06.008

Naznin, F., Currie, G., and Logan, D. (2017). Key Challenges in Tram/streetcar Driving from the Tram Driver's Perspective - A Qualitative Study. *Transp. Res. Part F Traffic Psychol. Behav.* 49, 39–48. doi:10.1016/j.trf.2017.06.003

OSM Wiki (OpenStreetMap Wiki contributors) (2020). Austria/Nahverkehr Wien. Available at: https://wiki.openstreetmap.org/wiki/Austria/Nahverkehr_Wien#Stra.C3.9Fenbahnlinien (Accessed January 28, 2022).

Peng, F., Zhao, Y., Chen, T., Zhang, X., Chen, W., Zhou, D., et al. (2018). Development of Robust Suboptimal Real-Time Power Sharing Strategy for Modern Fuel Cell Based Hybrid Tramways Considering Operational Uncertainties and Performance Degradation. *Appl. energy* 226, 503–521. doi:10.1016/j.apenergy.2018.05.092

Stadtwerke Saarbrücken, S. (2018). *Zahlenspiegel 2018*. Saarbrücken: Stadtwerke Saarbrücken Holding GmbH.

Sagberg, F., and Sætermo, I. E. (1997). Traffic Safety of Tram Transport. TØI Report 367. Available at: https://www.toi.no/getfile.php/138906-1208933888/Publikasjoner/T%C3%98I%20rapporter/1997/367-1997/sum-367-97.pdf (Accessed February 9, 2022).

Schachner, M., Sinz, W., Thomson, R., and Klug, C. (2020). Development and Evaluation of Potential Accident Scenarios Involving Pedestrians and AEB-Equipped Vehicles to Demonstrate the Efficiency of an Enhanced Open-Source Simulation Framework. *Accid. Analysis Prev.* 148, 105831. doi:10.1016/j.aap.2020.105831

Špirk, S. (2021). Utilization of the Validated Windshield Material Model in Simulation of Tram to Pedestrian Collision. *Materials* 14, 265. doi:10.3390/ma14020265

Städtische Verkehrsbetriebe Bern (2022). Bernmobil - Fahrgastzahlen. Available at: https://geschaeftsbericht.bernmobil.ch/de/zahlen-und-fakten/bernmobil-in-zahlen/?oid=68&lang=de#fahrzeuge (Accessed on February 17, 2022).

Swedish Government Offices (1965). Health in Offices and Shops 1965. *Br. Med. J.* 2, 1130–1131. doi:10.1136/bmj.2.5470.1130-a

Technical Committee CEN/TC (2019). *Railway Applications - Vehicle End Design for Trams and Light Rail Vehicles with Respect to Pedestrian Safety*. Brussels: European Committee for Standardization, 30.

Transports publics genevois (2022). Transports Publics Genevois. Available at: https://www.tpg.ch/fr/rapports-annuels (Accessed February 17, 2022).

TSK Praha (2022). Technická Správa Komunikací Hlavního Města Prahy. Available at: https://www.tsk-praha.cz/wps/portal/root/nabidka-sluzeb/rocenky (Accessed on February 17, 2022).

UIC: International union of Railways (2009). *UIC: International Union of Railways*. France: ERRAC Road Map.

UITP : International Association of Public Transport (2019). Public Transport Trend 2019. Available at: https://cms.uitp.org/wp/wp-content/uploads/2020/06/PT_Trends2019_Executive_Summary.pdf (Accessed February 9, 2022).

Verkehrsbetriebe Karlsruhe, V. B. K. (2020). *Die VBK in Zahlen*. Karlsruhe: Verkehrsbetriebe Karlsruhe GmbH.

Verkehrsbetriebe Zürich, V. B. Z. (2020). Fahrleistungen. Available at: https://www.stadt-zuerich.ch/vbz/de/index/die_vbz/portraet/zahlen_fakten/angebot.html (Accessed on February 17, 2022).

Verkehrsverbund Berlin-Brandenburg, V. B. B. (2021). *Verbundbericht*. Berlin-Brandenburg GmbH.

Verkehrsbetrieb Potsdam, S. (2015). Zahlen und Fakten. Verkehrsbetrieb Potsdam GmbH ViP. Available at: https://web.archive.org/web/20150424002625/http://www.swp-potsdam.de/swp/de/verkehr/ueber-uns-vip/zahlen_und_fakten-vip/zahlen_und_fakten.php (Accessed April 27, 2022).

Verkehrsverbund, O. Ö. (2022). Stadtverkehr. VBB Susanne Henckel. Available at: https://www.ooevv.at/?seite=stadtverkehr&sprache=DE (Accessed February 17, 2022).

Wiener Linien (2020). Betriebsangaben. Available at: https://www.wienerlinien.at/media/files/2020/wl_betriebsangaben_2019_deutsch_358274.pdf (Accessed February 21, 2022).

Wiener Linien, W. (2021). Description of the OGD Files for the Data Platform of the Wiener Linien. Available at: https://www.wienerlinien.at/ogd_realtime/doku/ogd/wienerlinien_ogd_Beschreibung.pdf (Accessed February 21, 2022).

Yamazaki, R. (2018). *Strada Bortfallshandbok 2018 – Information Om Täckning Och Bortfall I Rapportering till Transportstyrelsens Vägolycksdatabas*. Örebro.

Conflict of Interest: CL and PH are employed by Siemens Mobility Austria GmbH, PK worked for Siemens Mobility Austria GmbH.

The remaining authors declare that the research was conducted in the absence of any commercial or financial relationships that could be construed as a potential conflict of interest.

Publisher's Note: All claims expressed in this article are solely those of the authors and do not necessarily represent those of their affiliated organizations, or those of the publisher, the editors and the reviewers. Any product that may be evaluated in this article, or claim that may be made by its manufacturer, is not guaranteed or endorsed by the publisher.

frontiers | Frontiers in Future Transportation

ORIGINAL RESEARCH
published: 27 June 2022
doi: 10.3389/ffutr.2022.883951

Effects of Automated Emergency Braking and Seatbelt Pre-Pretensioning on Occupant Injury Risks in High-Severity Frontal Crashes

Ekant Mishra[1]*, *Krystoffer Mroz*[1], *Bengt Pipkorn*[1,2] and *Nils Lubbe*[1,2]

[1]Autoliv Research, Vårgårda, Sweden, [2]Division of Vehicle Safety, Department of Mechanics and Maritime Sciences, Chalmers University of Technology, Gothenburg, Sweden

In high-severity crashes, occupant protection is challenging. Automated Emergency Braking (AEB) and seatbelt pre-pretensioning (PPT) are means to improve occupant protection; the purpose of this study was to quantify their effects on occupant injury risks in high-severity full-frontal crashes by Finite Element (FE) simulations. The SAFER Active average male Human Body Model was used as an occupant substitute. The crash pulses used were from separate full-frontal crash simulations using a Honda Accord FE model. The vehicle interior model comprised a seat, an instrument panel, a three-point pretensioned seatbelt system with a load-limiter of 3.1 kN force level, and a frontal passenger airbag. The effects of AEB and PPT were evaluated by simulating a 1 g pre-crash braking scenario for 0.5 s, with and without AEB, for three different PPT force levels: 0, 300, and 600 N. The impact speed of 80 km/h was reduced to 69 km/h by AEB. When neither system was activated, the predicted risk for an occupant to sustain two or more fractured ribs (NFR2+) was 100% for both 45- and 65-year-old male occupants. The risks were reduced when the AEB was activated, particularly for the 45-year-old occupant. When the AEB was activated, the risks of concussion and rib fractures were reduced; upper neck tension forces, pelvis Anterior Superior Iliac Spine (ASIS) forces, and lower extremity forces were also reduced. Increasing the PPT forces reduced the rib fracture risk further (to about 48% for a 45-year-old occupant with 600 N PPT force). The reduced speed due to AEB resulted in a lower concussion risk (from 71.3% to 31%). However, the concussion risk increased slightly with increased PPT forces.

Keywords: human body model, concussion, rib fracture, finite element simulations, pre-crash, crash

OPEN ACCESS

Edited by:
Yong Han,
Xiamen University of Technology, China

Reviewed by:
Pengpeng Xu,
South China University of Technology, China
Tariq Usman Saeed,
Purdue University, United States
Jing Huang,
Hunan University, China

***Correspondence:**
Ekant Mishra
ekant.mishra@autoliv.com

Specialty section:
This article was submitted to Transport Safety, a section of the journal Frontiers in Future Transportation

Received: *25 February 2022*
Accepted: *30 May 2022*
Published: *27 June 2022*

Citation:
Mishra E, Mroz K, Pipkorn B and Lubbe N (2022) Effects of Automated Emergency Braking and Seatbelt Pre-Pretensioning on Occupant Injury Risks in High-Severity Frontal Crashes. Front. Future Transp. 3:883951. doi: 10.3389/ffutr.2022.883951

INTRODUCTION

Traffic safety continues to be a major health issue (World Health Organization, 2018). The travelling speed of a motor vehicle is a major factor influencing the probability and severity of a crash (Aarts and Van Schagen, 2006). Crash severity increases with speed: the greater the energy at impact, the more likely severe injuries to the occupants (Farmer, 2019). Crash testing that compared occupant injury risks at three crash speeds, 64, 80, and 90 km/h, illustrated that these increases in speed can have deadly consequences (Kim et al., 2021). Facial fractures and severe brain injuries were much more likely at 80 and 90 km/h compared to 64 km/h, due to contact of the head with the instrument panel (known as "strike through") (Kim et al., 2021).

The safe speed limit for head-on collisions is considered to be 80 km/h, at least in Sweden (Eugensson et al., 2011). Beyond 80 km/h, the responsibility for ensuring safety should be on the road infrastructure design rather than the vehicle (Eugensson et al., 2011). However, as seen from crash testing, the risk of severe injuries, particularly to the head can be high at 80 km/h (Kim et al., 2021).

Avoiding collisions entirely or reducing impact speeds, two ways to reduce injury risk for vehicle occupants, can be at least partly achieved with active safety systems like Automated Emergency Braking (AEB). Low-speed AEB systems are on average estimated to decrease real-world rear-end crashes with injuries by 45% and all rear-end collisions (irrespective of injury) by about 38% (Fildes et al., 2015; Cicchino, 2017).

However, not all AEB systems are equal. Different AEB designs can differ substantially in activation logic; moreover, depending on the situation they respond to, they activate at different times (Dahl et al., 2018). Typically, the AEB activates as late as possible to still avoid a collision by braking, with further delay to account for the possibility of avoiding a collision by steering, which often is less time consuming than braking at higher speeds (Brännström et al., 2014). According to Lindman et al. (2010), the AEB systems typically brake fully (up to 1 g, only limited by road friction) after a ramp up. Situation criticality rarely requires, and the possibility of steer avoidance rarely allows for decelerations longer than 1 s; however, they are often longer than 0.5 s (Brännström et al., 2014; Spitzhüttl and Liers, 2019).

Pre-crash braking by AEB can displace occupants forward because of inertial forces (Schoeneburg et al., 2011). Even without AEB, driver-initiated evasive maneuvers (braking, steering) attempting to avoid crashes are frequent (Mages et al., 2011). As a result, occupant displacement just before the crash is common. During emergency maneuvers, occupants' forward head excursions can reach up to 400 mm, although there is substantial variability (Reed, 2021). Excursion and deviations from the standard seating position may increase injury risks, due to altered interactions with the passive restraint systems (Mages et al., 2011; Boyle et al., 2020). Restraint systems adapting to these posture changes may prevent the likelihood of injuries (Boyle et al., 2020).

Systems such as seatbelt pre-pretensioning (PPT) can be activated in the pre-crash phase (even before any occupant movement) if an impending crash is detected in advance by environmental sensors using e.g., radar or video (Mages et al., 2011). While PPT systems tense the seatbelt and reduce belt slack in the pre-crash phase, they can even reduce the forward excursions significantly and return the occupants to their normal position (Mages et al., 2011). Moreover, reducing occupant forward displacement by pre-pretensioning in combination with the reduced impact speed due to AEB might reduce injury risks even further than AEB alone (Östh et al., 2015).

It is also important to capture the occupant response in pre-crash scenarios, since previous volunteer studies evaluating the effects of braking have determined that muscle contraction plays an important role in the forward displacement of occupants and the belt interaction forces (Ejima et al., 2007; Olafsdottir et al., 2013; van Rooij et al., 2013). Several active human body models (HBMs) exist today, Finite Element (FE) and multi-body; they employ different muscle activation strategies to reproduce the vehicle occupant pre-crash muscular response (Meijer et al., 2013; Östh et al., 2015; Devane et al., 2019). These models can predict occupant kinematics and injuries in addition to reproducing the pre-crash occupant response. The SAFER Active Human Body Model (SAFER A-HBM) is one such model, having actively controlled cervical, lumbar, and upper extremity muscles (Olafsdottir et al., 2013; Östh et al., 2015). It is an average male FE model based on the Total Human Body Model for Safety (THUMS) version 3 with updated head, neck, ribs, and lumbar spine (Kleiven, 2007; Iraeus and Pipkorn, 2019; Pipkorn et al., 2019). It has been validated for predicting whole-body kinematics, rib fractures, and concussions in frontal impacts, the most common car occupant injuries (Kleiven, 2007; Iraeus and Pipkorn, 2019; Pipkorn et al., 2019). It has also been validated for predicting pre-crash kinematics in emergency braking maneuvers with and without pre-pretensioned seatbelts by means of data from volunteer tests (Olafsdottir et al., 2013; Östh et al., 2015; Ólafsdóttir et al., 2019).

Previously, researchers have studied the combined effect of AEB and PPT on the occupant injury risks. Matsuda et al. (2018) investigated the influence of both braking and steering on the injury risks for frontal (56 km/h) and side collisions (32 km/h) using the versions 4 and 5 of the THUMS; the latter has active muscles. They also studied the effect of a pre-crash seatbelt. While they reported lower injury risks with the pre-crash seatbelt, the results with AEB but without pre-crash seatbelt were not conclusive (Matsuda et al., 2018). Östmann et al. also studied the effects of AEB and an electrical reversible seatbelt retractor (Östmann and Jakobsson, 2016). In frontal impacts with a travelling speed of 64 km/h, occupant accelerations were reduced by up to 70% due to AEB induced reduced impact speeds. However, they did not study any detailed injury criteria. Moreover, their simulations with the reversible retractor were inconclusive, as they did not terminate successfully (Östmann and Jakobsson, 2016). Saito et al. showed that increasing PPT forces led to reduced thoracic injury risk in addition to lower forward displacements in the pre-crash phase (Saito et al., 2016). However, they did not evaluate any strain-based injury risks (Saito et al., 2016). As noted, these studies either considered travelling speeds lower than the safe speed limit at 80 km/h (Eugensson et al., 2011; Östmann and Jakobsson, 2016; Matsuda et al., 2018) or did not evaluate any strain-based injury risk (Saito et al., 2016). We believe it is important to simulate travelling speeds up to 80 km/h, to develop better restraint systems to protect the occupants, as severe injuries occur at these speeds (Kim et al., 2021).

This study aimed to evaluate the effects of AEB and seatbelt PPT on the occupant injury risks and loadings in high-severity full-frontal crashes using the SAFER A-HBM.

MATERIALS AND METHODS

SAFER Active Human Body Model

Version 9.0.1 of the SAFER A-HBM was used to represent a passenger occupant. The SAFER A-HBM represents a 50th percentile male with a weight of 77 kg and a height of 175 cm (Robbins, 1983). It consists of approximately 127,000 solid elements, 108,000 shell elements, and 2,500 one-dimensional elements. The muscles are modelled with 1D Hill-type

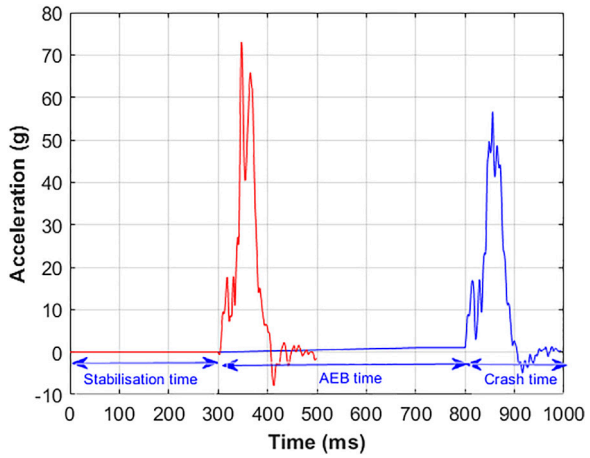

FIGURE 1 | Crash and AEB pulses. The red curve represents the crash pulse for the No_AEB+0N simulation. The blue curve represents the AEB and the crash pulse for the simulations with AEB and crash phases. The first 300 ms in both curves represent the stabilization time.

elements, and a closed-loop control strategy is followed for the muscle activation (Larsson et al., 2019).

Simulation Conditions

The simulation matrix consisted of one driving speed, the safe speed of 80 km/h, and two different impact speeds, without AEB at 80 km/h and with AEB at 69 km/h. The crash pulses (**Figure 1**) were extracted from separate full-frontal crash simulations using a Honda Accord FE model, model year 2011 (Singh et al., 2016). The Honda Accord FE model has been validated for full frontal barrier test at 56 km/h and 40% offset frontal crash test at 64 km/h (Singh et al., 2016). The No_AEB+0N simulation represents driving speed and impact speeds of 80 km/h with no AEB or PPT. The simulations AEB+0N, AEB+300N, and AEB+600N represent an 80 km/h traveling speed and a 69 km/h impact speed in addition to PPT forces of 0, 300, and 600 N, respectively, as shown in **Table 1**. We chose a conservative, but realistic, duration of 0.5 s AEB, based on previously published data (Brännström et al., 2014; Spitzhüttl and Liers, 2019). The 1 g AEB pulse we used had a ramp up time of 0.4 s. The 69 km/h impact speed in AEB simulations was calculated based on the driving speed of 80 km/h and the 0.5 s 1 g AEB.

The total simulation time for the No_AEB+0N simulation was 500 ms, which comprised an initial 300 ms model stabilization time (so that the SAFER A-HBM achieved equilibrium between the seat and the model and muscle activations were initialized) and a 200 ms crash phase. The total time for the simulations with AEB was 1,000 ms, which included the 500 ms pre-crash AEB duration. Both the pre-crash and the crash phases were simulated in the same run, without restarting the simulation. All the simulations were carried out using LS-DYNA explicit FE solver, double precision version R9.2.0 (LSTC, Livermore, CA, United States).

Vehicle Interior and Restraint Systems

All the simulations were carried out for a belted, upright occupant seated in the passenger compartment of a midsize European car, which includes a state-of-the-art three-point seatbelt, frontal passenger airbag, and a deformable seat. The SAFER A-HBM was positioned in the FE model of the vehicle seat used in previous volunteer tests (Olafsdottir et al., 2013; Larsson et al., 2019).

The seatbelt comprises a b-pillar mounted shoulder retractor with pretensioning and load-limiting (3.1 kN) and an outboard lap belt pretensioner. The models of the shoulder retractor, lap belt pretensioner and webbing material properties, as well as the complete belt system, have been validated in-house (at both component and system levels) to match the performance of their mechanical counterparts. Validation information of the belt system is provided in the **Supplementary Figure S1**. The belt was routed tightly around the pelvis and chest, with the pelvis Anterior Superior Iliac spine (ASIS) points as the guiding points for the lap belt, and the shoulder belt portion crossing the middle of the sternum. The seatbelt model was used with and without a PPT at different force levels to prevent forward excursion of the SAFER A-HBM from the initial position during braking. The PPT was triggered with the onset of the AEB pulse. The retractor pretensioner and lap-belt pretensioner were activated 5 and 15 ms after crash initiation, respectively. The two different PPT force levels caused the belt to pull in about 80–110 mm of webbing. The retractor pretensioner further pulled-in between 20 and 40 mm of webbing, depending on the different simulation conditions. The belt pay-out in the No_AEB+0N condition was about 480 mm; it ranged between 340 and 370 mm for the other conditions, with more pay-out for the lower PPT force. The seatbelt pull-in and pay-out, and the shoulder and lap belt forces are shown in **Supplementary Figure S3**.

The airbag model was a based on a state-of-the-art frontal passenger airbag for a midsize European car, with a volume of 112 L and two ventilation holes of diameters of 45 mm. A validation of the airbag model is included in the **Supplementary Figure S2**. The airbag pressure was increased by reducing the ventilation hole area by 70% for all load cases, a technique that prevents a possible strike through of the head into the instrument panel (Boyle et al., 2020). The airbag was activated

TABLE 1 | Simulation matrix.

Simulation	Driving speed (km/h)	AEB time (s)	Impact speed (km/h)	Pre-pretensioner force (N)
No_AEB+0N	80	0	80	No PPT
AEB+0N	80	0.5	69	No PPT
AEB+300N	80	0.5	69	300
AEB+600N	80	0.5	69	600

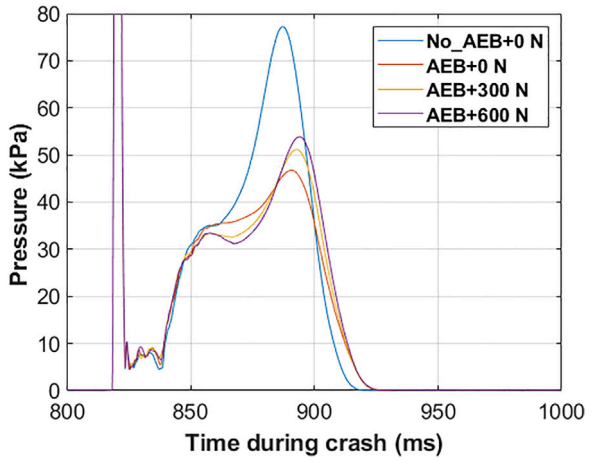

FIGURE 2 | Airbag pressures for the different simulation conditions.

14 ms after crash initiation. In the 69 km/h crash, peak in-crash airbag pressures of 47–53 kPa were measured, as shown in **Figure 2**. In comparison, the airbag pressure measured in an unmodified model (with normal ventilation hole areas) in a standard 56 km/h full-frontal crash is about 30 kPa, as shown in **Supplementary Figure S4**.

Occupant Kinematics and Injury Assessment

The maximum forward displacements for the head (head center of gravity), chest (T8), and pelvis (center of gravity H-point) relative to the vehicle displacements were compared for the different simulations.

We followed the HBM assessment criteria recommended in the SAFE-UP project to evaluate the risks of head, neck, thorax, lumbar spine, and pelvis injuries (Östling et al., 2022). The effect of AEB and PPT on the head and thorax injury risks were evaluated by comparing the AIS2 risk of concussion for an average male occupant and the AIS2+ risk of two or more fractured ribs (NFR2+) for a 45-year-old and a 65-year-old male occupant. The AIS2 concussion risk was calculated based on the maximal principal strain in the brain tissue (Kleiven, 2007). We also computed the head injury criterion (HIC15). The NFR2+ risks were estimated from the peak first principal strains in the cortical bone of each rib using a probabilistic method (Forman et al., 2012; Iraeus and Pipkorn, 2019; Pipkorn et al., 2019). The cumulative effects of AEB and PPT on head and thorax injury risks were also evaluated by calculating a joint probability of injury assuming independence of NFR2+ and AIS2 concussion risks, using the equation:

$$\boldsymbol{Pjoint} = 1 - (1 - \boldsymbol{Phead}) * (1 - \boldsymbol{Pchest}) \quad (1)$$

The upper neck tension forces (C1 vertebra) and lumbar spine compression forces (L1-L5 vertebrae) were measured using cross-section measurements with respect to a local coordinate system in each vertebral center (Mroz et al., 2022). For the pelvis loading, the resultant left, and right ASIS forces were measured using cross-sections on both sides of the pelvis, defined with respect to a local coordinate system (Mroz et al., 2022).

Furthermore, we also measured the resultant forces in the distal femurs and the proximal and distal tibias, as we expected leg-to-instrument panel contact. While these forces are not part of the SAFE-UP assessment criteria, they are included in the Euro NCAP frontal impact testing protocol (Euro NCAP, 2022). These forces were also measured using cross-sections of the bones (excluding soft tissues), defined with respect to a local coordinate system. The proximal and distal tibia forces were averaged. Note that the SAFER HBM is not validated to assess these cross-section force measurements. Therefore, the results should be read for trends, reduction or increases in forces, not absolute values.

RESULTS

Occupant Kinematics

Figure 3 compares the occupant forward displacements in the (A) pre-crash, and (B) crash phases. With the AEB alone, the occupant was already in a forward displaced position at the beginning of the crash phase. With increasing PPT force, the forward displacements in the pre-crash phase were reduced. However, the maximum forward displacements in the crash phase were only marginally affected by the AEB. The maximum forward pelvis and chest displacements varied negligibly with PPT. On the other hand, the maximum forward head displacement increased as PPT force increased. The head, chest, and pelvis trajectories in the XZ plane are shown in **Supplementary Figure S5**. The postures of the SAFER A-HBM at the beginning of the crash phase (the end of the pre-crash phase) and at the maximum forward head position during crash are shown in **Supplementary Figure S6**.

Injury Assessment

The NFR2+ risk for both the 45-year and 65-year-old male occupants in the No_AEB+0N simulation was 100%. The risks were reduced with the AEB in the AEB+0N simulation, particularly for the 45-year-old occupant. Additionally, as shown in **Figure 4**, the NFR2+ risk decreased further with the increase in PPT force.

AEB also reduced the concussion risk; the AIS2 concussion risk for the AEB+0N simulation was less than half of the No_AEB+0N simulation, as illustrated in **Figure 4**. However, the concussion risk increased with the increase in PPT force. The HIC15 value also increased with increase in PPT force, from 551 in the AEB+0N simulation to 1270 in the AEB+600N simulation, compared to 2610 in the No_AEB+0N simulation. The joint probability of injury calculated using **Eq. 1** was lowest in the AEB+0N simulation for rib fractures for 45-year-old and concussion and in the AEB+600N simulation for rib fractures for 65-year-old and concussion.

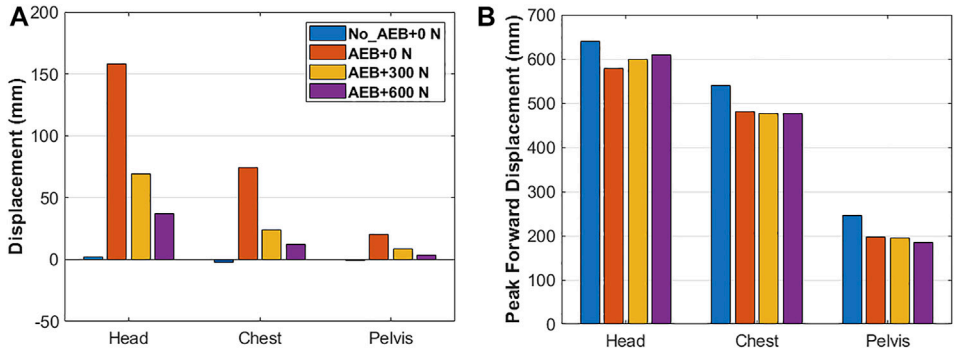

FIGURE 3 | Head, chest, and pelvis forward displacements: **(A)** at the beginning of crash phase and **(B)** peak values in crash phase. Note: Y-axis scales differ.

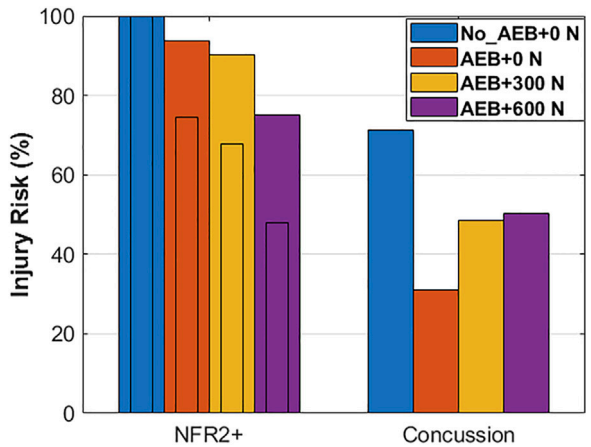

FIGURE 4 | NFR2+ risk for 45-year-old (narrow bars) and 65-year-old (wide bars) male occupants, and AIS2 concussion risk for a male occupant of unspecified age.

For the other body regions, the forces in the No_AEB+0N simulation (**Supplementary Table S1**) were normalized to 100%. The forces in other simulations are shown as a percentage of the normalized values in **Figure 5**. The maximum upper neck (C1) tension force decreased to about 60% for the simulations with AEB. There was no clear trend in the upper neck tension forces as PPT force increased.

The model-predicted maximum lumbar spine compression forces in the L1–L5 vertebrae were not affected by AEB or PPT. In all the simulations, the maximum compression force was measured in the L5 vertebra.

Resultant forces for the left and the right ASIS were lower for the AEB+0N simulation than the No_AEB+0N simulation. However, PPT force either increased or did not affect the ASIS forces.

Leg-to-instrument panel contact occurred in all the simulations. The resultant forces in the femur ranged from 1.3 to 1.7 kN for all conditions, except for 3.1 kN in the left femur in the No_AEB+0N simulation. The left tibia force in the AEB simulations were about 70% of the force in the No_AEB+0N simulation. For the right tibia, the effect of AEB was insubstantial, but some effect of PPT was seen as the forces were lower.

The sum of all percentage values across all assessments (except head and chest) comes to 800% in the No_AEB+0N, 614% in AEB_0N, 609% in AEB+300N, and 637% in AEB+600N simulations.

DISCUSSION

This study evaluated the effect of AEB and seatbelt PPT on the occupant injury risks and loadings in high-severity frontal car crashes by performing FE simulations of the SAFER A-HBM in the passenger position.

AEB reduced the AIS2 concussion and NFR2+ risks due to the reduced impact speed. The NFR2+ risk further reduced when increasing the PPT force, perhaps due to the occupant sitting in a position closer to the upright position at the beginning of the crash due to the PPT. Previous studies have shown that occupant postures due to pre-crash effects significantly influence the injury risks (Bose et al., 2008; Woitsch and Sinz, 2014). In contrast, the AIS2 concussion risk increased with increased PPT force. This is likely due to airbag interaction: higher PPT forces reduced initial displacement during the pre-crash braking and delayed the first airbag contact. The highest airbag pressures were observed for the highest PPT force, increasing linear acceleration of the head (as indicated by HIC15 values) and, in turn, brain strain and concussion risk.

The upper neck tension force decreased substantially due to the AEB-induced impact speed reduction. However, there was no considerable effect of the PPT. Neither AEB nor PPT substantially influenced lumbar spine compression. The highest loading was measured in the L5 vertebra in all the simulations. The reduced impact speed due to AEB also decreased the pelvis ASIS forces but the PPT either increased or did not affect the forces. This is likely due to the shorter pelvis frontal displacements (up to 20 mm) compared to the head and the chest (up to 160 mm and 75 mm, respectively). Even though increasing PPT forces reduced pelvis displacements in the pre-crash phase, the magnitudes and thus the effect of PPT were considerably lower to influence the pelvis ASIS forces in crash.

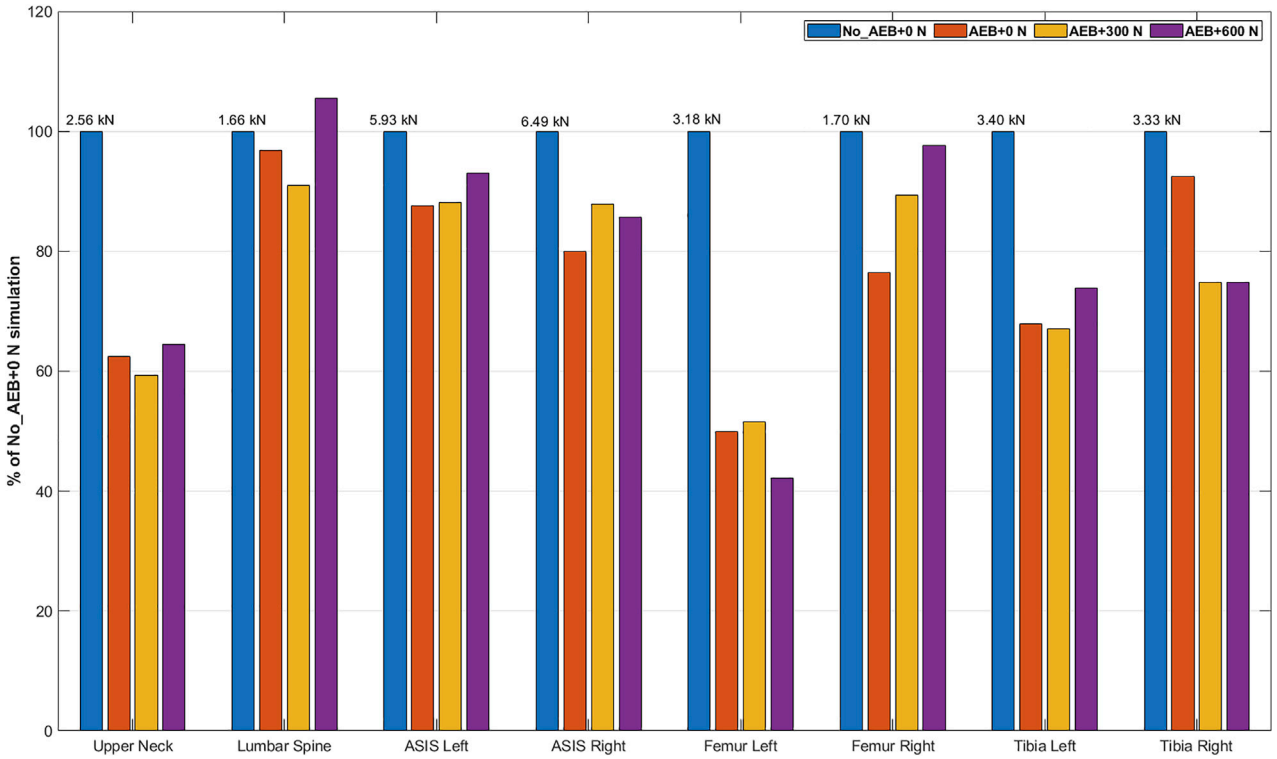

FIGURE 5 | Comparison of the upper neck tension forces, lumbar spine compression forces, and ASIS, femur, and tibia resultant forces across the four simulations. The values on the top of each blue bar represent the peak forces of each body region in the No_AEB+0N simulation which were normalized to 100%.

The lap belt forces and the pelvis displacements in the crash phase followed the same trend as the pelvis ASIS forces, i.e., they were reduced due to AEB but mostly unaffected by PPT.

The leg to instrument panel contact was severe in the No_AEB+0N simulation, particularly on the left leg which explains the high forces in the left femur and left tibia. The left leg hits the glove box near its hinge, while the right leg hits near the center of the glove box. This, along with the higher severity of the No_AEB+0N simulation could explain the high forces in the left leg in the No_AEB+0N simulation. With the increase in PPT force, femur and tibia forces decrease as the leg to instrument panel contact is less severe. There is no consistent relationship between the increase in PPT force and the femur and tibia forces.

AEB was shown to substantially reduce injury risks at high impact speeds, even with an AEB duration of only 0.5 s. However, the reduced impact speed does not linearly translate to injury risk and loading reductions to all body regions as pre-crash occupant displacement and interaction with the vehicle interior and restraint systems substantially influence loading to the body regions and injury risks as well. These findings are consistent with previous studies which have also reported a mixed effect of PPT on injury risks (Saito et al., 2016; Matsuda et al., 2018). The injury reduction effect of AEB needs to be studied with an integrated safety analysis (Matsuda et al., 2018), analyzing the effect of interventions in the pre-crash and crash-phase together. Advanced occupant restraints, such as PPT, can ameliorate the effects of AEB as shown in this study and previous studies (Mages et al., 2011; Woitsch and Sinz, 2014; Östh et al., 2015).

Current crash test standards do not consider these aspects when evaluating occupant safety (Mages et al., 2011; Schoeneburg et al., 2011). Updates are needed. The current crash test standards should be adapted to an integrated active and passive safety evaluation. A first step could be to allow for pre-crash activation of restraints within existing passive safety assessment methods as already considered by Euro NCAP (Euro NCAP, 2017). Further, it has been demonstrated that speed reduction achievable by AEB can also be replicated in physical testing (Berg et al., 2011). However, current crash test dummies are not validated for pre-crash kinematics, and results of such physical testing therefore questioned. Virtual assessment with active HBM would allow seamless and biofidelic assessment of the pre-crash and crash phase. Harmonized integrated virtual assessment was developed in the OSCCAR project, a particular focus is on the validation of all components like vehicle environment, restraint systems, and HBM (Eggers et al., 2021). HBM-based assessment criteria for kinematics and injury can then be evaluated following a standardized virtual test procedure for occupant positioning, belt installation, etc. (Eggers et al., 2021).

We have analyzed the effects of AEB and PPT on occupant injury risks and loadings in high-severity crashes. However, there are limitations. The generalizability of these results can be questioned because the model represents one occupant in an upright sitting position wearing a seatbelt with no slack. The key

real-world aspects regarding variability of occupants, seating postures, AEB pulses, crash pulses, restraint systems and their trigger times are important and should be considered in future studies. In particular, the effect of age and BMI should be considered as they significantly affect the head forward displacements in braking (Reed et al., 2018).

A major simplification is the increased airbag pressure by decreasing ventilation hole area to avoid strike through, as injury risks in strike-though conditions could not be evaluated with the models used. Current production airbags do not achieve such high pressures. A pressure of about 30 kPa is considered normal for a full-frontal crash at 56 km/h impact speed. Even if the effect of increasing airbag pressure on strike through has been studied before (Boyle et al., 2020), our focus in this study was not to study airbags. Other systems e.g., dual-depth airbags, adaptive airbags, or adaptive venting exist that similarly can reduce risks of strike-through and can be investigated in more detail.

The Honda Accord FE model used to extract the crash pulses has also not been validated for crashes at an impact speed of 80 km/h.

There are limitations in the HBM as well. As injury risk curves for the neck, lumbar spine, pelvis, and lower extremity were not available, only qualitative comparisons were possible.

CONCLUSION

In this study, the effects of AEB and seatbelt pre-pretensioning on the occupant injury risks and loadings at high-severity crashes were evaluated. The FE simulation results using the SAFER A-HBM show that AEB results in substantially lower rib fracture risk, lower concussion risk, lower neck forces, lower pelvis ASIS forces, and lower forces in the lower extremities. There was little effect of AEB on the lumbar spine compression forces.

Adding a PPT reduced rib fracture risk: the higher the force, the higher the reduction. PPT has negligible effect on the upper neck tension, lumbar spine compression, and pelvis ASIS forces. Moreover, there was no clear relationship between PPT force and femur and tibia forces. However, increasing PPT force increased concussion risk which can be attributed to the delayed first airbag contact.

The lowest joint injury probability for rib fractures and concussion was at 0 N PPT for 45-year-old and at 600 N PPT for 65-year-old, the lowest loading to other body regions at 300 N PPT. While variations in occupant anthropometrics, crash conditions and restraint characteristics are needed, it appears nevertheless necessary to study AEB and restraint performance not in isolation, as currently done in regulation and rating programs, but together in an integrated safety analysis.

DATA AVAILABILITY STATEMENT

The original contributions presented in the study are included in the article/**Supplementary Material**, further inquiries can be directed to the corresponding author.

AUTHOR CONTRIBUTIONS

EM: methodology, formal analysis, visualization, project administration, simulations, and writing—original draft. KM: methodology, formal analysis, writing—original draft, reviewing and editing. BP: conceptualization, supervision, funding acquisition, and writing—reviewing and editing. NL: conceptualization, supervision, resources, methodology, and writing—reviewing and editing. All authors contributed to the article and approved the submitted version.

FUNDING

This work was carried out as part of the Active Human Body Models for virtual occupant response, Step 4, and Step 5 projects, which have received funding from FFI (Strategic Vehicle Research and Innovation), by VINNOVA, the Swedish Transport Administration, the Swedish Energy Agency, and the industrial partners (Autoliv Research, Dynamore Nordic AB, and Volvo Cars).

ACKNOWLEDGMENTS

The authors would like to thank our partners at SAFER—The Vehicle and Traffic Safety Centre at Chalmers, specifically Chalmers University of Technology, Dynamore Nordic AB, and Volvo Cars for their joint efforts in developing the SAFER HBM. The authors would also like to thank Dr. K. Mayberry for language revisions.

SUPPLEMENTARY MATERIAL

The Supplementary Material for this article can be found online at: https://www.frontiersin.org/articles/10.3389/ffutr.2022.883951/full#supplementary-material

REFERENCES

Aarts, L., and Van Schagen, I. (2006). Driving Speed and the Risk of Road Crashes: A Review. *Accid. Analysis Prev.* 38, 215–224. doi:10.1016/j.aap.2005.07.004

Berg, A., Rücker, P., and Domsch, C. (2011). "Presentation and Discussion of a Crash Test Using a Car with Automatic Pre-crash Braking," in Proceedings, ESV 2011, Gothenburg, Sweden, 11–318.

Bose, D., Crandall, J. R., Untaroiu, C. D., and Maslen, E. (2008). "Influence of Pre-collision Occupant Properties on the Injury Response during Frontal Collision," in IRCOBI Conference, Bern, Switzerland, 135–147.

Boyle, K., Fanta, A., Reed, M. P., Fischer, K., Smith, A., Adler, A., et al. (2020). Restraint Systems Considering Occupant Diversity and Pre-crash Posture. *Traffic Inj. Prev.* 21, S31–S36. doi:10.1080/15389588.2021.1895989

Brännström, M., Coelingh, E., and Sjöberg, J. (2014). Decision-Making on when to Brake and when to Steer to Avoid a Collision. *Int. J. Veh. Saf.* 1 (7), 87–106. doi:10.1504/ijvs.2014.058243

Cicchino, J. B. (2017). Effectiveness of Forward Collision Warning and Autonomous Emergency Braking Systems in Reducing Front-To-Rear Crash Rates. *Accid. Anal. Prev.* 99, 142–152. doi:10.1016/j.aap.2016.11.009

Dahl, J., de Campos, G. R., Olsson, C., and Fredriksson, J. (2018). Collision Avoidance: A Literature Review on Threat-Assessment Techniques. *IEEE Trans. Intell. Veh.* 4, 101–113. doi:10.1109/tiv.2018.2886682

Devane, K., Johnson, D., and Gayzik, F. S. (2019). Validation of a Simplified Human Body Model in Relaxed and Braced Conditions in Low-Speed Frontal Sled Tests. *Traffic Inj. Prev.* 20, 832–837. doi:10.1080/15389588.2019.1655733

Eggers, A., Schießler, M., Ott, J., Peldschus, S., Mayer, C., Berger, A., et al. (2021). *WP5 - Success Stories HBM Virtual Testing Procedures*.

Ejima, S., Ono, K., Holcombe, S., Kaneoka, K., and Fukushima, M. (2007). "A Study on Occupant Kinematics Behaviour and Muscle Activities during Pre-impact Braking Based on Volunteer Tests," in Proceedings of Ircobi (International Research Council on the Biomechanics of Injury) Conference 2007, Held Maastricht, the Netherlands, September 2007, 31–45.

Eugensson, A., Ivarsson, J., Lie, A., and Tingvall, C. (2011). "Cars Are Driven on Roads, Joint Visions and Modern Technologies Stress the Need for Co-operation," in The 22nd ESV Conference, Washington, DC.

Euro NCAP (2017). *Euro NCAP 2025 Roadmap, in Pursuit of Vision Zero*.

Euro NCAP (2022). *Full Width Frontal Impact Testing Protocol*. Euro NCAP.

Farmer, C. M. (2019). *The Effects of Higher Speed Limits on Traffic Fatalities in the United States, 1993–2017*. Arlington, United States: Insurance Institute of Highway Safety.

Fildes, B., Keall, M., Bos, N., Lie, A., Page, Y., Pastor, C., et al. (2015). Effectiveness of Low Speed Autonomous Emergency Braking in Real-World Rear-End Crashes. *Accid. Anal. Prev.* 81, 24–29. doi:10.1016/j.aap.2015.03.029

Forman, J. L., Kent, R. W., Mroz, K., Pipkorn, B., Bostrom, O., and Segui-Gomez, M. (2012). "Predicting Rib Fracture Risk with Whole-Body Finite Element Models: Development and Preliminary Evaluation of a Probabilistic Analytical Framework," in Annals of Advances in Automotive Medicine/Annual Scientific Conference (Association for the Advancement of Automotive Medicine), 109.

Iraeus, J., and Pipkorn, B. (2019). "Development and Validation of a Generic Finite Element Ribcage to Be Used for Strain-Based Fracture Prediction," in Proceedings of the IRCOBI Conference, Florence, Italy, 193–210.

Kim, W., Kelley-Baker, T., Arbelaez, R., O'Malley, S., and Jensen, J. (2021). *Impact of Speeds on Drivers and Vehicles–Results from Crash Tests*. Arlington, United States: Insurance Institute of Highway Safety.

Kleiven, S. (2007). Predictors for Traumatic Brain Injuries Evaluated through Accident Reconstructions. *Stapp car crash J.* 51, 81–114. doi:10.4271/2007-22-0003

Larsson, E., Iraeus, J., Fice, J., Pipkorn, B., Jakobsson, L., Brynskog, E., et al. (2019). "Active Human Body Model Predictions Compared to Volunteer Response in Experiments with Braking, Lane Change, and Combined Manoeuvres," in International Research Council on Biomechanics of Injury (IROCBI 2019), Florence, Italy, Sept 11–13, 349–369.

Lindman, M., Ödblom, A., Bergvall, E., Eidehall, A., Svanberg, B., and Lukaszewicz, T. (2010). *Benefit Estimation Model for Pedestrian Auto Brake Functionality*. Hannover: 4rd International Conference on Expert Symposium on Accident Research.

Mages, M., Seyffert, M., and Class, U. (2011). "Analysis of the Pre-crash Benefit of Reversible Belt Pre-pretensioning in Different Accident Scenarios," in Proceedings of the 22nd ESV Conference, Washington, DC.

Matsuda, T., Yamada, K., Hayashi, S., and Kitagawa, Y. (2018). "Simulation of Occupant Posture Changes Due to Evasive Manoeuvres and Injury Predictions in Vehicle Frontal and Side Collisions," in Annu Proc IRCOBI Conf., Athens, Greece, 512–523. IRC-18-81.

Meijer, R., Elrofai, H., Broos, J., and van Hassel, E. (2013). "Evaluation of an Active Multi-Body Human Model for Braking and Frontal Crash Events," in Proceedings, ESV 2013, Seoul, South Korea. Washington, DC: NHTSA.

Mroz, K., Östling, M., Klug, C., Höschele, P., and Lubbe, N. (2022). Supplementing Future Occupant Safety Assessments with Severe Intersection Crashes Selected Using the SAFER Human Body Model. *SAE Int. J. Transp. Saf.* 10. doi:10.4271/09-10-02-0011

Ólafsdóttir, J. M., Östh, J., and Brolin, K. (2019). "Modelling Reflex Recruitment of Neck Muscles in a Finite Element Human Body Model for Simulating Omnidirectional Head Kinematics," in IRCOBI Conference Proc., Florence, Italy, 308–323.

Olafsdottir, J. M., Östh, J., Davidsson, J., and Brolin, K. (2013). "Passenger Kinematics and Muscle Responses in Autonomous Braking Events with Standard and Reversible Pre-tensioned Restraints," in Ircobi Conference 2013, Gothenburg, Sweden, 602–617.

Östh, J., Brolin, K., and Bråse, D. (2015). A Human Body Model with Active Muscles for Simulation of Pretensioned Restraints in Autonomous Braking Interventions. *Traffic Inj. Prev.* 16, 304–313. doi:10.1080/15389588.2014.931949

Östling, M., Daddetta, G. A., Lubbe, N., Silva, J. L. d., and Zimmer, A. (2022). "Safe-Up D4.2: Architecture of Passive Safety Systems (No. D4.2)," in *Proactive SAFEty Systems and Tools for a Constantly UPgrading Road Environment*.

Östmann, M., and Jakobsson, L. (2016). "An Examination of Pre-crash Braking Influence on Occupant Crash Response Using an Active Human Body Model," in Proceedings of the IRCOBI Conference, Malaga, Spain, 14–16.

Pipkorn, B., Iraeus, J., Björklund, M., Bunketorp, O., and Jakobsson, L. (2019). Multi-scale Validation of a Rib Fracture Prediction Method for Human Body Models," in Proceedings of the IRCOBI Conference, Florence, Italy, 175–192.

Reed, M. P. (2021). *The Importance of Considering Human Variability when Assessing Occupant Protection*.

Reed, M. P., Ebert, S. M., Jones, M. L. H., Park, B.-K. D., Hallman, J. J., and Sherony, R. (2018). Passenger Head Kinematics in Abrupt Braking and Lane Change Events. *Traffic Inj. Prev.* 19, S70–S77. doi:10.1080/15389588.2018.1481957

Robbins, D. H. (1983). *Anthropometric Specifications for Mid-sized Male Dummy, Volume 2, and for Small Female and Large Male Dummies*. Final report. Vol. 3. Ann Arbor, Michigan: The University of Michigan Transportation Research Institute.

Saito, H., Matsushita, T., Pipkorn, B., and Boström, O. (2016). "Evaluation of Frontal Impact Restraint System in Integrated Safety Scenario Using Human Body Model with PID Controlled Active Muscles," in Proceedings of the International Research Council on Biomechanics of Injury Conference, Malaga, Spain, 248–260.

Schoeneburg, R., Baumann, K.-H., Fehring, M., Ag, D., and Cars, M. (2011). "The Efficiency of PRE-SAFE Systems in Pre-braked Frontal Collision Situations," in Proceedings of the 22nd ESV Conference, Washington, DC, 11–0207.

Singh, H., Kan, C.-D., Marzougui, D., Morgan, R. M., and Quong, S. (2016). *Update to Future Midsize Lightweight Vehicle Findings in Response to Manufacturer Review and IIHS Small-Overlap Testing (No. Report No. DOT HS 812 237)*. Washington DC, USA: National Highway Traffic Safety Administration.

Spitzhüttl, F., and Liers, H. (2019). "Calculation of the Point of No Return (PONR) from Real-World Accidents," in 26th International Technical Conference on the Enhanced Safety of Vehicles (ESV): Technology: Enabling a Safer Tomorrow, Eindhoven, Netherlands (National Highway Traffic Safety Administration).

van Rooij, L., Pauwelussen, J., den Camp, O. O., and Janssen, R. (2013). "*Driver Head Displacement during (Automatic) Vehicle Braking Tests with Varying Levels of Distraction*," in 23rd ESV Conference on Enhanced Safety of Vehicles, May 27–30. Seoul, Korea: NHTSA.

Woitsch, G., and Sinz, W. (2014). Influences of Pre-crash Braking Induced Dummy–Forward Displacements on Dummy Behaviour during EuroNCAP Frontal Crashtest. *Accid. Anal. Prev.* 62, 268–275. doi:10.1016/j.aap.2013.10.012

World Health Organization (2018). *Global Status Report on Road Safety 2018: Summary*. Geneva: World Health Organization.

Conflict of Interest: The authors work at Autoliv Research, located in Vårgårda, Sweden. Autoliv Research is part of Autoliv (https://www.autoliv.com), a company that develops, manufactures, and sells for example protective safety systems to car manufacturers. Results from this study may impact how Autoliv choose to develop their products.

Publisher's Note: All claims expressed in this article are solely those of the authors and do not necessarily represent those of their affiliated organizations, or those of the publisher, the editors and the reviewers. Any product that may be evaluated in this article, or claim that may be made by its manufacturer, is not guaranteed or endorsed by the publisher.

frontiers | Frontiers in Future Transportation

TYPE Original Research
PUBLISHED 22 August 2022
DOI 10.3389/ffutr.2022.914481

OPEN ACCESS

EDITED BY
Yong Han,
Xiamen University of Technology, China

REVIEWED BY
Guibing Li,
Hunan University of Science and Technology, China
Xiaowei Li,
Xi'an University of Architecture and Technology, China

*CORRESPONDENCE
Felix Ressi,
felix.ressi@tugraz.at

SPECIALTY SECTION
This article was submitted to Transport Safety,
a section of the journal
Frontiers in Future Transportation

RECEIVED 06 April 2022
ACCEPTED 19 July 2022
PUBLISHED 22 August 2022

CITATION
Ressi F, Leo C, Klug C and Sinz W (2022), Protection challenges in seat positions with large rearward adjustment in frontal collisions: An approach using stochastic human body model simulations.
Front. Future Transp. 3:914481.
doi: 10.3389/ffutr.2022.914481

Protection challenges in seat positions with large rearward adjustment in frontal collisions: An approach using stochastic human body model simulations

Felix Ressi*, Christoph Leo, Corina Klug and Wolfgang Sinz

Vehicle Safety Institute, Graz University of Technology, Graz, Austria

Novel seat positions enabled by self-driving cars have been investigated in various studies in recent years. However, there is little research on the effect of increased rearward seat adjustments. To predict challenges associated with the possibility to move the seat further backwards in the car than currently possible as driver, appropriate methods have to be defined. A detailed human body model, a THUMS v4.1 in particular, tissue-based injury risk evaluation methods, a generic vehicle interior and a Latin hypercube design of experiments taking the variability of real-world crashes into account was established. In a first step, 200 simulations at current representative seat positions and a driving occupant posture were performed. The results were then compared to field data from an accident database to evaluate the accuracy of the method. The predictions exceeded the injury risks for the abdomen, head, and upper extremities, while underestimating the risk for thoracic and lower extremity injuries. A good match was observed for injuries of the neck and spine. In a second step, the 200 simulations were run again, but with the seat adjusted rearwards significantly. In this seat configuration, with the exception of the head and the upper extremities, increased injury risks were predicted for all body regions. The highest increases affected the lower extremities (+28%)—predominantly pelvic fractures—and the neck (+9%). In addition, (partial) submarining occurred in almost 50% of cases with the rearward adjusted seat—as opposed to none in the conventional seat position. The established method could be used in future studies to design safety measures addressing these identified potential safety risks.

KEYWORDS

occupant safety, novel seat configurations, accident data analysis, human body models, stochastic analysis and modelling, injury prediction

1 Introduction

Car occupants still account for 64% of road traffic fatalities in the United States (US) and 48% in Europe respectively (WHO, 2018). Not having met the previous goal of halving road traffic fatalities between 2010 and 2020 (European Commission, 2021), the European Union (EU) has set an even more ambitious goal for 2050: "Vision Zero," i.e., zero road fatalities and no serious injuries (European Commission, 2018). Likewise, the US have recently adopted a road safety vision striving to eliminate crashes which result in death or serious injury (US DOT, 2022). While such considerable reductions will not be achieved with measures in a single area, institutions in Europe and the United States have emphasized the important role automated vehicles could play in increasing road safety (UNECE, 2018; NSTC and US DOT, 2020). While ideally, they should avoid all accidents, in reality, accidents will still occur (Milakis et al., 2017). Therefore, they need to provide a high degree of passive safety for their occupants—at least equivalent to that of conventional, modern passenger cars (NHTSA, 2022). This can be seen as a kind of fallback in case a crash occurs. However, automated vehicles potentially pose a particular challenge to the same passive restraint systems, which are designed to provide the occupant safety fallback. Aside from the expected safety benefits, automated vehicles also enable drivers to take novel seat positions when there is no need for them to control the vehicle (Poulard et al., 2020). Examples for such positions include seats rotated about the z-axis, more reclined backrests or seats which are moved rearwards, away from the vehicle controls. Some of these possible configurations are already available to passengers in conventional vehicles. In a recent study, which analyzed in-car videos, passengers were found to position their seat "full-rear on the seat track 23% of the time and rearward of the mid-track position in 92% of frames" (Reed et al., 2020). Assuming that occupants on the driver's side, who are not engaged in driving the vehicle, behave similar to passengers in conventional vehicles, this highlights the relevance of the large rearward adjustments for occupants in automated vehicles. While it is believed that this change in occupant position could affect restraint system performance in frontal collisions (Ressi et al., 2019; Reed et al., 2020), the effects of this seat adjustment on occupant injury risk are currently not fully understood.

In a simulation study, Laakmann et al. (2019) demonstrated increased injury measures in what they refer to as "working position." Here, the seat was put in its rearmost position and the backrest was reclined by an additional 15° from its 25° standard configuration. Therefore, the effect of the longitudinal adjustment cannot be isolated from these results. An anthropomorphic test device (ATD) was used to model the occupant and assess injury metrics. Compared to the standard driving position, the injury assessment metrics for the head, neck, acetabulum, and the tibia increased the most. By updating the restraint systems (most notably the seat design and airbag geometry), the authors showed that with the exception of the tibia bending moment all considered injury measures could be lowered below their respective upper performance limits as proposed for the updated US NCAP tests (NHTSA, 2015). In the study, the occupant is modelled using a THOR ATD. Studies have shown limitations when using crash test dummies for evaluations in novel seat configurations, even when using this state-of-the-art device (Poulard et al., 2020).

In a study focusing on kinematics and the occurrence of submarining, Gepner et al. (2019) investigated the influence of various combinations of backrest recline angle and knee bolster (KB) position. The different KB positions can also be thought to represent different longitudinal seat adjustment relative to a fixed KB. To model the occupant, a human body model was used. Specifically, three anthropometries (female 5th, male 50th, and male 95th percentile) of the Global Human Body Model Consortium's occupant simplified (GHBMC-OS) model. With the backrest in the upright position, no submarining occurred for any of the three anthropometries in any KB configuration (near, standard, far, and no KB). Due to the chosen modeling approach, which detaches the knee bolster from the interior to represent different seat configurations by means of altered KB positions, the feet are always in the same position relative to the footwell. In reality, if different distances to the KB are the result of longitudinal seat adjustments, they are also going to lead to different distances between the feet and the footwell. This in turn would influence the loading of the lower extremities and subsequently the whole occupant. The driver side was not investigated in the study, as focus was set on the passenger side.

At least in the United States, vehicles are currently exclusively occupied by a driver 58% of the time (Reed et al., 2020). The self-driving mode offered in the first self-driving vehicles on the market is only going to be available in certain conditions, meaning the driver's seat is still going to be occupied in any case. This underlines the importance of addressing the driver's side too—particularly in case the vehicle's controls are not retracted when it is in self-driving mode.

In previous studies, mainly crash pulses from rigid wall crash tests were applied. While it can be argued that this kind of load case is well understood and widely used to represent a kind of worst case, it also only represents a single scenario (a full overlap high severity collision). Since they are the basis for occupant safety assessments, the restraint system parameters are usually optimized for these load cases. Investigating a broader range of possible scenarios in such simulation studies could improve the understanding of injury risks in load cases which are not a core part of the vehicle performance specifications. Also, robust occupant protection in these non-standard scenarios could be essential when considering the goal of eliminating road traffic fatalities and serious injuries, i.e., "Vision Zero" (European Commission, 2021; US DOT, 2022).

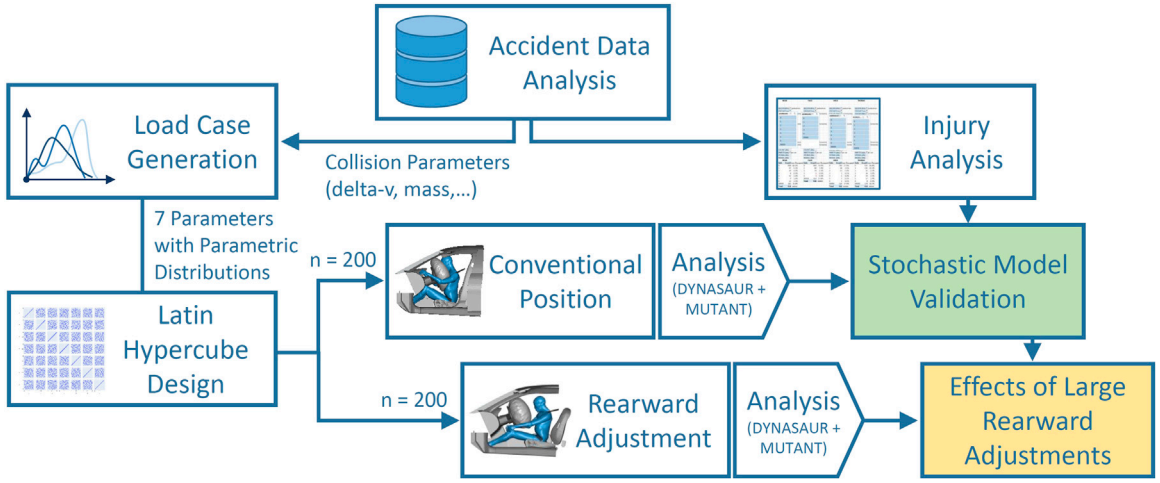

FIGURE 1
Graphical representation of the approach of the present study.

A previous study, aiming to replicate the injury frequencies found in a dataset from the Initiative for Harmonization of Global In-depth Traffic Accident Data (IGLAD) with a human body model (HBM), included a range of frontal crash pulses (Ressi et al., 2020). A Total Human Model for Safety (THUMS) v4.02 adult male 50th percentile (AM50) HBM was positioned in a generalized vehicle interior with varied restraint system parameters and subjected to various crash pulses. While the relative frequencies of injuries to the spine and the lower extremities predicted by the HBM (strain-based assessment of cortical bone fracture) matched the injury prevalence in the real-world accident sample well, this was not the case for all body regions. Particularly for the brain and the internal organs, the strain-based criteria used in the HBM (strain thresholds of 0.3 and 0.4 were used) overestimated the injury frequency found in the real-world data. Although the vehicle interior model used in the study was generalized, it was a proprietary model provided by an OEM. A number of model input parameters were varied to account for differences in the vehicle fleet. Nevertheless, a more generic average vehicle interior would be an ideal basis in this context. Furthermore, while a range of crash pulses was used, they were based on rigid wall crash tests. In their discussion, the authors acknowledged that using crash loads from real-world collisions is likely to represent an improvement (Ressi et al., 2020).

In conclusion, there are several studies (even beyond the ones cited above) addressing specific issues related to the effects of large rearward seat adjustments on occupant safety. What is lacking though, is a more generic perspective, enabling a broader understanding of the occupant safety related challenges, which novel seat configurations like increased rearward adjustments could imply. The present study introduces an approach which aims to estimate these challenges by addressing the following key points:

- Utilization of a generic vehicle interior (GVI) representing a driver's side, combined with a
- Detailed human body model, enabling tissue-based injury prediction, subjected to a
- Broad range of real-world loading conditions instead of crash test load cases, facilitating the
- Investigation of the effects of various generic seat adjustments with
- Comparisons to injury rates derived from real-world accidents.

2 Materials and methods

An overview of the methods used in the present study is shown in Figure 1.

Initially, data from the Initiative for Harmonization of Global In-depth Traffic Accident Data (IGLAD) accident database were analyzed. Filters were applied and the remaining cases were analyzed with respect to the most severe injuries occurring in each body region. In a separate analysis, parametric distributions were fitted to the collision parameters (e.g., delta-v, mass) of these cases. Additional parameters, representing the variability in the restraint systems (e.g., the airbag trigger time), with their respective distributions were derived from literature. In total, seven parameters were then combined in a Latin hypercube design resulting in 200 individual parameter combinations. In the first simulation phase, these 200 cases were run with the human body model (HBM) in a generic interior model (GVI) in a

conventional seat configuration. The results of these stochastic simulations were then analyzed and the HBM injury predictions were compared to the injury analysis based on the IGLAD sample. Hence, the accuracy of the HBM-based injury prediction for different body areas was evaluated. Subsequently, in the second simulation phase, the simulations were run again. The same parameters were re-used, apart from the seat position. The latter was varied between 150 and 250 mm rearwards of the conventional position, representing a novel seat configuration enabled by self-driving cars. In the final step, the results from the HBM injury predictions of the two sets of simulations were compared. Based on this analysis, the protection challenges in seat positions with large rearward adjustment in frontal collisions were estimated. The following sections describe the individual steps in more detail.

2.1 Accident data analysis

IGLAD data from 2007 until 2019 were used as the basis for the accident data analysis. The sample was filtered similarly to the previous study (Ressi et al., 2020). Specifically, only cases with two participants, at least one of them being a passenger car were included. Only frontal collisions (main deformed vehicle area: front) with other passenger cars, SUVs, vans or light trucks were considered. Filters were also applied to only include cases with a principal direction of force (PDOF) between 11 and 1 o'clock and exclude cases with small-overlap (i.e., cases without engagement of the longitudinal beams), unknown change in velocity due to the collision (delta-v) or unknown vehicle mass. Collisions where rollover occurred were not considered. The cases were then filtered for belted male drivers. This resulted in 694 cases, 52 of which were dropped because no information of the maximum injury severity according to the abbreviated injury scale (MAIS) (Association for the Advancement of Automotive Medicine, 1998) per body region was available. A Weibull distribution was fitted to the delta-v values of the remaining cases using python (v3.9, library "Reliability Engineering toolkit for Python" v0.8.1). Figures and parameters are provided in Supplementary Material. Subsequent to the parameter identification for the delta-v distribution, the sample was filtered further, to only include cases within a certain delta-v range for the injury assessment. Specifically, only cases with delta-v between 26 and 68 km/h were considered. The reason behind setting a lower threshold was to create a consistent dataset, to which the finite element simulations (described in Section 2.2) could be compared to. The median delta-v value in the IGLAD sample was found to be 26 km/h. However, based on other studies, injury risks for delta-v below this value are expected to be only minor. For instance, Weaver et al. (2015) reported a maximum of 4% AIS2+ risk at this delta-v. Therefore, our focus was on the upper half of the data and 26 km/h was selected as the lower boundary for the simulations. The upper limit was chosen to exclude cases in which delta-v was above the values typically found in crash test data. To get an estimate for a suitable limit, data from moderate overlap crash tests from the Insurance Institute for Highway Safety (IIHS) were analyzed. In these tests, the vehicle impacts a deformable barrier at 64.4 km/h with an overlap of 40% (IIHS, 2021), representing a vehicle to vehicle collision (IIHS, 2022). The mean delta-v observed in the 43 analyzed tests was 68 km/h, which was subsequently chosen as an upper threshold for the further analysis. Additionally to setting the upper delta-v threshold, cases with large intrusions were omitted as this was out of scope for the current study focusing on potential risks for rearward adjusted seat positions. Specifically, this was based on the value of the maximum extent of penetration, as defined by the Collision Deformation Classification (CDC) and cases above extent 5 were excluded.

The remaining 290 cases were then used to derive the two other distributions needed for the stochastic simulations. A Weibull distribution was fitted to the vehicle mass and a normal distribution was fitted to the PDOF (figures and parameters provided in Supplementary Material). All cases were assessed with respect to the struck side of the collision partner. The collisions were divided into three groups, depending on whether the front of the striking passenger car struck the opponent in the front (F2F), the side (F2S) or the back (F2B). With 50.9%, the majority of collisions were in the F2F configuration, followed by F2S (38.6%) and F2B (10.5%) collisions.

With all filters applied, the MAIS injuries of the 290 drivers in the sample were analyzed at body region level. In order to obtain relative MAIS + injury frequencies for each body region, the number of MAIS injuries at each level (MAIS6 up to MAIS1) was cumulated and divided by the total number of cases.

Finally, the age distribution in the sample was determined in order to aid age-based injury assessment. A majority of 60% of drivers in the real-world sample was between 17 and 41 years old, 26% between 41 and 65 and 14% were between 65 and 89 years of age. A histogram illustrating this distribution is provided in the Supplementary Material.

2.2 Stochastic finite element simulations

2.2.1 Generic vehicle interior

To model the vehicle, an available open-source generic vehicle interior (GVI) model (Iraeus and Lindquist, 2016) obtained from the openVT platform was used. The model was originally derived from laser scans of 14 cars and validated with their respective crash test data to analyze driver rib fractures in nearside oblique frontal accidents (Iraeus, 2015; Iraeus and Lindquist, 2016). Variants of the model have since been used to analyze the influence of crash pulse parameters on rib fractures (Iraeus and Lindquist, 2020) and study rib fracture risk as a function of age and rib strain (Larsson et al., 2021). For use in the

TABLE 1 Stochastically varied input parameters in the FE simulations.

Parameter	Unit	Distribution	Source
Delta-v	km/h	Weibull: scale = 32.2, shape = 1.7	IGLAD sample (n = 642, entire delta-v range)
Mass	kg	Weibull: scale = 1,474, shape = 5.3	IGLAD sample (n = 290, filtered delta-v range)
PDOF	°	Normal: μ = −5.4, σ = 19.2	IGLAD sample (n = 290, filtered delta-v range)
Pulse duration	ms	Normal: μ_{F2F} = 109.6, μ_{F2S} = 105, μ_{F2B} = 117.2, σ = 16.2	Iraeus and Lindquist, (2015)
TTF DAB	ms	Weibull: scale = 33.9, shape = 3.8	IIHS crash tests data (Supplementary Material)
SFLIM	kN	Normal: μ = 3.94, σ = 0.69	Iraeus, (2015)
Seat-X	mm	Uniform (0–25)	Based on average root-mean-square error (RMSE) for lower extremity landmark x-position in (Park et al., 2016)
Seat-X_{AD} (large rearward adjustment)	mm	Uniform (150–250)	Lower level based on seat travel in conventional modern vehicles (see Supplementary Table S1 in Supplementary Material)

present study, a number of modifications were made to the model. As only (oblique) frontal collisions were modelled in the present study, the parts used to model lateral collisions and lateral intrusions into the occupant compartment were removed. This resulted in a run time reduction of about 50%, which lead to an approximate total run time between 6:45 and 7:15 h on 32 cores for a simulation duration of 150 ms. Details on the hard- and software used in the present study are provided in the Supplementary Material. While the model can simulate intrusions into the passenger compartment by moving the end of the footwell towards the occupant, no cases with intrusions were considered in this study. Therefore, the open section on the inboard side of the footwell, which could accommodate for the deformations of the footwell material, was closed with elements of the same material as the footwell part. This was a precautionary measure to avoid contact instabilities in case the HBM feet were to slip into the crevice in simulated far-side oblique collisions.

2.2.2 Crash pulse generation

The application of crash loads in the GVI was modelled as a prescribed motion of the body in white. This means the model is accelerated in positive X direction (against the driving direction) as determined by the crash pulse from a standstill, similar to an inverse sled test.

A crash pulse can be calculated within the GVI model, based on a regression model derived from real-world crash data (Iraeus and Lindquist, 2015). The calculation uses an average crash pulse, to which five individually scaled eigenvectors are added. The resulting pulse is then scaled to the delta-v and crash pulse duration used for the current crash configuration. In their study, they also detail the regression models for each of the five eigenvalues which are used to scale the eigenvectors (Iraeus and Lindquist, 2015).

In the present study, only the normal distribution (which is a result of the regression model) for the pulse duration was considered (Table 1). For the eigenvalues, the means of the normal distributions from Iraeus and Lindquist (2015), calculated based on their respective regression models, were used. Only car-to-car collisions were considered in the present study, hence the IGLAD sample was filtered accordingly. Since no information on crash pulse duration was available in the IGLAD data, this parameter was estimated based on the regression model published by Iraeus and Lindquist (2015). For the vehicle mass, the parametric distribution derived from IGLAD was used.

2.2.3 Stochastic variation of input parameters

To approximate the average behavior of the vehicles in the IGLAD sample, seven input parameters for the model were varied stochastically. These were selected because they were found to have the highest practical significance in the original model (Iraeus, 2015) or were necessary as input for the pulse generation (mass). Table 1 lists these input parameters for the model and their respective properties.

Parametric distributions were used to specify the individual parameters. As described in Section 2.1, parametric distributions for delta-v, mass, and PDOF were derived from the filtered IGLAD sample. The parameters for the crash-pulse are described in the previous section.

No information on shoulder belt force limits (SFLIM) or airbag trigger times (time to fire driver airbag, TTF DAB) is included in the IGLAD data. Hence, the distribution for the shoulder belt force limit was adopted from the original GVI publication (Iraeus, 2015) and the trigger time distribution was approximated based on a set of moderate overlap crash tests (see Supplementary Material for details). Hence, the airbag deployment times for each simulated collision were selected without considering collision parameters (e.g., delta-v, time-history curves of acceleration, etc.). This does obviously not reflect how real-world airbag control units (ACUs) work. The algorithms determining whether (and when) to deploy airbags are proprietary and to the best knowledge of the authors, no generic ACU algorithm validated with real-world collisions is

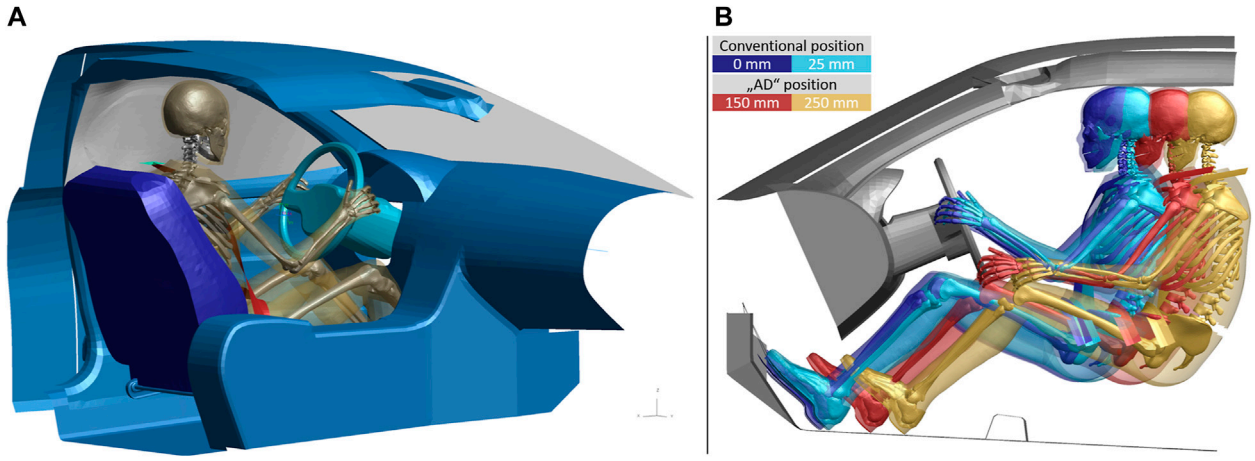

FIGURE 2
(A) Complete GVI model with the positioned HBM. **(B)** Visualization of posture differences and possible adjustment ranges for the simulations of the conventional seat position (blue and cyan HBMs on the left) and the large rearward adjustments (red and orange HBMs on the right). All distances given relative to the conventional position. Note that only the HBM's bony structures and parts of the skin are visualized for illustrative purposes.

available in literature. While in a previous study, a simple algorithm derived from rigid wall crash test data was presented (Ressi et al., 2020), it did not produce satisfactory results with the moderate overlap crash test data and was therefore rejected for the present paper. In a recent study using the GVI, the airbag TTD was estimated using the median value derived from event data recorders (Iraeus and Lindquist, 2020). Since the TTD values observed in the 43 moderate overlap crash tests varied between 16 and 52 ms for the same well-defined collision scenario (i.e., identical initial velocity, overlap, and barrier configuration), a random TTD selection was deemed more realistic for the present study than a single median value for all cases.

The final input parameter was the longitudinal seat position (Seat-X). For the initial set of simulations, to account for variation in the exact seat position, the seat (with the HBM) was moved rearwards up to 25 mm from the initial position. This maximum value was based on the regression model used for the posture prediction. The model specifies a root-mean-square error (RMSE) in X direction for each landmark. The RMSE values for the lower extremity landmarks (ankle, knee, and hip) are 21.8, 23.4, and 31.5 mm respectively. On average, this amounts to about 25.6 mm, which was rounded down to 25 mm. The seat adjustment was not modelled as a pure X displacement, but rather along the direction of the floor, which rises from the rear towards the front at an angle of approx. 2.8°. This angle can clearly be seen in Figure 2B. By applying the seat adjustment this way, intersections between the shoes and the floor can be avoided without the need to reposition the HBM. To avoid having to create a new belt fit for each of these seat positions, a simplification was made in moving the entire seat belt assembly with the seat and the occupant. While in reality, the shoulder belt routing would change slightly in each of the seat positions behind the initial position, the influence at a maximum seat movement of 25 mm was regarded to be negligible.

To create the population of stochastic simulations, a maximum projection Latin hypercube design (LHD) (Joseph et al., 2015) was created based on the seven parameters listed in Table 1. A matrix size of 200 combinations was chosen, which corresponds to almost three times the recommended minimum number of at least ten characteristic values per variable (Peduzzi et al., 1995). It was created using the MaxProLHD function (Joseph and Ba, 2018) implemented in R (R software, version 4.0.3; MaxPro package version 4.1–2). This function aims to achieve a uniform space filling (i.e., distribution of parameters) in the multi-dimensional design space (Joseph et al., 2015). The resulting design matrix contains 200 combinations of the seven specified continuous input factors, with the individual values for the factors taking values between zero and one. To use this design as input in the FE simulations and account for the respective parametric distributions, the factors had to be mapped to the values of the input parameters based on their respective cumulative distribution functions (CDFs) with the exception of the seat position. For the latter, the factor was scaled uniformly within the boundaries of the seat adjustment (conventional/self-driving), to obtain the desired position range. Since the normal distribution for the pulse duration depends on the collision type, the simulation matrix was randomly divided into three sub designs before the mapping—one for each collision type (F2F, F2S, and F2B). To map the results of the IGLAD sample to the simulations, the number of cases for each collision type was based on the respective share observed in the 290 real-world accidents (50.9%, 38.6%, and 10.5%). To take the filter range for the

delta-v values into account, the respective mapping was preceded by an additional step. Prior to the mapping based on the CDF, the CDF probabilities for the lower and upper limits were determined. These were then used to scale the delta-v factors in the LHD from values between [0, 1] and [0.49, 0.96]. A plot illustrating this procedure as well as scatter plot matrices of the simulation parameters are provided in the Supplementary Material.

2.2.4 Simulations with large rearward adjustment in self-driving cars

For the simulations with large rearward adjustments of the seat, the exact same parameter combinations for the collision and the restraint systems as for the initial simulation set were used again—except for the seat adjustment. This can be thought of as the same collisions re-occurring with the novel seat configuration. To determine reasonable values for the seat rearward adjustment (Seat-X_{AD} in Table 1), for a self-driving car the fore-aft travel of the driver seat of 16 vehicles, tested by the NTHSA in 2021, were evaluated (details provided in Supplementary Material). In these vehicles, the mean fore-aft travel for the driver seat was about 300 mm. This means that in these conventional vehicles, the driver could—on average—move their seat rearwards by 150 mm from the mid position before reaching the end of the seat tracks. Therefore, 150 mm was used as a lower limit for the seat adjustment, as this represents an amount of adjustment which is already available today. An additional 100 mm of rearward adjustment were chosen to define the maximum value of 250 mm. To make the setup more realistic, changes were introduced to the belt mounting and the occupant posture. The seat belt slip ring at the D-ring was positioned from the b-pillar to a position just above and behind the seat back to replicate the D-ring position of a belt integrated seat. While the D-ring was positioned realistically, it was still mounted rigidly to the vehicle structure rather than the seat back. This simplification was made to avoid re-modelling the seat back joint stiffness. In addition to the changes to the GVI, the occupant posture was adapted to reflect these changes. The arm position was changed from the standard driving posture to a relaxed posture. Also, the legs and feet were positioned symmetrically, as opposed to the footrest/accelerator configuration used in the initial set of simulations. Figure 2B illustrates the differences between the two postures and possible adjustment ranges. Note that in this image some parts of the model (including the seat) are hidden to aid the comparison of HBM postures and positions.

2.3 Occupant model

To model the occupant, a detailed finite element HBM was used. The selected model was version 4.1 of the Total Human Model for Safety (THUMS, Toyota Central R&D Labs., Nagakutes) 50th percentile adult male, which is freely available since June 2020 (Toyota Motor Corporation, 2020). According to the manual, the model was developed with LS-DYNA (Ansys LST, Livermore, CA) mpp s R9.2.0 (Toyota Motor Corporation and Toyota Central R&D Labs., 2021). The validation load cases were performed with LS-DYNA mpp s R7.1.3. Since we aimed to perform the simulations using LS-DYNA mpp s R12, the THUMS component validation set was re-run in this environment. Graphs comparing the simulation results of the two solver versions to the experimental data are provided in the Supplementary Material. In most body regions, the results were indistinguishable. The only case showing appreciable deviations from results with the earlier LS-DYNA release was the lateral ball impact to the pelvis (Guillemot et al., 1997). In this test, neither the original simulation results with R7.1.3 nor the simulation results with R12 fit the underlying experimental data perfectly. The loading condition modelled in this test is mostly relevant in side crashes. Since lateral collisions were not considered in the present study, the use of the more recent LS-DYNA release was deemed acceptable. All simulations evaluated for this study were subsequently run on the same hardware on a single computing node utilizing 32 CPUs. This should ensure consistent results with limited numerical noise (Östh et al., 2021). Before including the HBM in the GVI, it was scaled from the original unit system (s-mm-t-N) to the desired unit system (ms-mm-kg-kN) using Oasys PRIMER (pre-processing software PRIMER v18, Oasys Limited).

The HBM position and posture were determined based on a regression model derived from volunteer tests (Park et al., 2016). The seat position was adjusted slightly to match configuration 6 (seat height 270 mm) of the model setups from Park et al. (2016). The anthropometry of the HBM and the median age of the drivers in the IGLAD sample, where age was known (n = 282, 36 years), together with the measurements of relative seat and steering wheel position (which were taken from the GVI) were then fed into the regression model. It consists of two formulas for X and Z position of eight landmarks. Park et al. (2016) also specify the RMSE for each landmark coordinate. A simulation was then set up using the dummy tree file for the THUMS v4.1 model for Oasys PRIMER. The target position for this marionette method positioning simulation (Mohamed and Newlands, 2021) was defined as closely as possible to the regression model landmark positions. The arms were positioned to a standard driving posture. The resulting landmark positions on top of the final HBM posture in the GVI are provided in the Supplementary Material.

Generic shoes from a pedestrian model (Feist, 2018) were added to the HBM feet to achieve a more realistic interaction with the footwell and pedals. For the initial set of simulations, which were aimed at modelling a standard driving posture, the left foot was placed on the foot support and the right foot was placed on the accelerator pedal, which had to be pressed down to avoid intersecting the shoe. Subsequently, the seat was deformed by

TABLE 2 Injury metrics for the HBM simulations. Strain limits for cortical bones are provided for the ages of 77, 53, and 29 years.

AIS region	Body region		Deterministic strain limits (77, 53, 29 yo)	Literature source	Associated AIS severity
1	Head	Brain (strain-based—MPS50)	—	Fahlstedt et al. (2022)	2+
		Brain (kinematic—DAMAGE)	—	Gabler et al. (2019)	2–4+
		Skull (MPS99)	1.7%, 2.6%, 3.5%	Golman et al. (2014)	3+
3	Neck	C1—C7 (MPS99)	1.7%, 2.6%, 3.5%	Golman et al. (2014)	3
4	Thorax	Ribs (MPS99)	—	Larsson et al. (2021)	1–3
5	Abdomen	Liver, spleen (MPS95)	40%	Watanabe et al. (2011)	2–3+
		Submarining (kinematic)	—		2+
6	Spine	T1—T12, L1—L5 (MPS99)	1.7%, 2.6%, 3.5%	Golman et al. (2014)	3
7	Upper extr	Clavicle (MPS99)	1.7%, 2.6%, 3.5%	Golman et al. (2014)	2
		Ulna, Radius, Humerus (MPS99)	1.7%, 2.6%, 3.5%	Golman et al. (2014)	2–3
8	Lower extr	Pelvis (MPS99)	1.0%	Snedeker et al. (2003)	2–3
		Femur (MPS99)	1.7%, 2.6%, 3.5%	Golman et al. (2014)	3
		Tibia, Fibula (MPS99)	1.7%, 2.6%, 3.5%	Golman et al. (2014)	2–3

moving a rigidified version of the HBM in the final posture into the target position, determined by the regression model, and finally the seat belt was fitted. The complete resulting model, ready to be run, is shown in Figure 2A.

2.4 Human body model injury metrics

With the exception of the face, which was not evaluated due to a lack of injury metrics, injury metrics for each AIS body region were used to predict moderate or worse injuries (AIS2, AIS2+). Table 2 lists the used injury metrics, the strain threshold (if applicable) and the respective literature sources.

While ideally, all injuries in all body regions would be evaluated using injury risk curves (IRCs), most body regions lack model specific IRCs. As a result, the injury metrics listed in Table 2 are a combination of probabilistic (brain, ribs) and deterministic (other body regions) criteria. In the latter case, a strain limit was used to distinguish between cases with and without injury. In some cases, multiple metrics were defined for one body region (i.e., skull fracture and brain injury for the head or fractures in any cortical long bone of the upper extremities). To ensure consistency with the IGLAD data, which only features data on MAIS per body region, multiple injuries in one body region were summarized to one risk, by using the maximum risk for each parameter configuration. Mostly, strain-based criteria were used, utilizing one of the main advantages of a detailed HBM such as THUMS v4.1. While enabling detailed analyses on tissue level, this also facilitates omnidirectional assessment.

The brain was assessed using the 50th percentile principal strains (MPS50) of the whole brain with the injury risk function (IRF) for mild traumatic brain injury (mTBI) validated for the THUMS (Fahlstedt et al., 2022). Additionally, brain injury was assessed using the kinematics-based diffuse axonal multi-axial general evaluation (DAMAGE) criterion (Gabler et al., 2019). These two criteria were assessed independently, facilitating comparisons of their results.

Cortical bone fractures in the long bones (clavicle, humerus, radius, ulna, femur, tibia, and fibula), vertebrae, pelvis and skull were evaluated using 99th percentile principal strains (MPS99) (Ressi et al., 2020). Three age-dependent strain limits (3.5%, 2.6%, and 1.7%) were derived (Golman et al., 2014) based on the age distribution in the IGLAD sample. The sample was divided into three age groups (17–41, 41–65, and 65–89) and the strain limits were calculated based on the mean ages of these groups (29, 53, and 77).

For pelvic fractures, a 1% strain limit was used; independently of the age group (Snedeker et al., 2003).

For the thorax, only rib fractures were considered. The risk of a specific number of fractured ribs (NFR) was calculated using the probabilistic approach from Forman et al. (2012). The strains used in this evaluation were the maximum tensile principal strains based on the maximum integration point per rib. These were subsequeently converted into an injury risk per rib using an age dependent log-normal distribution (Larsson et al., 2021) and combined to an overall risk of 2 + rib fractures using the binomial function from Forman et al. (2012).

Abdominal injuries were assessed based on strains in liver and spleen using a strain limit of 40% (Watanabe et al., 2011) for the 95th percentile strains (Ressi et al., 2020). Additionally, each simulation was checked visually whether the lap belt moved upwards on the pelvis and slid off the iliac crests. For load cases without intrusions into the passenger compartment, abdominal injuries are mainly attributed to this phenomenon, commonly

referred to as submarining (Nakane et al., 2015). Cases in which submarining occurred (even if only on one side), were then associated with abdominal injury. As with the two metrics for brain injury, these two metrics for abdominal injury were assessed independently from each other.

To calculate a relative injury frequency with the deterministic criteria, the number of cases above the strain limit was cumulated and divided by the total number of simulations. For the cortical bones, in order to account for the age dependent strain limits, the number of cases above the strain limit was initially evaluated for each age group separately. Subsequently, a weighted sum (using the respective share of the age group from the field data) was calculated. This sum was then divided by the total number of simulations. To evaluate the injury frequency for the brain, the individual injury risks determined for each case were summed up and then divided by the total number of simulations. The rib fracture evaluation was performed similarly. First, the NFR2+ risk (i.e., the risk for two or more fractured ribs) for each case was determined using the age-adjusted risk for each age group. The sum of the age specific NFR2+ risks, weighted by the respective share of the age group was then calculated. This resulting predicted number of cases with two or more fractured ribs was then divided by the total number of simulations, resulting in a relative (with respect to the sample) risk for two or more fractured ribs.

Cases in which the added mass due to mass scaling exceeded 5% of the model mass or which terminated prematurely were dropped from the further analysis. For the remaining simulations, all injury metrics were calculated in the open-source post-processing tool DYNASAUR (Klug et al., 2018). The tool MUTANT (Luttenberger et al., 2019) was used to create combined tables of all simulations and all their criteria.

3 Results

The MAIS2+ body region level injury frequencies observed in the IGLAD sample, as well as the MAIS2+ injury prediction obtained with the HBM from the two simulation setups are listed in Table 2. For the head and the abdomen, the results for the two independent metrics described in Section 2.4 are provided in the table (with the respective strain-based criterion in the left column, kinematic in the right column). A table showing the IGLAD evaluation for all MAIS levels is provided in the Supplemental Material. The next sections briefly describe the results.

3.1 Accident data injury analysis

After applying all filter criteria, 290 cases involving drivers in frontal oblique collisions remained for further analysis. Of these, 27% were not injured (MAIS0), 24% sustained moderate or worse (MAIS2+), and 11% sustained serious or worse (MAIS3+) injuries. More severe injuries occurred in 7% of all cases. The first row in Table 3 lists the MAIS2+ body region level injury frequencies from the IGLAD sample. This shows that the most frequently injured body region was the thorax (11.6%). It is followed by the lower extremities (9.5%) and the head (6.5%). It has to be noted though, that the upper extremities and abdomen also exhibit very similar injury frequencies (6.3% and 5.6% respectively).

3.2 Stochastic model validation

The second line in Table 3 presents the results from the stochastic simulations with the conventional driving position. Starting the comparison with the head, the two individual injury metrics (50th percentile principal strains in the brain and DAMAGE) both result in predictions of approximately 30%. This means that compared to the head injury risk observed in the IGLAD sample of 6.5%, both predictions are considerably higher. The bar chart in Figure 3A illustrates these differences between the injury rates in the IGLAD data and the predicted injury rates from the HBM simulations. Similar to the head, also the two individual metrics for the abdomen (95th percentile principal strains in the liver/spleen and the presence of submarining) yield different results. While the strain-based metric predict abdominal injuries in all cases, a review of all simulations showed that in none of the cases submarining occurred. Figure 3A illustrates the resulting overprediction of 94.4% and resulting underprediction of 5.6% for the two metrics. The injury frequencies of the thorax and the lower extremities are lower in the simulations than those observed in the real-world accidents, while the injury frequencies of the upper extremities are

TABLE 3 MAIS2+ body region level injury frequencies from the IGLAD sample and the two sets of FE simulations with conventional and automated driving (AD) seat positions. To ensure consistency, only the 185 simulations which terminated normally in both sets were considered.

Source	Seat position	Head		Face	Neck	Thorax	Abdomen		Spine	UX	LX
IGLAD (n = 290)	—	6.5%		3.6%	0.7%	11.6%	5.6%		2.1%	6.3%	9.5%
FEA (n = 185)	Conventional (0–25 mm)	29.6%	28.8%	—	0.2%	1.0%	100%	0%	0.0%	14.7%	2.2%
FEA AD (n = 185)	Rear (150–250 mm)	24.1%	25.0%	—	9.2%	4.2%	100%	48.1%	3.7%	10.6%	29.9%

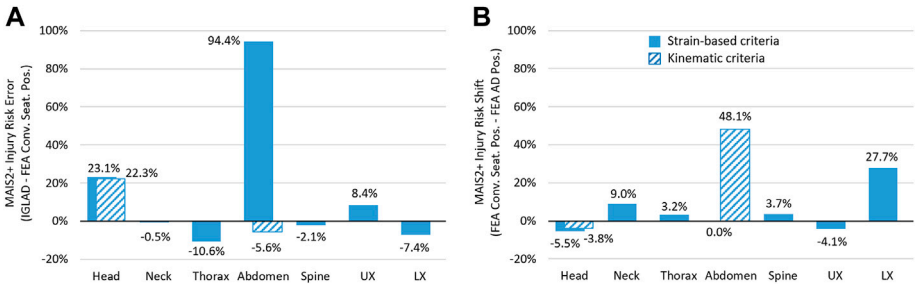

FIGURE 3
(A) Error between injury prediction from HBM and real-world accident data. **(B)** Shift in injury frequency as a consequence of the large rearward adjustments of the seat (using the criteria listed in Table 2).

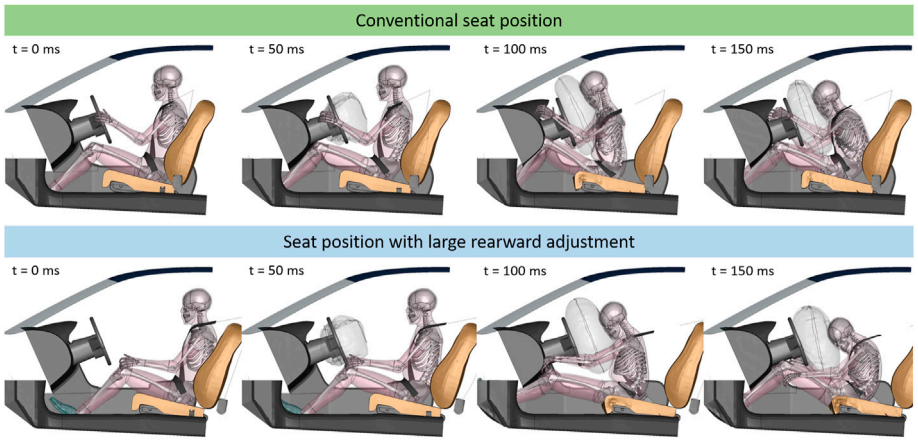

FIGURE 4
Still frames of case 557 (delta-v: 47 km/h). Top row shows kinematics for conventional seat position (21.8 mm behind max. forward position), lower row shows kinematics for seat adjusted 237.3 mm towards the rear. For visualization purposes, parts of the interior and HBM have been blanked.

overpredicted by the HBM. For the neck and the spine, the injury frequency observed in the real-world cases and the prediction based on the simulations is closely matched.

3.3 Effects of large rearward seat adjustments

The third line in Table 3 presents the results from the stochastic simulations with the seat in the rearward adjusted positions. Facilitating comparisons to the results in the conventional seat position, Figure 3B illustrates the shift in injury risk for each body region, based on the criteria listed in Table 3. The only body regions with reduced injury risk are the head and the upper extremities. In particular, the injury risk for the lower extremities is almost 28% higher in the simulations with the rearward adjusted seat. The risk for abdominal injuries is increased by almost 50% when using the presence of submarining as a metric, since in 89 of the 185 cases which were evaluated, the lap belt slid off the right iliac crest. With the strain-based criterion for abdominal organ injury predicting injuries in all cases—regardless of seat configuration—there is no difference between the two variants when evaluating this metric. Figure 4 shows still frames at four points in time from an exemplary simulation to facilitate the comparison of kinematics.

There are some noteworthy differences in terms of kinematics when comparing the two seat configurations. Due to the increased initial distance between the knees and the knee bolster, there is no load path into the femur. Therefore, the pelvis is only restrained by the lap belt. This leads to the legs extending and the feet impacting the footwell. Furthermore, in the rearward adjusted seat configuration, the thorax is restrained by the seat

belt almost exclusively and not by the airbag. Also, the steering column does not collapse and therefore does not absorb energy in this case. Another difference in kinematics concerns the upper extremities. In the conventional seat configuration, the hands are initially placed on the steering wheels. During the crash, the hands contact the instrument panel (IP) at an acute angle and slide up towards the windscreen. Due to the changed initial arm and seat position in the configurations with large rearward adjustments, the hands impact the IP at a more obtuse angle.

4 Discussion

4.1 Accident data injury analysis

The injury frequencies derived from the real-world accident database analysis are very similar to previously published data (Ressi et al., 2020). While the inclusion criteria differed slightly (most notably only cases with a PDOF of 0° were included in the previous study) both studies identified the thorax as the key injury region. With an injury rate of almost 10%, the present study identified the lower extremities as the second most injured body region. This notable difference to the 4% injury rate observed in the previous study can most likely be attributed to the lack of oblique crashes included due to the filter criteria. When filtering the current data set to only include head-on collisions, a lower extremity injury rate of less than 6% was observed, supporting this hypothesis (table showing IGLAD sample filtered for PDOF of 0° provided in the Supplemental Material). With 5.6%, abdominal injuries were considerably more prevalent in the present sample than previously (2%). Since limiting the analysis to head-on collisions also reduced the abdominal injury rate to 2.5%, this difference seems to be consistent with the different filter criteria. The remaining injury rates for the head, neck, spine and upper extremities were very similar.

4.2 Stochastic model validation

At an overall completion rate of 92.5%, the model robustness was deemed satisfactory. The premature terminations and excessive mass scaling (more than 5% of model mass) are mainly caused by unfavorable combinations of restraint system parameters in high severity crash pulses. At 96.5% (conventional seat position) and 93.5% (large rearward adjustments), the completion rates of the two individual sets of simulations were even higher. The study cited in the introduction, studying the effects of reclined seatbacks on kinematics and submarining, experienced completion rates as low as 67% for the GHMBC-OS 50th percentile model (Gepner et al., 2019). By excluding the results of simulations which did not meet the quality criteria in one of the configurations

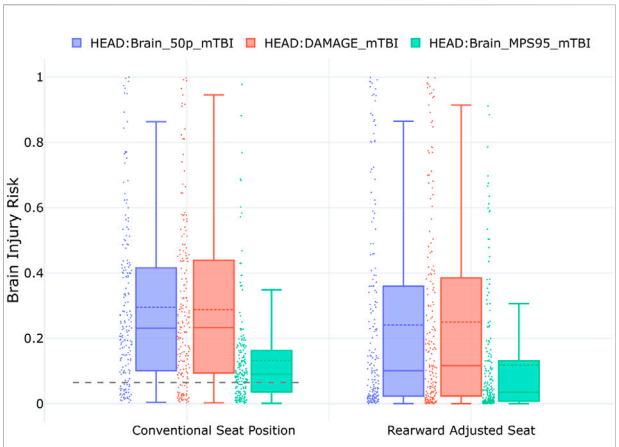

FIGURE 5
Boxplots for risk of mTBI based on three different brain IRFs. The three boxplots on the left show the results of the simulations with the conventional (n = 185), and the three on the right the results with the rearward adjusted seat position (n = 185). The gray dashed line represents the head injury risk observed in the IGLAD sample.

(conventional or rearward adjusted seat position) from both data sets, consistency was ensured.

When comparing the real-world data to the results from the simulations with the conventional seat position, mixed results were observed. While the absolute error with respect to injury risk for most body regions, as presented in Figure 3B, is below 10%, larger errors for the strain-based prediction for the abdomen (94%) and the head (23%) were observed. A similar overprediction of abdominal injuries was also observed in a previous study (Ressi et al., 2020) when using strain-based metrics. Abdominal MAIS2+ injuries were predicted for 100% of cases—for both seat configurations when applying the strain-based assessment. Considering that abdominal injuries only occurred in 5.6% of the real-world cases, this result does not seem plausible. However, when evaluating the simulations for submarining, none was observed in the conventional seat position. As a result, even though this represents an underprediction of 5.6%, it was deemed more plausible that no AIS2+ abdominal injuries (based on zero cases with submarining) should be predicted in these HBM simulations.

For the head, the injury risk error based on the strain-based criterion was 23%. Interestingly, at 22%, the error based on the kinematic criterion DAMAGE was almost identical. Using a different approach, Wu et al. (2022) found very similar differences in brain injury risk when comparing strain-based injury criteria calculated from crash test results to real-world accident data. There, for frontal collisions, the criteria based on principal strains in the GHBMC model overpredicted the real world injury rate by about 34% (Wu et al., 2022). As an additional comparison, the risk for mTBI, using the IRC presented by Wu et al. (2022) was also assessed in the present study. This risk curve

was developed with a GHBMC 50th percentile male and non-human primate brain models. Direct comparisons using IRFs developed for and from different models can be difficult (Wu et al., 2022). In the present study, the consideration of this brain injury metric represents an effort to check the strain-based results for plausibility. A plot illustrating the correlation between the two strain-based brain injury criteria is provided in the Supplemental Material. Figure 5 shows boxplots comparing brain injury risk evaluated with these three criteria: the mTBI risk based on 50th percentile strains (Fahlstedt et al., 2022), the mTBI risk based on the kinematic DAMAGE criterion (Gabler et al., 2019; Wu et al., 2022)—both listed among the metrics in —and the mTBI risk based on 95th percentile strains (Wu et al., 2022). As a reference, the 6.5% head injury risk observed in the IGLAD sample is represented in Figure 5 as a gray dashed line overlaid on the boxplots for the conventional seat position. A table listing the brain injury rates with the criteria mentioned above and additional boxplots for the risk of severe TBI are provided in the Supplemental Material.

The plots in Figure 5 show that for the conventional seat position, the mean brain injury risk (dashed lines in the boxplots) based on the 50th percentile principal strains is 29.6%. Notably, although it is based solely on the kinematics of the center of gravity of the HBM's head, the injury risk prediction based on DAMAGE is almost identical (mean of 28.8%). Compared to these two metrics, the IRF using 95th percentile strains predicts a considerably lower risk for mTBI (mean of 13.2%). The similarity between the results based on the IRF using MPS50 and DAMAGE is also remarkable when considering that they are based on very different data sources. While Fahlstedt et al. (2022) used lower-severity American football helmet measurements to derive the injury risk curves, Wu et al. (2022) created their risk curves from a combination of non-injurious tests with volunteers and tests with non-human primates. Even though DAMAGE is a kinematics-based criterion, it estimates the maximum principal strain in the brain. The criterion was assessed with 1747 head impacts, including volunteer, sports and automotive tests (Gabler et al., 2019). While the IRF using MPS95 is based on the same data as DAMAGE, the predicted risk is considerably lower. This can probably be attributed to the fact that the IRF was not tuned to the HBM used in the present study (THUMS v4.1) but to the GHBMC. The head injury criterion (HIC) was not used in the current study, as the poor correlation for brain injury risk prediction was shown in previous studies (Gabler et al., 2018).

In an earlier study with a THUMS v4.02 in a generalized interior, it was found that strain-based brain injury metrics overestimated the expected brain injury risk significantly (Ressi et al., 2020). In this study, AIS2+ brain injuries were predicted to occur in 95% of cases. Likewise, in the initial analysis in the present study, unrealistic brain injury risks in the range of 90% were observed. It was later discovered that these high strains were caused by a problem which occurs when scaling the unit system of THUMS v4.1 using the LS-Dyna keyword

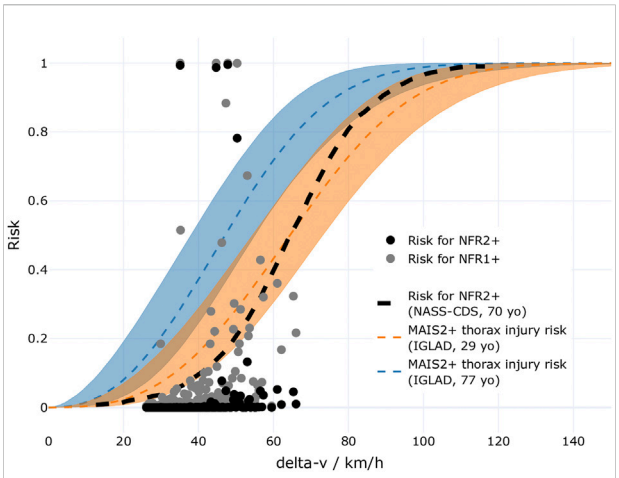

FIGURE 6
Comparison of MAIS2+ injury risk for the thorax based on the IGLAD sample (Weibull distributions for two age groups) and risks of NFR1+ and NFR2+ as a function of delta-v. The opaque areas around the curves indicate the 95th confidence intervals. Additionally, a risk curve for NFR2+ based on NASS-CDS data is shown.

*INCLUDE_TRANSFORM. After changing the way in which the HBM was scaled to the same unit system as the GVI (Section 2.3), lower strains were obtained, which are presented in the current paper. This indicates that the transformation integrated into LS-Dyna does not scale all necessary model parameters correctly, resulting in an excessively soft behavior of the brain. As the validation load cases, which were performed using LS-Dyna R12 for the present study, are provided in the THUMS base unit system, they were not affected by this issue. However, irrespective of these considerations, the injury risk observed in the IGLAD sample is still overpredicted by the simulations by 6.7%, 22.3% and 23.1% (based on MPS95, DAMAGE and MPS50 respectively). One important aspect in this could be the expected under-reporting of mTBI in accident databases (Wu et al., 2022), resulting in lower MAIS2+ head injury rates in the IGLAD sample. On the other hand, while the GVI was validated with crash test data from 14 vehicles using crash test dummies, the model was subsequently utilized primarily for strain-based rib fracture prediction (Iraeus, 2015; Iraeus and Lindquist, 2016; Iraeus and Lindquist, 2020; Larsson et al., 2021). Additional GVI model validation focusing on the head-airbag-interaction could potentially improve the results.

The HBM predicted AIS2+ thorax injuries (based on rib fractures) in only 1% of the cases. This is considerable lower than the 11.6% thoracic injury frequency observed in the IGLAD sample (listed in Table 2). To check these results for plausibility, the "Forman smoothed" IRF (Iraeus and Lindquist, 2020) was also implemented. While at 1.32%, this function predicted a slightly higher rate of AIS2+ thorax injuries, this rate is still considerably smaller than the real-world observation. Figure 6

shows a combination of plots. In the background, two Weibull distributions are shown. They were fitted to the thoracic AIS2+ injuries observed in the IGLAD sample as a function of delta-v. The two distributions are based on two age groups (mean of 29, and mean of 77 years). Additionally, the risk for NFR1+ and NFR2+ for a 77-year-old occupant, evaluated for each parameter combination in the stochastic simulation study, and a NFR2+ risk curve based on data from the United States' National Automotive Sampling System Crashworthiness Data System (NASS-CDS) (Larsson et al., 2021) are shown.

When visually comparing the MAIS2+ injury risk curve based on the IGLAD sample to the risks for NFR2+ predicted in the individual simulations, a lower risk prediction in the simulations is observed. This might be caused by the fact that MAIS2+ injury risk in IGLAD does not originate from rib fractures alone. Using data from NASS-CDS, rib fracture specific risk curves for delta-v have been published (Larsson et al., 2021). The NASS-CDS-based risk curve for a 70-year-old occupant for NFR2+ is also shown in Figure 6. This risk is at the lower confidence interval of the MAIS2+ thoracic injury risk curve for the 29-year-old occupant until approximately 50 km/h. Hence, at 50 km/h, a 55% risk for MAIS2+ thorax injuries (including rib fractures) for 77-year-old drivers can be estimated based on IGLAD, while the risk for NFR2+ for a 70-year-old according to NASS-CDS is estimated at about 18%. While the filter criteria are not identical, this underlines that there is a considerable amount of thoracic MAIS2+ injuries which cannot be attributed to fractured ribs. This might be one reason for the underestimation of thoracic injuries in the present study. Additionally, while the GVI has been used extensively in studies investigating rib fractures (Iraeus, 2015; Iraeus and Lindquist, 2016; Iraeus and Lindquist, 2020; Larsson et al., 2021), to the best knowledge of the authors, the present study is the first one using it with a THUMS v4.1. Also, the strain-based rib fracture risk function used in the present study was so far only validated for the SAFER HBM version 9 (Larsson et al., 2021). Using a rib fracture risk function specifically tuned for THUMS v4.1 could also help to further improve the results. Strain-based criteria were used instead of chest deflection, as PDOFs between -30° and +30° were investigated, which complicates finding a robust definition for chest deflection. Using chest deflection or other criteria for thoracic injury known from crash test dummies, as the viscous criterion (V*C), were developed for well-defined loading directions.

The injury metric for the neck, based on cortical bone fracture prediction, predicted an injury rate pretty much identical to the one observed in the IGLAD sample (0.2% and 0.7% respectively). Based on the same metric, no injuries to the thoracic or lumbar spine were predicted in the HBM simulations. While this represents an underprediction, at 2.1%, MAIS2+ injuries to the thoracic or lumbar spine were only observed in very few of the cases in the real-world sample anyway.

At 6.3%, upper extremity injuries were more common in the IGLAD data, but the simulations predicted an even higher injury rate of 14.7%. Part of the explanation for the overprediction might be related to the simplified representation of the instrument panel, which is modelled as rigid in most areas (Iraeus and Lindquist, 2016). However, closer inspection of the simulation results revealed that the majority of fractures in the cortical bones of the upper extremities are predicted in the left clavicle. Fractures to other bones in the upper extremities (mainly the right radius and ulna) only account for 0.9% of the simulations. This highlights the importance of belt routing, which is discussed further when comparing the results between the two seat configurations in Section 4.3. The lower extremities represent the second most frequently injured body region with 9.5% of the real-world cases. In the simulations, fractures are only predicted in 2.2% of configurations, all affecting the pelvis. While the argument that was made for thoracic injuries—that by only looking at fractures, an underestimation is to be expected—could be made for the lower extremities too, this claim cannot be backed by previous research. According to Forman et al. (2019), the majority of AIS2+ injuries for the upper and lower extremities in frontal collisions are fractures. The difference could be caused by the simplified modeling of the interaction of the legs with the GVI. This might on the one hand be related to the fact that the footwell does not feature a structure confining upward motion of the feet (cf. Figure 2B). On the other hand, different initial positions of the legs or other heterogeneities in the real-world like different shoes could be possible causes for the observed deviations. Particularly, the adequate modelling and the potential effects of shoes on lower extremity injury risk in occupant simulations is not well understood.

4.3 Effects of large rearward seat adjustments

The bar charts for the shift in injury risk between the two sets of simulations in Figure 3B shows that the injury risk for the head and the upper extremities is reduced. In contrast, all other injury risks are increased.

Most notably, the risk for abdominal injury, based on the occurrence of submarining (+48.1%) is increased substantially. In all cases with submarining, it occurred on the right (i.e., inboard) side. Mostly, the belt slipped off the right iliac crest shortly before the occupant motion reversed, i.e., before entering the rebound phase. Submarining with an earlier onset occurred in 16.8% of the cases. The issue of submarining of HBMs has been studied in a number of research publications, particularly with respect to seatback recline angles. Rawska et al. (2020) found that in some cases increased seat pan inclination could prevent submarining. While they did not investigate increased rearward adjustments directly, they discovered that

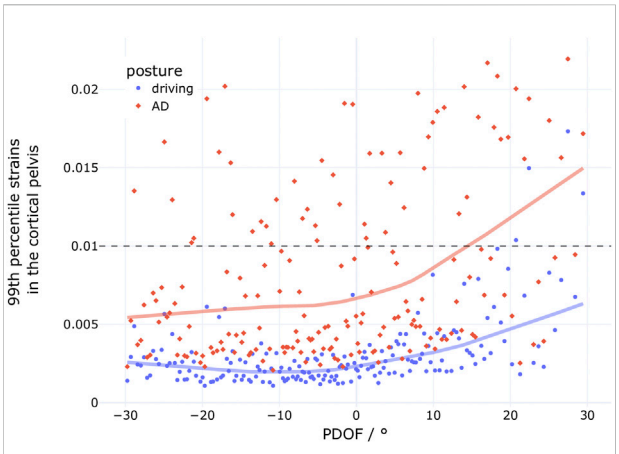

FIGURE 7
99th percentile strains of the cortical pelvis for the simulations with the conventional driving position (blue dots, n = 185) and the simulations with the rearward adjusted seat (AD, red diamonds, n = 185).

in the cases with no knee bolster also increased seat pan inclination could not prevent submarining (Rawska et al., 2020). In the present study, only a single seat back recline angle and a single seat pan inclination angle were used. Potentially, other combinations of these seat adjustments could have prevented submarining for some configurations. However, considering the findings of Rawska et al. (2020), it seems unreasonable that in absence of a load path through the femur (*via* a knee bolster for instance) submarining could be eliminated completely, without additional remedial measures. In any case, it is not completely understood if even state-of-the-art HBMs can adequately predict the occurrence of submarining. This can primarily be attributed to modelling simplifications (mainly for robustness reasons) of the adipose tissues between the skin and the pelvic bones. These tissues have found to be vital to adequately replicate the behavior observed in post mortem human subject (PMHS) tests investigating submarining (Gepner et al., 2018).

At 27.7%, the second highest increase in injury risk between the two seat configurations affected the lower extremities. In all of these cases, pelvic fractures occurred. In only two cases, also tibia fractures were predicted for a 77-year-old occupant. Overall, when weighting for the respective share of this age group in the IGLAD data, these two amount to about 0.3% of cases—but in both cases, pelvic fractures are predicted anyway. The low prevalence of non-pelvic lower extremity fractures in the simulations with the rearward adjusted seat further indicate that improvements to the footwell modelling in the GVI (in particular adding a roof to the footwell) could prove meaningful. Fractures in the pelvis were predicted by assessing the MPS99 in the cortical pelvis using a 1% threshold (Snedeker et al., 2003). Figure 7 shows the MPS99 for each simulation of the present study as a function of PDOF. For each of the two seat configurations (driving/AD), a locally weighted scatterplot smoothing line is shown. These lines illustrate that the pelvic strains tend to increase with increasing PDOF regardless of seat configuration. The reason for this is that with increasing PDOF, the pelvis started to impact the rigid center console in addition to the load introduced into the pelvis by the lap belt. The graph also

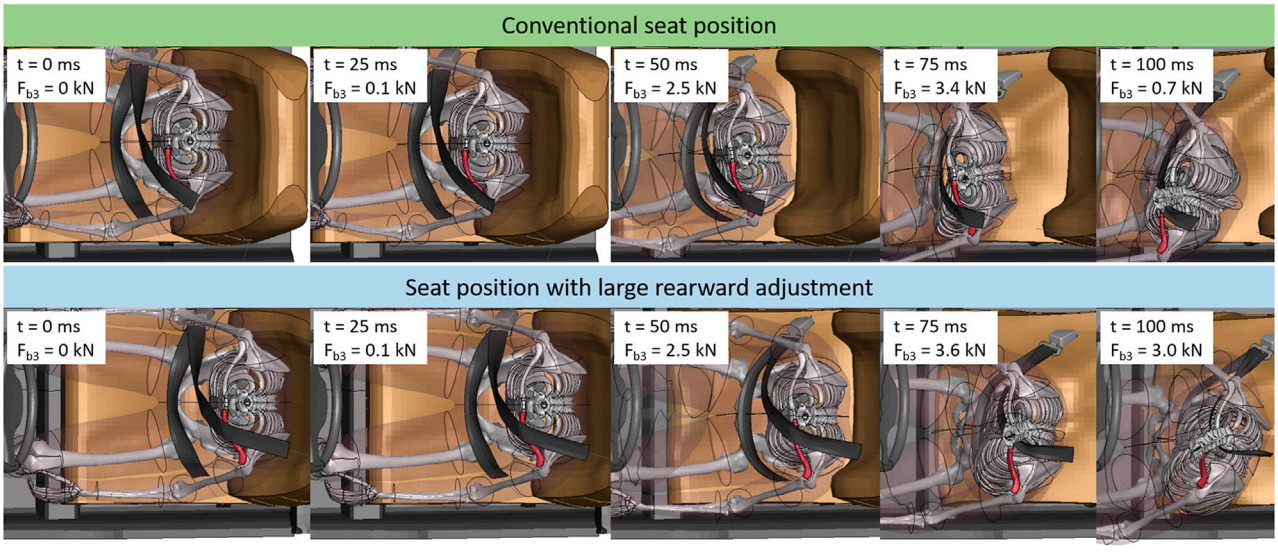

FIGURE 8
Still frames of case 513 (delta-v: 51 km/h, PDOF −16°). Top row shows kinematics for conventional seat position, lower row shows kinematics for rearwards adjusted seat. Time stamps and current shoulder belt force (F_{b3}) are provided. For visualization purposes, parts of the interior and HBM (most notably the head) are blanked and the left clavicle is highlighted in red.

highlights that the strains in the pelvis were always higher in the AD configuration than in the driving position.

Using THUMS v4.02, Peres et al. (2016), derived injury risk curves for pelvic fractures in lateral load cases. In their study, at 1% MPS99, the 95% confidence interval for AIS2+ injury risk is estimated between 23% and 65% for a 45-year-old and between 46% and 72% for a 65-year-old (Peres et al., 2016). While these risks are considerably lower than the 100% risk assumed in the present study, the highest strains observed in non-fracture cases in the study by Peres et al. (2016) were below 1.5% in both age groups. The MPS99 plot in Figure 7 illustrates that while only one case is above 1.5% with the conventional seat configuration, 30 cases exceed this value in the AD configuration. With this in mind, the substantial increase in predicted pelvic injuries seems plausible. In particular, when considering that the lap belt is the only significant load path to decelerate the pelvis directly, since the femurs are not being loaded through the knee bolster in the rearward adjusted seat positions because they are too far away (c.f. Figure 4).

The 9% increase in neck injury risk is considerable, especially when taking into account that in the simulations with the conventional seat configuration, the risk for neck injuries was close to zero. Likewise, the risks for the thorax (rib fractures) and the spine, which were underestimated in the standard driving position, are increased by 3.2% and 3.7% respectively. When taking into account the reduced effectiveness of the airbag in decelerating the torso and the changed loading of the spine (also visible in Figure 4) as a result of the increased distance to the airbag, this does not seem unreasonable. In this respect, it seems likely that potential countermeasures, designed to reduce spinal loads in (semi-) reclined seat positions (e.g., load limiting in the lap belt and seat track), could benefit occupants in interior configurations with increased rearward seat adjustments as well (Mroz et al., 2020).

For the head, the relative shift for all three criteria is well aligned. Based on MPS50 and DAMAGE, a decrease of 5.5% and 3.8% is predicted. For the metric using MPS95, a head injury risk reduction of 1.4% is predicted for the large rearward seat adjustments. When comparing the boxplots in Figure 5, they look similar for the driving position and the AD configuration in terms of their upper fences. At the same time, the lower fences are reduced in the AD configuration. Focusing on the individual injury risks in the plot, indicated by the dots next to the boxplots, it is obvious that the distribution changes considerably. While there are many cases with injury risk below 10%, reducing the median risks (solid horizontal line in each boxplot) accordingly, there are more cases above 60% injury risk for all three criteria, resulting in comparable mean risks (dashed horizontal line in each boxplot). One reason explaining the larger number of cases with lower risk could be that the brain injury risk was increased in the conventional seat position due to a slightly aggressive airbag setup, such that increasing the distance to the airbag and steering wheel actually improved the head-airbag-interaction in some

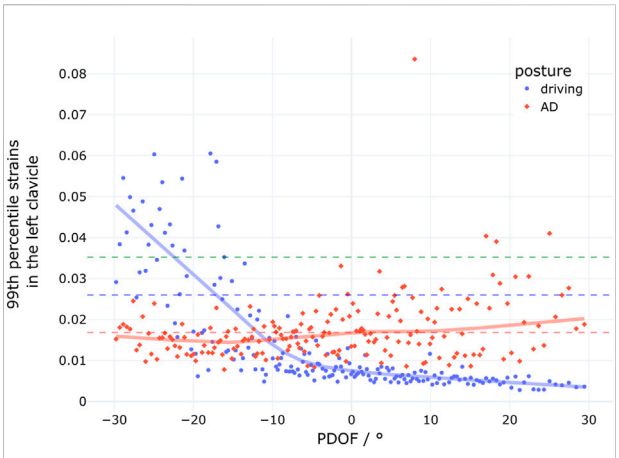

FIGURE 9
99th percentile strains of the cortical clavicle for the simulations with the conventional driving position (blue dots, n = 185) and the simulations with the rearward adjusted seat (AD, red diamonds, n = 185). The three dashed lines indicate the fracture thresholds for the three age groups.

cases. However, the larger number of cases with elevated risk also indicates that increased rearward seat adjustments can lead to problematic loads in the brain.

While some studies have underlined the importance of the upper extremities as a highly relevant body region not receiving adequate attention, it did not stand out in the present study. Compared to the conventional position, upper extremity injuries were even reduced by about 4% in the rearward adjusted seat positions. One potential reason behind this could be the fact that no contact is defined between the hands and the steering wheel rim, while in reality, this interaction might be an important source for upper extremity injuries. Just like in the conventional seat position, the bone most affected with fractures in the upper extremities was the left clavicle. Considering the reduced effect of the airbag in restraining the occupant's torso due to the increased distance, it seems counterintuitive that the probability for clavicle fracture would decrease. On closer inspection, it became obvious that this phenomenon can be attributed to the differences in the belt system between the two seat configurations. In the conventional driving position, the D-ring is mounted on the B-pillar. To replicate a belt-integrated seat, the D-ring was mounted generically behind and above the seat back on the outboard side (side view available in Figure 4). This lead to a belt routing with a slightly higher belt path, crossing the clavicle in the initial position. Figure 8 shows a comparison of the kinematics in a case with a PDOF of −16°.

In general, the belt kinematics are similar, with the belt slipping along the direction of the clavicle towards the neck of the occupant. The important difference is timing and the according load transferred through the shoulder belt. For the conventional seat position, the seat belt slides across the clavicle

in the time between 25 and 100 ms after t_0, when there is considerable force transferred *via* the shoulder belt (the maximum F_{b3} of 3.6 kN is reached at 81 ms). In contrast, in the configuration with the rearward adjusted seat, the belt is already at the proximal side of the clavicle when the belt is loaded. This explains why, even though the maximum belt force is higher (4.1 kN), the MPS99 in the left clavicle is considerably lower (AD position: 0.008, driving position: 0.035). Figure 9 further illustrates this relationship between the strains in the left clavicle and the PDOF for both seat configurations. The blue dots indicate the strains for each configuration with the standard driving position, the red diamonds the strains for the rearward adjusted seat, representing an automated driving (AD) position. For both groups, a locally weighted scatterplot smoothing line is shown. These lines illustrate the different behavior. For the conventional position, the strains increase with decreasing PDOFs, while for the AD position, the strains—on average—slightly increase with increasing PDOFs. The three dashed lines in green, blue and red in Figure 9 indicate the underlying fracture thresholds used for the respective age group (29, 53, and 77-year-old).

Although rarely life-threatening, injuries to the upper extremities can seriously affect the long term quality of life and lead to permanent medical impairment (Forman et al., 2019; Björklund et al., 2020). In the present study, in only 1.2% of cases upper extremity fractures *not* affecting the left clavicle were predicted (mostly affecting the radius and ulna). While the rigid material properties for the instrument panel in the GVI might exacerbate the effect of the rearward adjusted seat, a change in kinematics can be observed. When comparing the impact angle for the arms in the animations in Figure 4, it becomes clear that the design of the instrument panel needs to take potential collisions with the hands into account, ideally in terms of geometry and stiffness. Even though a reduction in upper extremity injuries was predicted in the present study, the results indicate that their mitigation might become more relevant in self-driving cars and the novel seat positions they enable.

4.4 Limitations

The presented approach has several limitations. Many of the inherent limitations have been discussed in the previous study using IGLAD data (Ressi et al., 2020). While using data from IGLAD offers the advantage of a more international perspective on vehicle safety by combining accident data from multiple countries, the injury data is only provided at MAIS level for each body region. For instance, this does not enable the distinction between skeletal and organ injuries.

While state-of-the-art FE HBMs, like the THUMS v4.1 used in the present study, provide detailed insights into strains in individual bones and soft tissues, they cannot be used to generate the level of detail needed to assign precise AIS codes. For example, the AIS injury severity can depend on whether a fracture is open or closed, the severity of rib fractures depends on potential complications (e.g., a hemo- or pneumothorax), and the severity of some injuries is determined by the estimated blood loss they caused or the surface area of organs affected by hematoma (Association for the Advancement of Automotive Medicine, 1998). Since this level of detail cannot be achieved with currently available HBMs, in case of ambiguities, a moderate injury (AIS2) or worse (AIS2+)—if applicable—was assumed.

Even if all injuries were known though, not all HBM body regions are yet covered by injury metrics with risk functions.

For the strain-based fracture assessment considering multiple age groups, no fracture was modelled in the HBM simulations. Rather than deleting elements exceeding a threshold, the strains were evaluated in post-processing and fractures assumed depending on the strain threshold (or rib fracture risk) for the age group in question. While this is a robust and commonly used method, it could be argued that in some circumstances, it might lead to unrealistic results. For instance, multiple fractured ribs could lead to reduced stability of the thorax, changing the loads on the internal organs, or a fractured clavicle could lead to changed thorax kinematics. However, this is not very likely in current state-of-the are restraint systems. Also, aside from the strain thresholds (and respective parameters for rib fracture risk curves), other age related changes (e.g., material properties, geometry, posture) were not taken into account.

In addition, only one anthropometry was considered. While using a wide range of occupants with different statures and masses would be a more realistic representation of the real-world collisions, the present study used the average male anthropometry, which has been the baseline for ATD testing for decades. Therefore, by not varying the anthropometry, the applicability of this model for a range of real-world occupants could be analyzed. To check whether the 50th percentile HBM

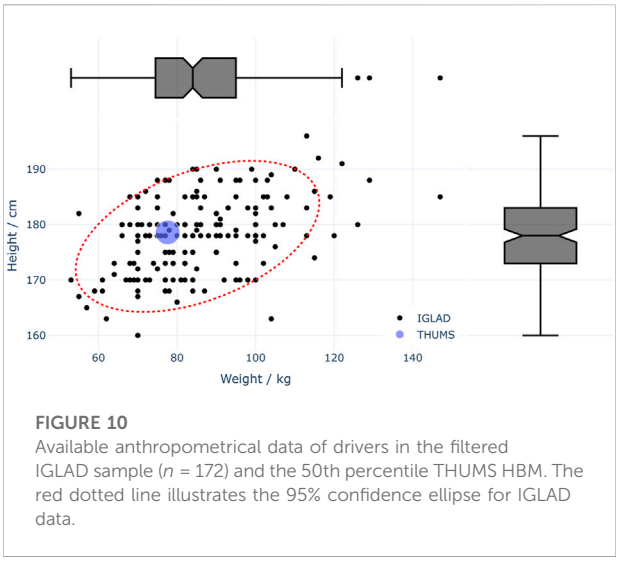

FIGURE 10
Available anthropometrical data of drivers in the filtered IGLAD sample (n = 172) and the 50th percentile THUMS HBM. The red dotted line illustrates the 95% confidence ellipse for IGLAD data.

adequately matched the anthropometries in the sample, its height and weight were combined in a plot with the height and weight of all drivers from the cases in the filtered IGLAD sample were this data were available. The plot, shown in Figure 10, illustrates that the height of the HBM (178.6 cm) was practically identical to the median height observed in the IGLAD sample (178 cm) while the HBM's mass (77.6 kg) was about 8% lower than the median mass from the real-world data (84 kg).

Aside from using only one occupant model, also only a single interior model was used. While the GVI was validated against crash test data in previous studies by the developers of the model (Iraeus and Lindquist, 2016), no additional validation was performed in the present study after introducing the modifications to model a generic belt integrated seat. Since only the belt routing was changed (the belt was not structurally integrated into the seat), a re-validation of the model was not deemed necessary. Nevertheless, as discussed in the previous section, the influence of the belt routing on clavicle fracture risk was found to be considerable. A systematic analysis, investigating the influence of belt routing on HBM kinematics and injury risk with respect to large rearward seat adjustments, could improve the understanding of the underlying phenomena and guide future interior and restraint system design.

To represent the variation in the vehicle fleet, the longitudinal seat position, restraint system parameters and crash pulse parameters were varied stochastically. In total, seven parameters were varied. Even though their selection was well motivated, more parameters and larger parameter ranges might be considered. For instance, depending on the vehicle, larger adjustments might be feasible in the future, but 100 mm were considered to be a reasonable starting point.

Furthermore, with a limit of 68 km/h, cases in which delta-v was much higher than in typical crash tests were excluded. While of course cases with higher delta-v are highly relevant to the goal of eliminating fatalities and serious injuries in road traffic accidents, they are very challenging with respect to occupant safety. The main concern with increased delta-v is the integrity of the safety cell. In a recent study, Kim et al. (2021) investigated the effects of increased impact speed based on an offset deformable barrier test. An average age vehicle model (model year 2010) was tested at the baseline impact speed of 64.4 km/h as well as at 80 km/h and 90 km/h, equivalent to an increase in kinetic energy of 54% and 95% respectively. While in the baseline test minimal occupant compartment intrusion was observed, the 54% increased kinetic energy resulted in some deformation (door opening, instrument panel, and brake pedal). The test with almost doubled kinetic energy lead to interior intrusions which were increased between 127 and 406 mm (5–16 inches) compared to the baseline test (Kim et al., 2021). Even though intrusions can be accounted for in the GVI model used in the finite element simulations, a relationship between crash loads and intrusions (location and extent) would be necessary for a meaningful representation. Lacking such a relationship, no intrusions were considered in the simulations, since no increased risk for rearward adjusted seat positions was expected.

While based on real-world data, the airbag trigger time was varied randomly. For future publications using a similar approach, a generic algorithm estimating realistic trigger times would be desirable. It is possible though, that to derive realistic yet generic trigger times, more information on the crash pulse is necessary than currently available from typical crash test or event data recorders.

Also, the chosen size of the design matrix could be considered a limitation. The robustness of the presented approach could be investigated by comparing results from different design matrices with varying sizes and see if they converge with increasing sample size.

To ensure consistency in presenting the results, 15 cases were dropped from the further analysis. These did not meet simulation quality criteria in at least one of the two simulation sets. While ensuring consistency, this also introduces bias. This is expected to lead to a degree of underprediction of injuries, since excessive mass scaling and error terminations often affect simulations with higher collision severities.

4.5 Outlook

Since the HBM theoretically enables omnidirectional injury prediction, this approach could potentially be used for any loading direction or seat configuration. In this respect, the present study can be seen as a starting point. The presented approach can aid the prioritization of new injury risk functions, which subsequently further improve future HBM-based injury prediction. By adjusting the loading conditions and seat configuration in the generic vehicle interior, the challenges with respect to occupant safety of countless potential future interior designs could be evaluated.

5 Conclusion

The results of stochastic simulations with an HBM in a conventional seat position were compared with injury rates observed in a sample taken from a real-world accident database showing different accuracies in the injury prediction capabilities of the applied method. While injury frequencies for the abdominal organs and head were overpredicted considerably, predicted injury rates were reasonable for the other body regions.

For simulations with the rearward adjusted seat, increased injury risk was observed for most body regions. The highest injury risk increases were predicted for the abdomen (+48%), the lower extremities (+28%) and the neck (+9%). These increases in

injury risk highlight that even small changes compared to conventional configurations require a reconsideration of conventional restraint systems.

Although there are limitations with respect to the injury prediction—particularly for the abdomen—with the used HBM, the potential of HBMs as useful tools for estimating future protection challenges is shown. The presented approach enables the identification of potential future protection challenges, before they are observable in accident databases, which can take decades. As a result, in ideal circumstances, by identifying and mitigating them before they arise, they will be never observed in real-world crashes.

Data availability statement

The raw data supporting the conclusion of this article will be made available by the authors, without undue reservation.

Author contributions

FR: Conceptualization, methodology, combined model development, stochastic parameter variation, setup and analysis of the finite element simulations, visualization, writing (original draft), reviewing, and editing. CL: Stochastic parameter variation and visualization. CK: Conceptualization, supervision, methodology, writing, reviewing, and editing. WS: Conceptualization, reviewing and editing. All authors contributed to the article and approved the submitted version.

Funding

This research received no specific grant from any funding agency. The publishing fees were supported by TU Graz Open Access Publishing Fund.

Acknowledgments

The authors thank Johan Iraeus for developing the generic interior model and granting the authors access to the model. The authors acknowledge the use of high performance computing resources provided by the IT Services (ZID) of Graz University of Technology. Furthermore, the authors acknowledge Toyota Motor Corporation for making the THUMS publicly available. The authors extend their thanks to Desiree Kofler for her support with the finite element simulations, to Gunther Konrad for his assistance in preprocessing the IIHS crash test data and to Bernd Schneider for his support with creating a space-filling simulation design which takes given parameter distributions into account.

Conflict of interest

The authors declare that the research was conducted in the absence of any commercial or financial relationships that could be construed as a potential conflict of interest.

Publisher's note

All claims expressed in this article are solely those of the authors and do not necessarily represent those of their affiliated organizations, or those of the publisher, the editors and the reviewers. Any product that may be evaluated in this article, or claim that may be made by its manufacturer, is not guaranteed or endorsed by the publisher.

Supplementary material

The Supplementary Material for this article can be found online at: https://www.frontiersin.org/articles/10.3389/ffutr.2022.914481/full#supplementary-material

References

Association for the Advancement of Automotive Medicine (1998). *Abbreviated injury scale 1990 update 1998*. Barrington, IL: AAAM.

Björklund, M., Risberg, J., Laudon, O., and Jakobsson, L. (2020). "Development of a hand and forearm impact test method and a study on influencing factors," in *Proceedings of the IRCOBI conference*. Munich, Germany: IRCOBI, 693–706.

European Commission (2018). COM(2018) 298 *Europe on the move: Sustainable mobility for Europe: Safe, connected, and clean*. Brussels: European Commission.

European Commission (2021). Road safety: 4000 fewer people lost their lives on EU roads in 2020 as death rate falls to all time low. Press release. https://ec.europa.eu/commission/presscorner/detail/en/IP_21_1767 (Accessed April 04, 2022).

Fahlstedt, M., Meng, S., and Kleiven, S. (2022). Influence of strain post-processing on brain injury prediction. *J. Biomech.* 132, 110940. (online first). doi:10.1016/j.jbiomech.2021.110940

Feist, F. (2018). *Shoes of THUMS pedestrian model*. Graz.

Forman, J. L., Kent, R. W., Mroz, K., Pipkorn, B., Bostrom, O., and Segui-Gomez, M. (2012). Predicting rib fracture risk with whole-body finite element models: Development and preliminary evaluation of a probabilistic analytical framework. *Ann. Adv. Automot. Med.* 56, 109–124. PMCID: PMC3503420.

Forman, J. L., Poplin, G. S., Shaw, C. G., McMurry, T. L., Schmidt, K., Ash, J., et al. (2019). Automobile injury trends in the contemporary fleet: Belted occupants in frontal collisions. *Traffic Inj. Prev.* 20, 607–612. doi:10.1080/15389588.2019.1630825

Gabler, L. F., Crandall, J. R., and Panzer, M. B. (2018). Development of a metric for predicting brain strain responses using head kinematics. *Ann. Biomed. Eng.* 46, 972–985. doi:10.1007/s10439-018-2015-9

Gabler, L. F., Crandall, J. R., and Panzer, M. B. (2019). Development of a second-order system for rapid estimation of maximum brain strain. *Ann. Biomed. Eng.* 47, 1971–1981. doi:10.1007/s10439-018-02179-9

Gepner, B., Joodaki, H., Sun, Z., Jayathirtha, M., Kim, T., Forman, J., et al. (2018). "Performance of the obese GHBMC models in the sled and belt pull test conditions," in *Proceedings of the IRCOBI conference*, 355–368.

Gepner, B., Rawska, K., Richardson, R., Kulkarni, S., Chastain, K., Zhu, J., et al. (2019). "Challenges for occupant safety in highly automated vehicles across various anthropometries," in *Proceedings of the 26th international technical conference on the enhanced safety of vehicles* (Washington DC: NHTSA).

Golman, A. J., Danelson, K. A., Miller, L. E., and Stitzel, J. D. (2014). Injury prediction in a side impact crash using human body model simulation. *Accid. Analysis Prev.* 64, 1–8. doi:10.1016/j.aap.2013.10.026

Guillemot, H., Besnault, B., Robin, S., Got, C., Le Coz, J. Y., Lavaste, F., et al. (1997). Pelvic injuries in side impact collisions: A field accident analysis and dynamic tests on isolated pelvic bones. *SAE Trans.* 106, 3624–3633.

IIHS (2022). About our tests: Frontal crash tests. Available at: https://www.iihs.org/ratings/about-our-tests#frontal-crash-tests (Accessed March 29, 2022).

IIHS (2021). *Moderate overlap frontal crashworthiness evaluation — crash test protocol*. Ruckersville, VA, USA: Insurance Institute for Highway Safety.

Iraeus, J., and Lindquist, M. (2020). Analysis of minimum pulse shape information needed for accurate chest injury prediction in real life frontal crashes. *Int. J. Crashworthiness* 1, 684–691. doi:10.1080/13588265.2020.1769004

Iraeus, J., and Lindquist, M. (2016). Development and validation of a generic finite element vehicle buck model for the analysis of driver rib fractures in real life nearside oblique frontal crashes. *Accid. Analysis Prev.* 95, 42–56. doi:10.1016/j.aap.2016.06.020

Iraeus, J., and Lindquist, M. (2015). Pulse shape analysis and data reduction of real-life frontal crashes with modern passenger cars. *Int. J. Crashworthiness* 20, 535–546. doi:10.1080/13588265.2015.1057005

Iraeus, J. (2015). *Stochastic finite element simulations of real life frontal crashes: With emphasis on chest injury mechanisms in near-side oblique loading conditions* ([Umeå, SWE]: University of Umeå). [dissertation].

Joseph, V. R., and Ba, S. (2018). *MaxPro: Maximum projection designs: R package*.

Joseph, V. R., Gul, E., and Ba, S. (2015). Maximum projection designs for computer experiments. *Biometrika* 102, 371–380. doi:10.1093/biomet/asv002

Kim, W., Kelley-Baker, T., Arbelaez, R., O'Malley, S., and Jensen, J. (2021). *Impact of speeds on drivers and vehicles – results from crash tests (technical report)*. Washington, DC, USA: AAA Foundation for Traffic Safety.

Klug, C., Luttenberger, P., Schachner, M., Micorek, J., Greimel, R., and Sinz, W. (2018). "Postprocessing of human body model results – introduction of the open source tool DYNASAUR," in Proceedings of the 7th International Symposium on Human Modeling and Simulation in Automotive Engineering, Berlin, Germany, October 18–19, 2018.

Laakmann, F., Zink, L., and Seyffert, M. (2019). New interior concepts for occupant protection in highly automated vehicles. *ATZ Worldw.* 4, 48–53. doi:10.1007/s38311-019-0012-8

Larsson, K.-J., Blennow, A., Iraeus, J., Pipkorn, B., and Lubbe, N. (2021). Rib cortical bone fracture risk as a function of age and rib strain: Updated injury prediction using finite element human body models. *Front. Bioeng. Biotechnol.* 9, 677768. doi:10.3389/fbioe.2021.677768

Luttenberger, P., Schachner, M., Rajinovic, S., Moser, J., Leo, C., and Sinz, W. (2019). *MUTANT functionality report*. Graz: University of Technology Graz.

Milakis, D., van Arem, B., and van Wee, B. (2017). Policy and society related implications of automated driving: A review of literature and directions for future research. *J. Intelligent Transp. Syst.* 21, 324–348. doi:10.1080/15472450.2017.1291351

Mohamed, G., and Newlands, G. (2021). "Human body model positioning using Oasys PRIMER," in Proceedings of the 13th European LS-DYNA Conference, Ulm, Germany, October 5–7, 2021.

Mroz, K., Östling, M., Richardson, R., Kerrigan, J., Forman, J., Gepner, B., et al. (2020). "Effect of seat and seat belt characteristics on the lumbar spine and pelvis loading of the SAFER human body model in reclined postures," in *Proceedings of the IRCOBI conference*, 470–486.

Nakane, K., Nojiri, M., Maekawa, R., Esaki, M., Suzuki, S., Masuda, Y., et al. (2015). "Analysis of abdominal injuries caused by the submarining phenomenon in the rear seat occupants," in *Proceedings of the 24th international technical conference on the enhanced safety of vehicles* (Gothenburg: NHTSA).

NHTSA (2015). *New car assessment program: Request for comments*. Washington DC: National Highway Traffic Safety Administration. Docket No. NHTSA-2015-0119.

NHTSA (2022). *Occupant protection for vehicles with automated driving systems*. Washington DC: National Highway Traffic Safety Administration. Docket No. NHTSA-2021-0003.

NSTC, and US DOT (2020). *Ensuring American leadership in automated vehicle technologies: Automated vehicles 4.0*. Washington DC: National Science & Technology Council and US Department of Transportation.

Östh, J., Pipkorn, B., Forsberg, J., and Iraeus, J. (2021). "Numerical reproducibility of human body model crash simulations," in *Proceedings of the IRCOBI conference*, 431–443. (Online).

Park, J., Ebert, S. M., Reed, M. P., and Hallman, J. J. (2016). Statistical models for predicting automobile driving postures for men and women including effects of age. *Hum. Factors* 58, 261–278. doi:10.1177/0018720815610249

Peduzzi, P., Concato, J., Feinstein, A. R., and Holford, T. R. (1995). Importance of events per independent variable in proportional hazards regression analysis II. Accuracy and precision of regression estimates. *J. Clin. Epidemiol.* 48, 1503–1510. doi:10.1016/0895-4356(95)00048-8

Peres, J., Auer, S., and Praxl, N. (2016). "Development and comparison of different injury risk functions predicting pelvic fractures in side impact for a Human Body Model," in *Proceedings of the IRCOBI conference*, 661–678.

Poulard, D., Lin, H., and Panzer, M. B. (2020). *Occupant safety in vehicles equipped with automated driving systems, Part 3: Biofidelity evaluation of GHBMC M50-OS against laboratory sled tests*. Washington DC: National Highway Traffic Safety Administration. Report DOT HS 812 905.

Rawska, K., Gepner, B., Moreau, D., and Kerrigan, J. (2020). Submarining sensitivity across varied seat configurations in autonomous driving system environment. *Traffic Inj. Prev.* 21, 1–6. doi:10.1080/15389588.2020.1791324

Reed, M. P., Ebert, S. M., Jones, M. L. H., and Hallman, J. J. (2020). Prevalence of non-nominal seat positions and postures among front-seat passengers. *Traffic Inj. Prev.* 21, 7–12. doi:10.1080/15389588.2020.1793971

Ressi, F., Kofler, D., Sinz, W., Tomasch, E., and Klug, C. (2020). "Key injury regions for passenger car drivers in frontal crashes: A comparison of results from IGLAD and finite element simulations using a human body model," in *Proceedings of the IRCOBI conference*, 137–155.

Ressi, F., Sinz, W., Geisler, C., Öztürk, A., D'Addetta, G. A., and Freienstein, H. (2019). "Estimating preliminary occupant injury risk distributions for highly automated vehicles with respect to future seat configurations and load directions," in Proceedings of the 26th ESV Conference, Eindhoven, Netherlands, June 10–13, 2019, 125–141.

Snedeker, J. G., Muser, M. H., and Walz, F. H. (2003). Assessment of pelvis and upper leg injury risk in car-pedestrian collisions: Comparison of accident statistics, impactor tests and a human body finite element model. *Stapp Car Crash J.* 47, 437–457. doi:10.4271/2003-22-0019

Toyota Motor Corporation (2020). Toyota offers free access to THUMS virtual human body model software. Available at: https://global.toyota/en/newsroom/corporate/32665896.html (Accessed March 02, 2022).

Toyota Motor Corporation, and Toyota Central R&D Labs (2021). *Total human model for safety (THUMS): AM50 occupant model version 4.1*.

UNECE (2018). *Resolution on the deployment of highly and fully automated vehicles in road traffic*. Geneve: United Nations Economic Commission for Europe.

US DOT (2022). *National roadway safety strategy*. Washington, DC: US Department of Transportation.

Watanabe, R., Miyazaki, H., Kitagawa, Y., and Yasuki, T. (2011). "Research of the relationship of pedestrian injury to collision speed, car-type, impact location and pedestrian sizes using human FE Model (THUMS v 4)," in *SAE technical papers*. doi:10.4271/2012-22-0007

Weaver, A. A., Talton, J. W., Barnard, R. T., Schoell, S. L., Swett, K. R., and Stitzel, J. D. (2015). Estimated injury risk for specific injuries and body regions in frontal motor vehicle crashes. *Traffic Inj. Prev.* 16, 108–116. doi:10.1080/15389588.2015.1012664

WHO (2018). *Global status report on road safety*. Geneve: World Health Organization.

Wu, T., Sato, F., Antona-Makoshi, J., Gabler, L. F., Giudice, J. S., Alshareef, A., et al. (2022). Integrating human and nonhuman primate data to estimate human tolerances for traumatic brain injury. *J. Biomech. Eng.* 144, 071003. (online first). doi:10.1115/1.4053209

frontiers | Frontiers in Future Transportation

TYPE Original Research
PUBLISHED 09 September 2022
DOI 10.3389/ffutr.2022.890776

OPEN ACCESS

EDITED BY
Robert Thomson,
Chalmers University of Technology, Sweden

REVIEWED BY
Jie Wang,
Changsha University of Science and Technology, China
Di Pan,
Xiamen University, China
Yong Han,
Xiamen University of Technology, China
Bengt Pipkorn,
Autoliv, Sweden
Chengyue Jiang,
Chongqing University of Technology, China

*CORRESPONDENCE
Wenle Lv,
lvwenle@tust.edu.cn

SPECIALTY SECTION
This article was submitted to Transport Safety,
a section of the journal
Frontiers in Future Transportation

RECEIVED 06 March 2022
ACCEPTED 26 July 2022
PUBLISHED 09 September 2022

CITATION
Li H, Lv W, Hynčík L, Zhou B, Zhao H, Cui S, He L and Ruan S (2022), Injury study of the 6-year-old pediatric thorax and abdomen in frontal sled tests using different computational models.
Front. Future Transp. 3:890776.
doi: 10.3389/ffutr.2022.890776

Injury study of the 6-year-old pediatric thorax and abdomen in frontal sled tests using different computational models

Haiyan Li[1], Wenle Lv[1]*, Luděk Hynčík[2], Bingbing Zhou[3], Hongqian Zhao[1], Shihai Cui[1], Lijuan He[1] and Shijie Ruan[1]

[1]Tianjin University of Science and Technology, Tianjin, China, [2]University of West Bohemia, Pilsen, Czechia, [3]Tianjin Quadrant Space Science and Technology Company, Limited, Tianjin, China

The correct use of a child restraint system (CRS) is an effective internationally recognized measure to protect the safety of child occupants which can reduce the probability of child road traffic accident deaths by 54–80%. Finite element (FE) analysis is one important method with which to study the protection of child occupants. The aim of this study was to investigate thoracic and abdominal injuries and the protective effect of CRS on child occupants in 6-year-old (6YO) children in a frontal sled test using different computational models. In this study, a verified FE model of a 6YO child occupant was placed in the FE model of a CRS with a three-point safety belt. In the simulation setup phase, the frontal sled simulation of the 6YO FE model was reconstructed by applying the AAMA pulse. Based on the simulation data of the Q6 dummy FE model (Q6) and the 6YO child Virthuman model (V6) from previous studies, the frontal sled test simulation of a verified 6YO child FE model with detailed anatomical structures (TUST IBMs 6YO) was carried out to analyze pediatric thorax and abdomen injuries under the same experimental conditions. According to the simulation results, the variation tendencies of the simulation responses such as chest acceleration and compression are consistent with each other, which can provide effective information for the design of a CRS. In addition, the simulation results of the TUST IBMs 6YO can provide a variety of simulation data, such as the maximum first principal strain value and nephogram, of the internal organs of the chest and abdomen, providing a theoretical basis for the performance analysis and later development of a CRS.

Abbreviations: AAMA, American Automobile Manufacturers Association; AIS, abbreviated injury scale; CRS, child restraint system; CT, computed tomography; ECER129, Economic Commission for Europe Regulation; FE, finite element; TUST IBMs 6YO, 6YO child FE model with detailed anatomical structures developed by Tianjin University of Science and Technology; HIC, head injury criterion; MBS, multibody system; PIPER, position and personalize advanced human body models for injury prediction; Q6, Q6 child dummy FE model; THUMS 3YO, total human model for safety 3-year-old; V6, virtual 6YO child model developed by automatic scaling; VC, viscous criterion.

KEYWORDS

child seat, occupant kinematics, frontal impact, chest and abdominal injury, finite element

1 Introduction

Cars have become a necessity for most families, and the use of CRS is gradually attracting the attention of young parents nowadays. Use of child dummies in sled tests is becoming more and more widespread in the later verification process of CRS design in spite of the limitations of the low recycling rate of dummies and large testing costs for enterprises. In addition to child dummies, multibody system (MBS) models are also widely used in CRS verification, while a child FE model with a detailed anatomy can better reflect the performance of the CRS, greatly reduce the costs of testing using numerical simulation, and be recycled during product development and upgrading.

Maňas et al. (2012) introduced the kinematic response and verification process of an MBS human model in a collision and explained its advantages and importance. Two kinds of MBS models, EUROSID 2 (fine model) and USSID (rough model), were introduced by Franz and Graf, 2000, where the materials were described in detail. A new type of CRS was introduced, and the performance of the seat model under the conditions of a frontal collision was studied by Cao et al. (2010), where it was shown that the seat can effectively protect children aged 3 and 6 years. In the study by Huang et al. (2016), it was found that the head displacement of the child MBS model was not sensitive to the waveform, but the pulse shape had a greater impact on the head and chest accelerations.

CRS research in developed countries in Europe and America started earlier, and the technology was more mature than that in China. Sled tests of 3- and 6-year-old children with a three-point safety belt and CRS were conducted in Beauchamp et al., 2005. With regard to the improvement of new test methods for CRS, Trosseille et al. (2001) studied the knowledge about child behavior and tolerance in the CREST project and put forward a new test procedure to determine the effectiveness of instrumentation. Jager et al., 2005 introduced earlier the feasibility of Q dummy series models in frontal impacts. Eggers et al. (2015) evaluated the safety of child occupants in the rear seats of vehicles through Q6 and Q10 dummies and concluded that the Q6 thorax was greatly affected by geometric parameters such as the safety belt and that the Q6 dummy can more truly reflect the injury mechanism of the thorax. Beillas et al. (2014) concluded that an upper deflection sensor can better evaluate the chest injury of the Q6 dummy by comparing the injury of the Q6 dummy with that of the FE model. Kim et al. (2014) conducted a sled test with the Economic Commission for Europe Regulation 129 (ECE R129) standard seat and Q6 child dummy seat and concluded that the safety belt anchor point can affect child injuries. Zhang et al. (2021) studied the effect of the belt restraint path on child occupant injury by reconstructing a sled test with a Q6 dummy model, and the simulation results showed that an optimized seat belt restraint path can effectively enhance the safety of child occupants. Maheshwari et al. (2019) compared and analyzed the responses of a Q6 child occupant FE model restrained in three types of CRS conditions on the FMVSS 213 test bench.

In terms of research into child chest injury, Ouyang et al. (2006) studied children in different age groups in frontal impact experiments. Due to the limitations of cadaver experiments, the researchers studied injury by developing FE models for simulation analysis. A 3-year-old child chest and abdomen FE model for the injury study was built by scaling the adult FE model based on measurements and statistics in Mizuno et al. (2005). Another method of model construction was to construct the chest and abdomen FE models with the actual human anatomical structures based on human computed tomography (CT) images. A detailed 10-year-old child chest FE model was developed and verified by reconstructing of a static loading experiment by Jiang. (2013). Lv et al. (2015) constructed a complete FE model of a 6-year-old (6YO) child pedestrian (FEM6) with detailed anatomical structures and verified it by reconstructing experiments and studying chest injury in lateral impacts, laying the foundation for the follow-up research of CRS. All these studies showed that a high biofidelic child FE model, which was scarce for 6YO child occupants, was a more realistic and reliable method for assessing child safety protection and injury. Therefore, it is necessary to investigate the effect of CRS on child injury with an intact 6YO occupant FE model, which has a realistic and detailed anatomical structure.

The present paper aims to study 6YO pediatric occupant thorax and abdomen injuries in terms of acceleration, deflection, and force utilizing a verified TUST IBMs 6YO in frontal sled simulations, which compares the results with those from the Q6 and V6 models obtained from Hyncik et al.'s study (2014) and the protective effect of CRS on child occupants. The first principal strain is regarded as an evaluation index to predict the injury of internal organs.

2 Model construction and simulation setup

The child biomechanical dummy is represented by the validated Q6 model (as reference); therefore, the comparison to this model corresponds to the comparison to the child dummy. Based on the numerical simulations of the Q6 dummy FE model and the V6 MBS model (Hyncik et al., 2014), the frontal sled test simulation of the verified TUST IBMs 6YO was carried out under the same experimental conditions.

TABLE 1 Dimensions of the 6YO child in this paper and the international standard.

Parameter	6YO child FE model	6YO child in the 50th percentile
Height (mm)	1135	1113
Mass (kg)	23.9	18.9
Chest width (mm)	207.4	216
Chest thickness (mm)	130.7	147
Chest circumference (mm)	573.8	598

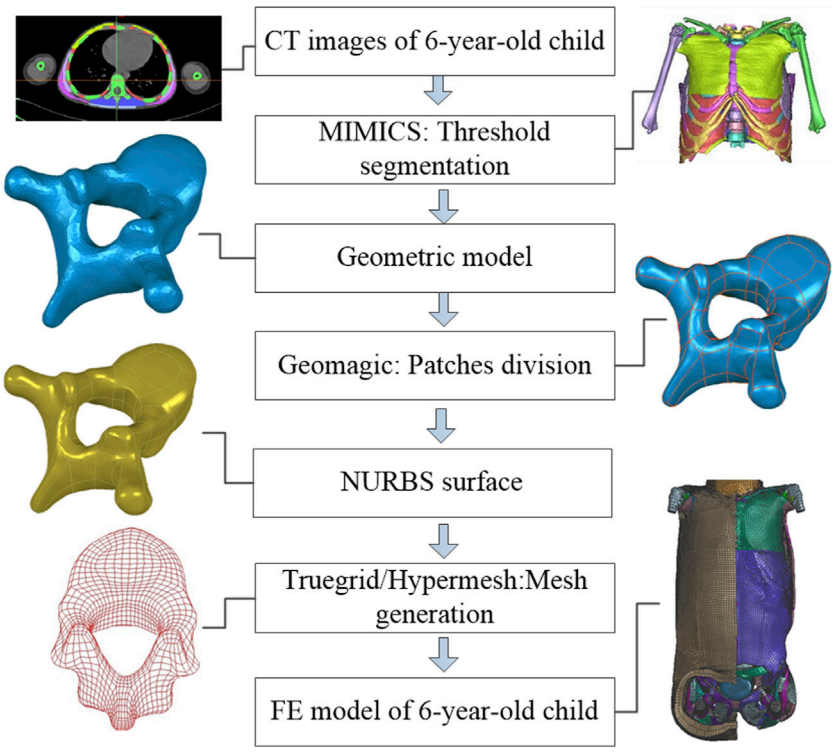

FIGURE 1
Construction process of pediatric FE model.

2.1 6-year-old child model

The TUST IBMs 6YO adopted in this paper conforms to the 50th percentile of the 6YO children's standard Human dimensions for Chinese minors, GB/T26158. The model is 1135 mm in height, 23.9 kg in weight, 207.4 mm in chest width, 130.7 mm in chest thickness, and 573.8 mm in chest circumference, as shown in Table 1.

The construction process for the child finite element model is as follows: first, the geometric model was extracted in Mimics 10.01 software by using the threshold segmentation method based on CT images of a 6YO child. The seated posture of the geometric model was obtained by rotating each part according to the seat angle. Then the geometric model was smoothed and divided into patches to obtain a patch model by using Geomagic 8.0. Finally, the FE model was constructed based on the geometric model by using Truegrid v2.1.0 and Hypermesh 12.0. In the FE model, cancellous bone, internal organs, muscle, fat, the spinal cord, cartilage, intervertebral discs, and other tissues were modeled by a hexahedral solid element, while cortical bone, ligament, skin, and the end plate were modeled by a shell element. The vertebral body was

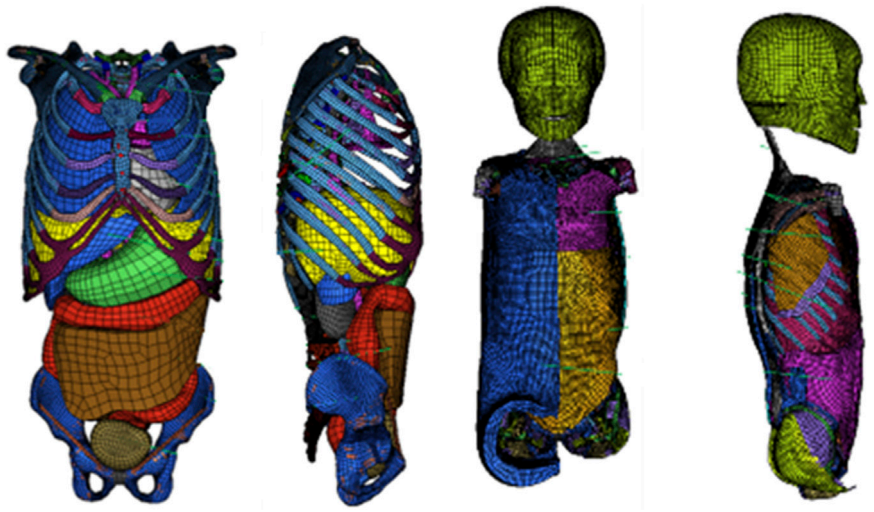

FIGURE 2
FE models of chest and abdomen of TUST IBMs 6YO including bones and internal organs (left) and muscle (right).

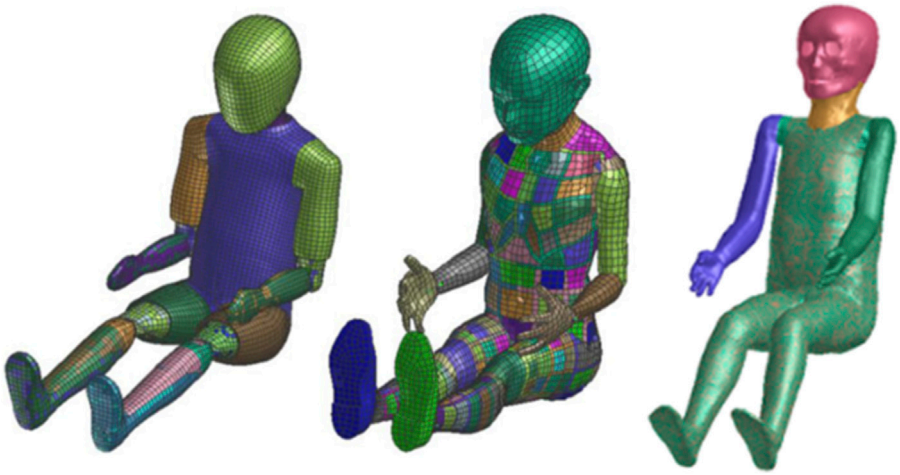

FIGURE 3
Q6 child dummy model (left). V6 child Virthuman model (middle) and TUST IBMs 6YO (right).

connected with the intervertebral disc by common nodes, which was the same for the connection between bone and muscle, skin, and fat. The contact between viscera and bone and different viscerae was defined as the surface–surface contact. The detailed construction process of the pediatric FE model is shown in Figure 1.

The material properties used in the 6YO child FE model were obtained from the literature (Untaroiu et al., 2005; Zhao and Norwani, 2007; Jiang et al., 2012; Lv et al., 2015; Lv WL. et al., 2016; Li et al., 2017a) and obtained by scaling adult material properties, which are summarized in Supplementary Appendix SA by Li et al. (2020). It should be noted that the scaling factor was obtained based on the existing child and adult tissue material parameters. The validity of the 6YO child FE model was verified by reconstructing several cadaver experiments (see Supplementary Appendix SB), and the simulation results were in good agreement with the experimental data, which indicated that this scaling method was feasible and reasonable to obtain child material under current conditions.

TABLE 2 Model data for the 6YO child.

Parameter	Q6	V6	TUST IBMs 6YO
Sitting height (mm)	601	653	671
Shoulder height (mm)	362	395	372
Shoulder width (mm)	305	262	217
Chest depth (mm)	141	180	172
Hip width (mm)	223	200	229
Buttocks to knee (mm)	366	350	315

The number of elements in the thorax and abdomen of TUST IBMs 6YO is 236,507. The model includes internal organs, skeletal tissues, muscles, ligaments, skin, and fat, as shown in Figure 2, which had been verified through the reconstruction of frontal impacts at different velocities (Ouyang et al., 2006; Ouyang et al., 2015) and lateral impact experiments at several angles (Shaw et al., 2006; Viano et al., 1989) in the literature (frontal impacts: Lv et al., 2015; Cui et al., 2016; lateral impacts: Lv et al., 2016b). Detailed information of the 6YO child FE model validation at the sub-model level is summarized in Supplementary Appendix SB by Li et al. (2020).

Figure 3 shows the Q6 child dummy model., 2013, the V6 child Virthuman model, and the TUST IBMs 6YO. The weight of the Q6 dummy is 22.98 kg, and the height is 1143 mm. The V6 child Virthuman model has a height of 1140 mm and a weight of 19 kg, which was obtained by scaling an adult model according to the relevant database of 6–7-year-old child heights (Hyncik et al., 2014).

The V6 child takes a step forward in human body modeling. V6 is a child human body model developed from an adult human body model (Vychytil et al., 2014) by a scaling algorithm based on actual anthropometric data (Hyncik et al., 2013). Both the geometry and stiffness are scaled to reconstruct a 6YO child's biomechanical properties. The model has been previously validated (Hyncik et al., 2013, 2014).

The TUST IBMs 6YO model was a finite element model of a 6YO child with detailed anatomical structures based on CT data. The V6 model was a special hybrid model that benefits from combining the MBS approach with deformable elements to enable injury assessment for a variety of impacts. The Q6 model was a full finite element model developed by Humanetics (2013), including inner and outer segments as a virtual copy of the physical Q6 child dummy, which was validated to correspond to the Q6 physical dummy response (Humanetics, 2013).

Body size is an important parameter for collision analysis, and the body sizes are shown in Table 2. The corresponding relationship can be effectively analyzed by body size. According to the size data of the three child models, each model has its own characteristics. The child FE model has a lower shoulder width, while other data correspond to each other.

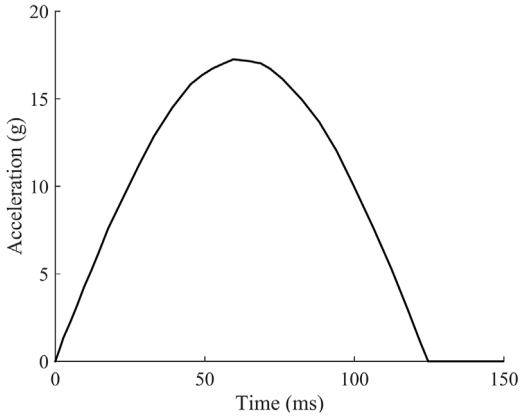

FIGURE 4
Frontal sled-AAMA sled pulse (the reproduce of the curve has been approved by the author Hyncik).

2.2 Safety seat FE model

In this paper, the FE model of CRS was built based on the geometric model of a child safety seat currently on the market using the pre-processing software HyperMesh 12.0. It consists of 1,231,296 elements, 32,570 shell elements, and 1,198,726 solid elements. The majority of the safety seat components were modeled by solid elements. The contact (*SYMMETRIC NODE-TO-SEGMENT WITH EDGE TREATMENT) in Pam-Crash software was used to model the boundary condition between the safety seat back portion and vehicle seat. The majority of the safety seat body was modeled as plastic material, while the padding was modeled as foam material. Furthermore, the three-point safety belt for a vehicle is built for the CRS, which is made of elastic isotropic material.

2.3 Simulation setup

The frontal sled simulation of the 6YO FE model was reconstructed by loading with the American Automobile Manufacturers Association (AAMA) pulse (Franz and Graf, 2000) (see Figure 4) in Virtual Performance Solutions 8.0. The simulation setup of the 6YO FE model was consistent with those of Q6 and V6 model simulations.

The sled consists of an ECE R16 seat. The sled and the seat models are taken from previous studies (Hyncik et al., 2014). The model is positioned in the seat, and a sliding contact interface (*SYMETRIC NODE-TO-SEGMENT WITH EDGE TREATMENT) is defined between the body and the seat. A three-point belt system is developed to model a C-pillar mounted belt restraint system. The simulation setups of the virtual 6YO child model and FE model are shown in Figure 5.

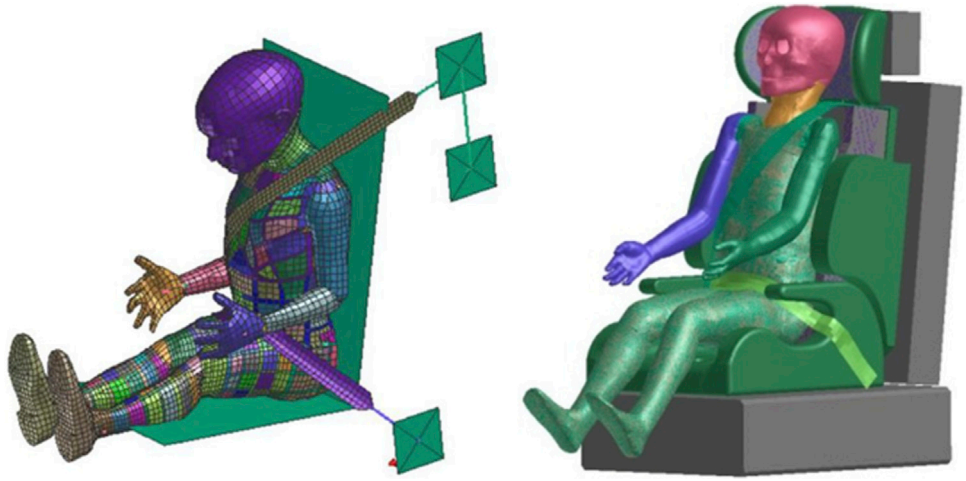

FIGURE 5
V6 (left) and TUST IBMs 6YO (right) in the frontal sled simulations (the reproduce of the Figure about V6 has been approved by the author Hyncik).

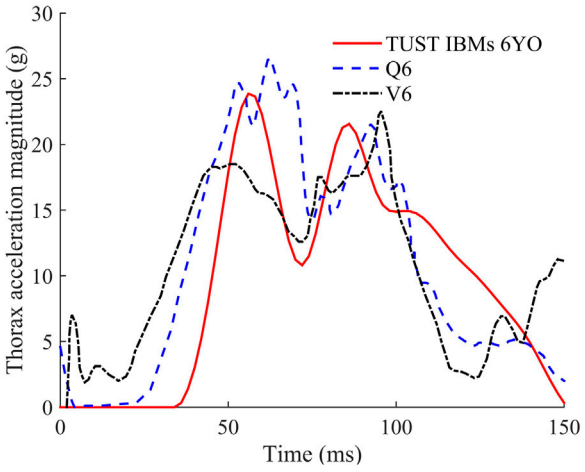

FIGURE 6
Thorax acceleration curves in frontal sled simulations.

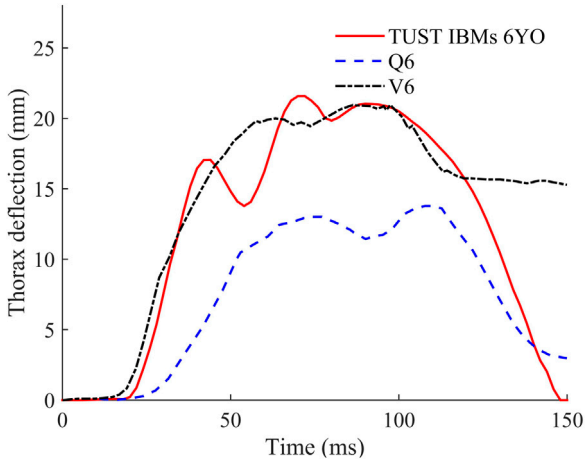

FIGURE 7
Thorax deflection curves in frontal sled simulations.

3 Results and discussion

The thorax acceleration, thorax deflection, shoulder belt force, and lap belt force curves obtained from the simulation results are compared with the corresponding curves of Q6 and V6 obtained from Hyncik et al.'s study (Hyncik et al., 2014), as shown in Figure 6, Figure 7, Figure 8, and Figure 9, and the reproduction of the curves was approved by the author Hyncik.

From Figures 6–9 and Table 3, it can be seen that there are two obvious peaks in the thorax acceleration curves of TUST IBMs 6YO, Q6, and V6, particularly 21.56 g/23.86 g, 21.52 g/27 g, and 23 g/18.51 g, respectively, while the maximum thorax accelerations are 23.86, 27, and 23 g, respectively. The variation tendency of the thorax acceleration curve of TUST IBMs 6YO agrees with those by Han et al. (2017) and Peng (2017), where simulations with a total human model for safety 3-year-old (THUMS 3YO) child FE model showed greater maximum thorax accelerations (Han et al., 2017). Possible reasons for the difference in maximum thorax acceleration could be associated with body weight and soft tissue energy absorption levels.

According to the variation tendencies of thorax deflection curves of TUST IBMs 6YO, Q6, and V6, there are two obvious peaks of 17.05 mm/21.58 mm, 14 mm/13, and 19.72 mm/21 mm in the corresponding curves, respectively. The maximum thorax

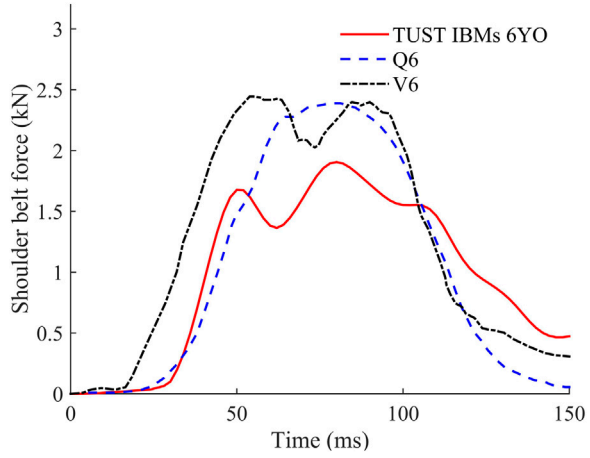

FIGURE 8
Shoulder belt force curves in frontal sled simulations.

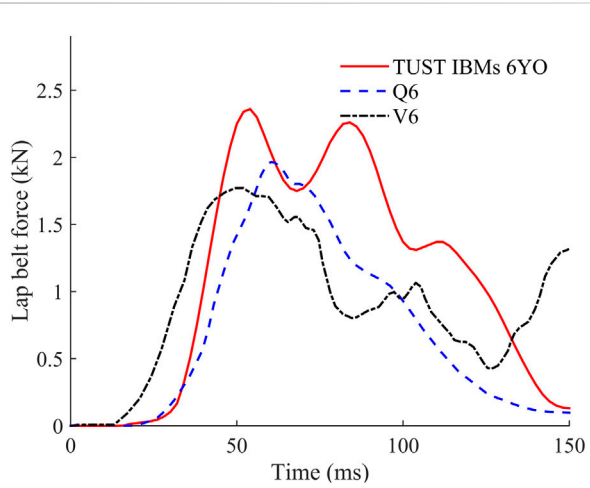

FIGURE 9
Lap belt force curves in frontal sled simulations.

TABLE 3 Maximum values for TUST IBMs 6YO, V6, and Q6.

Parameter	TUST IBMs 6YO	V6	Q6
Maximum thorax acceleration (g)	23.86	23	27
Maximum thorax deflection (mm)	21.58	21	14
Maximum shoulder belt force (kN)	1.91	2.53	2.48
Maximum lap belt force (kN)	2.36	1.77	1.96

deflections are 21.58, 14, and 21 mm in TUST IBMs 6YO, Q6, and V6, respectively. The maximum shoulder/lap belt forces of TUST IBMs 6YO, Q6, and V6 are 1.91 kN/2.36 kN, 2.48 kN/1.96, and 2.53 kN/1.77 kN, respectively. The maximum shoulder/lap belt load values of TUST IBMs 6YO (1.91 kN/2.36 kN) were much greater than those from low-speed, non-injurious frontal sled tests, which were conducted using male human volunteers with the sled acceleration pulse by Arbogast et al. (2009). The variation tendencies of shoulder/lap belt force curves of TUST IBMs 6YO agree well with those by Giordano et al. (2017), where simulations with the position and personalize advanced human body models for injury prediction (PIPER) scalable child model showed a greater maximum shoulder/lap belt force, and possible reasons could be associated with the muscle modeling method. The TUST IBMs 6YO thoracoabdominal muscle models with detailed anatomical structures were constructed based on the CT data of a 6YO child, which could better simulate the geometric characteristics and the direction of force transmission of the muscles, rather than using an equivalent muscle like that in the PIPER scalable child model.

The variation tendencies of the thorax acceleration, thorax deflection, shoulder belt force, and lap belt force curves of TUST IBMs 6YO are in good agreement with the corresponding curves of Q6 and V6. In addition, the difference between TUST IBMs 6YO, Q6, and V6 in acceleration and deflection in the thorax is caused by the different thorax structure of the models. The different response to the safety belt in the unloading stage of the thoracoabdominal contact force is caused by the impact of the simple seat model used in V6 during the unloading stage.

It can be seen from Figure 7 that the thorax deflections of TUST IBMs 6YO and V6 are greater than those of Q6, which is caused by the high thorax stiffness of Q6. Figures 8, 9 show that the maximum shoulder belt force of TUST IBMs 6YO is smaller than those of V6 and Q6, while the opposite is true for the lap belt force. The reason for the different simulation results of the three models is due to the different structure and geometry of the models. From Figures 7, 8, the value of thorax deflection of TUST IBMs 6YO was close to that of V6, while the value of shoulder belt force of TUST IBMs 6YO was smaller than that of V6 in the time interval 0–100 ms, which indicated that the thorax total stiffness of TUST IBMs 6YO was smaller than that of V6. It can also be seen that the thorax total stiffness of V6 was greater than that of Q6.

The thorax injury indexes include the viscosity criterion (V*C) and abbreviated injury scale (AIS). The V*C value represents the change rate of chest deformation relative to time (see Eq. 1), which is used to evaluate the damage to chest soft tissue.

$$V^{*}C = V(t)C(t) = \frac{d[D(t)]}{dt}\frac{D(t)}{b} \tag{1}$$

Here, $D(t)$ is the time function of chest compression and b is the initial chest thickness.

The correlation between (V*C)max and chest injury has been investigated in thoracic impact experiments with human cadavers in the literature (Viano, 1989; Cavanaugh et al., 1993; Pintar et al., 1997), which provides data support for the prediction of chest injury. Therefore, (V*C)max is used as an index to evaluate chest injury in this article. The chest injury

TABLE 4 Detailed information of injury threshold of the 6YO child.

Parameter	Chest $(VC)_{max}$	Abdomen $(VC)_{max}$	Abdomen $F_{max}C_{max}$
Scale factor	$0.6562^{1/2}$	$0.6562^{1/2}$	$0.642^{2} \times 0.6562$
Adult injury threshold	1.3 (m/s)	1.4 (m/s)	1540 (N)
Injury threshold of the 6YO child	1.053 (m/s)	1.134 (m/s)	417 (N)

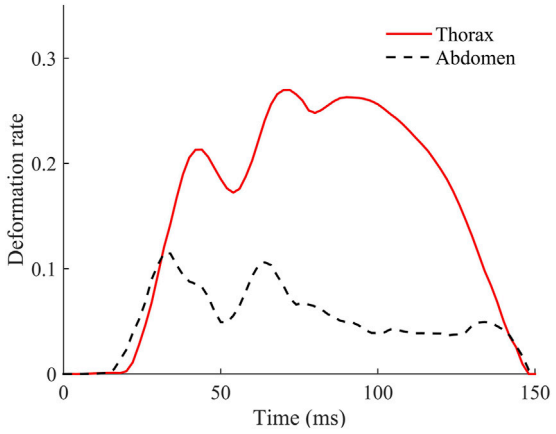

FIGURE 10
Thorax and abdomen deformation rate curves of TUST IBMs 6YO.

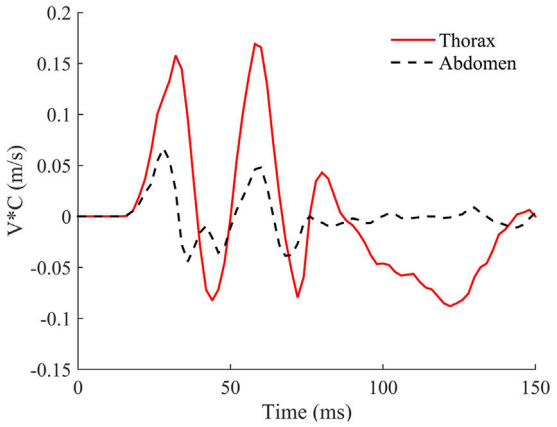

FIGURE 11
Thorax and abdomen V*C curves of TUST IBMs 6YO.

threshold (VC)max of lateral impacts was obtained from Ivarsson et al.'s (2004) study, and the relationship between injury threshold (VC)max of frontal impacts and lateral impacts was obtained from Viano et al.'s (1989) study. The chest and abdomen injury thresholds of frontal impacts are shown in Table 4.

The injury level formula is the relationship between the AIS and compression ratio of the chest and abdomen obtained by Viano et al. (1989), as shown in Eq. 2, where C is the chest compression index, which refers to the ratio between chest compression and chest thickness.

$$AIS = -3.78 + 19.56C \quad (2)$$

The ratio between the AIS of a 6YO child and the compression of the chest and abdomen is obtained according to the height ratio between children and adults as follows in Eq. 3.

$$AIS = -2.48 + 12.71C \quad (3)$$

The deformation rate, V*C, FmaxCmax of the thorax and abdomen, the trunk angle, and the maximum first principal strain of internal organs are obtained from the frontal sled simulation, as shown in Figure 10, Figure 11, Figure 12, Figure 13, and Figure 14. In addition, Table 5 shows the injury parameters of the thorax and abdomen for TUST IBMs 6YO.

From Figure 10 and Table 5, it can be seen that the maximum deformation rates of the chest and abdomen of TUST IBMs 6YO are 26.97 and 11.49%, respectively. According to Eq. 3, the thorax AIS of TUST IBMs 6YO is 0.925 with the maximum deformation rate of the chest 26.97%, which indicates that the child injury is mild in the frontal sled simulation. The maximum V*C values of the thorax and abdomen of TUST IBMs 6YO are 0.169 and 0.06, respectively, which do not reach the corresponding injury thresholds of 1.053 and 1.134, while the probability of AIS 4+ is 25% (Ivarsson et al., 2004), which indicates that the thorax and abdomen of TUST IBMs 6YO have a higher probability of slight or no injury. From Figures 10, 11, the maximum deformation rate and V*C values of the thorax are greater than those of the abdomen due to the difference in the effect of the seat belt on the thorax and abdomen.

The injury thresholds of the first principal strain of heart contusion and laceration were defined in this paper as 30% and 62.6 ± 6.9%, respectively, according to Yamada's (1970) study. The maximum first principal strain of the lungs (28.4%) was used to reflect pulmonary contusion, which was obtained by combining experiment and FE simulation results by Gayzik (2008). From Figures 12, 13, it is known that the maximum first principal strain of the heart is 11.8% at 68 ms, which is caused by the compression of the heart, sternum, and the fourth and fifth ribs under the seat belt. By comparing the maximum first principal strain and injury threshold of the heart, the result shows that there are no

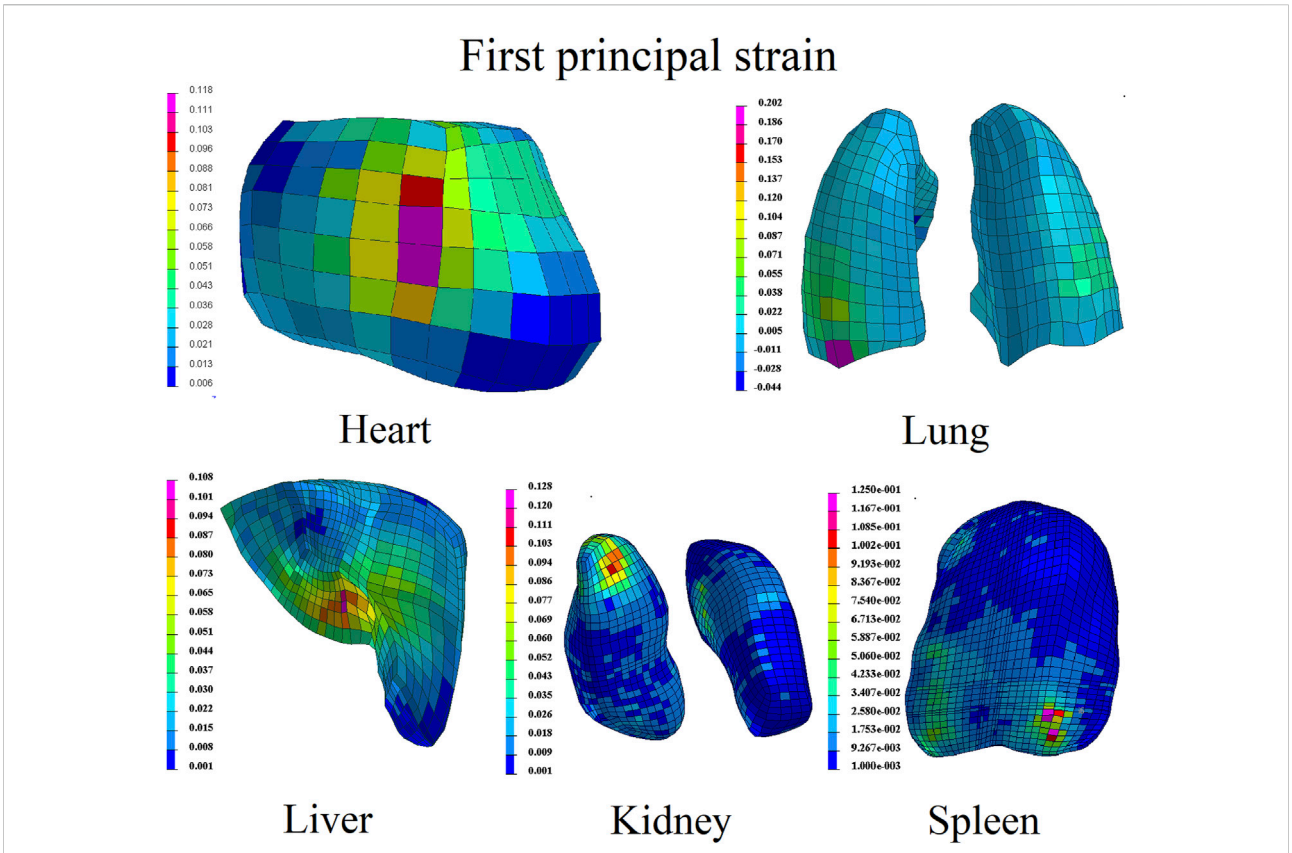

FIGURE 12
Maximum first principal strain diagrams of internal organs in TUST IBMs 6YO.

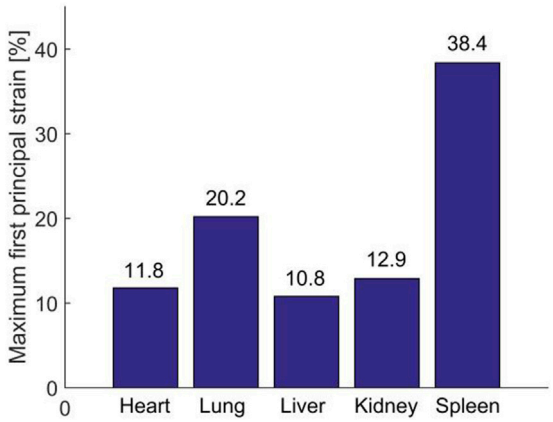

FIGURE 13
Maximum first principal strains of internal organs for TUST IBMs 6YO.

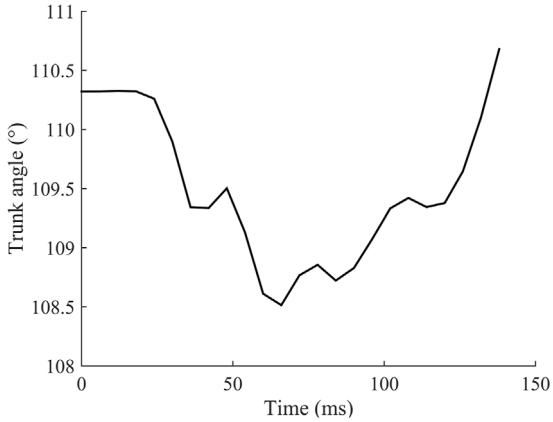

FIGURE 14
Trunk angle curve of TUST IBMs 6YO.

contusions or lacerations in the heart. The maximum first principal strain of the lungs is 20.2% at 38 ms, which does not reach the injury threshold (28.4%), and indicates that no pulmonary contusion occurred. The pressure of the safety belt is large during the motion process, which can easily cause lung damage from the ribs. Therefore, the safety belt cushion should be added in the

TABLE 5 Injury parameters of the thorax and abdomen for TUST IBMs 6YO.

Parameter	TUST IBMs 6YO	Injury Threshold
Chest (V^aC)max (m/s)	0.169	1.053[a]
Abdominal (V^aC)max (m/s)	0.06	1.134[a]
Chest AIS	0.925	-
Abdominal AIS	0	-
Chest compression rate (%)	26.97	-
Abdominal compression rate (%)	11.49	-
Chest FmaxCmax (N)	514.05	-
Abdominal FmaxCmax (N)	242.63	417**

[a]significant level: 0.01 ** significant level: 0.04.

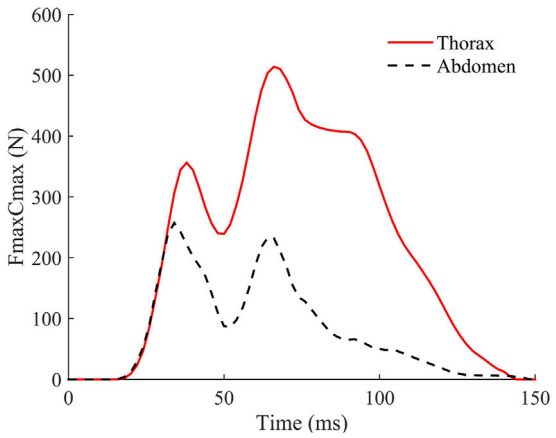

FIGURE 15
Thorax and abdomen FmaxCmax for TUST IBMs 6YO.

safety belt design, which can effectively reduce the damage to the lungs. The distributions of the first principal strain in the heart and lungs are consistent with those in the study by Tang (2018), where simulations with the THUMS 3YO occupant model showed a larger first principal strain, and possible reasons could be associated with the element type and boundary definition type. The heart and lungs in TUST IBMs 6YO were constructed using a hexahedral solid element rather than a tetrahedral solid element like that in the THUMS model. The boundary condition of the heart and lungs in TUST IBMs 6YO was defined as surface to surface contact, which could better simulate the actual boundary conditions, rather than using shared boundary node setting like that in the THUMS model. The tolerance value of the first principal strain of the liver was defined in this paper as 30% according to Melvin et al.'s (1973) study. The maximum first principal strain values of the liver, spleen, and kidney are 10.8% (at 38 ms), 38.39% (at 76 ms), and 12.9% (at 54 ms), respectively. The maximum first principal strain of the liver is smaller than the corresponding injury threshold, which indicates no injury to the liver. The maximum first principal strain values of the liver and kidneys are due to the extrusion of the liver/kidney and the stomach, while the maximum first principal strain of the spleen appears on account of the contact of the ribs with the spleen and the diaphragm under the action of the safety belt, see Supplementary Appendix SC. It can be seen from the data that the injury risks to internal organs of children such as the heart, lungs, liver, and kidneys during the kinematic response are lower, indicating that these organs are better protected than the spleen.

The definition of the trunk angle is the angle between the line of the hip joint and shoulder joint and the horizontal. From Figure 14, the maximum trunk angles are 108.51° and 110.67°. The greater the change in trunk angle, the more obvious the submarining trend, which represents a higher injury risk of the child's abdomen due to the compression of internal organs after the lap belt slipped over the iliac crests, which is consistent with the study by Adomeit and Heger, 1975. The abdomen is easily injured at 66 and 138 ms.

The FmaxCmax injury parameter value is a comprehensive injury evaluation index, which is obtained from the product of the maximum contact force between the thorax and the seat belt and the thorax compression ratio. The thorax injury risk increases with the increase of the FmaxCmax value. The experimental analysis by Untaroiu et al. (2012) shows that FmaxCmax and the intrusion speed of children's safety belts are the best indices to predict injury. Figure 15 shows the variation tendency of FmaxCmax of TUST IBMs 6YO. The maximum FmaxCmax value of the abdomen 240.63 N is smaller than the corresponding injury threshold 417 N obtained from Table 5, which indicates that there is no probability of AIS 4 + abdominal injury. The FmaxCmax value of the chest is greater than that of the abdomen in the time interval of 35–140 ms.

There are a few limitations to the study: 1) the study focuses on the specific topic of a 6YO thorax and abdomen comparison in a frontal sled test simulation. Future work could address thorax and abdomen injuries in lateral impact simulation. 2) Most of the material parameters of TUST IBMs 6YO are obtained by scaling those of the adult, which will be continuously updated as technology develops. 3) Injury thresholds for children were obtained by scaling the adult injury thresholds, which need to be further verified in future studies.

4 Conclusion

The paper demonstrates that the variation tendency of thorax acceleration, the intrusion of the thorax safety belt, and the shoulder/lap belt force in Q6, V6, and TUST IBMs 6YO are consistent with each other. The thorax total stiffness of the Q6, V6, and TUST IBMs 6YO models shows a decreasing trend. According to the injury index of the TUST IBMs 6YO in the motion process, it can be seen that the injury risks of the thorax and abdomen are relatively high at 80 ms, and better emergency measures should be provided to better protect the thorax and abdomen and reduce the injury. In addition, the child safety seat should be improved, addressing the injuries of the thorax and abdomen to achieve the best protection. The paper shows the greater advantages of the simulation output data of the child FE model with detailed anatomical structures to better reflect the performance of the child safety seat and provide more specific data for improving the CRS.

Data availability statement

The original contributions presented in the study are included in the article/Supplementary Material; further inquiries can be directed to the corresponding authors.

Author contributions

The author's contributions are as follows: HL was in charge of the whole trial; WL, LH, and BZ wrote the manuscript; HZ, SC, LH, and SR assisted with simulation calculation and analyses.

Funding

This work was supported by the National Natural Science Foundation of China (Grant No. 81471274, 81,371,360, and 81,201,015) and by the European Regional Development Fund-Project "Application of Modern Technologies in Medicine and Industry" (Fund No.CZ.02.1.01/0.0/0.0/17_048/0,007,280).

Conflict of interest

Author BZ was employed by Quadrant Space Science and Technology Company, Limited.

The remaining authors declare that the research was conducted in the absence of any commercial or financial relationships that could be construed as a potential conflict of interest.

Publisher's note

All claims expressed in this article are solely those of the authors and do not necessarily represent those of their affiliated organizations or those of the publisher, the editors, and the reviewers. Any product that may be evaluated in this article or claim that may be made by its manufacturer is not guaranteed or endorsed by the publisher.

Supplementary material

The Supplementary Material for this article can be found online at: https://www.frontiersin.org/articles/10.3389/ffutr.2022.890776/full#supplementary-material

References

Adomeit, D., and Heger, A. (1975). Motion sequence criteria and design proposals for restraint devices in order to avoid unfavorable biomechanic conditions and submarining. *Stapp Car Crash Conf.* 19, 139.

Arbogast, K. B., Balasubramanian, S., Seacrist, T., Maltese, M. R., Garcia-Espana, J. F., Hopely, T., et al. (2009). Comparison of kinematic responses of the head and spine for children and adults in low-speed frontal sled tests. *Stapp Car Crash J.* 53, 329–372. doi:10.4271/2009-22-0012

Beauchamp, L., Beuse, N., and Doyle, S. (2005). *Child restraint dynamic performance evaluation in a 48 km/h (30 mph) sled test*. Washington: NHTSA Technical report.

Beillas, P., Soni, A., Chevalier, M. C., et al. (2014). "Q6 dummy thoracic response and diagonal belt interactions: Observations based on dummy testing and human and dummy simulations," in Proceedings of the IRCOBI Conference Proceeding, Berlin, Germany, September 10–12, 2014. Paper IRC-14-39.

Cao, L. B., Chen, H., Ren, X. J., and Ou Yang, Z. G. (2010). Study on an integrated child safety seat. Applied Mechanics and Materials. *Trans. Tech. Publ.* 34, 517–522. doi:10.4028/www.scientific.net/amm.34-35.517

Cavanaugh, J. M., Zhu, Y., Huang, Y., et al. (1993). "Injury and response of the thorax in side impact cadaveric tests," in Proceedings of the 37th Stapp Car Crash Conference, San Antonio, TX, November 1, 1993, 199–221. SAE Paper #933127.

Cui, S. H., Chen, Y., Li, H. Y., Cao, D. C., and Ruan, S. J. (2015). Development and validation for the finite element model of child head. *J. Med. Biomechanics* 30 (5), 452. doi:10.3871/j.1004-7220.2015.05.452

Cui, S. H., Shan, L. L., Li, H. Y., He, L. U., Lyu, W. L., Ruan, S. J., et al. (2016). Development and validation of a 6-year-old occupant thorax finite element model and impact injury analysis. *Chin. J. Automot. Eng.* 6 (6), 418Chinese. doi:10.3969/j.issn.2095-1469.2016.06.05

Eggers, A., Schnottale, B., and Ott, J. (2015). "Sensitivity of Q10 and Q6 chest measurements to restraint and test parameters," in Proceedings of the 24th International Technical Conference on the Enhanced Safety of Vehicles, Gothenburg, Sweden, June 8–June 11, 2015.

Franz, U., and Graf, O. (2000). "Accurate and detailed LS-DYNA FE models of the US-and EUROSID: A review of the German fat project," in Proceedings of the 6th International LS-DYNA Conference, Dearborn, MI, April 9–April 11, 2000.

Gayzik, F. S. (2008). *Development of a finite element based injury metric for pulmonary contusion*. Winston-Salem: Wake Forest University.

Giordano, C., Li, X., and Kleiven, S. (2017). Performances of the PIPER scalable child human body model in accident reconstruction. *PLoS ONE* 12(11), e0187916. doi:10.1371/journal.pone.0187916

Han, Y., Pan, D., Ouyang, J., Qian, L., Mizuno, K., and Anguo Cang, A. (2017). Study of chest injuries to 3YO child occupants seated in impact shield and 5-point

harness CRSs. *Traffic Inj. Prev.* 19(3), 274–279. doi:10.1080/15389588.2017.1385780

Haut, R. C., and Atkinson, P. J. (1995). "Insult to the human cadaver patellofemoral jointEffects of age on fracture tolerance and occult injury," in Proceeding of the 39th Stapp Car Crash Conference, San Diego, CA, November 1, 1995, 39, 281.

Huang, Y., Ji, P. J., Ma, L. C., et al. (2016). A study on crash waveform dispersion and its effects on the responses of child restraint system. *Automot. Eng.* 38 (4), 440. doi:10.19562/j.chinasae.qcgc.2016.04.008

Hyncik, L., Cechova, H., Kovar, L., and Blaha, P. (2013). *On scaling virtual human models*. U.S. and Canada: SAE Technical Paper. 2013-01-0074.

Hyncik, L., Mana, J., Spicka, J., Špirk, S., and Kovar, L. B. (2014). *Development of 6 years old child virtual model by automatic scaling*. U.S. and Canada: SAE Technical Paper. 2014-01-2028.

Ivarsson, B. J., Crandall, J. R., and Longhitano, D. (2004). *Lateral injury criteria for the 6-year-old pedestrian - Part I: Criteria for the head, neck, thorax, abdomen and pelvis*. U.S. and Canada: SAE Technical Papers.

Jager, K. D., Ratingen, M. V., Lesire, P., Guillemot, H., Schnottale, B., Tejera, G., et al. (2005). "Assessing new child dummies and criteria for child occupant protection in frontal impact," in Proceedings of the 19th ESV conference, Washington, DC, June 6–June 9, 2005, TNO–LAB–BASt–IDIADA–UTAC.

Jiang, B. H., Cao, L. B., Mao, H. J., Wagner, C., Marek, S., and Yang, K. H. (2012). Development of a 10-year-old paediatric thorax finite element model validated against cardiopulmonary resuscitation data. *Comput. Methods Biomechanics Biomed. Eng.* 17 (11), 1185–1197. doi:10.1080/10255842.2012.739164

Jiang, B. H. (2013). *Development of finite element model and study of injury mechanisms for pediatric thorax*. Changsha: Hunan University.

Kajzer, J., Matsui, Y., Ishikawa, H., Günter, S., and Ulrich, B. (1999). *Shearing and bending effects at the knee joint at low-speed lateral loading*. Warrendale: SAE Special Publications.

Kerrigan, J. R., Ivarsson, B. J., Bose, D., Madeley, N. J., Millington, S. A., Bhalla, K. S., et al. (2003). ". Rate-sensitive constitutive and failure properties of human collateral knee ligaments," in Proceedings of the International Research Council on the Biomechanics of Impacts (IRCOBI) Conference, Lisbon (Portugal), September 25–26, 2022.

Kim, S., Ryu, H., Kim, Y., Baek, S., Kim, M., and Park, J. (2014). The study on the effect of seatbelt anchorage points using Q6 in sled test. *J. Auto-vehicle Saf. Assoc.* 6 (2), 49.

Li, H. Y., Cui, Z. Y., Cui, S. H., et al. (2017a). Development and validation of pelvic finite element model for a 6-year-old child. *Chin. J. Automot. Eng.* 7 (2), 100.

Li, H. Y., Li, K., Huang, Y. Q., Lv, W., Cui, S., He, L., et al. (2020). Validation of a finite element model with six-year-old child anatomical characteristics as specified in Euro NCAP Pedestrian Human Model Certification (TB024). *Comput. Methods Biomechanics Biomed. Eng.* 24 (6), 76–90. doi:10.1080/10255842.2020.1810677

Li, H. Y., Pan, Y. F., Ruan, S. J., et al. (2017b). Analysis of growth plate material property effect on knee injury of six-year-old child occupant. *Yiyong Shengwu Lixue/journal Med. Biomechanics* 32 (3), 213. doi:10.16156/j.1004-7220.2017.03.002

Luck, J. F., Nightingale, R. W., Yin, S., Kait, J. R., Loyd, A. M., Myers, B. S., et al. (2013). Tensile failure properties of the perinatal, neonatal, and pediatric cadaveric cervical spine. *Spine* 38 (1), E1–E12. doi:10.1097/brs.0b013e3182793873

Lv, W. L., Ruan, S. J., Li, H. Y., Cui, S., He, L.-J., and Wang, C.-X. (2016a). Development and validation of finite element model for 6-year-old pediatric neck. *J. Med. Biomechanics* 31 (2), 95–101. in Chinese. doi:10.3871/j.1004-7220.2016.02.095

Lv, W. L., Ruan, S. J., Li, H. Y., Cui, S., and He, L. (2015). Development and validation of a 6-year-old pedestrian thorax and abdomen finite element model and impact injury analysis. *Int. J. Veh. Saf.* 8 (4), 339–356. doi:10.1504/ijvs.2015.074378

Lv, W. L., Ruan, S. J., Li, H. Y., Cui, S. H., He, L. J., Wang, C. X., et al. (2016b). "Injury analysis of a six-year-old child pedestrian thorax in lateral/oblique impact," in Proceedings of the Eighth International Conference on Measuring Technology and Mechatronics Automation (ICMTMA), Macau, China, March 11–12, 2016: IEEE Computer Society, 352–358.

Lv, W. L., Ruan, S., Li, H. Y., Cui, S., and He, L. (2016c). Abdominal injury analysis of a 6-year-old pedestrian finite element model in lateral impact. *Int. J. Veh. Saf.* 9 (1), 85–100. doi:10.1504/ijvs.2016.077155

Maheshwari, J., Duong, N., Sarfare, S., and Belwadi, A. (2019). "Responses of a 6-year-old ATD restrained in a booster child seat on the FMVSS 213 test bench, proposed upgraded test bench and a vehicle seat in simulated frontal impacts," in Proceedings of the 26th International Technical Conference on The Enhanced Safety of Vehicles (ESV) - Conference Proceedings, Eindhoven, Netherlands, June 10–13, 2019.

Mañas, J., Kovář, L., Petřík, J., Čechová, H., and Špirk, S. (2012). Validation of human body model VIRTHUMAN and its implementation in crash scenarios. *Adv. Mech. Des.* 8, 351–356. doi:10.1007/978-94-007-5125-5_46

Melvin, J. W., Stalnaker, R. L., Roberts, V. L., et al. (1973). "Impact injury mechanisms in abdominal organs," in Proceedings of the 17th Stapp Car Crash Conference, Coronado, CA: Society of Automotive Engineers.

Mizuno, K., Iwata, K., Deguchi, T., Ikami, T., and Kubota, M. (2005). Development of a three-year-old child FE model. *Traffic Inj. Prev.* 6 (4), 361–371. doi:10.1080/15389580500255922

Nahum, A. M., Smith, R., and Ward, C. (1977). "Intracranial pressure dynamics during head impact," in Proceedings of 21st Stapp Car Crash Conference, New Orleans, LA: Society of Automotive Engineers 337–336.

Ouyang, J., Liu, C., Zhu, Q., Zhong, S., and Li, Z. (2015). Abdominal impact study on paediatric cadaveric subjects. *Int. J. Veh. Saf.* 8 (4), 287–298. doi:10.1504/ijvs.2015.074369

Ouyang, J., Xu, Y., Chen, W., Zhong, S., Zhu, Q., Zhao, W., et al. (2005). Biomechanical assessment of the pediatric cervical spine under bending and tensile loading. *Spine* 30 (24), E716–E723. doi:10.1097/01.brs.0000192280.53831.70

Ouyang, J., Zhao, W., Xu, Y., Chen, W., and Zhong, S. (2006). Thoracic impact testing of pediatric cadaveric subjects. *J. Trauma Inj. Infect. Crit. Care* 61 (6), 1492–1500. doi:10.1097/01.ta.0000233711.07823.40

Ouyang, J., Zhu, Q. A., Zhao, W. D., Xu, Y. q., Chen, W. s., and Zhong, S. z. (2003). Experimental cadaveric study of lateral impact of the pelvis in children. *1 Jun yi xue xue bao* 23 (5), 397.

Peng, L. Y. (2017). *Research on protective performance of child restraint system based on dummy, simulation and animal experiment*. China: Xiamen University of Technology. Master Thesis.

Pintar, F. A., Yoganandan, N., Hines, M. H., Maltese, M. R., McFadden, J., Saul, R., et al. (1997). "Chestband analysis of human tolerance to side impact," in Proceedings of the 41st Stapp Car Crash Conference, Lake Buena Vista, FL, November 12, 1997, 63–74. SAE Paper #973320.

Prange, M. T., Luck, J. F., Dibb, A., Van Ee, C. A., Nightingale, R. W., and Myers, B. S. (2004). Mechanical properties and anthropometry of the human infant head. *Stapp Car Crash J.* 48, 279–299. doi:10.4271/2004-22-0013

Q6 child dummy Model (2013). *Q6 child dummy Model*. Michigan: Humanetics. Release Version 1.0.

Shaw, J. M., Herriott, R. G., Mcfadden, J. D., Donnelly, B. R., and Bolte, J. H. (2006). Oblique and lateral impact response of the PMHS thorax. *Stapp Car Crash J.* 50 (1), 147.

Spicka, J., Manas, J., and Hyncik, L. (2015). Frontal impact response of a virtual low percentile six years old human thorax developed by automatic down-scaling. *Appl. Comput. Mech.* 9, 41. doi:10.4314/ahs.v3i3.6851

Tang, H. C. (2018). *Study on 3-year-old child occupant thoracic dynamic response and injury parameters in frontal impact*. China: Xiamen University of Technology. Master Thesis.

Trosseille, X., Cassan, F., and Schrooten, M. (2001). *Child restraint system for children in cars–CREST results*. U.S. and Canada: SAE Technical Paper.

Untaroiu, C., Darvish, K., Deng, B., and Wang, J. T. (2005). A finite element model of the lower limb for simulating pedestrian impacts. *Stapp Car Crash J.* 49 (11), 157. doi:10.4271/2005-22-0008

Untaroiu, C. D., Bose, D., Lu, Y. C., Riley, P., Lessley, D., and Sochor, M. (2012). Effect of seat belt pretensioners on human abdomen and thorax: Biomechanical response and risk of injuries. *J. Trauma Acute Care Surg.* 72 (5), 1304–1315. doi:10.1097/ta.0b013e3182472390

Viano, D. C. (1989).Biomechanical responses and injuries in blunt lateral impact," in Proceedings of the 33rd Stapp Car Crash Conference. U.S. and Canada: SAE Technical Paper, 113–142. SAE Paper #892432.

Viano, D. C., Lau, I. V., Asbury, C., King, A. I., and Begeman, P. (1989). Biomechanics of the human chest, abdomen, and pelvis in lateral impact. *Accid. Analysis Prev.* 21 (6), 553–574. doi:10.1016/0001-4575(89)90070-5

Vychytil, J., Manas, J., Cechova, J., et al. (2014). *Scalable multi-purpose virtual human model for future safety assessment*. U.S. and Canada: SAE Technical Paper. 2014-01-0534.

Yamada, H. (1970). *Strength of biological materials*. Baltimore: Williams & Wilkins.

Zhang, X. R., Wang, H. T., and He, J. (2021). Research on seat belt restraint path for child booster seats. *Chin. J. Automot. Eng.* 11 (1), 59–65. in Chinese.

Zhao, J. Z., and Norwani, G. (2007). Biomechanical analysis of hard tissue responses and injuries with finite element full human body model. *ESV Conf.* 9, 07.

frontiers | Frontiers in Future Transportation

TYPE Original Research
PUBLISHED 20 October 2022
DOI 10.3389/ffutr.2022.913852

OPEN ACCESS

EDITED BY
Yong Han,
Xiamen University of Technology, China

REVIEWED BY
Feng Zhu,
Johns Hopkins University, United States
Costin D. Untaroiu,
Virginia Tech, United States
Bharath Koya,
Wake Forest Baptist Medical Center, United States

*CORRESPONDENCE
Bernd Schneider,
bernd.schneider@tugraz.at

SPECIALTY SECTION
This article was submitted to Transport Safety, a section of the journal Frontiers in Future Transportation

RECEIVED 06 April 2022
ACCEPTED 03 October 2022
PUBLISHED 20 October 2022

CITATION
Schneider B, Kofler D, D'Addetta GA, Freienstein H, Wolkenstein M and Klug C (2022), Approach for machine learning based design of experiments for occupant simulation.
Front. Future Transp. 3:913852.
doi: 10.3389/ffutr.2022.913852

Approach for machine learning based design of experiments for occupant simulation

Bernd Schneider[1]*, Desiree Kofler[1], Gian Antonio D'Addetta[2], Heiko Freienstein[2], Maja Wolkenstein[2] and Corina Klug[1]

[1]Vehicle Safety Institute, Graz University of Technology, Graz, Austria, [2]Robert Bosch GmbH, Stuttgart, Germany

The complexity of crash scenarios in the context of vehicle safety is steadily increasing. This is especially the case on the way to mixed traffic challenges with non-automated and automated driving vehicles. The number of simulations required to design a robust restraint system is thus also increasing. The vast range of possible scenarios here is causing a huge parameter space. Simultaneously biofidelic simulation models are resulting in very high computational costs and therefore the number of simulations should be limited to a feasible operational range. In this study, a machine-learning based design of experiments algorithm is developed, which specifically addresses the issues when designing a safety system with a limited number of simulation samples taking diversity of the occupant and accident scenario into account. In contrast to an optimization task, where the aim is to meet a target function, our job has been to find the critical load case combinations to make sure that these are addressed and not missed. A combination of a space-filling approach and a metamodel has been established to find the critical scenarios in order to improve the system for those cases. It focuses specifically on the areas that are difficult to predict by the metamodel. The developed method was applied to iteratively generate a simulation matrix of a total of 208 simulations with a generic interior model and a detailed FE human body model. Kinematic and strain-based injury metrics were used as simulation output. These were used to train the metamodels after each iteration and derive the simulation matrix for the next iteration. In this paper we present a method that allows the training of a robust metamodel for the prediction of injury criteria, considering both varying load cases and varying restraint system parameters for individual anthropometries and seating postures. Based on that, restraint systems or metamodels can be optimized to achieve the best overall performance for a huge variety of possible scenarios with a specific focus on critical scenarios.

KEYWORDS

design of experiments, metamodel, finite element simulation, human body model, occupant safety, virtual testing, machine learning (ML)

1 Introduction

By means of virtual testing, the assessment of real-world safety instead of the protection in standard load cases is enabled (Freienstein et al., 2019; Luttenberger et al., 2020). The number of scenarios occurring in the real world however, is resulting an enormous parameter space. Furthermore, autonomous driving will enable new seating postures (Poulard et al., 2020) and as a result will therefore increase the overall complexity and the efforts required to safeguard occupant protection even more effectively. At the same time, biofidelic simulation models cause high computational costs and therefore the number of simulations should be limited to a feasible range. To control this increasing number of influencing variables and load cases, methods are needed to understand and scan the complex parameter space in an efficient way.

Adequate design of experiments is playing an increasingly important role in this. If no metamodel is chosen in advance, model-free designs are applied. So-called space-filling experimental designs are model-free designs that are very common for computer simulation. In such approaches, the whole parameter space is covered as uniformly as possible. An important aspect here is that the design is not only space-filling for the entire parameter space but also for subspaces (e.g., when only one parameter or a subset of parameters is being examined). When this is the case, the design is said to have good projection properties. Another point to consider is that the input parameters of the computer simulation can be of different types such as continuous, discrete or categorical and these need to be handled by a DoE algorithm. The points of a design can be chosen all at once, which is termed a one-shot strategy, such as in Joodaki et al. (2021) where a Latin Hypercube sampling was used. If results of experiments are intended to have an influence on the selection of new design points, a sequential strategy can be applied (Gan and Gu, 2019). (Provost et al., 1999; Crombecq et al., 2009; Draguljić et al., 2012; Pronzato and Müller, 2012).

Metamodels, sometimes also referred to as "surrogate models", are often used to describe the relationship between the input parameters and simulation outputs of interest. They can be used to find correlations between physical inputs and outputs of a given system. Many different metamodels are available for regression such as LASSO, k-nearest neighbors (k-NN), neural nets, support vector machines (Xia et al., 2018), decision trees, random forest (RF), gradient boosting and Gaussian process regression (GPR). It is usually not known in advance which model will be the best for a specific task so different models have to be tested. To evaluate the performance of a metamodel the available data set is split in training and test data. The model is trained with the training data and the performance is measured on the test data. Usually the split is done by randomizing the data and then using a certain percentage as training and the rest as test data. In an iterative approach, a further split into training and test data can also be used. The results of the last iteration of the sequential design can be used as test data and the rest as training data. Metamodels usually have several input parameters, so called hyperparameters, which have to be chosen by the user. In order to find the best set of hyperparameters cross-validation is generally used. Tuning of the machine learning hyperparameters was shown to be essential to achieve a metamodel with high accuracy (Williams, 2006; Watt et al., 2020; Joodaki et al., 2020).

In previous studies in the context of occupant safety and crashworthiness, the aim was to use a combination of metamodels and design of experiments mainly for optimization tasks. For such problems, different types of metamodels are used ranging from support vector regression (Xia et al., 2018) to even combinations of metamodels (Gan and Gu, 2019; Joodaki et al., 2020). Another approach was proposed in Adam and Untaroiu (2011) and Untaroiu and Adam (2013) where first a classification of pre-crash occupant postures was performed and a genetic algorithm was then used to optimize the restraint system for the different classes. In Perez-Rapela et al. (2020) neural networks in combination with Monte Carlo simulations are used to account for occupant response variability in the assessment of safety systems. An overview of design optimization for structural crashworthiness can be found in Fang et al. (2017). Other studies in the field of vehicle safety have tried to use metamodels for on-board prediction. In Bance et al. (2021) a lumped parameter model together with polynomial chaos expansion uncertainty quantification is used for on-board occupant injury risk prediction. Another example is the prediction of an occupant model's response to time-varying accelerations for applications inside the vehicle for restraint system control units with a metamodel aiming to work in real-time (Kneifl et al., 2022). For this task, a non-intrusive model order reduction with long short-term memory is used (Kneifl et al., 2022).

In summary, metamodels are trained to predict the response for different combinations of input parameters. The accuracy of the metamodel prediction for specific combinations of input-parameters depends to a great extent on the parameter-space covered by the training dataset and testing is only done within the parameter-space covered by the test dataset. Therefore, an appropriate design of experiments for deriving the test and training datasets plays an essential role.

For the development of restraint systems the parameters are usually varied in a defined scenario catalogue. This scenario catalogue tends to be the load cases tested in regulations or consumer information testing. However, ideally these scenario catalogues should cover a wide range of scenarios to finally design a robust restraint system and not to miss potentially critical scenarios, likely to happen in the field (Perez-Rapela et al., 2020).

Since we cannot apply a full factorial design of experiments due to the high computational costs, a smarter method is needed to select the simulation cases. For safety-relevant simulations, it is important to cover especially the critical areas within our

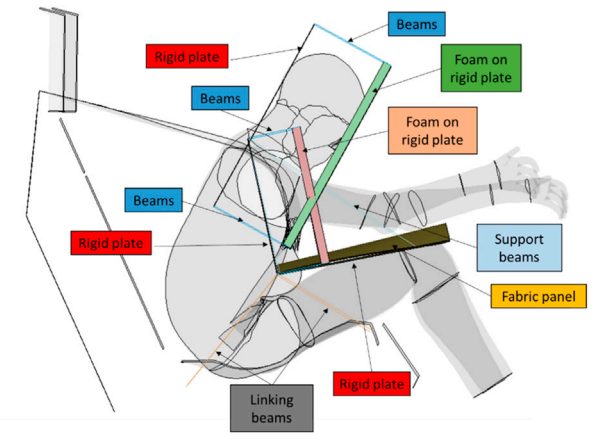

FIGURE 1
Assembly of the simplified airbag load chain representation. Each foam panel contacts only the corresponding body region e.g. head (green), thorax (orange) and femur (yellow). Each panel is connected to a rigid plate (red) *via* beams (blue). The head and thorax panel are connected to the femur panel *via* support beams (light blue). The entire construction is connected to the seat structure *via* linking beams (grey) to keep the generic airbag in place.

parameter space for the development of metamodels or for optimizing the restraint systems. The question arises in this context, of how we can, with a limited number of simulations, focus on the critical areas of the design space if these are unknown when starting the simulation study. This is particularly challenging, as the criticality is determined by a combination of intrinsic and extrinsic factors as well as the applied safety system (Perez-Rapela et al., 2020).

In our study, we have addressed this question and investigated how to select data points in the parameter space that are most useful for training a metamodel and learning about the restraint system performance. Our aim was to gather the maximum quantity of information relevant for occupant protection from a given number of simulations. An intelligent design of experiments for occupant simulation was developed for this purpose, which aims to automatically select simulations in areas that are difficult to control. To demonstrate the methodology, the effect of different loading directions, anthropometries and seating postures for the design of a generic restraint system and the resulting occupant loads was analysed.

2 Materials and methods

2.1 Data generation

2.1.1 Simulation environment

For development and testing of the methodology, an exemplary simulation study was performed. A finite element simulation model was set up, consisting of a generic seat with belt, a simplified airbag load chain representation (SALCR) and the human body model (HBM) THUMS v4.02. The SALCR includes three foam panels, which are attached to a rigid plate, see Figure 1. The characteristics of the generic airbag can be adjusted by changing the stiffness of the beams connected to the head and thorax panels to simulate different stiffnesses (mass flows). Furthermore, by changing the factor of distribution of stiffness between the two panels different loading paths corresponding to different shapes of airbags are simulated. After a maximal deflection of 300 mm, the stiffness of the beams is increased significantly to simulate a contact of the HBM with the vehicle interior. The femur panel consists of a fabric sheet which enables the support of the SALCR on the HBM thighs. This generic setup was chosen in order to represent the same initial conditions for each simulation run by a seat bounded restraint system. Thereby influences of an eventual deviation in airbag deployment are eliminated and the same initial distance between the HBM and the SALCR is provided. In order to check the plausibility of the effects of the SALCR, a comparison of the forces was made with a simulation model based on the vehicle of the oblique THOR Accord model (downloaded on 11.03.2020), that is equipped with a serial driver and passenger airbag model (Singh et al., 2018). A table with adjusted parameters of the airbag model compared to the downloaded version can be found in the Supplementary Material. Since no steering wheel is present in the simulation setup, the comparison is made with the passenger airbag model of the Honda Accord. The plots for the comparison of the forces can be found in the Supplementary Material. Amplitude and shape are comparable for the belt forces as well as the SALCR/airbag contact forces, but a time shift in force between the serial airbag and the conceptual system used in this study is observed, which is caused by the difference in support and deployment. The ISO 18571 (ISO, 2014) scores for the comparison of belt force and airbag forces can be found in the Supplementary Material. Anyhow, no exact replication of one restraint system was targeted. Instead the aim was to enable easy parameter variation over a wide range. Therefore, the developed conceptual SALCR was found to be an appropriate simplification.

Two different occupant anthropometries were chosen for the investigations. The THUMS v4.02 50th percentile male (AM50) model was utilized as basis. For analysis of anthropometric differences, THUMS was used in its baseline size (height: 1.78 m, mass: 77 kg). Since a consistent THUMS v4.02 model version was not available for the fifth percentile anthropometry, a scaled version of the baseline was used (height: 1.53 m, mass: 46 kg). The model was scaled only, to keep everything else consistent.

An upright and a lounge positioned model were generated for both anthropometries. The upright model equals the available THUMS v4.02 occupant model and the lounge

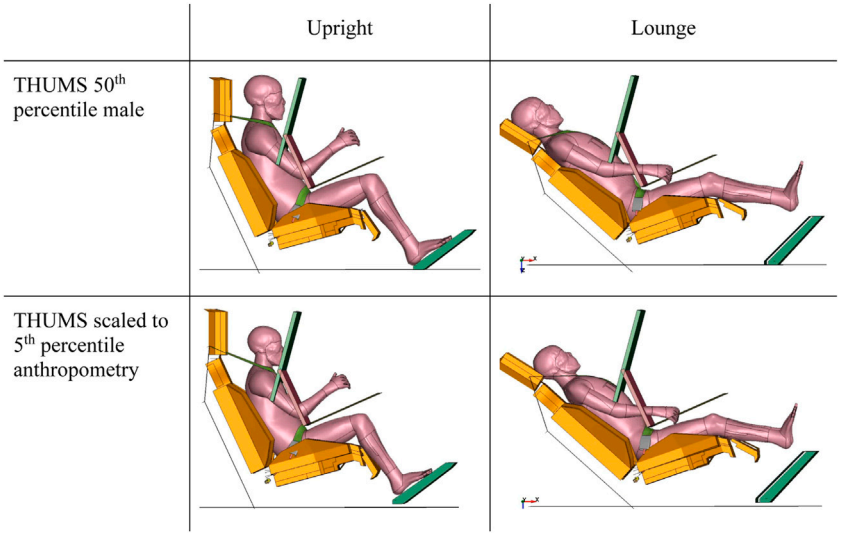

FIGURE 2
AM50 and AF05 THUMS models in upright and lounge seating position.

TABLE 1 Simulation configurations for crash pulse generation.

Pulse name	Crash configuration	v HO [km/h]	v OPP [km/h]	α [°]	m HO [-]	m OPP [-]	acc HO max in x [g]	acc HO max in y [g]
FF56	Wall, frontal	56	0	-	Heavy	Rigid wall	44.4	2.9
Center_0	Centre, centre	40	50	0	Heavy	Heavy	31.8	11.7
Center_45	Centre, centre	40	50	45	Heavy	Heavy	27.5	26.9
Center_m45	Centre, centre	40	50	-45	Heavy	Heavy	23.6	26.9

model was generated by positioning the THUMS v4.02 pedestrian model. Figure 2 illustrates the final simulation models. The lounge model basically represents a reclined seating position that allows a relaxed occupant posture. The generic airbag was positioned with the bottom edge aligning with the lap belt. The footrest was transformed to provide adequate foot support for both models in upright position.

2.1.2 Crash pulses

To investigate occupant behaviour for different loading conditions, acceleration-time pulses were generated by finite element simulations (Höschele et al., 2022) with a simulation model based on the vehicle of the oblique THOR Accord model (Singh et al., 2018) (downloaded on 11.03.2020). The description of the crash configuration is based on the "Volvo parametric crash configuration" (Wagström et al., 2019). Table 1 lists the configuration of the simulations by which the four pulses were generated. The values, such as velocity (v), mass (m) and acceleration (acc), of the host vehicle are indicated with HO and the values of the oncoming vehicle or wall encountered are indicated with OPP.

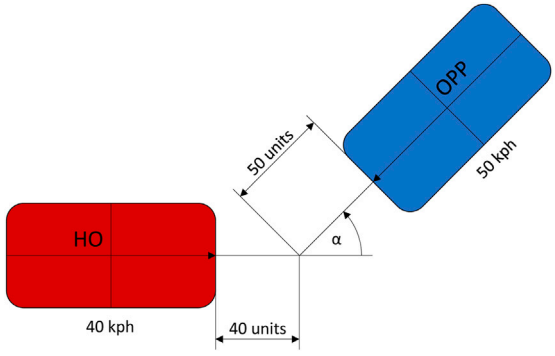

FIGURE 3
Sketch of the Center_45 oblique impact scenario.

TABLE 2 Parameters to be varied with corresponding values and ranges.

Parameter	Value	Quantity
Anthropometry	• THUMS v4.02 a.m.50 (AM50) • THUMS v4.02 a.m.50 scaled (AF05)	2
Seating position	• Upright • Lounge	2
Pulse	• FF56 • Center_45 • Center_0 • Center_m45	4
Stiffness of the SALCR beams	• 750 kN–3,000 kN	continuous
Distribution of the stiffness of SALCR beams	• 33%–66% (100% corresponds to 100% stiffness on the head panel)	continuous
Belt load limiter	• 60%–100% (100% corresponds to 1.95 kN)	continuous

The full-frontal load case FF56 was generated by a vehicle impact on a rigid wall with 56 km/h. The other pulses were generated by vehicle-to-vehicle impact scenarios with both Honda Accord models of equal mass and vehicle velocities of 40 and 50 km/h respectively. The two oblique impact scenarios Center_m45 and Center_45 were simulated with ±45° impact angle. Figure 3 shows a sketch of the configuration of the Center_45 oblique impact.

For each simulation, the acceleration was recorded in the centre console of the host vehicle, whereby the accelerations in x- and *y*-direction as well as the rotational acceleration about the *z*-axis were output. Plots of the pulses for each axis can be found in the Supplementary Material. These data were used as input for the HBM simulation environment, whereby the acceleration was applied only on the seated HBM model. The load was not applied to the generic airbag model in order to isolate the HBM airbag interaction behaviour and avoid overlaid loadings on the SALCR due to HBM contact and global acceleration.

2.1.3 Simulation and evaluation

The simulation models were parameterised and boundary conditions for the individual parameters were defined. Table 2 summarizes all varied parameters and the corresponding values or thresholds of the baseline occupant simulation model. It contains a combination of categorical and continuous parameters.

The parameters chosen by the developed DoE method, were automatically inserted in the simulation decks. Simulations were performed on a HPC cluster using LS-Dyna R9.2.1. A single simulation took about 24 h on 80 cores and produced an output of about 5 GB.

The evaluation of the simulation results was conducted with the in-house developed tool "dynasaur"[1] (Klug et al., 2018) from the LS-Dyna binout files. The injury criteria HIC15, Brain 95th percentile strain (Brain 95p), NIC and Rib fracture 1 + risk (Forman et al., 2012) were implemented in the "dynasaur" calculation procedure and evaluated automatically. For the kinematic injury criteria HIC and NIC, accelerometers were positioned in the THUMS model at the head center of gravity, center of C1 and T1 and connected to the bony structure with an interpolation constrained (*CONSTRAINED_INTERPOLATION). Accelerations were filtered with CFC 1000 before further processed. The 95th percentile strain for the brain was calculated from the element time histories. For the rib fracture assessment, the procedure from Forman et al. (2012) and the smoothed risk curve (Larsson et al., 2021) from Forman et al. (2012) for a 45 year old person were applied using the maximum principle strain at the mid-surface per rib to calculate the fracture risk per rib, combined with the probabilistic function to the overall risk of 1 + rib fractures.

2.2 Feedback loop

The basic idea of the feedback loop is a combination of a DoE algorithm, which can select a number of points from a set of candidate points, and a metamodel. Any type or combination of metamodels that has good predictive quality can be trained and applied based on the specific problem. Based on the predictions of the metamodel a subset of the set of candidate points is selected. How this subset is chosen can vary, depending on the specific task and goal. This procedure of the feedback loop is illustrated in Figure 4.

The start and end of the feedback loop are colored blue. The boxes colored black indicate algorithms and boxes related to candidate points are colored green. To start the feedback loop, 64 simulations are selected using a Latin hypercube design (LHD). Finite element simulations are carried out with these input parameters to obtain the simulation results. For further designs, the existing design is augmented with candidate points which are randomly selected points in the design space. The selection of a subset of candidate points is done with the help of metamodels. The goal is to achieve good prediction of the metamodel on the whole parameter space. The following procedure was used:

1 https://gitlab.com/VSI-TUGraz/Dynasaur.

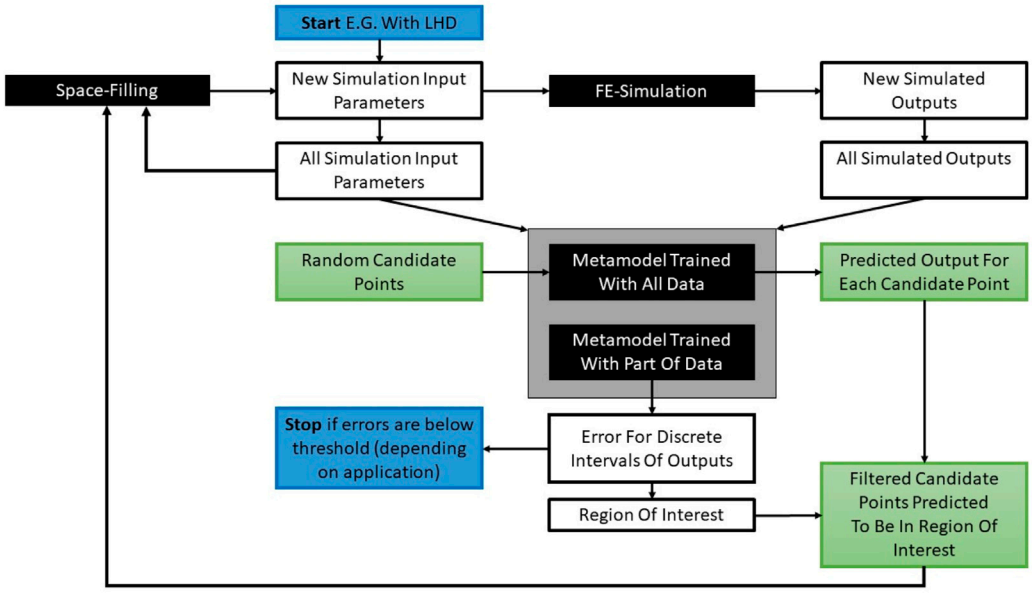

FIGURE 4
Basic principle of feedback loop combining DoE algorithm and metamodel.

- For each injury criterion of interest, a metamodel is trained and the performance is measured on the test set.
- The range of predicted values for the whole set (training and testing) is split in ten bins with equal spacing.
- For each of the bins the mean of the absolute error of values from the test set is calculated. However, based on the previous simulations, not all bins contain data points. There can be bins in which there are no predictions for the test set and therefore no error can be calculated. The mean error for such bins is considered zero.
- The bin with the highest mean error is selected as a region of interest.
- The metamodel is retrained with the full data set and predictions are made for the one million candidate points. The subset of these points where the prediction falls into the interval with the highest mean error is used for the augmentation of the design.
- This is done for all the injury criteria of interest.

This method was termed the "highest mean criterion". A visualization of the steps can be found in the Supplementary Material. From these subsets of candidate points the load cases are selected by a space-filling algorithm. The same number of load cases are selected for each injury criteria (i.e., 8 for iteration 4, which consisted of a total of 32 simulations, considering four injury criteria). The selected parameters are used as input parameters for the simulations of the next iteration.

As space-filling DoE algorithm the MaxPro approach (Joseph et al., 2020) was chosen. It can be seen as an extension to the maximin Latin hypercube design. The maximum projection (MaxPro) criterion ensures that the design is not only space-filling for the entire parameter space but also for subspaces. The MaxPro criterion can also be extended for multiple types of factors. It can create sequential designs and is available as implementation in R.

The selection of a subset of candidate points is done with the help of metamodels. Cross-validation is used for the selection of the metamodel and the hyperparameters of the metamodel. For this the Python machine learning module scikit-learn[2] (Pedregosa et al., 2011) was used. No scaling of the input parameters was performed since it did not improve the prediction accuracy. Since the k-NN algorithm performed best for the first iterations of data, it was used throughout the study unless stated otherwise.

To show the behaviour of the algorithm using known functions the Styblinski-Tang function as well as Mishra's bird function (Mishra, 2006) (not constrained) were chosen. These functions are also used in the context of optimization which is not the goal in this work. A Latin hypercube design was used to create the first design. Additional design points were created by augmenting the initial design with candidate points using MaxPro. For the Styblinski-Tang function 32 points were created with LHD and 32 points by augmentation whereas for Mishra's bird function 16 points were created with LHD and 16 points by augmentation. For the "highest mean criterion" the first design points created by the LHD were used for training a GPR metamodel

2 https://scikit-learn.org/stable/.

und the remaining design points were used for testing in the first step. In each iteration 32 new points were created for the Styblinski-Tang function and 16 new points for Mishra's bird function. For the "highest mean criterion" one-fourth of the points were chosen using the described approach and the remaining points were chosen using the space filling MaxPro algorithm. Choosing the remaining points with MaxPro was done to prevent the "highest mean criterion" from getting stuck in one area. For the MaxPro approach all points in one iteration were created with MaxPro. To compare the two approaches a GPR metamodel was trained using the created design points. The difference of the two functions and the trained metamodels was evaluated on a grid with 1,001 points in x and y direction respectively.

2.3 Sensitivity study

A sensitivity study was performed to investigate if the metamodel is able to learn from the results of different configurations, such as different pulses, anthropometry and seating position. The available data is split into two sets S1 and S2. For the pulses the set S1 comprises all the data with pulse FF56, the second set S2 comprises the rest of the data. For the anthropometry the set S1 comprises the data with the AF05 HBM and for the seating position S1 comprises the data with the HBM in upright position. The first set is randomly split into a set $S1_{part}$ that contains 80% of the set S1 and a test set $S1_{test}$ that contains the remaining 20% of the set S1. To investigate different sizes of training data from the set S1, 25%, 50%, 75%, and 100% of the set $S1_{part}$ are used as training data $S1_{train}$. A metamodel is trained, firstly with only the set $S1_{train}$ and secondly with the union of set $S1_{train}$ and S2. The test set is both times $S1_{test}$. As a metamodel GPR is used since for k-NN the split into the sets is already done inherently.

To quantify the importance of the different input parameters for the metamodel, a score is calculated for each parameter using "permutation feature importance" according to (Breiman, 2001). For this, a trained metamodel with good prediction quality is needed. The values for each feature are permuted one after the other. If the feature is important, the prediction quality decreases. The permutation feature importance is calculated as the prediction score of the metamodel for the original data, minus the prediction score for the permutated data. A mean permutation feature importance can be calculated by repeating the procedure for different permutations. (Breiman, 2001).

3 Results

3.1 Design of experiments

The comparison of the maximum error of the "highest mean criterion" and MaxPro for the Styblinski-Tang function as well as Mishra's bird function can be seen in Figure 5. For the Styblinski-Tang function the maximum absolute error decreases faster with the exception of the second iteration. After eight iterations the errors for both approaches are approximately the same. The points chosen by the "highest mean criterion" focus on the boundary where there is a steep increase of the Styblinki-Tang function. For Mishra's bird function again the maximum absolute error decreases faster until the sixth iteration. For the last two iterations the MaxPro approach shows the lower maximum absolute error.

For the finite element simulations the first design was created with Latin Hypercube sampling. Then three iterations were made with no restrictions to the candidate points. Following on from this three iterations were made with the "highest mean criterion". A summary of all iterations and the applied approach is shown in Table 3.

Figure 6 shows boxplots of the absolute error in the predictions from the test data of the four different injury criteria. The first three iterations are with no restrictions on the set of candidate points, iterations four to six were designed with the "highest mean criterion". It can be seen that the error increases when switching to the "highest mean criterion" in iteration 4. Only in the case of Brain 95p does it stay roughly the same. This behaviour is intended since the new cases are chosen in areas where the prediction error is highest. The error declines for Brain 95p and NIC in the last iteration but more iterations would be necessary to confirm this trend.

3.2 Prediction quality of the metamodels

The prediction quality of the two metamodels k-NN and GPR is tested with two different splits into training and test data. For the first split the results of the iterations 0 to 5 of the data set are used as training data and the results of iteration six are used as test data. For the second split, the whole data set with all 208 simulations was utilized to also take the data points of the last iteration into account. The k-NN and the GPR metamodels were thus trained with 80% of the randomized whole data set (iteration 0–6). The prediction is then tested on the remaining 20% of the data set. The resulting R^2 values are summarized in Table 4. Plots with a comparison of simulation results and prediction can be found in the Supplementary Material.

The predictions for the kinematic-based criteria HIC15 and NIC are very good ($R^2 > 0.9$), with the exception of k-NN for the iteration based split. It can be seen, that the prediction is more challenging for strain-based criteria like Brain 95p and especially the rib fracture risk. For HIC15, Brain 95p and NIC GPR shows almost equal or better results compared to k-NN, whereas for Rib fracture 1+ k-NN is more stable. Using 80% of the entire randomized data set as training data increases the accuracy of the metamodels as expected.

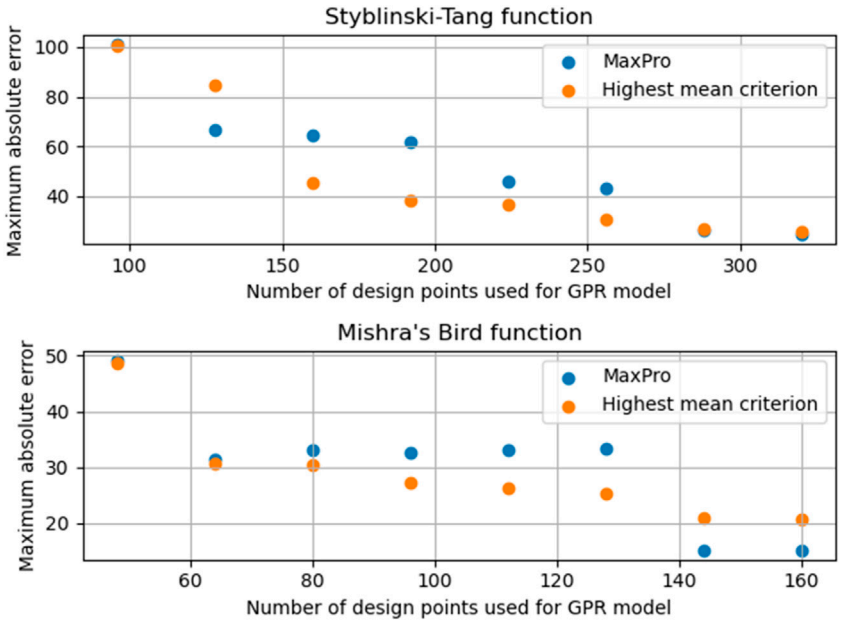

FIGURE 5
Maximum absolute error of the GPR metamodel trainined with the design points created by the MaxPro algorithm and the "highest mean criterion" respectively.

TABLE 3 Iterations of simulations with corresponding selection approach.

Iteration	Simulations	Quantity	DoE approach
0	1–64	64	Latin Hypercube
1	65–80	16	MaxPro
2	81–112	32	MaxPro
3	113–144	32	MaxPro
4	145–176	32	"Highest mean criterion"
5	177–192	16	"Highest mean criterion"
6	193–208	16	"Highest mean criterion"

3.3 Sensitivity study

One split into two sets S1 and S2 was carried out for the anthropometry. The set S1 comprises all the simulations with the AF05 HBM model and the set S2 comprises the simulations with the AM50 HBM model. The results can be seen in Table 5. As expected, the calculated R^2 score decreases with a reduced size of the training set. No clear trend emerges for the comparison of the results with and without added data from the set S2. But in most cases adding data from set S2 leads to similar or worse R^2 values. Similar results can be observed for the split of the data based on pulses and seating position which can be found in the Supplementary Material. This leads to the conclusion that combining simulations with different anthropometries, pulses or seating positions does not help to reduce the necessary number of simulations at least if they are not described by continuous parameters which is the case in this study.

To see the influence of the different input parameters on the metamodel the permutation feature importance (Breiman, 2001) for the HIC15 was determined. The GPR metamodel was trained with 80% of the whole data set for this purpose. The permutation feature importance calculation for the test set was repeated ten times, so mean and standard deviation are stated in Table 6. The pulse has the highest feature importance followed by seating position and anthropometry. The feature importance of the parameter stiffness, distribution and belt load limiter are significantly lower.

4 Discussion

4.1 Limitations

The focus of this study was the development of a method for a fully automatic design of experiments, enabling to learn as much as possible from a limited number of simulations. The focus was not set on the metamodel and therefore using the metamodel for designing a system, additional simulations would

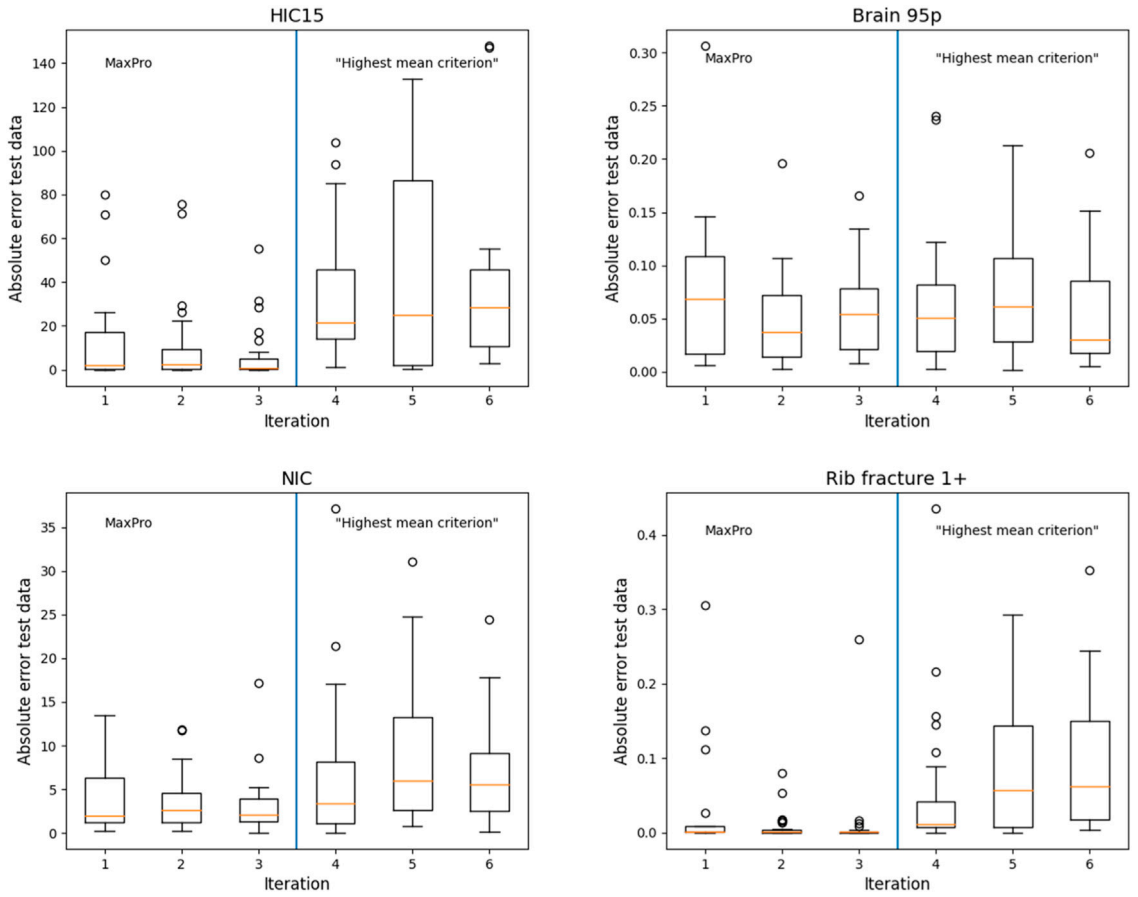

FIGURE 6
Boxplots with absolute error of the predictions on the test data for all iterations.

TABLE 4 R^2 values for predictions with k-NN and GPR metamodels for two different splits into training data and test data.

	Training data iteration 0-5, test data iteration 6		Training data 80% of all iterations, test data 20% of all iterations	
	R^2 k-NN	R^2 GPR	R^2 k-NN	R^2 GPR
HIC15	0.66	0.91	0.97	0.99
Brain 95p	0.89	0.89	0.95	0.93
NIC	0.86	0.98	0.98	0.98
Rib fracture 1+	0.33	0.22	0.78	0.59

be needed. This becomes evident when looking at the prediction of the rib fracture risk.

The description of the loading scenario was very discontinuous and not described with parameters. In future studies, the pulses should be described in an improved way, using parameters characterising the shape and amplitude. Furthermore, when using more than two anthropometries and more than two seating postures, it might be better to derive a metamodel, which can learn from the different scenarios.

A simplified seat-mounted restraint system was used in order to represent the same initial conditions for each simulation run. Although the comparison with a conventional vehicle shows a

10.3389/ffutr.2022.913852

TABLE 5 Results of sensitivity study for splitting the anthropometry.

Number of test data: 20	Only AF05 data used for training (S1)		AM50 data set added for training (S2)	
	Number of training data	R^2	Number of training data	R^2
HIC15	78	0.97	188	0.97
	58	0.96	168	0.96
	39	0.94	149	0.95
	19	0.84	129	0.91
NIC	78	0.75	188	0.7
	58	0.72	168	0.57
	39	0.52	149	-0.11
	19	−0.01	129	-1.51
Brain 95p	78	0.98	188	0.98
	58	0.97	168	0.98
	39	0.97	149	0.99
	19	0.87	129	0.97
Rib fracture risk 1+	78	0.64	188	0.67
	58	0.62	168	0.61
	39	0.75	149	0.56
	19	0.55	129	0.36

TABLE 6 Permutation feature importance for HIC15.

Features	Stiffness	Distribution	Belt load limiter	Anthropometry	Seating position	Pulse
Mean	0.043	0.048	0.06	0.128	0.149	2.128
Standard deviation	0.027	0.022	0.013	0.032	0.034	0.281

similar magnitude and duration of the contact forces, the timing of the applied restraint system is shifted, as it was not deploying. The advantage of the comparable distance is related with a higher distance compared to an airbag which is deploying. Therefore, the results of this study cannot be directly transferred to a real restraint systems.

Two functions were used to show the differences of the proposed "highest mean error" approach and the space-filling MaxPro algorithm. Since the differences depend on the chosen function as well as parameters such as number of design points per iteration a more thorough examination of the proposed algorithm should be conducted in the future. This could lead to a better understanding of the behaviour and to further improvement of the "highest mean error" approach.

The goal of the proposed approach is to achieve good prediction of the metamodel on the whole parameter space and not missing any important regions. The prediction error was increasing for the data from the finite element simulations with our applied procedure. This is an indication that we would have not seen these problems in our metamodel if we would have continued with the space-filling approach. But it is difficult to show that no important regions have been overlooked without being able to simulate every point.

The proposed approach is intended for cases where the number of simulations is limited, e.g., because of limited time or computational resources. If a very large number of simulations can be performed the whole design space could be scanned instead.

4.2 Simulation setup

A parameterised, robust simulation model is needed to train the metamodels. Before starting the parameter variation, the simulation of all extreme load cases should prove the model's stability. Outliers of simulation results should be always checked manually, as they affect the design of the next iteration. The Human Body Model applied in the current simulations was very robust, but issues in the belt and restraint system interactions (sticky nodes) were observed in single simulations, which required changes of the contact settings such as contact stiffness and search frequency.

It should be checked in advance if the variance in the input parameters leads to significant changes in the results. Originally, it was planned to vary only the angle, but not the collision speed. However, this led to a spread in some of the injury criteria that was too small and therefore did not fulfil the purpose of the study. To achieve a higher range in injury criteria values, the pulse FF56 was added.

4.3 Design of experiments

With the DoE approach of the current study it was not intended to perform a classic optimization approach as in Xia et al. (2018), Gan and Gu (2019) or Joodaki et al. (2021), but to learn as much as possible from a limited number of simulations. Defining the aim of a design of experiments approach is essential. In the concept phase, there was some discussion on whether certain areas of a predicted outcome could be excluded, since the output values were either too high or too low. This was inspired by the approach of Gan and Gu (2019), who developed an algorithm, in which an important region was defined and points that lie within that region were chosen by preference for the next iteration. Ultimately, however, an approach of this kind appeared to be too subjective for our application, since it was found to be difficult to draw a line objectively without running the risk ever and again of missing something essential. Instead of this, the areas of the metamodel with the highest insecurities were defined as the areas, which we should examine more closely as a means of avoiding misleading conclusions. Rooting out the causes of non-stable behaviour is of great importance, especially for safety applications.

On examining the average errors per iteration, it is apparent that the errors in iteration four and five were much higher than those in the previous iterations, but with a decreasing trend for the last iteration. This trend should ideally proceed further. Applying the developed method helps to reveal critical areas. When errors do not increase, even when focusing on those areas with the biggest errors, we were confident that missing important regions would be unlikely.

Metamodels of an entirely acceptable quality within a large parameter space were derived, despite only 208 simulations having been performed. To estimate the number of simulations that would be needed for a full factorial analysis, a discretization of the continuous variable in the current study has to be assumed. A discretization with ten data points each for beam stiffness, distribution of stiffness as well as the belt load limiter would lead to a total of 16,000 simulations for the full parameter space.

4.4 Metamodel

Within the DoE, the metamodel was trained with the k-NN method, although for the final results GPR showed better accuracy. For the first set of iterations, however, k-NN is much more stable and the risk of misleading interpretations is lower. The reason for this might be the small number of data sets at the beginning together with the aforementioned inability to learn from different configurations. For the first training data set with 64 simulations, only eight simulations are with the same pulse, anthropometry and seating position. In the future also combinations of different metamodels could be tested.

Surprisingly the prediction of the metamodel did not seem to improve with data from other configurations. This might be caused by non-continuous and too different configurations. Training the metamodel and performing the DoE for each configuration separately meant that a significantly greater number of simulations would needed. Anthropometry, posture and pulse should be varied in the future more continuous to achieve better learning effects in between the scenarios.

Metamodels were trained to predict four different injury criteria, which were each of a different type. The highest prediction accuracy was achieved for the kinematics-based criteria HIC and NIC, which are mainly applied for dummies and have limited meaningfulness for HBMs. The prediction of the strain-based criteria seemed to be more challenging for the metamodel. The most complex injury criteria applied in this study, the probabilistic rib fracture risk assessment, was the most difficult to predict. To calculate the probabilistic rib fracture risk assessment, the maximum strain of each rib is derived and used as input for the risk calculation per rib which is finally combined to an overall rib fracture risk using a binomial function. In contrast to the brain 95th percentile strain, more complexity layers are thus added, which the metamodel must learn. In future an attempt could be made to predict the strains within the individual rib using metamodels and then to perform the remaining evaluation steps manually.

Ultimately, of course more data is always better. The level of needed accuracy of the metamodel strongly depends on where it should be applied. The metamodel developed in this study can be used to distinguish between critical and non-critical areas for the generic restraint system that was used and prioritize input-parameters for future studies.

5 Conclusion

A DoE approach has been established focusing on those metamodel areas, which are more difficult to predict than others. An approach of this kind is recommended for safety-relevant problems with expensive generation of training data. Instead of optimizing the restraint system to run more and more simulations in "non-critical" areas, the developed algorithm specifically focuses on the more challenging areas to avoid misjudgement in these for the metamodel. This can help engineers to reveal the most critical areas, which should be prioritized to improve the robustness of the study using the individually feasible number of simulations that can be generated as effectively as possible.

Further research is needed in order to also be able to predict more complex injury criteria and further understand the learning effects from the categorical parameters describing the scenarios, such as anthropometry and posture.

Data availability statement

The raw data supporting the conclusions of this article will be made available by the authors, without undue reservation.

Author contributions

BS carried out the data analysis. BS and CK performed the manuscript preparation. DK designed and carried out the simulations. CK supervised the data analysis and the method development. GD, HF, and MW provided comments, feedback, and edited the manuscript. All authors contributed in continuous discussion on the method, read and approved the final manuscript.

Funding

Open access funding provided by Graz University of Technology Open Access Publishing Fund.

Acknowledgments

The authors would like to acknowledge the use of high-performance computing resources provided by the IT Services (ZID) of Graz University of Technology. We would also like to thank the Toyota Motor Corporation and Toyota Central R&D Labs for providing the academic license of the THUMS v4.02 AM50 occupant model.

Conflict of interest

The authors GD, HF, and MW are employed by Robert Bosch GmbH.

The remaining authors declare that the research was conducted in the absence of any commercial or financial relationships that could be construed as a potential conflict of interest.

The study was part of the DoSim project that has been funded by the Robert Bosch GmbH within the Mercedes/Bosch Tech Center i-protect. The funder had the following involvement in the study: Problem formulation and discussion of results.

Publisher's note

Supplementary material

The Supplementary Material for this article can be found online at: https://www.frontiersin.org/articles/10.3389/ffutr.2022.913852/full#supplementary-material

References

Adam, T., and Untaroiu, C. D. (2011). Identification of occupant posture using a Bayesian classification methodology to reduce the risk of injury in a collision. *Transp. Res. Part C Emerg. Technol.* 19, 1078–1094. doi:10.1016/j.trc.2011.06.006

Bance, I., Yang, S., Zhou, Q., Li, S., and Nie, B. (2021). A framework for rapid on-board deterministic estimation of occupant injury risk in motor vehicle crashes with quantitative uncertainty evaluation. *Sci. China Technol. Sci.* 64, 521–534. doi:10.1007/s11431-019-1565-9

Breiman, L. (2001). Random forests. *Mach. Learn.* 45, 5–32. doi:10.1023/A:1010933404324

Crombecq, K., Couckuyt, I., Gorissen, D., and Dhaene, T. (2009). "Space-filling sequential design strategies for adaptive surrogate modelling," in *Proceedings of the first international conference on soft computing Technology in civil, structural and environmental engineering*. Editors B. Topping and Y. Tsompanakis (UK: Civil-Comp Press Stirlingshire).

Draguljić, D., Santner, T. J., and Dean, A. M. (2012). Noncollapsing space-filling designs for bounded nonrectangular regions. *Technometrics* 54, 169–178. doi:10.1080/00401706.2012.676951

Fang, J., Sun, G., Qiu, N., Kim, N. H., and Li, Q. (2017). On design optimization for structural crashworthiness and its state of the art. *Struct. Multidiscipl. Optim.* 55, 1091–1119. doi:10.1007/s00158-016-1579-y

Forman, J. L., Kent, R. W., Mroz, K., Pipkorn, B., Bostrom, O., and Segui-Gomez, M. (2012). Predicting rib fracture risk with whole-body finite element models: Development and preliminary evaluation of a probabilistic analytical framework. *Ann. Adv. Automot. Med.* 56, 109–124.

Freienstein, H., Kolatschek, J., and D'Addetta, G. A. (2019). *Sicherheit zukünftiger hochautomatischer Fahrzeuge im Mischverkehr – anforderungen, Lösungskonzepte und Potenzialabschätzungen*. VDI-Tagung Fahrzeugsicherheit, Düsseldorf, Germany 12.

Gan, N., and Gu, J. (2019). Hybrid meta-model-based design space exploration method for expensive problems. *Struct. Multidiscipl. Optim.* 59, 907–917. doi:10.1007/s00158-018-2109-x

Höschele, P., Smit, S., Tomasch, E., Östling, M., Mroz, K., and Klug, C. (2022). Generic crash pulses representing future accident scenarios of highly automated vehicles. *SAE Int. J. Trans. Saf.* 10, 1–26. doi:10.4271/09-10-02-0010

ISO (2014). *Road vehicles - objective rating metric for non-ambiguous signals ISO/TS 18571:2014(E)*. Geneva, Switzerland: ISO (Accessed January 29, 2020).

Joodaki, H., Gepner, B., and Kerrigan, J. (2020). Leveraging machine learning for predicting human body model response in restraint design simulations. *Comput. Methods Biomech. Biomed. Engin.* 24, 597–611. doi:10.1080/10255842.2020.1841754

Joodaki, H., Gepner, B., Lee, S.-H., Katagiri, M., Kim, T., and Kerrigan, J. (2021). Is optimized restraint system for an occupant with obesity different than that for a normal BMI occupant? *Traffic Inj. Prev.* 22, 623–628. doi:10.1080/15389588.2021.1965131

Joseph, V. R., Gul, E., and Ba, S. (2020). Designing computer experiments with multiple types of factors: The MaxPro approach. *J. Qual. Technol.* 52, 343–354. doi:10.1080/00224065.2019.1611351

Klug, C., Luttenberger, P., Schachner, M., Micorek, J., Greimel, R., and Sinz, W. (2018). "Postprocessing of human body model results – introduction of the open source tool DYNASAUR," in Proceedings of the 7th international symposium: Human Modeling and Simulation in automotive engineering (CARHS). Berlin, Germany: CARHS.

Kneifl, J., Hay, J., and Fehr, J. (2022). Real-time Human Response Prediction Using a Non-intrusive Data-driven Model Reduction Scheme. *IFAC-PapersOnLine* 55, 283–288. doi:10.1016/j.ifacol.2022.09.109

Larsson, K.-J., Blennow, A., Iraeus, J., Pipkorn, B., and Lubbe, N. (2021). Rib cortical bone fracture risk as a function of age and rib strain: Updated injury prediction using finite element human body models. *Front. Bioeng. Biotechnol.* 9, 677768. doi:10.3389/fbioe.2021.677768

Luttenberger, P., Feist, F., Kofler, D., Sinz, W., D'Addetta, G. A., Freienstein, H., et al. (2020). "Assessment of future occupant restraint principles in autonomous vehicles," in 2020 IRCOBI Conference Proceedings, Farmington Hills, Michigan, USA: International Research Council on the Biomechanics of Injury IRCOBI 431–455.

Mishra, S. K. (2006). Some new test functions for global optimization and performance of repulsive particle swarm method. *SSRN J*, 24. doi:10.2139/ssrn.926132

Pedregosa, F., Varoquaux, G., Gramfort, A., Michel, V., Thirion, B., Grisel, O., et al. (2011). Scikit-learn: Machine learning in Python. *J. Mach. Learn. Res.* 12, 2825–2830.

Perez-Rapela, D., Forman, J. L., Huddleston, S. H., and Crandall, J. R. (2020). Methodology for vehicle safety development and assessment accounting for occupant response variability to human and non-human factors. *Comput. Methods Biomech. Biomed. Engin.* 19, 384–399. doi:10.1080/10255842.2020.1830380

Poulard, D., Lin, H., and Panzer, M. B. (2020). *Occupant safety in vehicles equipped with automated driving systems, Part 3: Biofidelity evaluation of GHBMC M50-OS against laboratory sled tests*. Report No. DOT HS 812 905. National Highway Traffic Safety Administration Washington, D.C., USA.

Pronzato, L., and Müller, W. G. (2012). Design of computer experiments: Space filling and beyond. *Stat. Comput.* 22, 681–701. doi:10.1007/s11222-011-9242-3

Provost, F., Jensen, D., and Oates, T. (1999). "Efficient progressive sampling". In *Proceedings of the fifth ACM SIGKDD international conference on knowledge discovery and data mining*. Editor U. Fayyad (New York, NY, USA: ACM)), 23–32.

Singh, H., Ganesan, V., Davies, J., Paramasuwom, M., and Lorenz, G. (2018). *Vehicle interior and restraints modeling development of full vehicle finite element model including vehicle interior and occupant restraints systems for occupant safety analysis using THOR dummies*. Washington, DC, USA: NHTSA. Report No. DOT HS 812 545.

Untaroiu, C. D., and Adam, T. J. (2013). Performance-based classification of occupant posture to reduce the risk of injury in a collision. *IEEE Trans. Intell. Transp. Syst.* 14, 565–573. doi:10.1109/TITS.2012.2223687

Wagström, L., Leledakis, A., Östh, J., Lindman, M., and Jakobsson, L. (2019). "Integrated safety: Establishing links for a comprehensive virtual tool chain," in Proceedings of the 26th ESV conference proceedings. (Washington, DC, USA: NHTSA).

Watt, J., Borhani, R., and Katsaggelos, A. K. (2020). *Machine learning refined: Foundations, algorithms, and applications*. New York, NY, USA: Cambridge University Press.

Williams, C. K. I. (2006). *Gaussian processes for machine learning*. The MIT Press.Cambridge, MA, USA.

Xia, L., Liu, W., Lv, X., and Gu, X. (2018). A system methodology for optimization design of the structural crashworthiness of a vehicle subjected to a high-speed frontal crash. *Eng. Optim.* 50, 634–650. doi:10.1080/0305215X.2017.1334774

frontiers | Frontiers in Future Transportation

TYPE Original Research
PUBLISHED 30 November 2022
DOI 10.3389/ffutr.2022.914489

OPEN ACCESS

EDITED BY
Yong Han,
Xiamen University of Technology, China

REVIEWED BY
Hua-Lei Yin,
Nanjing University, China
Andre Eggers,
Federal Highway Research Institute, Germany

*CORRESPONDENCE
Maria Eichlseder,
maria.eichlseder@iaik.tugraz.at
Corina Klug,
corina.klug@tugraz.at

SPECIALTY SECTION
This article was submitted to Transport Safety, a section of the journal Frontiers in Future Transportation

RECEIVED 06 April 2022
ACCEPTED 09 November 2022
PUBLISHED 30 November 2022

CITATION
Galijatovic E, Eichlseder M, Heindl SF and Klug C (2022), Integrity of virtual testing for crash protection.
Front. Future Transp. 3:914489.
doi: 10.3389/ffutr.2022.914489

Integrity of virtual testing for crash protection

Esma Galijatovic[1,2], Maria Eichlseder[1]*, Simon Franz Heindl[2] and Corina Klug[2]*

[1]Institute of Applied Information Processing and Communications, Graz University of Technology, Graz, Austria, [2]Vehicle Safety Institute, Graz University of Technology, Graz, Austria

The interest in virtual testing is globally rapidly increasing because of several advantages compared to physical tests in laboratories. In the area of passive car safety, finite element simulations can be used to get further insights, use more biofidelic human models and make the overall assessment more robust by incorporating more variety in the virtual testing load cases. For a successful implementation of virtual testing in regulations or consumer information, the integrity of the procedure has to be ensured. As car simulation models used within the virtual testing are usually not shared with the evaluation institutions due to intellectual property (IP) issues, this is a challenging task. Stringent validation and certification procedures are needed and it has to be ensured that the models used in these steps are the same as the ones used for the virtual testing. In this paper, we developed a secure procedure for model version control. Through analysis of possible threats for both sides, car manufacturer and evaluation institution, we defined requirements, which the new procedure should satisfy. These requirements state that the integrity and authenticity of all shared documents should be protected, as well as the confidentiality of the simulation model. By considering all prerequisites, we developed an architecture for a new procedure. This architecture uses cryptographic algorithms such as hash functions and digital signatures to ensure integrity and authenticity, as well as secure computation mechanisms such as Intel Software Guard Extensions (SGX). In our proof-of-concept implementation, we demonstrated how a secure wrapper around LS-DYNA can produce a signed report to authenticate the input model files based on a hash tree and link them to the simulation results. The evaluation institution can use a matching verification tool to verify that the models were not manipulated compared to other simulation runs or the qualification process. The developed procedure can be used for trustworthy implementation of virtual testing into consumer information or regulation for the assessment of car safety with strengthened integrity. Further research is needed to develop comparable procedures for other simulation software packages or ideally integrate it directly into the simulation software.

KEYWORDS

car safety, consumer testing, integrity, confidentiality, hash function, digital signature, virtual testing

1 Introduction

The interest in virtual testing for vehicle safety assessments is globally rapidly increasing because of several advantages compared to physical tests in laboratories. Loading conditions can be varied as well as the anthropometry of the humans to enable a more robust assessment. Furthermore, integrated assessments linking pre- and in-crash phase and the use of biofidelic Human Body Models (HBMs) without hardware limitations are enabled. Thereby, instead of crashing a real car in a physical crashtests, a virtual replication of the car model is used and tested virtually in a simulated crash. (Huizinga et al., 2002; van Ratingen, 2020).

For a successful implementation of virtual testing, the integrity of the procedure has to be ensured. All involved parties and the end-consumers buying and driving the evaluated cars have to trust the procedure and potential manipulation must be prevented. As IP protected information is included in the virtual car models, this is a challenging task. Stringent procedures are needed to ensure quality of the model comparability in between such virtual tests (repeatability and reproducibility). The principle of such a procedure is shown in Figure 1.

The applied simulation models depend on the application case and the overall setup is often a combination of vehicle and occupant models. The models have to qualify for use in virtual testing by fulfilling requirements on the validation and/or comparability level. Thereby, general requirements (mass, geometry, output specifications..) are checked and model responses are compared with target responses from experiments and/or reference simulations. The assessment institution is inspecting shared results and documentation to certify the simulation models. Eventually, the qualified simulation models are used to run the virtual testing loadcases. The evaluation institution is inspecting the simulation results for plausibility (quality checks, consistency with qualification..) and considers the results of the virtual testing loadcases for the overall vehicle assessment. To replicate different loadcases, parts of the simulation models need to be changed "dynamic parts". Other parts of the model remain unchanged between qualification and virtual testing and also within the virtual testing procedure (named "static" the figure). It has to be ensured that the models used in the qualification steps are the same as the ones used for the virtual testing and cannot be manipulated in between. (Eggers et al., 2013; Klug et al., 2019; van Ratingen, 2020).

Currently, virtual testing procedures are still very rare in the area of car safety. In the European New Car Assessment Programme (Euro NCAP) (Euro NCAP 2022) pedestrian assessment of cars with deployable systems (i.e., pop-up bonnets), the first certification procedure for virtual human models to be used in the assessment procedure was defined. In this application case, the virtual tests—simulations where car models are crashing pedestrian models in different statures—are used to derive the boundary conditions for the physical tests. To qualify the virtual human models, they are used in reference simulations with generic car models and their response is compared to reference curves. Those simulations are very well-defined and as every user has access to the same generic car models, they are comparable among different users. This is done to qualify the simulation models and environments (cluster, used solver version) for use in virtual testing. Results and documentation of these reference simulations are shared with Euro NCAP and there inspected for plausibility. If Euro NCAP judges the all requirements are fulfilled and the reference simulations are within the corridors, the virtual human models qualify for the next step. There, the human models are impacted with the simulation models of the series-production cars to be evaluated. Both types of simulations are done by the car manufacturers, basically exchanging in the simulation setup only the generic vehicle models of the reference simulations with the models of the series-production cars for the assessment simulations. The consistency between the simulation setups and the virtual human models has to be documented and is checked based on the provided outputs. However, the integrity check purely relies on this documentation and the provided data and changes of the models are not trackable by third parties. In this case, this is accepted, as the simulations are only used as prerequisite for phyisical tests. For all simulations, quality criteria have to be fulfilled and plausibility of simulation results is inspected by Euro NCAP. (Klug et al., 2019).

Further applications of virtual testing are under development, where the simulation results should be used for the assessment itself and not only as prerequisite (Linder et al., 2020; van Ratingen, 2020). Therefore, the integrity of simulation results and used simulation models will play an steadily increasing role and further improvements might be needed.

In information security research and cryptology, data integrity is a central, well-studied security property. Cryptographic standards provide algorithmic solutions to protect the integrity of files, including hash functions (NIST FIPS 180-4, 2015), message authentication codes (MACs) (NIST FIPS PUB 198-1, 2008), and digital signatures (NIST FIPS PUB 186-4, 2013). These algorithms take as input a file and a suitable digital key (a symmetric key for MACs or the private key of an asymmetric keypair for signatures) and produce a fixed-size authentication tag, fingerprint, or signature to certify the integrity of the file. This can later be checked with the corresponding verification key (the same symmetric key for MACs or the public key of an asymmetric keypair for signatures) to verify that the file has not been modified. However, applying these generic algorithms to protect specific assets in practice is often challenging. The main difficulties include proper key management, secure implementation, and suitable adaptation based on the desired notion of integrity (e.g., if the asset includes parts that may be changed, if the asset is distributed across several locations or changes over time, taking metadata into account, and many other aspects).

The aim of our study was to explore possible solutions to improve integrity of the procedure and the files used in virtual testing by exploring methods from information security research and cryptology. The ambition was to define an enhanced procedure and investigate a proof-of-concept implementation.

2 Materials and methods

To investigate how the integrity of virtual testing could be further improved, the following methods were applied: First, we performed a threat analysis to structure potential problems, second, we developed and evaluated concepts to solve them, and third, we implemented a proof of concept in conjunction with a selected finite element (FE) software package, namely LS-DYNA (ANSYS - LST, 2021).

2.1 Threat analysis

The threat analysis was performed based on the current procedure for the assessment of active bonnets, having already future applications in mind, where the crash safety assessment itself is based on virtual load cases directly. Threats for the organisation performing the assessment as well as for the car manufacturer were considered based on discussions with different stakeholders.

2.2 Building blocks of the virtual testing procedure and the developed solutions

2.2.1 Simulations for virtual testing

For virtual testing in the field of vehicle safety, multibody or finite element simulations are performed. Different software packages are therefore used in the car industry. The main structure among the processes is very similar among the different Finite Element (FE) software packages. The current proof-of-concept implementation was done exemplary in combination with the FE software package LS-DYNA. The input files for LS-DYNA are plain text files that consist of ASCII-characters. All input files have to follow a certain format and structure. This includes a limited set of specific keywords, followed by respective values. By that, model elements and equations available in LS-DYNA are defined. Input files can also be encrypted, which means that keywords and related input parameters are only readable by LS-DYNA as it has the corresponding decryption key. When initiating the simulation, only one main input file is inserted into LS-DYNA, but many other files can be included by reference to achieve segregation of different components. These additional files are added using *INCLUDE and *INCLUDE PATH keywords. Outputs are binary files generated by LS-DYNA, which contain the simulation results (ANSYS LST, 2021).

An exemplary simulation setup for a simple “cube” example is shown in Figure 2. In this example, the files in the lower box remain unchanged (static parts of simulation model) throughout the procedure, while the main. key and Loadcase.inc. files are modified to change the loading conditions (dynamic parts of simulation model). This model is also used as demonstrator in the feasibility study.

As simulations for virtual testing are usually large models, simulations are performed on high-performance computing (HPC) clusters. These clusters are highly secured and connection to outside world is very restricted.

2.2.2 Cryptographic signature schemes and hash functions

Cryptographic or digital signing is a procedure that ensures the integrity and authenticity of a message (Diffie and Hellman, 1976; Rivest et al., 1978). This procedure is used when it is crucial to know who sent the specific message and ensure it was not altered in transit. Additionally, once a person signs a message with a digital signature, they can no longer repudiate their signature. This property is called non-repudiation. These procedures use asymmetric public-key cryptography with a key-pair of public and private keys, where the private key is used for signing by the sender, and the public key is used for verification by the receiver (Diffie and Hellman, 1976). Only a person that owns a private key can generate a signature, so digital signatures can not be forged. We have used two cryptographic signature schemes in this study: RSA (Rivest–Shamir–Adleman) and ECDSA (Elliptic Curve Digital Signature Algorithm), both standardized by US National Institute of Standards and Technology (NIST, 2013). The security of the RSA algorithm is based on the hardness of the integer factorization problem (Rivest et al., 1978), while ECDSA is analogue of the Digital Signature Algorithm (DSA) algorithm using elliptic curves (Miller, 1985; Koblitz, 1987). These schemes are considered secure against “classical adversaries”, but would suffer a drastic loss of security in case of potential future “quantum adversaries” that have access to a large quantum computer. For this reason, NIST is currently searching for a “post-quantum”-safe replacement (NIST, 2020). Once such a post-quantum signature algorithm has been standardized, it can serve as a secure drop-in replacement for current algorithms provided that the increased cost of these algorithms (larger signatures, larger keys, slower computation) is compatible with the application. These are not to be confused with quantum signature algorithms (Gottesman and Chuang, 2001; Lu et al., 2021), which require that the system itself uses a quantum-bit public key and thus a dedicated quantum communication infrastructure. For this reason, they cannot serve as replacements in the context discussed in this paper.

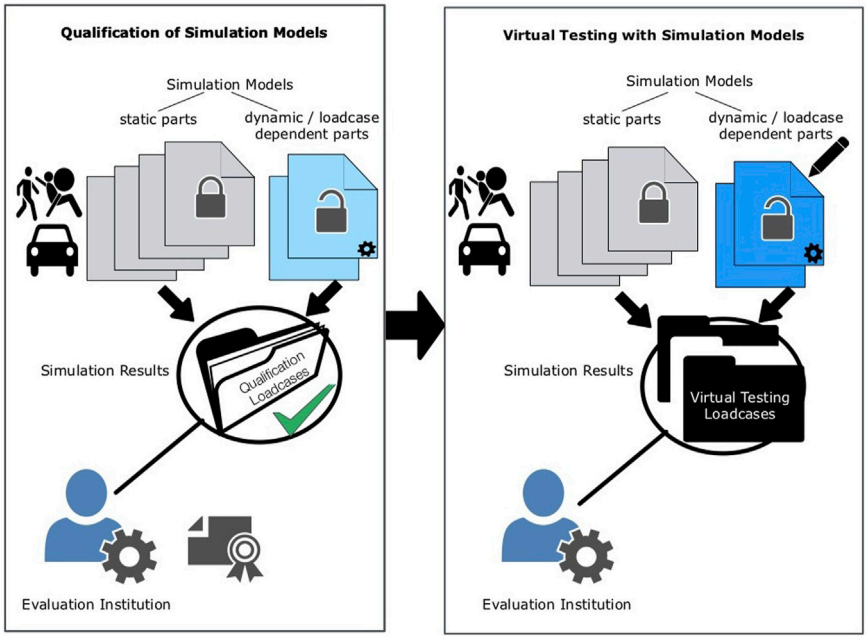

FIGURE 1
Possible implementation of virtual testing procedure where evaluation institution has access to simulation results.

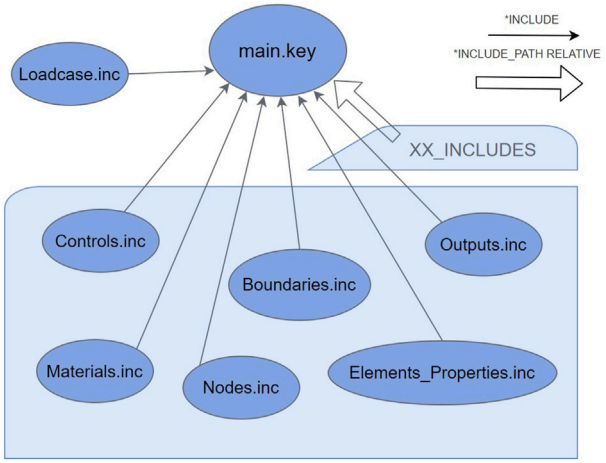

FIGURE 2
Simple "cube" example to illustrate the input file structure.

Additionally, all these cryptographic signature schemes rely on a cryptographic hash function to map input files of arbitrary length to a hash value, or tag, of fixed length that serves as a secure fingerprint (Damgård, 1989; Merkle, 1989). Secure cryptographic hash functions offer preimage resistance (i.e., it is infeasible for an attacker to find files that map to a given hash tag) and collision resistance (i.e., it is infeasible for an attacker to prepare two different files that map to the same hash tag). Hash functions and digital signatures are widely used as building blocks in cryptographic protocols (e.g., Transport Layer Security (TLS) for https or blockchains), file integrity (e.g., peer-to-peer (P2P) downloads), version control (e.g., git), and many other applications.

2.2.3 Secure enclaves

Secure enclaves (or Trusted Execution Environments) are secure subsystems of a computer with an aim to ensure confidential computing. Code executed in a secure enclave is protected from inspection or manipulation by other untrusted software, including higher privilege levels such as the operating system. This protects the confidentiality and integrity of the data processed by this trusted code. Thus, a program can run its most sensitive computations in a secure enclave; for example, the secure enclave can securely store cryptographic keys and allow their use only by the trusted cryptographic implementation and on this machine. The switch from unprotected, untrusted code to protected, trusted code in a secure enclave is implemented by a special interface (i.e., Intel's call gate). One of the most prominent examples is Intel SGX (Intel, 2021) that can be used for key management, enhanced application and data protection, hardware-enhanced content protection, and more. They are entirely isolated from other processes, including the operating system. Intel SGX as a security mechanism is used in the developed procedure for private key management. This mechanism requires proper hardware support in terms of the secure enclave component inside of the processor.

3 Results

3.1 Threat analysis

The main threat for the evaluation institution is a mismatch of models used within the different steps of the procedure or a mismatch between simulation input files and outputs. These mismatches can either happen on purpose (e.g. optimised models for each loadcase separately) or as consequence of an error and could cause:

- A model is used by the car manufacturer for virtual testing that does not qualify for virtual testing as inconsistent model versions are used within the process.
- The simulation results shared have not been derived using the qualified models.

Leakage of confidential information is another possible threat. For car manufacturers, it is of great importance to keep simulation models confidential. Simulation model files contain protected intellectual properties, which is why they have to be protected against access from untrusted third parties. Simulation output binary files may also include confidential information since it may include information about the simulation model. Furthermore, the shared results also have to be protected against changes (by intention or accident).

Based on the threat analysis, we define the following requirements:

1) A unique identifier for a simulation model is needed to check consistency and protect integrity.
2) Some files are modifiable, others have to be consistent throughout all steps.
3) Some of the files contain confidential information of the car manufacturer or suppliers (e.g., material models), while load case-relevant information such as acceleration curves are not considered confidential. Confidential information has to be protected.
4) It has to be traceable from which simulation models the simulation results were computed.
5) The authenticity of the shared simulation results have to be ensured. Any modification of the exported results by any party must be detectable.

3.2 Architecture of the proposed approach

Based on these requirements, we developed a procedure and implemented a proof-of-concept.

3.2.1 Wrapper

A wrapper script was developed to read in the simulation files, run the simulation, extract the results, and calculate unique identifiers for each input and output file. As first step all simulation model files are read in, checked and hashed to generate the unique model identifier. Then the simulation is started using the cluster-specific shell script, which also specifies which simulation model is run. To avoid manipulation of the shell script, which is starting the simulation file in the time between hashing the input files and running the simulation, the wrapper is storing the content of the shell script internally and exports it into a new script file which is finally executed after the hashing was completed. As soon as the simulation terminates, the outputs of interest are extracted from the generated binout files into. csv files, which is then hashed too. Finally, all identifiers are listed in a report (i.e., a Portable Document Format (PDF) file) that needs to be signed. The process is shown in Figure 3.

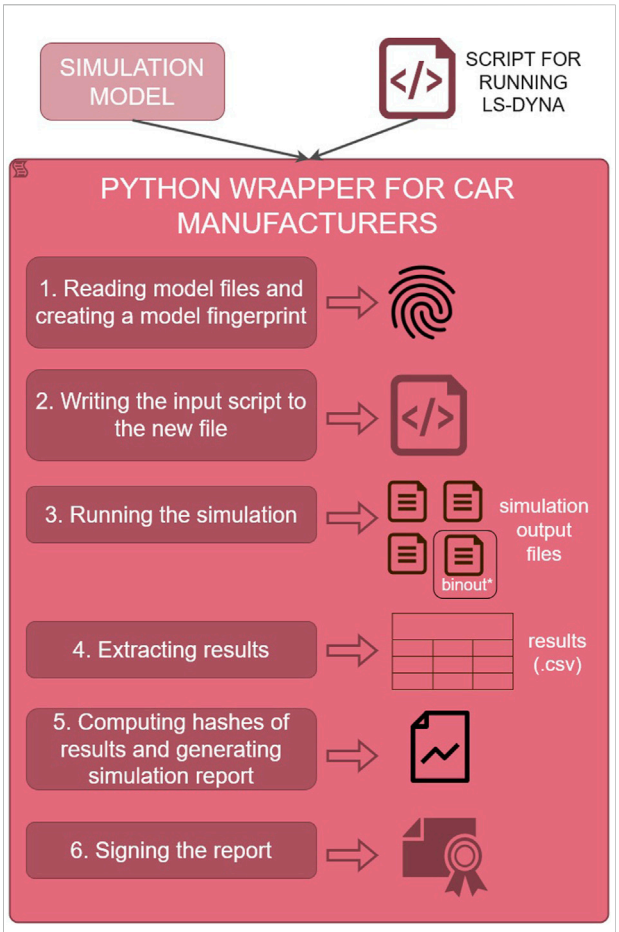

FIGURE 3
Structure of the developed wrapper for use by the car manufacturer for running simulations, extracting results and signing simulation reports, including unique identifiers of inputs and results.

3.2.2 Read in the simulation files

Since the simulation model generally consists of multiple files cross-linked by INCLUDE keywords, we need a dedicated

strategy to compute the hash. Any change in the file contents, file names, or file structure should produce a different hash. One simple approach is to concatenate the contents of all files and compute a model hash from this string. However, this design conflicts with the requirement of permitting a selected class of changes in some of the files as it would be not possible to distinguish between allowed and prohibited modifications. Therefore, we propose a different approach and represent the simulation model files as a tree structure, where one main file forms a root node and other files it includes form its child nodes. These child nodes can in turn contain other files. Knowing this, we can create a tree structure that captures all relevant information about the model and use it to compute the hash. Each node should contain information about file paths, file contents (hash of the contents), and files included (child nodes). An example of information kept in one node is:

This tree structure is convertible to a string that can be used for the computation of a SHA-256 hash, which is included in the final simulation report as the final model hash. With this method, it is clearly visible which files were changed within the procedure. Those files should not include any IP protected information and could be therefore shared with the evaluation institutions, while the IP protected information is clearly trackable with the unique identifier without access to the protected files by third parties. When this algorithm processes a single file, it first reads its content into a variable. Next, it looks for *INCLUDE PATH or *INCLUDE PATH RELATIVE statements, and if they exist, it adds these paths into the list of folders. The created list of folders contains all folders where the algorithm looks for child nodes. After, the algorithm searches for all *INCLUDE statements and processes the child nodes first. When all child nodes are added to the children list field (if there were any), the algorithm computes the SHA-256 hash of the contents and sets the corresponding field in the structure. This function then returns and continues the recursion until all files are visited.

Another important point is that the algorithm returns an error if a cycle is introduced. Assume, for example, that file X. key includes file Y. key, which includes file Z. key. If file Z. key includes file X. key, a cycle is introduced, and this is not an allowed situation. Therefore, the graph of files must be a tree (cycle-free). This situation is prevented by having a list of visited files forwarded through the recursion. This list contains hashes of all visited files. Then, when the file contents are read, and a hash is computed, it is first checked whether the hash of a current file exists in a visited files list. If not, the algorithm continues, and if this file was already visited, the algorithm raises an exception. Furthermore, to avoid that the user is overwriting parameters in the static files with keywords in the dynamic files, the inputs are also checked for duplicate parameters. If available, the input checker could in the future also look for forbidden keywords in the dynamic files.

After this object is created, it is translated into a string, and the final SHA-256 hash is computed from it. If any file is even slightly changed, this hash would be different. The tree structure here resembles tree structure showed in Figure 2. The only difference is that nodes contain additional information, as described previously.

3.3 Running the simulation

Setting up all needed parameters and variables for the simulation can be done using a shell script. This allows the person that is running the simulation to specify the cluster-specific settings (e.g. which LS-Dyna executable to use, License Server, Number of CPUs and the main simulation file which should be run). After the input script is processed, the simulation can be started. However, there is a time gap between reading the script and processing inputs and starting the simulation. This time gap could lead to a Time Of Check To Time Of Use (TOCTTOU) problem. Having such a problem could allow a malicious user to use one input script for preprocessing, then change the contents of the input script while the preprocessing is still under way and start the simulation with a completely different input script. To prevent this, we write the content of the input script to a new file with a random name and start the simulation using this newly generated file.

3.3.1 Simulation output

Typically, LS-DYNA outputs consist of several binary files, some of which contain confidential information about the model and data needed for the assessment of the car. The python libary “Dynasaur” (Klug et al., 2018; Schachner et al., 2022) was used to extract the outputs of interest from the binary output files and exports it into two CSV files (one including time series and one including scalars, such as injury criteria). These files can be shared with the evaluation institution, as they include the requested results used for plausibility checks and assessment (e.g. trajectories, acceleration signals, contact forces, calculated injury and quality criteria), but no IP protected information.

To track which model was used to produce these results and to ensure that results were not changed afterwards, another SHA-256 hash is calculated and included in the simulation report.

3.3.2 Simulation report

The simulation report includes the unique identifiers (hashes) of the simulation model and the simulation results. When all information about the model and results has been collected, a simulation report can be generated.

The report includes a table of hashes as illustrated in Figure 4 for the “cube” example of Figure 2. The final car model hash is presented in the first row, while relative file paths and hashes of their contents are included in the following rows. The final three rows contain CSV file hashes (two hashes computed from documents containing extracted results) and the time and

SIMULATION RESULTS

Model hash	06eb3f641e1559c4ce814270fcd687147e3516a7770eeb769d2d67b63fc3b1a3
main_val.key	86f5798104a723c866aaeb4e94ce15efe067f5109d61fddfd3cba453709242de
-XX_Includes\Controls.inc	1f1a0528482390aefba7ada8b52b986581ff76e00550e1660a033d8f4a53a623
-XX_Includes\Nodes.inc	b2b2ef0ac72d437764b8eeebf29e700cf72b7d3c2c0cb54d85e038f60967b146
-XX_Includes\Elements_Properties.inc	3c2b9259939d70182b72aa16a1a376c52b2defaf86647ee1242ba9909cd2798e
-XX_Includes\Materials.inc	1c441b83e4f11a60355b301f89624b39913686a9651d1d88223ce2e1e378272a
-XX_Includes\Boundaries.inc	0ddfe4ba9d284a640bf9293bd670ba7232626ae8fe1c11ad619c3d41ed940a5b
-XX_Includes\Outputs.inc	24547478a280131d22050e19f7ced470cf68beb9246467f0f0afde25ec3d5071
CSV output hash	0a36f64aba6ebd61544e7d687086036de7e66242d389e4d8f37bc6184d2ac787
CSV criteria output hash	9ecc118154ce71198a8979e2f958b83281223530efdc04df87e4d988e2f5fb28
Time and Date	2021-09-13 16:52:59.141017 Central European Daylight Time

FIGURE 4
Exemplary structure of the simulation report based on the "cube" example of Figure 2.

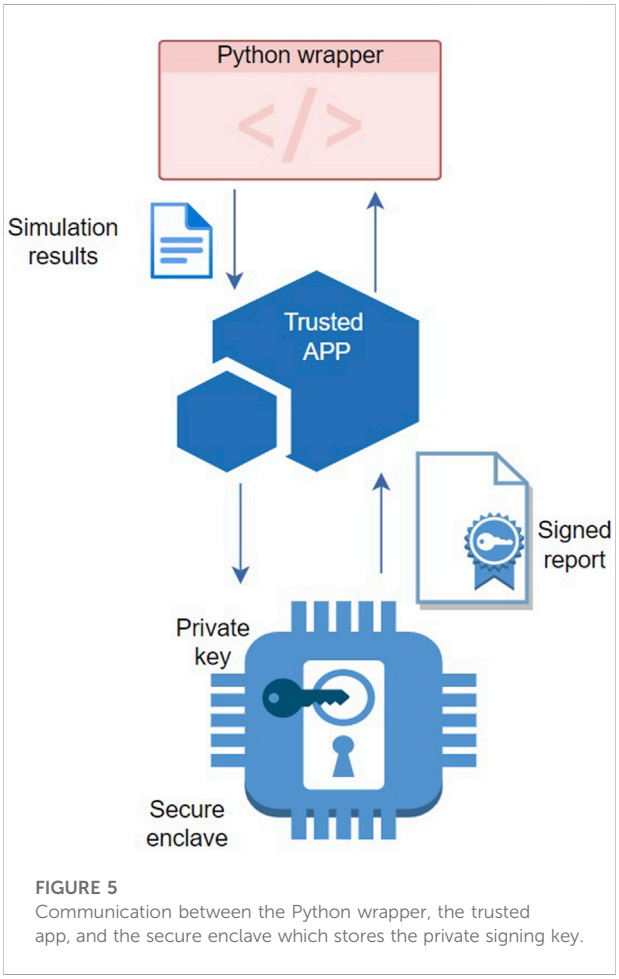

FIGURE 5
Communication between the Python wrapper, the trusted app, and the secure enclave which stores the private signing key.

date when the report is created. Invoking the build method over the document variable, a PDF document is generated and ready for signing. The report is saved to in a "Results"-folder along with the generated CSV files to be shared with the evaluation institution.

3.4 Signing approaches

When the model and results hashes are computed and included in the simulation report, it is necessary to prevent anyone from changing them, i.e., manipulating the report. This can be ensured by the evaluation institutions by signing the simulation report with a digital signature. Then, only the owner of the private signing key can create valid reports. However, as the report is created by the car manufacturer, managing this private key is challenging. In the following sections, we discuss several potential approaches.

3.4.1 Hiding the private key in a secure enclave

In this approach, the private key is created and stored in Intel SGX, as shown in Figure 5.

When the key is generated and stored inside the secure enclave, nobody can access it except the machine on which it was generated. Since the key would be generated for each car manufacturer separately, there would not be a unique key that belongs to the evaluation institution, but all of these signatures can be verified and used accordingly. A disadvantage of this approach is that there has to be hardware support. Car manufacturers must have secure enclaves in their processors on the HPC clusters or otherwise this approach cannot be used. The other disadvantage is that the car manufacturers could still use the private key for signing. Thus, it is necessary to bind the key to the process that generated it and thus limit its use, for example using remote attestation. That way, only the report generated by the script could be signed using that approach. The

evaluation institution or a trusted third party hides the key inside the secure enclave of the car manufacturer's clusters and binds the key only to the script that runs the simulation.

To generate the signing key and sign the report using secure enclaves, in this solution, we use the Intel SGX application from Nevis (2020). It consists of two internal applications. The first one is the gateway application, which is an untrusted application that prepares the enclave and invokes its functions. The second one is the trusted application that runs in the Intel SGX enclave. It invokes the function *via* the Intel SGX ECALL mechanism.

The trusted app has two functionalities, key generation and data signing. In the key generation part, the trusted application generates a key pair for the ECDSA signature scheme, which consists of a private key and a public key. The private key is needed for signing and must be kept protected, while the public key can be exported to be used for verification of signatures. Technically, the private key is saved inside the enclave and encrypted using the Advanced Encryption Standard with Galois/Counter Mode (AES-GCM) algorithm that uses the encryption key derived from the silicon and the enclave's SIGNER measurement register. This way, the private key data is sealed and can only be unsealed in the same enclave on the same machine that created it.

The application can be used with simple commands to generate the public-private key pair and to sign the data. The key generation command generates a public key in Privacy-Enhanced Mail (PEM) format and stores it in the results directory. This file needs to be forwarded to the evaluation institution for signature verification. The private key and its associated information are stored in sealeddata. bin, protected by Intel SGX. The script first checks whether this file already exists in the root folder and generates the new key only if it does not. This prevents an attacker from causing denial-of-service by deleting the sealeddata. bin file. The command for signing needs the sealeddata. bin file to know which key to use for signing. In our proof-of-concept implementation, the resulting signature is stored in a Report. signature file next to the PDF report to be signed.

3.4.2 Signing by the person that runs the simulation

If secure enclaves are not available on the used hardware, signing could alternatively be performed by a person. This approach assumes a contact person who takes responsibility for model integrity. For the implementation in the proof-of-concept demonstration code, we use the "PDFNetPython" Python library to create a digital signature (PDFTron Systems Inc, 2001). To sign the PDF report using the PDFNetPython library, it is first necessary to create a signing widget in the document. This allows the user to create a field in a PDF document where the signature will be placed. The exact place of a field can be set using coordinates as parameters. There is also a possibility to add an image that will visually represent the signature. After the signature field is added, it is used to create a digital signature field object. This object is then saved to a variable, on which signing method is invoked using the private key file and the password which secures the private key file.

The signature algorithm used by this method is RSA with a key length of 2048 bit with SHA-256 hashing. The key file used as a parameter is in PKCS#12 file format (PFX filename extension) protected with a password. This file is exported using OpenSSL (The OpenSSL Project Authors, 2022). This approach improves the previous procedure significantly since it limits the time for potential model manipulation. However, model integrity could still potentially be subverted by a technically highly skilled adversary on the car manufacturer's side; this approach assumes a certain amount of trust between the responsible contact person and the evaluation institution.

3.5 Check of integrity

To prove that the procedure was performed properly, the evaluation institution needs to check if the received signed "Simulation Report" is consistent with the extracted simulation output files. Therefore, we developed a script as proof-of-concept implementation for the evaluation institution to perform the verification of the signature and the verification of the hashes (model hash and result hash). To check the integrity of the results, the testing institution computes the hash from the content of the result CSV file and compares it with the hash given in the report. If computed hash is the same, the integrity of CSV is preserved, since the hash given in the report is protected with a signature.

4 Discussion

4.1 Evaluation

4.1.1 Overview

In summary, our solution consists of several layers of protection which address different aspects of the problem:

- The hash function construction in the wrapper protects integrity of the simulation model: it records the details of the simulation model so that any differences can be detected. However: anyone could write down any hashes they like, i.e., this is not sufficient against a malicious actor, only against accidental errors.
- The signature protects the authenticity of the report: only the owner of the private key can produce a valid signed report and thus certifies the contents. This also provides non-repudiation, i.e., the owner of the private key cannot

deny having signed the report. However, access to this key must be restricted with organizational and/or technical measures. For example, it could be assigned to a trusted, personally responsible person.

- The trusted execution environment restricts the usage of the private key to a particular device and a particular trusted small program that implements the signing procedure. This prevents various kinds of misuse and implementation attacks. However, this signing procedure could still be invoked with malicious input (e.g., fake output of the simulation software by manipulating the interaction with this software; however, with the given setup, it would be very easy to trace who is responsible in case such a manipulation is suspected, and to check whether this was the case).
- A remote attestation setup (not implemented due to lack of network on target systems) could restrict who can invoke the trusted code and could monitor each invocation externally for further security if desired and feasible.

Next, we discuss the properties of this solution, as well as potential alternatives, in more detail.

4.1.2 Security

The developed procedure significantly improves the integrity and authenticity of related files by addressing the main threats identified. A cryptographic way to ensure the integrity of the simulation results was established. Unique model fingerprints are generated and documented to avoid that model files could be manipulated within the virtual testing procedure. Digital signatures guarantee the authenticity of a document and prevent repudiation.

4.1.3 Performance

The procedure brings only minor additional work for users and small computational overheads. To measure the real-time overhead, we run two processes over the mentioned cube example. One process is just the running the simulation, while the other process is started by running the implemented wrapper script (with the responsible person signing). The simulation (the baseline procedure without the wrapper) on the cube example lasted 13.0072 s, while the new procedure lasted 21.3379 s. When comparing these two times, it seems like there is a considerable time overhead (8.3307 s). However, taking into account that LS-DYNA simulations for real-world examples may often last even for several hours, the time overhead of 8.33 s is negligible and indistinguishable. The time overhead will be similar for a complex simulation since the same number of hashes, reports and CSV files are generated. Of course, if the complex solution has more files, the overhead will increase. However, it will still be within 1 minute, which is again negligible compared to a several-hour long simulation.

4.2 Limitations

While many mentioned threats are addressed, there are still some threats that one should be aware of. Since the simulation is not done in a protected environment, malicious users could still harm the procedure (e.g., by manipulation of the LS-DYNA executable), but a higher amount of criminal energy would be needed for that. Another threat is that the execution of the closed-source FE software itself can not be fully protected from manipulation; in particular, the signing procedure is currently not tied securely to the FE software (using remote attestation or similar mechanisms) and could thus be invoked separately by other processes on the same computer. The procedure with signing requires secure enclaves working on the computer hardware where simulations are run (e.g., HPC cluster at the car manufacturer). If this is not available, manual signing could be done, but this lowers the security level of the procedure.

The developed procedure requires that the files which can be modified do not contain IP protected information, so that the content can be inspected by the evaluation institution. Otherwise, additional contents and not allowed manipulations could be not avoided with the developed procedure. However, as load cases mostly differ in acceleration pulses and this is not supposed to be confidential information, our developed procedure could be used for such applications. If their are other use cases in the future where it would be needed to modify confidential parts of the model in between load cases another script checking the keywords in the changed files. This would require a list of allowed and forbidden keywords in the changeable files. Another approach could be Audits by trusted third parties underlying non-disclosure agreements. Our procedure would be still helpful for such audits as the information which files were changed in which loadcase is provided.

The procedure as such and the hash function also work on encrypted files, as the hash can be also calculated for the ciphertext to ensure its consistency between simulations. However, encrypted files cannot be audited and therefore parameters overwriting other parts of the models could be hidden in there. If parameters are defined multiple times, the developed wrapper could not identify it. Therefore, the current procedure can be not applied if the simulation setup consists of encrypted dynamic (load case dependent) parts. If static parts are encrypted, the procedure still works but is a bit weaker because duplicate parameters cannot be identified. The procedure was applied within this paper only for an easy example to make it more readable and easier to follow for the reader. Within the development phase it was also applied to bigger files with dummy models, which are closer to the final use case. It was found that the procedure works consistently, also with more complex files and file structures, basically changing only the result shown in Figure 4.

The procedure does not replace quality and plausibility checks of the simulations. This has to be done based on shared simulation results by the evaluation institution. The procedure just supports the evaluation institutions by documenting from which simulation models results were generated and which parts of the models were modified in between which steps of the procedure.

4.3 Alternative signing approaches

For report signing, it is necessary to have a private key known only by the evaluation institution or a trusted third party (e.g., LS-DYNA) and not by the car manufacturer. However, it is challenging to generate and safely store such a key. Several approaches were discussed within the development of the procedure described in this paper. The "secure enclave" approach was finally implemented and described within this paper. As the secure enclave approach still has the drawback that it might not be available on a certain hardware and the approach with a responsible person signing the report requires trust in this person, further alternatives should be investigated in the future, as we discuss next.

4.3.1 Using the private key from LS-DYNA

One option is to use LS-DYNA's private encryption key, which is intended for internal input file encryption and decryption in LS-DYNA. Using this key would be very convenient since it would solve both key generation and storage problems. Nevertheless, the level of provided security would depend on how well this key is protected. Only limited documentation on this embedded encryption method is publicly available, preventing alternative uses or security evaluation of this mechanism. Another option requring support from FE software developers is to hide the newly generated key inside the FE software binary.

4.3.2 Storing the private key on a server

Signing could also be done on a trusted third-party server. The implemented wrapper would have to create the final report and upload it to the server. Then, the server uses the stored key, signs the received document, stores corresponding details in a log file, and returns it to the wrapper.

This option has a significant shortcoming preventing its use given our requirements: The HPC clusters of car manufacturers typically do not have internet access or any connection to the outside world on purpose for security reasons, particularly due to the confidentiality of the files processed on these machines. Nonetheless, access to licence servers is needed also on these clusters. When the simulation is started, FE software could for example send the ID of the device to a licence server and receive "YES" if the machine has a valid license or "NO" otherwise. An idea based on this finding is to store the key on the very same machine as the licence server. This is, however, an unsuitable solution because of the possible responses from the server—it is not able to return a signed document but only a "YES/NO" answer. This would have to be changed to enable this option.

4.4 Future work

Additionally to the before discussed improvements for the signing, there are also other ways to further improve the procedure: Most importantly, the integration of the procedure in the FE software itself would make the procedure more easier to implement as the car manufacturer's clusters and further improve the security of the procedure because the wrapper functionalities would be embedded in the binary of the FE software. An input checker could check the keywords the files to avoid forbidden changes of the model especially when the dynamic parts of the simulation models cannot be inspected because of IP issues. Additional types of simulation results such as videos of animations could be also added to the procedure in the future, applying the same approaches, because basically every file can be hashed and the procedure therefore extended to everything where changes should be identified. Overall, our procedure is just addressing the integrity of a virtual testing procedure. Other future work has to focus on the development of the qualification criteria for the simulation models and the definition and assessment of the virtual testing loadcases.

5 Conclusion

In this paper, we propose a new and secure procedure for virtual testing of IP-protected simulation files. Security mechanisms, such as hash functions, digital signatures and secure enclaves are used to ensure the necessary security requirements. The proposed procedure makes it possible to trace which parts of the simulation model have been subject to modification without disclosing IP-protected information. Furthermore, the consistency between the simulation results and the input files can be checked. This ensures that models used in the previous qualification procedures was indeed used throughout the virtual test and that results were generated with the qualified models and therefore significantly improves the integrity of the procedure. We have implemented a proof-of-concept for the FE software package LS-DYNA and made it publicly available. Implementation for other simulation software packages (not necessarily restricted to FE software) is subject of future work. Further research is also needed to address known drawbacks of the proposed procedure (e.g. improve security of the signing process). The developed method is an enabler for increasing the integrity of virtual tests in consumer information

or vehicle safety assessment regulations and could be implemented directly in FE software packages in the future.

Data availability statement

Publicly available datasets were analyzed in this study. This data can be found here: The code developed in this study is available *via* https://openvt.eu/Integrity_check/proof-of-concept-scripts.

Author contributions

EG wrote the first draft of the manuscript, performed the threat analysis and implemented the derived procedure in the sample code presented. ME wrote the parts of the manuscript focusing on security and supervised EG on the security aspects. CK wrote the virtual testing sections of the manuscript and supervised EG on the application aspects. ME and CK commented on the study. SH had the initial idea of such an approach and critically reviewed the manuscript. All authors contributed to the revision of the manuscript, read and approved the submitted version.

Funding

The master's thesis in which this study was performed has received support from the VIRTUAL project funded by the European Union Horizon 2020 Research and Innovation Program under Grant Agreement No. 768960.

Acknowledgments

The authors would like to thank colleagues from Dynamore and Scale for fruitful discussions of different possibilities for implementation.

Conflict of interest

The authors declare that the research was conducted in the absence of any commercial or financial relationships that could be construed as a potential conflict of interest.

Publisher's note

All claims expressed in this article are solely those of the authors and do not necessarily represent those of their affiliated organizations, or those of the publisher, the editors and the reviewers. Any product that may be evaluated in this article, or claim that may be made by its manufacturer, is not guaranteed or endorsed by the publisher.

References

ANSYS - LST (2021). Ls-dyna. Available at: https://www.lstc.com/products/ls-dyna.

ANSYS-LST (2020). Keyword user's manual. *LS-DYNA*. https://www.dynasupport.com/manuals/ls-dyna-manuals/ls-dyna_manual_volume_i_r13.pdf

Damgård, I. (1989). A design principle for hash functions. *Adv. Cryptol.* 435, 416–427. doi:10.1007/0-387-34805-0_39

Diffie, W., and Hellman, M. E. (1976). New directions in cryptography. *IEEE Trans. Inf. Theory* 22, 644–654. doi:10.1109/TIT.1976.1055638

Eggers, A., Schwedhelm, H., Zander, O., Izquierdo, R. C., Polanco, J. A. G., Paralikas, J., et al. (2013). "Virtual testing based type approval procedures for the assessment of pedestrian protection developed within the eu-project imviter," in NHTSA, editor, The 23rd ESV Conference Proceedings (NHTSA).

Euro NCAP (2022). European new car assessment programme. Available at: https://www.euroncap.com/en.

Gottesman, D., and Chuang, I. (2001). Quantum digital signatures. doi:10.48550/arxiv.quant-ph/0105032

Huizinga, F., Ostaijen, R., and Slingeland, A. (2002). A practical approach to virtual testing in automotive engineering. *J. Eng. Des.* 13, 33–47. doi:10.1080/09544820110090304

Intel (2021). Intel software guard extensions. Available at: https://software.intel.com/content/www/us/en/develop/topics/software-guard-extensions.html.

Klug, C., Luttenberger, P., Schachner, M., Micorek, J., Greimel, R., and Sinz, W. (2018). "Postprocessing of human body model results – introduction of the open source tool dynasaur," in CARHS, editor, 7th International Symposium: Human Modeling and Simulation in Automotive Engineering.

Klug, C., Feist, F., Schneider, B., Sinz, W., Ellway, J., and van Ratingen, M. (2019). "Development of a certification procedure for numerical pedestrian models," in NHTSA, editor, The 26th ESV Conference Proceedings (NHTSA).

Koblitz, N. (1987). Elliptic curve cryptosystems. *Math. Comput.* 48, 203–209. doi:10.1090/s0025-5718-1987-0866109-5

Linder, A., Davidse, R. J., Iraeus, J., John, J. D., Keller, A., Klug, C., et al. (2020). *VIRTUAL-a European approach to foster the uptake of virtual testing in vehicle safety assessment*. In 8th Transport Research Arena TRA 2020, April 27-30, 2020, Helsinki, Finland.

Lu, Y. S., Cao, X. Y., Weng, C. X., Gu, J., Xie, Y. M., Zhou, M. G., et al. (2021). Efficient quantum digital signatures without symmetrization step. *Opt. Express* 29, 10162–10171. doi:10.1364/OE.420667

Merkle, R. C. (1989). A certified digital signature. *Adv. Cryptol.* 435, 218–238. doi:10.1007/0-387-34805-0_21

Miller, V. S. (1985). Use of elliptic curves in cryptography. *Adv. Cryptol.* 218, 417–426. doi:10.1007/3-540-39799-X_31

Nevis, B. S. (2020). Gateway key provisioning and secure signing using intel® software guard extensions. Available at: https://software.intel.com/content/www/us/en/develop/articles/code-sample-gateway-key-provisioning-and-secure-signing-using-intel-software-guard.html.

NIST (2008). *FIPS PUB 198-1: The keyed-hash message authentication code (HMAC)*. Gaithersburg, MD: National Institute of Standards and Technology: Federal Information Processing Standards Publication.

NIST (2013). *FIPS PUB 186-4: Digital signature standard (DSS)*. Gaithersburg, MD: National Institute of Standards and Technology: Federal Information Processing Standards Publication.

NIST (2015). *FIPS 180-4: Secure hash standard (SHS)*. Gaithersburg, MD: National Institute of Standards and Technology: Federal Information Processing Standards Publication.

NIST (2020). *Nistir 8309: Status report on the second round of the NIST post-quantum cryptography standardization process*. Gaithersburg, MD: National Institute of Standards and Technology Interagency or Internal Report.

PDFTron Systems Inc (2001). Digitally sign pdf files in python (2001-2021). Available at: https://www.pdftron.com/documentation/samples/py/DigitalSignaturesTest.

Rivest, R. L., Shamir, A., and Adleman, L. M. (1978). A method for obtaining digital signatures and public-key cryptosystems. *Commun. ACM* 21, 120–126. doi:10.1145/359340.359342

Schachner, M., Micorek, J., Luttenberger, P., Greiml, R., Klug, C., and Rajinovic, S. (2022). Dynasaur - dynamic simulation analysis of numerical results. Available at: https://gitlab.com/VSI-TUGraz/Dynasaur.

The OpenSSL Project Authors (2022). The openssl project. Available at: https://www.openssl.org/.

van Ratingen, M.Update on virtual testing in safety assessments from euro ncap (2020). VIRTUAL OSCCAR workshop: Progress in Virtual Testing for automotive application. Available at: http://www.ircobi.org/wordpress/downloads/2020-virtual-osccar.pdf.

frontiers | Frontiers in Future Transportation

TYPE Original Research
PUBLISHED 31 January 2023
DOI 10.3389/ffutr.2023.931780

OPEN ACCESS

EDITED BY
Yong Han,
Xiamen University of Technology, China

REVIEWED BY
Daisuke Ito,
Kansai University, Japan
Emilia Szumska,
Kielce University of Technology, Poland

*CORRESPONDENCE
Arne Keller,
keller@agu.ch

SPECIALTY SECTION
This article was submitted to Transport Safety, a section of the journal Frontiers in Future Transportation

RECEIVED 29 April 2022
ACCEPTED 09 January 2023
PUBLISHED 31 January 2023

CITATION
Keller A and Krašna S (2023), Accelerations of public transport vehicles: A method to derive representative generic pulses for passenger safety testing.
Front. Future Transp. 4:931780.
doi: 10.3389/ffutr.2023.931780

Accelerations of public transport vehicles: A method to derive representative generic pulses for passenger safety testing

Arne Keller[1]* and Simon Krašna[2]

[1]AGU Zürich, Zürich, Switzerland, [2]Faculty of Mechanical Engineering, University of Ljubljana, Ljubljana, Slovenia

Investigating the postural balance and stability of standing passengers of public transport in laboratory or numerical tests requires generic test pulses, which replicate the acceleration/deceleration characteristics of common public transport vehicles such as buses or trams. We propose a method to generate such test pulses based on measured acceleration time series. The method consists of an automated splitting algorithm, an expansion in Legendre polynomials and a weighted mean to obtain average pulses which are not dominated by the events of highest magnitude. As a demonstration, the method is applied to acceleration time series obtained on public buses in normal operation, resulting in scalable generic pulse shapes. These can be used as the basis of a standardised framework for physical and virtual testing addressing the standing passenger problem.

KEYWORDS

public transport, non-collision incidents, acceleration time series, legendre polynomials, generic acceleration pulses

Introduction

Public buses and trams are not only environmentally friendly and affordable but are also a safe means of transportation compared to other modes of urban transport such as private cars, powered two-wheelers and bicycles (Morency et al., 2018; European Commission, 2022). Nevertheless, using public transportation to travel is not without risk. Most injuries that passengers sustain while using public transportation occur without the vehicle being involved in a road collision (Kirk et al., 2003) (so-called non-collision incidents). Particularly standing passengers can lose their balance and fall due to the acceleration and deceleration behaviour of the vehicle; Elvik (2019) estimated the risk of falling in a moving public transport vehicle as 0.3–0.5 per million passenger kilometres and 0.7–1.7 per million passengers in relation to boarding and exiting the vehicle. The injury risk is higher for female and elderly passengers (Halpern et al., 2005; Kendrick et al., 2015; Li et al., 2017). In addition to these safety concerns, passenger dissatisfaction with the comfort and smoothness of the ride is also one of the major reasons to avoid bus service (Karekla and Tyler, 2018).

To understand the typical injury mechanisms in non-collision incidents, both the postural balance of a person standing on a moving surface and the nature of the acceleration perturbations typically challenging the balance of a bus or tram passenger have been studied. While the postural balance of a person standing on a moving surface is not directly the subject of this study, the work in this field using either laboratory experiments with voluntary participants (e.g., (Carpenter et al., 2005; Robert et al., 2007; Tokuno et al., 2010)) or computational models that simulate the human body (Palacio et al., 2009; Aftab et al., 2016) is still a primary research motivation. The acceleration signal of a typical public transport

journey is of a duration that by far exceeds the range of motion of a laboratory sled experiment and the duration that can be replicated in a human body model simulation within reasonable computation time. Therefore, the characteristic features of the acceleration perturbations must be 1) understood and 2) condensed into short pulses that can be applied in a computer simulation or in the laboratory.

In early research on the acceleration behaviour of public transport vehicles, the focus was mostly on defining comfort or safety thresholds for acceleration magnitudes and jerks (Hoberock, 1977; Brooks et al., 1978), while the structure of the acceleration pulses was not investigated in further detail. The first study that considered the influence of acceleration pulses on the postural balance of standing passengers was completed by Graaf and Van Weperen (1997), who measured acceleration time series on buses and trams and used similar perturbations in treadmill experiments with volunteer participants. More recently, several authors studied the acceleration time series of buses (Zaworski et al., 2007) and subway trains (Powell and Palacín, 2015) with a focus on passenger (dis)comfort. The shape of average emergency braking pulses was investigated by Turkovich et al. (2011); Schubert et al. (2017) measured acceleration pulses during a study with a bus in test driving conditions using volunteers. However, a closer analysis of the acceleration time series was not the main objective of their work. To date, the most systematic study investigating the structure and shape of acceleration pulses was completed by Kirchner et al. (2014). These authors expanded time-normalised acceleration and deceleration pulses in a Legendre series, enabling the quantification of the relevant properties of the pulses and the comparison of different acceleration events in terms of similarity coefficients. They also suggested a method to choose a representative example out of a given set of pulses (i.e., the one with the highest mean mutual similarity).

Despite the research completed thus far, with a goal of providing suitable input data for computational and laboratory studies of the standing passenger problem, there are still significant gaps in both knowledge and methodology. Representative sets of field data are still rare in the current literature. In addition, there is no method to automatically derive meaningful average acceleration and deceleration pulses from larger data sets. Even though the method presented by Kirchner et al. (2014) already allows for a systematic comparison of different acceleration and deceleration events, their method is not readily applicable to larger datasets, as it requires manual splitting of the acceleration signals. Furthermore, an averaging method taking into account all events of a set (instead of only choosing a representative example) is still lacking in the literature.

In this work, we address this methodological gap by expanding the (Kirchner et al., 2014) method to an automatically applicable algorithm that can be used for datasets of much larger sizes. Furthermore, we propose a weighted-mean method to compute an average pulse from a given set of acceleration and deceleration pulses. As a demonstration of the method, we present a set of real-life acceleration data recorded on public buses during their normal operation in city traffic, from which we derive generic acceleration and deceleration pulses representing the typical behaviour of the vehicles under consideration.

Even though a combination of theoretical work and field data analysis, this article still follows the structure ”Materials and methods—Results—Discussion—Conclusion” typical for a data analysis work. The section ”Materials and methods” contains a somewhat longer theoretical section, explaining the proposed data analysis method, including some theoretical background on Legendre expansions and a description of the new ”weighted mean” approach and the splitting algorithm. The remaining parts focus on the application of the new method to the dataset. For the reader interested in the deeper mathematical details of the weighted mean approach, more information is provided in the appendix.

Materials and methods

Data analysis method

The time series analysis method presented here is based on a Legendre expansion of a scalar function with support [0, 1], which represents a time-normalised acceleration or deceleration event. Therefore, the raw datasets (i.e., the time series of the longitudinal acceleration component) first have to be filtered and split into acceleration and deceleration events. Then, normalisation and Legendre expansion of the data is completed. The resulting coefficient sets can be used for similarity analysis and the computation of representative average pulses. The implementation of the data analysis method was achieved in Python using the SciPy and Pandas packages (McKinney, 2010; Virtanen et al., 2020). All scripts are available under the terms of the GPL licence on the OpenVT platform.[1]

Preprocessing and automatic splitting

The one-dimensional raw acceleration data are Butterworth filtered (second order, cutoff frequency $\omega_0 = 0.75\ \frac{\text{rad}}{\text{s}}$) to remove high-frequency oscillations. The resulting acceleration signal is split according to the following three-step algorithm:

- Constant phases are identified as intervals that are longer than a certain duration, which by default is 100 time steps, and the change of the signal per time step is lower than a certain threshold, which by default is 0.005 standard deviations of the entire signal. After cropping out these constant phases, a set of raw pulses remains.
- On each of the remaining raw pulses, a discrete Fourier transformation is applied and the maximum of the spectrum is determined. If the peak occurs at a frequency > 0, i.e., there is predominant oscillating behaviour, then the pulse is split into multiples of the period associated with the peak frequency, and if the spectral maximum occurs at 0, i.e., there is no predominant oscillating behaviour, then the peak is not split.
- For each of the resulting subpulses, the cumulative sum is calculated (as an approximate estimate of the resulting speeds) and the absolute maximum of the result is determined. Depending on whether the maximum occurs 1) close to the start of the subpulse, 2) close to the end of the subpulse, or 3) somewhere in between subpulses, the subpulse is identified as 1) a deceleration event (DEC), 2) an acceleration

1 https://openvt.eu/Acceleration_tools/Bus_data_and_tools.

event (ACC) or 3) a split at the occurrence of the maximum of an ACC and a DEC event[2].

As a result of the splitting algorithm, for the given time series, two sets of functions representing the acceleration signals of the ACC and the DEC events, respectively, are obtained. For further treatment, these functions are time-normalised to a unity interval, resulting in the functions

$$f_i^I\colon [0,1] \mapsto \mathbb{R}, \tag{1}$$

where $1 \le i \le M_I$ is the number of the event in the given set and $I \in \{A_1, A_2, \ldots, , D_1, D_2, \ldots\}$ is an identifier representing the different sets of ACC pulses (A_n) and DEC pulses (D_m), respectively. That is, if only one acceleration time series is considered, the algorithm results in one set of ACC pulses and one of DEC pulses, so the identifier could be $I \in \{A_1, D_1\}$, while for each additional time series under consideration, one more ACC and DEC set is added to the list.[3]

Legendre expansion

Expansions in Legendre polynomials are a known and useful tool, e.g., in image processing (Paton, 1975). The mathematical properties of these expansions and their convergence are well documented in the scientific literature. For an overview, see Wang and Xiang (2012). Kirchner et al. (2014) suggested a Legendre expansion of acceleration pulses due to the convenient properties of the Legendre polynomials on a unit interval.

As opposed to the most common representation on the interval $[-1, 1]$, in this work, the shifted Legendre polynomials on the support $[0, 1]$ are used. For any non-negative integer n, the nth polynomial is defined as

$$P_n\colon [0,1] \mapsto \mathbb{R}, \tag{2}$$

$$P_n(x) = \frac{1}{n!}\frac{\mathrm{d}^n}{\mathrm{d}x^n}\left(x^2 - x\right)^n. \tag{3}$$

These polynomials obey the orthogonality relation

$$\int_0^1 P_k(x) P_l(x)\,\mathrm{d}x = \frac{1}{2k+1}\delta_{kl}, \tag{4}$$

on which the Legendre expansion is based.

The time-normalised functions in Eq. 1 can be approximated by a series of Legendre polynomials,

$$f_i^I(x) = \sum_{k=0}^{N} c_{i,k}^I P_k(x) + (R_N)_i^I(x) \approx \sum_{k=0}^{N} c_{i,k}^I P_k(x), \tag{5}$$

where N is the order of the approximation and $(R_N)_i^I(x)$ are the residual functions. The decay of the residuals with N depends on the behaviour of the complex continuation of the function f on a Bernstein ellipse. In general, this decay cannot easily be estimated. For further details see, e.g., Wang and Xiang (2012). However, for our purposes, it can be stated that choices on an order of magnitude of $N = 10$ to $N = 200$ are reasonable, in a trade-off of approximation quality and computational cost.

Using the orthogonality relation Eq. 4, the $N + 1$ Legendre coefficients can be written as

$$c_{i,k}^I = (2k+1)\int_0^1 f_i^I(x) P_k(x)\,\mathrm{d}x. \tag{6}$$

Please note that, for the sake of the clarity, we will in the following often use a somewhat sloppy notation and denote the coefficient $c_{i,k}^I$ by $c_{i,k}$ provided that it is clear from which set I the corresponding pulse f_i^I is taken.

Our implementation offers two ways to compute the Legendre coefficients: 1) a numerical evaluation of the integrals in Eq. 6 using a Gauss-Legendre quadrature with the roots of the highest-order polynomial as integration points (to which the data are interpolated using a cubic spline interpolation) and 2) a least-squares fit of the data with Eq. 5 (this method avoids evaluating the integrals explicitly). Method (ii) tends to be faster, and method (i) is more stable for coefficients of higher order[4].

The Legendre approximation reduces the number of degrees of freedom for each pulse to a small number of coefficients; the use of 40–70 coefficients is mostly sufficient, except if jerks are to be estimated. In addition, this approximation provides a straightforward way to compare the shapes of different pulses (see section "Similarity analysis").

Analysis of time-normalised acceleration and deceleration pulses

Once the Legendre representations (5) have been computed, several methods can be employed to compare the different pulses.

Jerk estimation

The jerk, i.e., the time derivative of acceleration, is known to be of fundamental importance for passenger (dis)comfort and safety (Graaf and Van Weperen, 1997). Nevertheless, this quantity (and particularly its peak value) is not necessarily easy to estimate from acceleration time series, as numerical differentiation schemes tend to be unstable for noisy data.

Once the Legendre coefficients of a given pulse are known, we compute the Legendre representation of the time derivative according to Phillips (1988). The corresponding Legendre expansion provides up to a scaling factor due to the time normalisation, an approximation of the jerk as a function of normalised time. This method avoids using a finite differences scheme[5]. However, this method requires the computation of a higher number of Legendre coefficients.

For the jerk as time derivative of acceleration, is has to be taken into account whether or not the acceleration pulses under consideration are time-normalised. The jerk estimation method for time-normalised pulses described above yields a jerk with respect to normalised time, with a dimension of acceleration. If the "true" jerk

2 By definition, for ACC events, the cumulative acceleration is >0, while for DEC events, the cumulative acceleration is negative.

3 Of course, the sets can also be re-combined in different ways—we leave it to the reader to come up with suitable indexing in this case. In places where only the pulses of one set (e.g., one ACC set) are compared with each other, we will drop the identifier I altogether to make the notation less clumsy.

4 According to Hale and Townsend (2016), it would be possible to further speed up this computation by using a method similar to the fast Fourier transformation. This approach could be a good way to make the method more suitable for larger data quantities.

5 According to Lu et al. (2013), this method performs significantly better than the finite differences scheme and even has advantages over approaches based on polynomial interpolation.

(dimension acceleration over time) is of interest, the jerk with respect to normalised time has to be divided by the duration of the pulse under consideration. In the results section, the histograms for the measured pulses always show the jerk with respect to time, while the jerks of the mean and maximum similarity pulses are specified with respect to normalised time.

Similarity analysis

The similarity analysis in terms of Legendre coefficients has been described by Kirchner et al. (2014). For two time-normalised ACC or DEC pulses f and g, the similarity coefficient is defined as

$$s[f,g] = \frac{\langle f,g\rangle}{\sqrt{\langle f,f\rangle\langle g,g\rangle}}, \tag{7}$$

where $\langle .,. \rangle$ represents the L2 scalar product. Similarity coefficients can be applied to compare time-normalised pulses of different sets without taking into account their magnitudes. We will, however, in the following focus on similarities between pulses of the same set.

Let $\left\{f_1^I \ \ldots \ f_M^I\right\}$ be a set of M time-normalised pulses (all either ACC or DEC pulses) with identifier I (in the following, only this one set of pulses will be considered, so we will drop the identifier I in the notation). Using a Legendre expansion to order N, the similarity coefficient within the set can be expressed in terms of the Legendre coefficients $c_{i,k}$, $c_{j,k}$ of the pulses f_i and f_j as

$$s_{ij} \coloneqq s\left[f_i, f_j\right] = \frac{\sum_{k=0}^{N} \frac{c_{i,k}c_{j,k}}{2k+1}}{\sqrt{\sum_{l=0}^{N} \frac{(c_{i,l})^2}{2l+1} \sum_{m=0}^{N} \frac{(c_{j,m})^2}{2m+1}}}. \tag{8}$$

For the M different pulses f_i of the set under consideration, a symmetric similarity matrix of dimensions $M \times M$ containing the $M(M+1)/2$ independent similarity coefficients is obtained.

Average/representative example: Maximum similarity and mean pulses

The similarity coefficients s_{ij} within a given set are the basis for different methods to define a representative average or to select a representative example for the shape characteristics of a set of time-normalised events without over-representing high-magnitude events. Kirchner et al. (2014) suggested considering the mean similarity coefficient of each pulse f_i out of the set I, which is defined as

$$\bar{s}_i = \frac{1}{M} \sum_{j=0}^{M} s_{ij}. \tag{9}$$

As a representative example, the pulse out of the set with the highest mean similarity coefficient is chosen,[6]

$$f_{\text{maxsim}}^I = f_i \in \left\{f_1^I \ \ldots \ f_M^I\right\}: \ \bar{s}_i = \max_{k\in\{1\ \ldots M\}} \bar{s}_k. \tag{10}$$

This pulse can now either be written as time-normalised function or as Legendre expansion. We will refer to this method as the "maximum similarity pulse method" and to the resulting pulse f_i as the "maximum similarity pulse".

While the maximum similarity pulse method allows choosing a representative example out of a set of pulses, in many applications (particularly when creating input to experimental or numerical tests), it is more appropriate to use an average that takes into account the shape of all pulses of the set to some extent. Given that measured acceleration signals are typically sets with different magnitudes but similar shapes, simply calculating an arithmetic mean would not be very useful, as it would be dominated by pulses with the highest magnitude.

As a method to calculate such a representative average of the shapes of different pulses, we suggest considering a weighted mean over a given set with the inverse of the L_2-norm of each pulse as weight. The Legendre coefficients of this weighted mean pulse can be written as[7]

$$\bar{c}_k = a_0 \frac{1}{M} \sum_{i=1}^{M} \frac{c_{i,k}}{\sqrt{\sum_{l=0}^{N} \frac{(c_{i,l})^2}{2l+1}}}, \ k = 0 \ \ldots \ N, \tag{11}$$

where M, again, is the overall number of pulses in the given set, a_0 is an arbitrary (but constant) scaling factor, and N is the order of the Legendre approximation. The time-normalised acceleration pulse corresponding to these coefficients is given by the generic expression of the Legendre series (Eq. 5) with zero residuals, $\sum_{k=0}^{N} \bar{c}_k P_k(x)$. It can be shown (see appendix) that out of all Legendre series of order N, the multiples of this pulse have the highest possible mean similarity with the pulses of the set.[8] As this holds for any multiple of the pulse define d by these coefficients, the maximisation of the mean similarity only defines the mean pulse up to a multiplicative factor. Therefore, Eq. 11 contains an unknown scaling factor a_0. The choice of the scaling factor is up to the user; a reasonable choice depends on the application. For example, the peak acceleration of the mean pulse could be adapted to the needs of a laboratory or numerical test, or it could be used to normalise either the L2-norm of the pulse or the peak acceleration to 1, so a time- and acceleration-normalised pulse would be obtained. In the examples given in the Results section, we choose a_0 as the arithmetic mean of the peak accelerations of the pulses of the input set, so a_0 contains some information about their magnitude. However, it shall be stressed that different choices of the normalisation are possible and can makes sense according to the desired application. In the following sections, the pulse defined by the coefficients in Eq. 11 will be referred to as the "mean pulse" (or "unconstrained mean pulse") and the method as the "(unconstrained) mean pulse method."

Due to the cutting algorithm and varying terrain gradients, measured acceleration pulses that are cut out of an acceleration time series tend to be offset or lopsided. Therefore, the mean pulses defined by the coefficients in Eq. 11 do not generally equal zero when $x = 0$ or $x = 1$. However, with a laboratory setting and computer simulations in mind, it is interesting to derive a version of the mean pulse that maximises the mean similarity with all pulses

6 It could potentially be that this definition is not unique—that is, that there are two pulses with the same mean similarity coefficient. This is, however, unlikely in measured acceleration pulses.

7 Note that, as opposed to the previous sections, where given time-normalised acceleration pulses were approximated and analysed in Legendre series, we take the opposite approach now and define a new pulse by defining its Legendre coefficients.

8 The mean similarity coefficient of this pulse is by construction ≥ that of the maximum similarity pulse, as the maximum similarity pulse is the pulse *within the given set* which has the highest mean similarity coefficient, while the mean pulse manifests the highest mean similarity coefficient theoretically possible in any Legendre expanded pulse of order N.

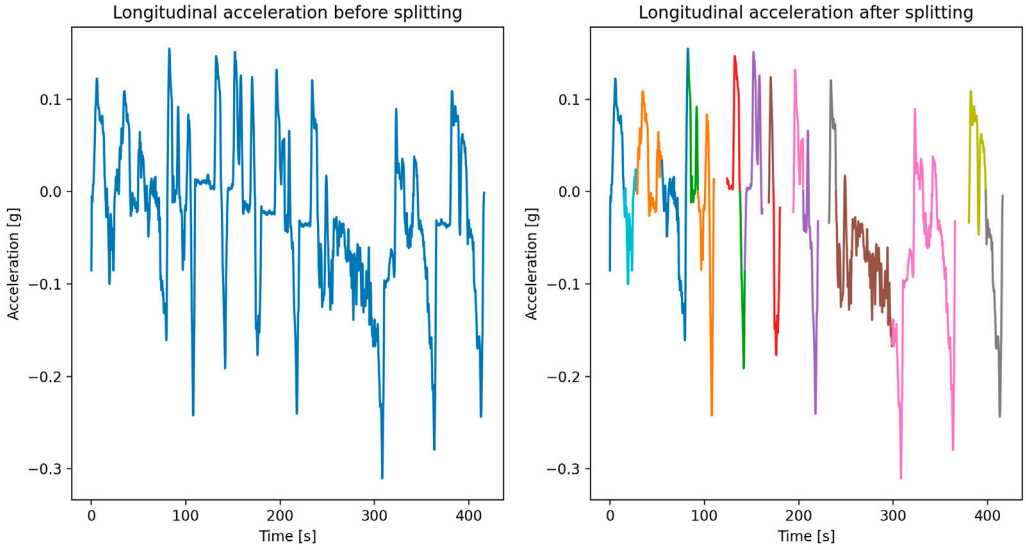

FIGURE 1
Example of a Butterworth filtered acceleration signal before and after splitting for ride no. 1 of an electric vehicle.

under consideration while starting and ending at zero. With the definitions

$$\bar{c} = \sum_{k=0}^{N} \bar{c}_k, \tag{12}$$

$$\tilde{c} = \sum_{k=0}^{N} \bar{c}_k (-1)^k, \tag{13}$$

we define the Legendre coefficients

$$\bar{c}_k^0 = \bar{c}_k - \frac{(2k+1)\left(N+1-(-1)^{N+k}\right)}{N(N+1)(N+2)}\left[\bar{c} + (-1)^k \tilde{c}\right], \quad k = 0, \ldots, N. \tag{14}$$

As for the "mean pulse" method, the corresponding time-normalised acceleration pulse can be computed according to Eq. 5, $\sum_{k=0}^{N} \bar{c}_k^0 P_k(x)$. It can be shown (see appendix) that 1) these pulses equal 0 at $x = 0$ and $x = 1$ and 2) that the multiples of this Legendre series have the highest possible mean similarity coefficients with all pulses of the given set for all Legendre series of order N starting and ending at 0.

Again, given that the similarity coefficients are invariant with respect to multiplication with a positive constant factor, this series is uniquely defined only up to multiplicative scaling. The scaling factor is contained implicitly in $\bar{c}_k, \bar{c}$ and $\tilde{c}$. That is, the resulting Legendre coefficients are not normalised to an L2-norm of 1 but can be re-scaled in any desired way by adapting this scaling factor. For the scaling, the same holds as for the unconstrained mean pulse method. This method will be referred to as the "constrained mean pulse method" in the following sections.

Measurements and data

A set of measurements was carried out on several bus lines of the Zurich public transportation network under normal operating conditions. Data were collected on electric and diesel-powered vehicles. The instrument used was a commercially available mobile phone (Samsung Galaxy S5) equipped with an application designed to read out the onboard sensors (three-axial accelerometer, gyroscope, and GPS) every 0.02 s. The instrument was manually aligned with the vehicle and held in place during travel. As the main interest of this study lies on accelerations in the primary direction of travel of the vehicle, the following analysis will be focused on the longitudinal acceleration component. A total of 6 time series of longitudinal acceleration data were obtained (the raw data are displayed in Supplementary Figures S1, S2 in the supplementary material).

Results

Splitting algorithm, Legendre analysis

Each of the time series measured was split into acceleration and deceleration events according to the splitting algorithm. As an example, the splitting of one of the time series (after Butterworth filtering) is shown in Figure 1. In total, the splitting of the normal operation datasets resulted in 99 ACC events with magnitudes up to 0.215 g and 97 DEC events. In the latter, there was one event with an exceptionally high magnitude of −0.7 g, which was caused by the erroneous handling of the measuring device. This pulse was ignored in the further analysis, resulting in 96 DEC events up to −0.279 g. Histograms of the magnitudes and durations of all events are shown in Figure 2. As a last step to prepare for the Legendre analysis, the events were normalised in time. All time-normalised events are displayed in Supplementary Figure S3 in the supplementary material.

For all events under consideration, Legendre expansion up to order $N = 10$ (i.e., 11 coefficients), $N = 50$ and $N = 200$ have been computed.

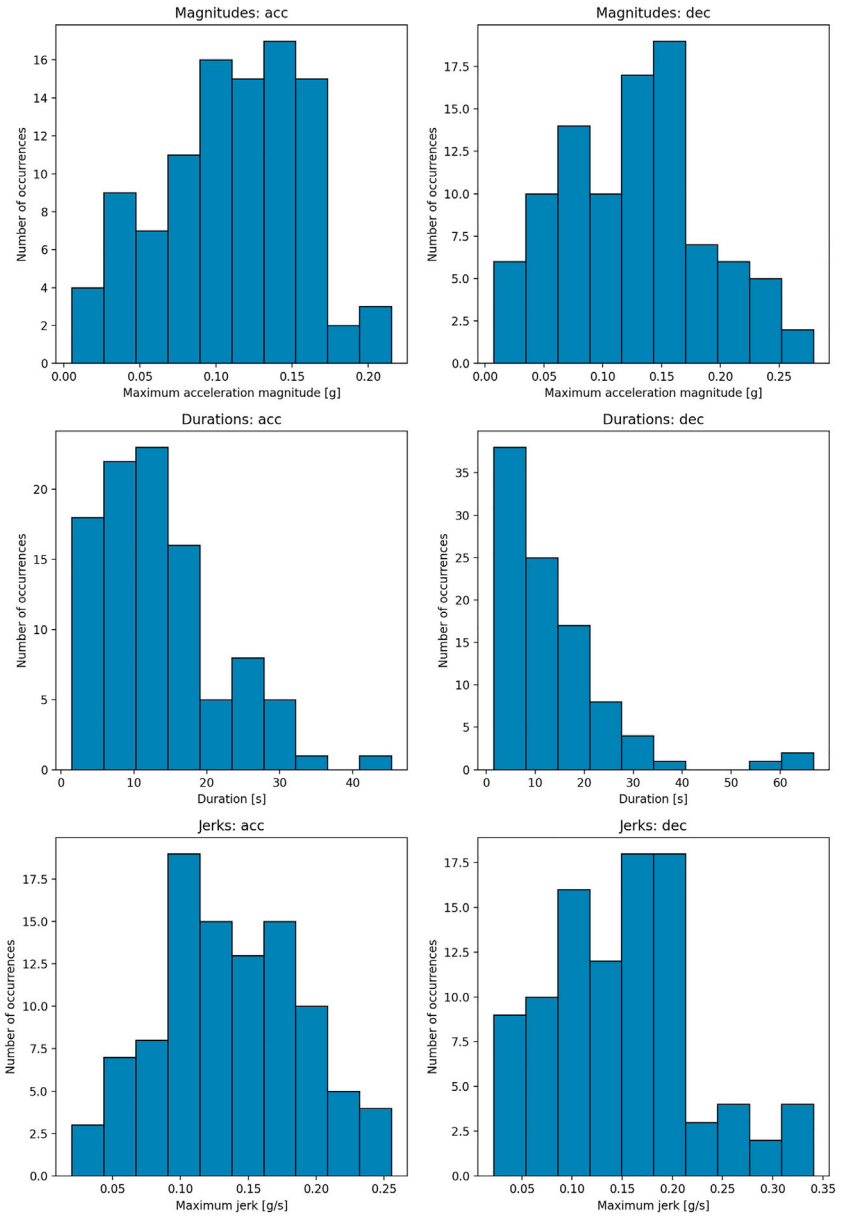

FIGURE 2
Histograms of acceleration magnitudes, peak jerk values and pulse duration for all vehicle types.

Mean pulse method and maximum similarity pulses

Both the mean pulse method (constrained and unconstrained) and the maximum similarity method were evaluated as average over all vehicle types (i.e., electric and diesel vehicles) as well as separately for the different types. Figure 3 shows the results of the three methods with all vehicles taken into account, while the results according to vehicle type can be found in the Supplementary Material. Note that the unconstrained mean pulses have been computed with coefficients up to $N = 50$, while the constrained mean pulses were obtained with a rather rather low ($N = 10$) number of coefficients. The application of the constrained method only makes sense with such a low number of coefficients; with a higher value of N, the pulses tend to converge to the unconstrained ones with a discontinuity jumping to 0 in the beginning and the end.

The maximum similarity pulses displayed in Figure 3 have been measured on electric vehicles. They do not only represent the pulses of maximum mean similarity overall, but also within the category "electric vehicles."

As pointed out in the Methods section, the mean pulse methods are only defined up to a constant scaling factor. In the results shown, the scaling was chosen in a way to scale the peak acceleration according to the arithmetic mean of the peak acceleration of the set of pulses under consideration.

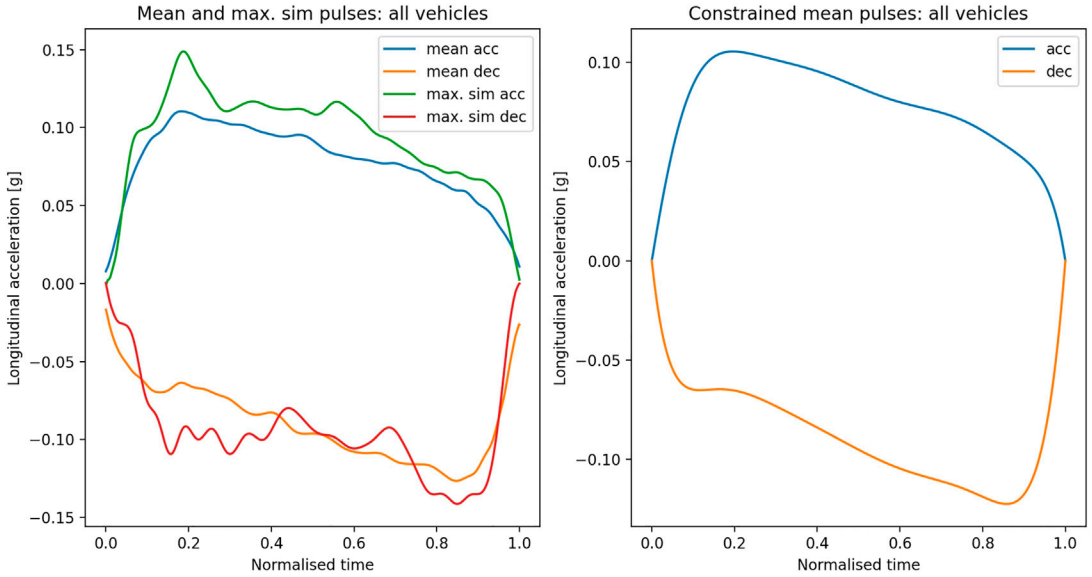

FIGURE 3
Average acceleration and deceleration pulses. Left: computed according to the "unconstrained mean pulse method" (coefficients up to order $N = 50$) and the "maximum similarity method." Right: computed according to "constrained mean pulse method" (coefficients up to $N = 10$). All vehicle types.

TABLE 1 Mean similarity coefficients of the average pulses according to maximum similarity (ms) and mean pulse (mp) method.

Pulse method, direction	Mean similarity coefficient
mp acc	0.826
ms acc	0.821
mp dec	0.791
ms dec	0.776

Similarity coefficients

While similarity analysis is not the primary focus of this work, sets of similarity coefficients enable the comparison of the performance of the mean pulse and maximum similarity pulse methods. The mean similarity coefficients of the average pulses according to the unconstrained mean pulse method and the maximum similarity method with the full set of ACC and DEC pulses, respectively, are given in Table 1. Furthermore, an evaluation of the similarity coefficients between the mean pulse and the maximum similarity pulse yields 0.9958 (ACC) and 0.984 (DEC). These results have been obtained as averages over all vehicle types.

Jerk estimate

For each of the events under consideration, the Legendre coefficients of the jerk time series have been evaluated based on a Legendre representation with 200 coefficients. As an example, the jerk with respect to normalised time is shown for the maximum similarity and (unconstrained) mean pulses in Figure 4. Furthermore, the distribution of the peak jerk values (with respect to time) is presented in Figure 2 for all vehicle types and in Supplementary Figure S7 in the supplementary material separately for the different vehicle types.

Discussion

In non-collision incidents involving public transportation vehicles, standing passengers are often subjected to balance perturbations due to the acceleration and deceleration of the vehicle. The balance recovery and mitigation of possible injury depend on the perturbation pulse properties, as presented in biomechanical studies (Karekla and Tyler, 2018; Krašna et al., 2021). However, typical bus acceleration and deceleration pulses are difficult to replicate in a laboratory setup. Therefore, for research on the safety of standing passengers, it is essential that the main features of the acceleration and deceleration pulses are properly described. Nevertheless, the research on this topic is scarce compared to research and literature on the safety of, e.g., seated passengers in cars. Kirchner et al. (2014) presented a method of extraction of the pulse characteristics based on Legendre polynomial expansion, which can be considered the current standard and which the method presented here has to be compared to.

Splitting and Lagrange representation

As shown in Figure 1, by using the splitting algorithm, the larger spikes in acceleration and deceleration are consistently detected even though at some points, the trained eye would probably have subdivided some events into several ACC and DEC pulses during manual splitting. This is also apparent from the unequal number of ACC and DEC pulses. However, the more regularly shaped events in the test drive dataset are clearly recognised by the splitting algorithm.

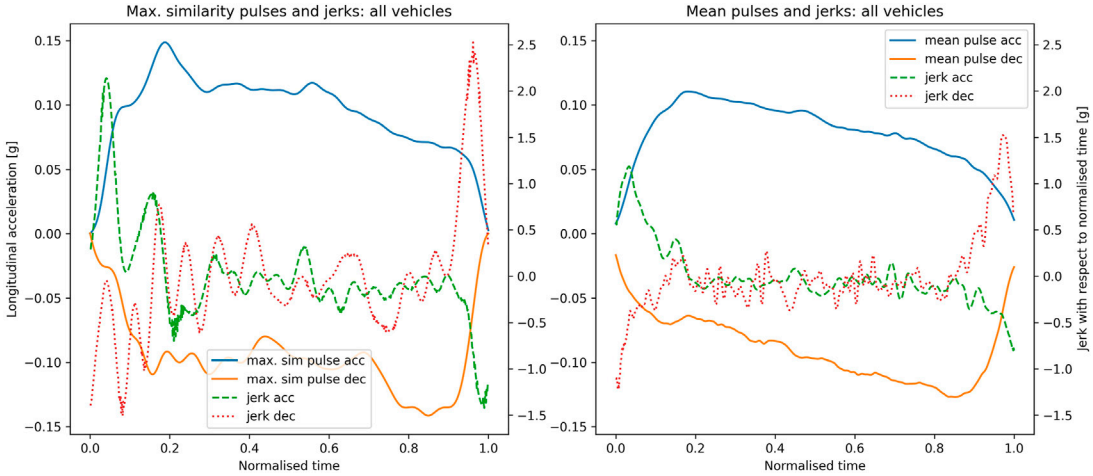

FIGURE 4
Jerk estimates for maximum similarity pulses (left) and unconstrained mean pulses (right), with coefficients up to N = 200 for all vehicle types.

It is clear that manual splitting, as in Kirchner et al. (2014), would improve the quality of pulse splitting in difficult cases. However, an automatic splitting is required as soon as the datasets increase in size. Manual splitting is also used to remove subjective estimates from the analysis. Therefore, we consider it important to develop the splitting algorithm further.

The Legendre representations generally deliver excellent fits of the time-normalised ACC and DEC pulses. With coefficients up to order $N = 50$ evaluated, an excellent agreement (mean adjusted $R^2 = 0.9987$) is reached, while the fits with 11 coefficients reach approximately $R^2 = 0.95$. It is dependent upon the application whether a higher accuracy of the fits or a lower number of coefficients is desirable.

Maximum similarity vs mean pulse method

Both the maximum similarity method and the (un)constrained mean pulse method aim at extracting a representative example or average from a number of events with different magnitudes without being dominated by the events with the highest magnitude. The maximum similarity method has been suggested by Kirchner et al. (2014) and can be considered the quasi-standard so far to derive test pulses for laboratory and numerical tests of the postural balance of standing passengers.

The mean pulse method yielded acceleration pulse of average magnitude 0.11 g and deceleration magnitude 0.13 g, while the maximum similarity method resulted in higher pulse magnitudes (Figure 2; Figure 3). This is comparable to the results reported by Kirchner et al. (2014) and Palacio et al. (2009) based on the measured data obtained in a similar setup during regular operation of a city bus, as well as the typical values presented by Kuhn (2013), 0.08–0.11 g for average acceleration and 0.12–0.15 g for deceleration. The peak values occurred at the beginning of the acceleration pulse and at the end of the deceleration pulse, in accordance with experimental observations (Schubert et al., 2017). The peak values of the jerk were 1.0 g/s for acceleration pulse and 1.5 g/s for deceleration pulse in the mean pulse method, while higher values and more noise was observed in the maximum similarity method (Figure 2; Figure 4). Therefore, it can be stated that the mean pulse method captures the key characteristics of the acceleration/deceleration pulses that may be used for representation of balance perturbations for the standing passengers.

Direct comparison of the unconstrained mean pulse and maximum similarity results (Figure 3) shows that the results are surprisingly similar; an observation, which is confirmed by the mutual similarity coefficients >0.993. Both methods manage to capture typical features of acceleration and deceleration pulses, such as a strong rise in the beginning followed by a slower decrease and a drop in the end. Also the constrained mean pulses show the typical features, even though in a less detailed way due to the lower order N of the Legendre expansion. The mean similarities of the mean pulse results with the underlying sets are slightly higher than those of the maximums similarity pulses (see Table 1), which reflects the fact that the mean pulse method is based on an optimisation of mean similarity coefficients.

While the maximum similarity method selects one element of the underlying set of pulses, the mean pulse method, when applied to a larger set, converges to a result which 1) is not very sensitive to addition or removal of single pulse from the underlying set and 2) levels out random features of the pulses of the set (average property). Hence, the resulting mean pulses are much smoother than the maximum similarity pulses.

The goal of the mean pulse method is to define test pulses to study the postural balance of standing passengers in presence of acceleration perturbations based on acceleration data sets measured in public transport vehicles. The generation of such test pulses can be done either by applying the mean pulse results directly as test pulses, or by scaling their magnitude to a lower and upper bound to define corridors for the test pulse. In both cases, the convergence and average property of the mean pulse method is an advantage, as similar sets of measured pulses result in similar mean pulses which, furthermore, can be scaled in a meaningful way.

It could be argued that the smoothness of the mean pulses actually is a disadvantage when applied as test pulses for the standing passenger problem, as it could lead to less severe test conditions compared to the spikes and random oscillations observed in the measured acceleration pulses (and, therefore, also in the maximum

similarity pulses). Indeed, from the distribution of jerk over time in Figure 4, it is apparent that the maximum similarity pulses do come with higher peak accelerations and jerks. However, the peak values appear at roughly similar times (the peak in the absolute value of the acceleration appears after the first rise, while positive and negative peak jerks appear in the first rise or the last drop). Given that peak jerks and peak accelerations together with the points in time when they appear are the relevant quantities for the severity of an acceleration perturbation to standing passengers (Krašna et al., 2021), the severity of the maximum similarity pulse seems not to be due to the random peaks and oscillations, but rather due to features which are also present in the mean pulses. Therefore, the mean pulses, scaled in time and magnitude to the desired severity, likely provide sufficiently realistic and convenient input to numerical or physical tests, given the advantages discussed above.

Conclusion

In this study, a novel method is presented to define representative average shapes of acceleration and deceleration pulses of public transport vehicles based on measured acceleration time series. This method consists of a combination of automated splitting, Legendre polynomial fits, similarity coefficients and a weighted-mean approach to capture the average shapes without being dominated by events of large magnitude. To test the method and present some pulse shapes as first results, a dataset collected on buses in normal operation was considered, allowing a comparison of the new mean pulse method and the (established) maximum similarity method.

The results show that the proposed method is capable of automatically extracting meaningful representative averages out of the datasets, which due to the weighting are not dominated by the events of the strongest magnitude. Due to the average properties of the method, the mean pulses are free of the random oscillations typically occurring when choosing a representative example out of the set. The proposed method enables the generation of well-defined representative acceleration/deceleration pulses while taking into account the real-life perturbation characteristics observed in field data. The perturbation pulses obtained with the mean pulse method can be applied as scalable test pulses, e.g., in sled experiments with volunteer participants assessing the safety and reaction of standing passengers subject to acceleration/deceleration perturbations. Furthermore, due to the automated splitting algorithm, the method can be applied also to larger datasets and mean pulses representative of more exhaustive data can be generated in a straightforward way.

The newly emerging finite element human body models capable of replicating standing passengers will likely offer a particularly interesting application of the mean pulse method: with these models, also higher severity perturbations with increased injury risk can be tested. The test pulses for these can be obtained from the mean pulse method, either by scaling the existig pulses or by applying it to field data sets containing emergency driving manoeuvres.

Data availability statement

The datasets presented in this study can be found in online repositories. The names of the repository/repositories and accession number(s) can be found below: OpenVT platform: https://openvt.eu/Acceleration_data_and_tools.

Author contributions

AK developed the concept of the average pulse method and contributed to the data analysis. SK contributed to the data analysis. Both authors contributed equally to writing the article.

Funding

This work has been created as part of project VIRTUAL and has received funding from the European Union's Horizon 2020 research and innovation programme under grant agreement No 768960.

Acknowledgments

The authors would like to thank Jakob Gross (AGU Zürich) for carrying out the measurements of bus accelerations and Markus Muser and Kai-Uwe Schmitt (both AGU Zürich) for helpful discussions and ideas. Furthermore, we would like to thank two reviewers for constructive comments and valuable input.

Conflict of interest

AK was employed by AGU Zürich.

The remaining author declares that the research was conducted in the absence of any commercial or financial relationships that could be construed as a potential conflict of interest.

Publisher's note

Supplementary material

The Supplementary Material for this article can be found online at: https://www.frontiersin.org/articles/10.3389/ffutr.2023.931780/full#supplementary-material

References

Aftab, Z., Robert, T., and Wieber, P.-B. (2016). Balance recovery prediction with multiple strategies for standing humans. *PLOS ONE* 11, 1–16. doi:10.1371/journal.pone.0151166

Brooks, B., Edwards, H., Fraser, C., Levis, J., and Johnson, M. (1978). "Passenger problems on moving buses," in Mobility for the Elderly and the Handicapped. The

International Conference on Transport for the Elderly and Handicapped. Loughborough University of Technology Florida State University, Tallahassee.

Carpenter, M. G., Thorstensson, A., and Cresswell, A. G. (2005). Deceleration affects anticipatory and reactive components of triggered postural responses. *Exp. brain Res.* 167, 433–445. doi:10.1007/s00221-005-0049-3

Elvik, R. (2019). Risk of non-collision injuries to public transport passengers: Synthesis of evidence from eleven studies. *J. Transp. Health* 13, 128–136. doi:10.1016/j.jth.2019.03.017

European Commission (2022). *Annual statistical report on road safety in the EU, 2021 (European road safety observatory. Brussels, European commission, directorate general for transport).*

Graaf, B. D., and Van Weperen, W. (1997). The retention of blance: An exploratory study into the limits of acceleration the human body can withstand without losing equilibrium. *Hum. factors* 39, 111–118. doi:10.1518/001872097778940614

Hale, N., and Townsend, A. (2016). A fast FFT-based discrete Legendre transform. *IMA J. Numer. Analysis* 36, 1670–1684. doi:10.1093/imanum/drv060

Halpern, P., Siebzehner, M., Aladgem, D., Sorkine, P., and Bechar, R. (2005). Non-collision injuries in public buses: A national survey of a neglected problem. *Emerg. Med. J.* 22, 108–110. doi:10.1136/emj.2003.013128

Hoberock, L. L. (1977). A survey of longitudinal acceleration comfort studies in ground transportation vehicles. *J. Dyn. Syst. Meas. Control* 99, 76–84. doi:10.1115/1.3427093

Karekla, X., and Tyler, N. (2018). Reducing non-collision injuries aboard buses: Passenger balance whilst walking on the lower deck. *Saf. Sci.* 105, 128–133. doi:10.1016/j.ssci.2018.01.021

Kendrick, D., Drummond, A., Logan, P., Barnes, J., and Worthington, E. (2015). Systematic review of the epidemiology of non-collision injuries occurring to older people during use of public buses in high income countries. *J. Transp. Health* 2, 394–405. doi:10.1016/j.jth.2015.06.002

Kirchner, M., Schubert, P., and Haas, C. T. (2014). Characterisation of real-world bus acceleration and deceleration signals. *J. Signal Inf. Process.* 5, 8–13. doi:10.4236/jsip.2014.51002

Kirk, A., Grant, R., and Bird, R. (2003). "Passenger casualties in non-collision incidents on buses and coaches in great Britain," in Proceedings of the 18th International Technical Conference on the Enhanced Safety of Vehicles, May 2003 (Nagoya, Japan), 19–22. Available at: https://www-nrd.nhtsa.dot.gov/departments/esv/18th/

Krašna, S., Keller, A., Linder, A., Silvano, A. P., Xu, J.-C., Thomson, R., et al. (2021). Human response to longitudinal perturbations of standing passengers on public transport during regular operation. *Front. Bioeng. Biotechnol.* 9, 680883. doi:10.3389/fbioe.2021.680883

Kuhn, W. (2013). *Fundamentals of road design.* Southampton, United Kingdom: WIT Press.

Li, D., Zhao, Y., Bai, Q., Zhou, B., and Ling, H. (2017). Analyzing injury severity of bus passengers with different movements. *Traffic Inj. Prev.* 18, 528–532. doi:10.1080/15389588.2016.1262950

Lu, S., Naumova, V., and Pereverzev, S. V. (2013). Legendre polynomials as a recommended basis for numerical differentiation in the presence of stochastic white noise. *J. Inverse Ill-posed Problems* 21, 193–216. doi:10.1515/jip-2012-0050

McKinney, W. (2010). "Data structures for statistical computing in python," in *Proceedings of the 9th Python in science conference*. Editors S. van der Walt and J. Millman, 51–56.

Morency, P., Strauss, J., Pépin, F., Tessier, F., and Grondines, J. (2018). Traveling by bus instead of car on urban major roads: Safety benefits for vehicle occupants, pedestrians, and cyclists. *J. urban health* 95, 196–207. doi:10.1007/s11524-017-0222-6

Palacio, A., Tamburro, G., O'Neill, D., and Simms, C. K. (2009). Non-collision injuries in urban buses—Strategies for prevention. *Accid. Analysis Prev.* 41, 1–9. doi:10.1016/j.aap.2008.08.016

Paton, K. (1975). Picture description using Legendre polynomials. *Comput. Graph. Image Process.* 4, 40–54. doi:10.1016/0146-664x(75)90020-9

Phillips, T. N. (1988). On the Legendre coefficients of a general-order derivative of an infinitely differentiable function. *IMA J. Numer. Analysis* 8, 455–459. doi:10.1093/imanum/8.4.455

Powell, J., and Palacín, R. (2015). Passenger stability within moving railway vehicles: Limits on maximum longitudinal acceleration. *Urban Rail Transit* 1, 95–103. doi:10.1007/s40864-015-0012-y

Robert, T., Beillas, P., Maupas, A., and Verriest, J.-P. (2007). Conditions of possible head impacts for standing passengers in public transportation: An experimental study. *Int. J. crashworthiness* 12, 319–327. doi:10.1080/13588260701433552

Schubert, P., Liebherr, M., Kersten, S., and Haas, C. T. (2017). Biomechanical demand analysis of older passengers in a standing position during bus transport. *J. Transp. Health* 4, 226–236. doi:10.1016/j.jth.2016.12.002

Tokuno, C. D., Cresswell, A. G., Thorstensson, A., and Carpenter, M. G. (2010). Age-related changes in postural responses revealed by support-surface translations with a long acceleration–deceleration interval. *Clin. Neurophysiol.* 121, 109–117. doi:10.1016/j.clinph.2009.09.025

Turkovich, M. J., Van Roosmalen, L., Hobson, D. A., and Porach, E. A. (2011). The effect of city bus maneuvers on wheelchair movement. *J. Public Transp.* 14, 147–169. doi:10.5038/2375-0901.14.3.8

Virtanen, P., Gommers, R., Oliphant, T. E., Haberland, M., Reddy, T., Cournapeau, D., et al. (2020). SciPy 1.0: Fundamental algorithms for scientific computing in Python. *Nat. Methods* 17, 261–272. doi:10.1038/s41592-019-0686-2

Wang, H., and Xiang, S. (2012). On the convergence rates of Legendre approximation. *Math. Comput.* 81, 861–877. doi:10.1090/s0025-5718-2011-02549-4

Zaworski, J. R., Hunter-Zaworski, K., and Baldwin, M. (2007). Bus dynamics for mobility-aid securement design. *Assist. Technol.* 19, 200–209. doi:10.1080/10400435.2007.10131877

Appendix A: Derivation of pulses of maximum mean similarity (proof of Eqs 11, 14)

Pulses not constrained to 0

Let each of the time-normalised acceleration pulses f_i, $i = 1 \ldots M$, be approximated by $N + 1$ Legendre coefficients $c_{i,k}$, where $k = 0 \ldots N$. We seek to find a pulse $\bar{f}$ given by a Legendre expansion with coefficients $\bar{c}_k$, $k = 0 \ldots N$, that maximises the mean similarity coefficient

$$\bar{s}(\bar{c}_k) = \frac{1}{M}\sum_{j=1}^{M} \frac{\sum_{k=0}^{N} \frac{\bar{c}_k c_{j,k}}{2k+1}}{\sqrt{\sum_{l=0}^{N} \frac{(\bar{c}_l)^2}{2l+1} \sum_{m=0}^{N} \frac{(c_{j,m})^2}{2m+1}}}. \tag{A1}$$

To facilitate the notation, we define the normalised version of the coefficients $c_{i,k}$ as

$$\alpha_k^j = \frac{c_{i,k}}{\sqrt{\sum_{l=0}^{N} \frac{(c_{i,l})^2}{2l+1}}}, \tag{A2}$$

and in the same way the normalised version of the mean coefficients $\bar{c}_k$. This allows us to rewrite Eq. A1 as[9]

$$\bar{s}(\bar{\alpha}_k) = \frac{1}{M}\sum_{j=1}^{M}\sum_{k=0}^{N} \frac{\bar{\alpha}_k \alpha_k^j}{2k+1}. \tag{A3}$$

We need to optimise the $N + 1$ coefficients $\bar{\alpha}_k$ to find an extreme value of $\bar{s}$ while obeying the normalisation condition

$$\sum_{k=0}^{N} \frac{(\bar{\alpha}_k)^2}{2k+1} = 1, \tag{A4}$$

which assures that the resulting mean coefficients are still normalised to one. This can be achieved with the use of a Lagrange multiplier coupling the normalisation condition to Eq. A4. We thus need to find a minimum of the function

$$\bar{s}_\lambda(\bar{\alpha}_k) = \bar{s}(\bar{\alpha}_k) - \lambda \sum_{l=0}^{N} \frac{(\bar{\alpha}_l)^2}{2l+1}, \tag{A5}$$

where the Lagrange multiplier $\lambda \neq 0$ has to be determined after the optimisation in a way that the constraint is fulfilled. Then, the necessary condition for an extreme value of $\bar{s}$ constrained by the normalisation condition is

$$0 = \frac{\partial \bar{s}_\lambda}{\partial \bar{\alpha}_k} = \frac{1}{M}\sum_{j=1}^{M} \frac{\alpha_k^j}{2k+1} - 2\lambda \frac{\bar{\alpha}_k}{2k+1}, \quad k = 0 \ldots N. \tag{A6}$$

Provided that $\sum_{j=1}^{M} \alpha_k^j \neq 0$ for at least one index k, Eq. A6 is solved by the coefficients

$$\bar{\alpha}_k^\lambda = \frac{1}{2M\lambda}\sum_{j=1}^{M} \alpha_k^j, \quad k = 0 \ldots N. \tag{A7}$$

Inserting these coefficients into Eq. A4 yields two possible solutions for the Lagrange multiplier λ,

$$\lambda_\pm = \frac{\pm 1}{2M}\sqrt{\sum_{k=0}^{N} \frac{\left(\sum_{j=1}^{M} \alpha_k^j\right)^2}{2k+1}}. \tag{A8}$$

Thus, we have obtained two solutions $\bar{\alpha}_k^\pm$ to Eq. A6 for the two possible values $\lambda_\pm$. As the smooth function $\bar{s}(\bar{\alpha}_k)$ necessarily has a minimum and a maximum on the compact unit sphere with respect to the norm defined in Eq. A4, one of these solutions must be the minimum and the other one the maximum. Inserting the "+" solution into Eq. A3 yields

$$\bar{s}(\bar{\alpha}_k^+) = \frac{1}{2M^2\lambda_+}\sum_{i,j=1}^{M}\sum_{k=0}^{N} \frac{\alpha_k^i \alpha_k^j}{2k+1} = \frac{1}{2M^2\lambda_+}\sum_{k=0}^{N} \frac{\left(\sum_{i=1}^{M} \alpha_k^i\right)^2}{2k+1} > 0. \tag{A9}$$

In the same way, we obtain $\bar{s}(\bar{\alpha}_k^-) < 0$ for the "-" solution, which means that the positive solution is the maximum. The non-normalised coefficients $\bar{c}_k$ of the mean pulse given in Eq. 11 result from the normalised coefficients $\bar{\alpha}_k^+$ by re-scaling with a constant factor a_0, which absorbs the factor 2λ in Eq. A7. Given that the mean mutual similarity coefficient $\bar{s}(\bar{\alpha}_k)$ is invariant with respect to multiplication of the coefficients with a constant factor, the coefficients $\bar{c}_k$ realise the highest possible value of the mean mutual similarity coefficient.

In the case $\sum_{j=1}^{M} \alpha_k^j = 0 \;\forall\; k \in \{0, 1, \ldots, N\}$, even though the coefficients given in Eq. A7 still represent a solution of Eq. A6 for any $\lambda \neq 0$, they all equal 0, and thus, there is no possible choice of λ that would satisfy constraint (18). However, it is obvious from Eq. A3 that the function $\bar{s}(\bar{\alpha}_k)$ equals 0 everywhere, i.e., for any choice of coefficients $\bar{\alpha}_k$ or $\bar{c}_k$, normalised or non-normalised, the highest possible value 0 is assumed. Therefore, in particular, the coefficients $\bar{c}_k$ as given in Eq. 11 (which also happen to all equal 0) realise the highest possible value of the mean similarity coefficient $\bar{s}(\bar{c}_k)$, which completes the proof.

It is stressed that the second case occurs only if the set of pulses is in mean completely uncorrelated, which is highly unlikely in any context where the application of this method would be reasonable.

Pulses constrained to 0

Let the base set of pulses f_i, $i = 1, \ldots, M$, and the corresponding coefficients c_k^i, $k = 0, \ldots, N$, and normalised coefficients α_k^i be like those in the previous paragraph. We seek to derive $N + 1$ coefficients $\bar{c}_k^0$ and normalised versions $\bar{\alpha}_k^0$ which maximise the mean mutual similarity coefficient $\bar{s}(\bar{c}_k^0)$ while fulfilling the following constraints:

$$\sum_{k=0}^{N} \frac{(\bar{\alpha}_k^0)^2}{2k+1} = 1, \tag{A10}$$

$$\sum_{k=0}^{N} \bar{\alpha}_k^0 = 0, \tag{A11}$$

$$\sum_{k=0}^{N} \bar{\alpha}_k^0 (-1)^k = 0. \tag{A12}$$

While the first of these constraints is the normalisation condition, conditions (25) and (26) ensure that the corresponding pulse is zero at the ends of the considered interval,

$$0 = \bar{f}^0(0) = \sum_{k=0}^{N} \bar{c}_k^0 P_k(0) = \bar{f}^0(1) = \sum_{k=0}^{N} \bar{c}_k^0 P_k(1). \tag{A13}$$

9 Given that the similarity coefficient is invariant with respect to re-scaling the coefficients, we denote the mean similarity coefficient $\bar{s}$ with the same symbol whether it is meant as a function of the coefficient c_k or the coefficient α_k.

These three constraints can again be taken into account by using three Lagrange multipliers λ, μ, ν. We thus need to find a maximum of the function

$$\bar{s}_{\lambda\mu\nu}(\bar{\alpha}_k^0) = \bar{s}(\bar{\alpha}_k^0) - \lambda \sum_{l=0}^{N} \frac{(\bar{\alpha}_k^0)^2}{2l+1} - \mu \sum_{l=0}^{N} \bar{\alpha}_l^0 - \nu \sum_{l=0}^{N} \bar{\alpha}_l^0 (-1)^l, \tag{A14}$$

for which the necessary condition is

$$0 = \frac{\partial \bar{s}_{\lambda\mu\nu}}{\partial \bar{\alpha}_k^0} = \frac{1}{M} \sum_{j=1}^{M} \frac{\alpha_k^j}{2k+1} - 2\lambda \frac{\bar{\alpha}_k^0}{2k+1} - \mu - \nu(-1)^k, k = 0 \ldots N. \tag{A15}$$

This expression can be resolved for $\bar{\alpha}_k^0$,

$$\bar{\alpha}_k^0 = \frac{1}{2\lambda}\left[\frac{1}{M}\sum_{j=1}^{M}\alpha_k^j - (2k+1)\left(\mu + (-1)^k\nu\right)\right]. \tag{A16}$$

From this result, the Lagrange parameters have to be eliminated using the constraints (24)–(26). This is facilitated by the following definitions (assuming that $\lambda \neq 0$):

$$l = \frac{1}{2\lambda},\ m = \frac{\mu}{2\lambda},\ n = \frac{\nu}{2\lambda},\ \tilde{\alpha}_k = \frac{1}{M}\sum_{j=1}^{M}\alpha_k^j. \tag{A17}$$

Now, we can rewrite Eq. A16 as

$$\bar{\alpha}_k^0 = l\tilde{\alpha}_k - (2k+1)\left(m + (-1)^k n\right). \tag{A18}$$

Inserting this equation into the constraints (25) and (26) yields

$$0 = l\tilde{\alpha} - m\sum_{k=0}^{N}(2k+1) - n\sum_{k=0}^{N}(2k+1)(-1)^k, \tag{A19}$$

$$0 = l\tilde{\alpha} - m\sum_{k=0}^{N}(2k+1) - n\sum_{k=0}^{N}(2k+1)(-1)^k, \tag{A20}$$

$$0 = l\tilde{\beta} - m\sum_{k=0}^{N}(2k+1)(-1)^k - n\sum_{k=0}^{N}(2k+1), \tag{A21}$$

where the symmetric and anti-symmetric sums of the normalised coefficients

$$\tilde{\alpha} = \sum_{k=0}^{N}\tilde{\alpha}_k, \tag{A22}$$

$$\tilde{\beta} = \sum_{k=0}^{N}\tilde{\alpha}_k(-1)^k \tag{A23}$$

have been defined. By explicitly evaluating the finite sums in Eq. A19, A20 and A21 to

$$\sum_{k=0}^{N}(2k+1) = (N+1)^2, \tag{A24}$$

$$\sum_{k=0}^{N}(2k+1)(-1)^k = (N+1)(-1)^N, \tag{A25}$$

the system of equations can be solved for m and n:

$$m = \frac{l\tilde{\alpha}}{N(N+2)} - \frac{l(-1)^N\tilde{\beta}}{N(N+1)(N+2)}, \tag{A26}$$

$$n = \frac{-l(-1)^N\tilde{\alpha}}{N(N+1)(N+2)} + \frac{l\tilde{\beta}}{N(N+2)}. \tag{A27}$$

Given that both m and n are proportional to l, the latter appears in the result for $\bar{\alpha}_k^0$ only as a scaling factor, which allows for the normalisation of $\bar{\alpha}_k^0$. It is thus not necessary to compute l explicitly; rather, we can write the coefficients up to the scaling factor as

$$\frac{\bar{\alpha}_k^0}{l} = \tilde{\alpha}_k - \frac{(2k+1)\left(N+1-(-1)^{N+k}\right)}{N(N+1)(N+2)}\left[\tilde{\alpha} + (-1)^k\tilde{\beta}\right]. \tag{A28}$$

By replacing the expressions for $\tilde{\alpha}_k$, $\tilde{\alpha}$ and $\tilde{\beta}$ with their non-normalised counterparts $\bar{c}_k$, $\bar{c}$ and $\tilde{c}$, we obtain Eq. 14. The further argument that this value is actually a maximum for the positive choice of l works analogously to the previous paragraph. If $\bar{\alpha}_k^0 \neq 0$ for at least one k, a value for l exists that normalises the set of coefficients and it can be argued that the correlated version ($l > 0$) is the maximum (while the anti-correlated one represents the minimum). Also, the argument for the case $\bar{\alpha}_k^0 = 0\,\forall k$ applies as in the previous paragraph, which completes the proof.

frontiers | Frontiers in Future Transportation

TYPE Original Research
PUBLISHED 03 April 2023
DOI 10.3389/ffutr.2023.945599

OPEN ACCESS

EDITED BY
Robert Thomson,
Chalmers University of Technology,
Sweden

REVIEWED BY
David Kidd,
Insurance Institute for Highway Safety (IIHS), United States
Dustin Joshua Souders,
Clemson University, United States
Makoto Itoh,
University of Tsukuba, Japan

*CORRESPONDENCE
Fengwei Guo,
fengwei.guo@tugraz.at

SPECIALTY SECTION
This article was submitted to Transport Safety, a section of the journal Frontiers in Future Transportation

RECEIVED 16 May 2022
ACCEPTED 06 March 2023
PUBLISHED 03 April 2023

CITATION
Guo F, Fuchs A, Kirschbichler S, Sinz W, Tomasch E, Steffan H and Moser J (2023), Collection and classification of influence parameters for safety effectiveness of ADAS.
Front. Future Transp. 4:945599.
doi: 10.3389/ffutr.2023.945599

Collection and classification of influence parameters for safety effectiveness of ADAS

Fengwei Guo[1]*, Anton Fuchs[2], Stefan Kirschbichler[2], Wolfgang Sinz[1], Ernst Tomasch[1], Hermann Steffan[1] and Joerg Moser[1]

[1]Vehicle Safety Institute, Graz University of Technology, Graz, Austria, [2]Virtual Vehicle Research GmbH, Graz, Austria

Virtual scenario-based testing has become an acceptable method for evaluating safety effectiveness of advanced driver assistance systems (ADAS). Due to the complexity of the ADAS operating environment, the scenarios that an ADAS could face are almost infinite. Therefore, it is crucial to find critical scenarios to improve the efficiency of testing without compromising credibility. One popular method is to explore the parameterized scenario space using various intelligent search methods. Selecting parameters to parameterize the scenario space is particularly important to achieve good coverage and high efficiency. However, an extensive collection of (relevant) influence parameters is missing, which allows a thorough consideration when selecting parameters regarding specific scenarios. In addition, the general importance definition for individual influence parameters is not provided, regarding the potential influence of their variations on the safety effectiveness of ADAS, which can also be used as a reference while selecting parameters. Combining knowledge from different sources (the published literature, standardized test scenarios, accident analysis, autonomous vehicle disengagement, accident reports, and specific online surveys), this paper has summarized, in total, 94 influence parameters, given the general definitions of importance for 77 influence parameters based on cluster analysis algorithms. The list of influence parameters provides researchers and system developers a comprehensive basis for pre-selecting influence parameters for evaluating the safety effectiveness of ADAS by virtual scenario-based testing and helps check whether certain influence parameters can be a meaningful extension for the evaluation.

KEYWORDS

advanced driver assistance systems, influence parameters, scenario-based testing, safety effectiveness, cluster analysis

1 Introduction

Advanced driver assistance systems (ADAS) are designed besides other systems to make driving safer and more comfortable. To achieve effective and reliable functionality, most of the ADAS tend to become more complex systems that are sensitive to various parameters in real-world traffic. Thus, conventional validation based on only test drives is no longer realizable (Kalra and Paddock, 2016). Accordingly, scenario-based testing will be one feasible solution (Nalic, 2020) and offers advantages like raising the acceptance of customers for ADAS, reproducibility and extensible scenarios, and minimization of safety hazards during

testing (TÜV SÜD, 2021). In addition, high-fidelity simulation-based testing becomes a necessary step due to two main disadvantages of real-world testing: the extremely lengthy testing process and potential dangers (Sun et al., 2021). These facts underline the need for virtual scenario-based testing in safety certification and safety effectiveness evaluation of ADAS.

To comprehensively evaluate the potential of ADAS for accident avoidance and collision mitigation, ADAS should be tested with the entire scenario space and ideally parameterized with all influence parameters. Influence parameters are defined as parameters that describe a scenario and whose variation within that scenario could potentially affect the safety effectiveness of ADAS. The parameters can be clearly categorized using a model presented in the German research project PEGASUS. The model was designed to describe scenarios systematically with six independent layers, namely, the road level, traffic infrastructure, temporal modification of the former two layers, objects, environments, and digital information (PEGASUS METHOD, 2019). Due to the complexity of the scenarios and the generally huge number of superimposed influence parameters, the number of scenarios to be considered is virtually infinite.

Given the huge number of potential influence parameters, a possible solution could be to consider a limited number of influence parameters based on a pre-selection to develop test scenarios within a limited scenario space. Zhou and Re (2017) used relative distance, relative speed, and the relative moving direction between eGO and target vehicles in the parameterization and generation of test scenarios for an adaptive cruise control system. Ben Abdessalem et al. (2016) applied a multi-objective search to derive the most critical scenarios for a pedestrian detection vision-based system. Five parameters considered in the multi-objective search were identified through discussions with the domain expert, namely, the speed of the vehicle and the pedestrian, and the position and orientation of the pedestrian. In a research study by Chelbi et al. (2018), six influence parameters, namely, the relative distance, relative speed, temperature, humidity, weather event, and visibility, were included in the generation model of test scenarios for an autonomous emergency braking system. Similarly, values of eight demonstrative influence parameters, which are related to the kinematic status of eGO and target vehicles, were varied by Kluck et al. (2019) to create test scenarios for virtual ADAS verification and validation. Except for Chelbi et al. (2018), other researchers have focused only on the parameters related to the "objects" layer in the PEGASUS model.

Due to the strongly reduced number of influence parameters considered so far, which parameters should be additionally considered in the next step is the question. Extensive observation of every possible influence parameter is necessary. Several researchers have attempted to specify influence parameters across different categories. Different categories of influence parameters were defined and included in a scenario generation model called MaTeLo, which generates a test case for ADAS based on the Markov chain Monte Carlo method. The defined categories include weather conditions, structure of the road and the environments, behavior of the equipped vehicle, behavior of surrounding vehicles, pedestrians, and obstacles and disturbance. For each category, several examples of parameters were given (Raffaëlli et al., 2016). Gyllenhammar et al. likewise gave several examples for different categories, such as dynamic elements, connectivity, and other factors and scenarios (Gyllenhammar et al., 2020). Categorizing influence parameters in alignment with a clear scenario description structure, such as the PEGASUS model, and providing a comprehensive collection of parameters that fit into the defined categories can be an extensive observation. The parameters were all treated equally in the aforementioned research study, regardless of their potential to affect the safety effectiveness of ADAS. When determining parameters used to parameterize the scenario space, the general importance definition of each influence parameter can be a useful reference to combine with the consideration of the particular use case (specific types of ADAS and scenarios).

Based on the best knowledge of the authors, there is no list including overall potential influence parameters for ADAS safety effectiveness evaluation with corresponding general importance definitions available in the literature. Thus, an extensive collection of work of influence parameters and furthermore an importance definition for the parameters are necessary.

The purpose of this study is to provide information on a key aspect of virtual scenario-based testing, namely, scenario generation, by presenting a comprehensive list of influence parameters with general importance definitions that can be used by researchers and system developers. This list can be used in combination with a consideration of specific use cases to systematically select influence parameters for generating scenarios to evaluate the safety effectiveness of ADAS in scenario-based testing.

2 Materials and methods

2.1 Steps followed to carry out the research

1) Multiple sources were used to identify influence parameters and gather qualitative assessment information that measures the impact of these parameters on ADAS safety effectiveness.
2) Cluster analysis was applied based on features quantified from the qualitative assessment information collected to classify the identified influence parameters into different levels of importance.

2.2 Collection of influence parameters and corresponding qualitative assessment information

For an extensive collection of influence parameters, the following different sources were studied:

- Published literature
- Standardized tests
- Accident analysis
- Autonomous vehicle disengagement and accident reports
- Online surveys (expert knowledge)

The collection was carried out in two phases. First, a literature review including the published literature, standardized tests, accident analysis, autonomous vehicle disengagement, and accident reports was carried out to identify influence parameters and to obtain corresponding qualitative assessment information.

TABLE 1 Coverage of the knowledge of the 25 surveyed experts in different study fields.

	Synonym
$AD	ADAS OR (driver AND (assistant systems OR assistance)) OR ((automated OR autonomous OR intelligent OR unmanned) AND (vehicle OR driving OR car)) OR self-driving
$IP	(influence OR impact) AND (parameter OR factor)
$SG	Scenario AND (generation OR search OR definition OR creation)
$VV	Verification and validation OR (safety performance AND (test OR assessment OR evaluation))
$ODD	Operational design domain

TABLE 2 Coverage of the knowledge of the 25 surveyed experts in different study fields.

Study field	%
Car safety performance assessment	32
Accident analysis and accident reconstruction	44
Field operational test of ADAS or autonomous driving	12
Simulation of ADAS or autonomous driving	48
Research & development of ADAS or autonomous driving	48
Validation and verification of ADAS	4
Risk assessment (all vehicle types)	4
Safety and security	4

After aggregation, the identified influence parameters were summarized in a list and the qualitative assessments collected from various sources were documented appropriately. Second, the experts from relevant study fields were invited to participate in an online survey to evaluate the importance of the previously collected influence parameters regarding their impact on safety effectiveness of ADAS and to complete the list of influence parameters.

2.2.1 First phase: Literature review

The sources used in the collection of influence parameters and the corresponding methods or criteria used to identify influence parameters and extract qualitative assessment information are described in this subsection.

2.2.1.1 Published literature

A three-step literature search methodology was employed to identify relevant studies. The steps were as follows:

- Step 1: The search strings are defined as follows, where $AD, $IP, $SG, $VV, and $ODD represent the synonyms of the terms AD and ADAS, influence parameters, scenario generation, verification and validation, and operational design domain. The synonyms are listed in Table 1.

$$Search\ string = \$AD\ \mathbf{AND}\ (\$IP\ \mathbf{OR}\ \$SG\ \mathbf{OR}\ \$VV\ \mathbf{OR}\ \$ODD).$$

- Step 2: A literature search m was carried out on four electronic databases, namely, Scopus, SAE Mobilus, IEEE Xplore Digital Library, and Google Scholar, in order to include as many relevant studies as possible in the research.
- Step 3: The literature collected in Step 2 was screened to filter out studies that contain relevant information on the influence parameters. The snowballing method was applied to the filtered studies in order to identify any additional relevant studies in conjunction with a filtering process.

Thirty-one documents (Buehler and Wegener, 2005; Schmidt and Sax, 2009; Staender, 2010; Weitzel and Winner, 2013; Chen et al., 2014; Weitzel, 2014; Kurt et al., 2015; Seiniger and Gail, 2015; Wittmann et al., 2015; Zhang et al., 2015; Ben Abdessalem et al., 2016; Hasirlioglu et al., 2016; Raffaëlli et al., 2016; Doric, 2017; Hasirlioglu et al., 2017; Wittmann et al., 2017; Xia et al., 2017; Zhao et al., 2017; Zhou and Re, 2017; Chelbi et al., 2018,; Chelbi et al., 2019; Chen, 2018; Junietz et al., 2018; Kolk et al., 2018; Sander and Lubbe, 2018; Xia et al., 2018; Antona-Makoshi et al., 2019; Goodin et al., 2019; Kluck et al., 2019; Duan et al., 2020; Koné et al., 2020) were identified. From these studies, the influence parameters that meet one of the following criteria were identified and a preliminary grade (qualitative assessment) was assigned accordingly. The grades and corresponding criteria are as follows:

- "Important": The authors of the studies have identified the parameters as important or critical for the safety effectiveness of ADAS in their research or have used the parameters as a variant in ADAS testing.
- "Limitedly important": The authors considered the parameters important under certain conditions. For example, "Obvious conditions like friction coefficient are only relevant in few scenarios with strong accelerations." (Wittmann et al., 2015).
- "Mentioned": The authors have mentioned the parameters as potential influence parameters for ADAS.

2.2.1.2 Standardized tests

To identify influence parameters from standardized tests, the present test and rating protocols for ADAS from five standardized tests were reviewed. These five standardized tests are Euro NCAP (new car assessment program), U.S. NCAP, IIHS (Insurance Institute for Highway Safety), China NCAP, and JNCAP and cover four main automobile markets. The varied parameters between designed test conditions in a test scenario were identified as influence parameters and graded as important. For

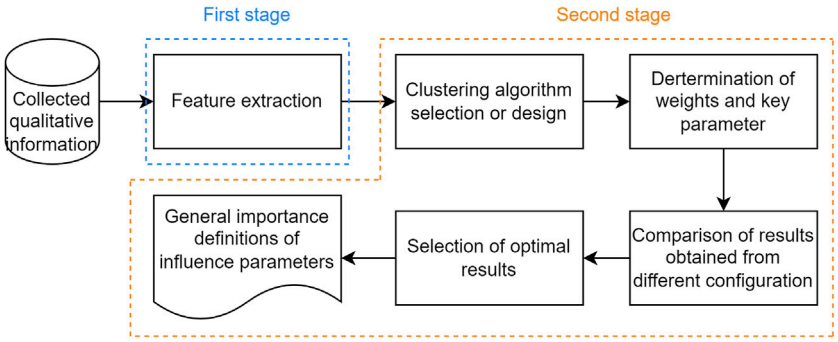

FIGURE 1
Flow diagrams of application of clustering analysis.

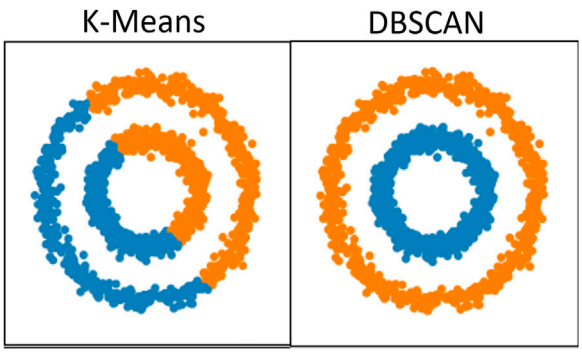

FIGURE 2
Comparison between K-means (distance-based) and DBSCAN (density-based). Reproduced from Comparing different clustering algorithms on toy datasets (2022).

example, according to Assessment Protocol–Vulnerable Road User Protection by Euro NCAP (2019), day or night, the light condition, speed of the eGO vehicle, size of the pedestrian, obstructed view, etc., are varied during the test. These factors were identified as influence parameters and rated as important.

2.2.1.3 Accident analysis

The IGLAD codebook (IGLAD, 2018) is a data scheme designed for a harmonized description of the accidents and is used to document in-depth information on accident cases provided by partners from nine countries in the database. In this codebook, 81 contributing factors, which have the main (most critical) influence on the triggering of the accident, were documented as the "main contributing factor" (IGLAD, 2018). Factors that are associated with the influence parameters previously collected from the literature and standardized tests are identified; for example, speeding is associated with the longitudinal speed of the eGO vehicle. The remaining factors were checked by the author if they are assumed to have a potential influence on the safety effectiveness of ADAS. These factors are eliminated as they are only relevant for human drivers, such as "alcohol" and "overtaking on the wrong side (undertaking)".

2.2.1.4 Autonomous vehicle disengagement and accident reports

California's Autonomous Vehicle Tester Program has allowed manufacturers to test their autonomous driving systems on public roads since 2014. Manufacturers testing vehicles in this program are required to report disengagement of the autonomous mode during testing (either because of technology failure or situations requiring the test driver/operator to take manual control of the vehicle to operate safely) and any collision that resulted in property damage and bodily injury within 10 days of the incident (California Department of Motor Vehicles, 2022). In addition, the causes of these disengagements and accidents are indicated. Favarò et al. (2017), Favarò et al. (2018), and Boggs et al. (2020) have studied these reports in detail and summarized the causes of the disengagement and the collision. Autonomous driving features, which correspond to SAE driving automation levels 3–5 (SAE On-Road Automated Vehicle Standards Committee, 2014), can be seen as an extension of ADAS features, which correspond to SAE driving automation levels 0–2. Therefore, these causes of disengagement and collision are also highly relevant to ADAS. From these research studies, the causes of disengagement and collision related to the external environment (including other road users, traffic infrastructure, and weather) were identified as influence parameters. The corresponding qualitative assessments include the cause of disengagement and cause of accidents, respectively. The other causes related to human factors (driver) and system failure were excluded.

2.2.2 Second phase: Identifying the importance of the influence parameters

In an online survey (created with Google Form (Google, 2021)), 25 experts evaluated the importance of the influence parameters collected from four sources in the first phase and their potential influence on safety effectiveness of ADAS. Invitations will be extended to experts through the networks of EVU (European Association for Accident Research and Analysis), P.E.A.R.S consortium (Wimmer et al., 2019), Virtual Vehicle Research Center, TU Graz, and TU Darmstadt. The invited experts will be required to have a minimum of 3 years of experience in the corresponding research discipline, as outlined in Table 2. The qualitative assessments include "Important," "Might be

TABLE 3 Evaluation and weight definition of features corresponding to different sources.

	Literature	Standardized test	Accident analysis	Cause of disengagement	Cause of the accident	Online survey
Comprehensive	No	No	No	Yes	Yes	Yes
Highly relevant	Yes	Yes	No	Yes	Yes	Yes
Weight	2/3	2/3	1/3	1	1	1

important," "Not important," and "Not applicable (in the case of missing knowledge of this parameter)." Additionally, the list of influence parameters was expanded by experts based on their experience. Table 2 shows the percentage of 25 participating experts who have research experience in the given study fields. The information was provided by the survey participants in a multiple-choice question. The choice includes the first five study fields listed in Table 2. The last three fields with only 4% coverage (corresponding to one expert) were added by experts. Almost half of the experts have experience in the study fields "Simulation" and "Research & Development" of ADAS or automated driving, which are relevant to the research topic of this paper.

2.3 Classification of influence parameters using cluster analysis

To generally classify the collected influence parameters into different importance levels by holistically considering the qualitative assessment information collected from different sources, a type of machine learning method called cluster analysis (Everitt, 2011) was applied. The influence parameters added by the experts in the online survey were excluded as they are not assessed by all experts. Cluster analysis is a group of methods used to distinguish a set of objects into several groups with similar characteristics (Everitt, 2011). It is an unsupervised learning method that needs neither predefinitions of the classes nor labeled training data for training the clustering model. Thus, cluster analysis is suitable to classify the collected influence parameters into different classes. The classification process includes two stages (as shown in Figure 1): feature extraction (quantization of collected qualitative assessment information) and application of the clustering algorithms (including selection of clustering algorithms, determination of weights and key parameters, comparison of clustering results, and selection of the optimal result for classification).

2.3.1 Feature extraction

The feature denotes a measurement of the importance of an influence parameter based on qualitative assessment information from a specific source and will be used as the predictors (Mathworks, 2021) in the cluster analysis. For each influence parameter, the qualitative assessment information collected from each source will be quantized as features corresponding to that source. To avoid distortion caused by different ranges of values, the extracted features are normalized (Lakshmanan, 2019). The extraction/quantization method used for each source is described as follows:

- Published literature: For a given influence parameter, an "important" or "limited important" assessment from the literature is assigned 3 points and "mentioned" 1 point. To rate the influence parameters as important or use them as varied parameters for test scenario generation, significantly higher justification efforts are required compared to mentioning them as potentially important. Therefore, to place more additional value on the "important" or "limited important" assessments, 3 points were given. The points are added and divided by the highest score of all parameters to be normalized to [0.000, 1.000].
- Standardized tests: The frequency that the influence parameter occurs in the five standardized tests will be extracted as the feature, which ranges in [0.000, 1.000]. For example, if the size of target objects will be varied in two tests (Euro NCAP and IIHS) out of the five tests, then the value is 0.400.
- Accident analysis: The feature is valued as either 1 or 0, which is a dummy variable (Eckstein et al., 1994), depending on if the influence parameter is documented in the IGLAD codebook as a main contributing factor.
- Autonomous vehicle disengagement and accident reports: Two features were extracted representing the cause of disengagement and the cause of accidents. Both features are valued using dummy variables (1 or 0), depending on if the influence parameter is the cause of the disengagement/accident.
- Online surveys: "Important" evaluation is counted as 3 points, "might be important" as 1 point, "Not applicable" as 0 points, and "not important" as −3 points. To give more weight to a clear evaluation ("important" and "not important"), which requires more reasoning efforts, than to an ambiguous evaluation ("might be important"), 3 points and −3 points were counted for "important" and "not important," respectively. The points are added and divided by the theoretical maximum total of points (75 points) to be scaled down to [−1.000, 1.000] (a minimal value of −1 occurs when all 25 experts evaluate the influence parameter as "not important" [25 (the number of experts) multiplied by −3 points and divided by 75)].

Features extracted from the published literature, standardized tests, and online survey are given by a ratio scale, and a higher value means more important. Features extracted from accident analysis and autonomous vehicle disengagement and accident reports are represented by dummy variables (1 or 0). A Boolean value of 1 (true) represents more important, while 0 (false) represents less important.

TABLE 4 Average silhouette width when using different methods and the number of clusters.

Average silhouette width		Number of clusters			
		3	4	5	6
Method	K-prototypes	0.642	0.42	0.443	0.502
	Ward	0.677	0.673	0.666	0.507

2.3.2 Application of cluster analysis

2.3.2.1 Used clustering algorithms

Considering both the assessment dimensions summarized by Wegmann et al. (2021) and our use case, the following assessment dimensions were considered to select appropriate clustering algorithms:

- Type of the dataset: In our use case, a mixed data structure is faced. The features corresponding to the source literature, standardized test, and online survey are numerical data, while those corresponding to source accident analysis and disengagement and accident reports are categorical data (dummy variables). The clustering algorithms applied should be applicable for datasets with a mixed data structure. According to our survey, the most common clustering algorithms applicable to mixed data structures are K-prototype (Huang, 1998) and algorithms based on Gower's distance (Gower, 1971).
- Shape of clusters: The goal is to classify influence parameters into different importance levels, which, in principle, is a distance-based clustering problem rather than a density-based clustering problem. Figure 2 shows the biggest difference between results achieved by applying a typical distance-based algorithm—K-means (Hartigan and Wong, 1979) and a typical density-based algorithm DBSCAN (density-based spatial clustering of applications with noise) (Ester et al., 1996). Two different colors (blue and orange) represent two clusters of objects separated by the clustering algorithm. K-means separates the objects by regions in the coordinate system, which means features of objects within the same cluster are all relatively similar, while DBSCAN separates the objects by shapes, which means that two objects with large differences in features can still be grouped into one cluster. Therefore, density-based clustering algorithms are not suitable for our application.
- Sensibility to the scale of features: Advantages of the definition of weights for features regarding their relevance and quality are shown in Chowdhury (2021). The relevance to the topic—safety effectiveness of ADAS and comprehensiveness of sources used in 2.1—also varies. Thus, the weights should also be dedicatedly defined for features corresponding to different sources. The weight can be interpreted as feature re-scaling factors (Chowdhury, 2021). The used algorithms must be sensitive to the scale of features, which means a distribution-based clustering method like the Gaussian mixed model (Sarkar et al., 2020) is not appropriate.
- Implementation: The algorithms used in this study must be implemented in existing Python packages. Specifically, the Python package used must natively support the definition of feature weights and the utilization of precomputed Gower's distance. If the package does not support these features, the required extension efforts must be reasonable.

Based on the assessment, the following clustering algorithms are determined for application.

- Ward's hierarchical clustering (Murtagh and Legendre, 2014) based on Gower's distance (Gower, 1971)
- K-prototypes (Huang, 1998)

2.3.2.2 Weight definition

As specified in section 2.2.2.1, it is necessary to define weights dedicatedly for different features. To determine the weights of features, two criteria (comprehensiveness and relevance) are used to evaluate the sources, from which features are extracted. The evaluations and determined weights are summarized in Table 3. Comprehensiveness assesses whether the sources cover all possible aspects related to safety effectiveness of ADAS so that influence parameters of certain aspects are not missed and qualitative assessments obtained are not biased. The literature research was carried out as extensively as possible. Nevertheless, completeness cannot be guaranteed. As for standardized tests, limited by the controllability of parameters like weather and light conditions, not every influence parameter is reflected in a standardized test, which leads to poor comprehensiveness. In accident analysis, main contributing factors in the IGLAD codebook are mostly summarized from accidents related to human-driven cars. Some factors that have an impact on ADAS are not summarized. These three sources are not comprehensive. The expert knowledge included in the online survey covers a wide range of relevant study fields. The influence parameter list evaluated by experts is a summarization of information from multiple sources. Disengagement and accident reports summarize the causes based on testing of autonomous vehicles on public roads, in which vehicles are exposed to real-world scenarios consisting of all possible influence parameters. These sources are comprehensive. Relevance measures the relevance of the information from the sources for the safety effectiveness of ADAS. In other words, the subject of study must be an ADAS or a subject that is functionally similar, such as an autonomous vehicle. Accident analysis is more relevant to human drivers than to ADAS, resulting in low relevance, while topics from other sources are highly relevant to the ADAS safety effectiveness. Features from sources (disengagement and accident reports, and online survey) that are both comprehensive and highly relevant were assigned the highest weight of 1. Features from sources (the literature and standardized test) that are highly relevant but not comprehensive were given the second highest weight of 2/3. The weight of the feature from the source (accident analysis) that is neither highly relevant nor comprehensive was defined as 1/3.

2.3.2.3 Key parameter definition—Number of clusters

Both methods selected in section 2.2.2.1 require defining a key parameter at implementation—the number of clusters. This key parameter determines the number of clusters to which the influence parameters can be assigned. There were already three different qualitative assessments in both the online survey and literature

TABLE 5 Influence parameters classified differently by K-prototype and Ward's hierarchical clustering (K-prototype: most important; Ward: less important).

Influence parameter	Literature	Accident analysis	Standardized test	AV* disengagement	AV* accident	Online survey
Longitudinal speed (eGO vehicle)	0.742	1	1.000	0	0	0.972
Initial position and alignment (eGO vehicle)	0.097	0	1.000	0	0	0.893
Visual obstruction	0.323	1	0.600	0	0	0.893

*AV stands for autonomous vehicle

TABLE 6 Statistical comparison between clusters with different importance levels.

	Literature	Online survey	Standardized test	AV* disengagement	AV* accident	Accident analysis
Most important	0.367	0.865	0.875	62.5	62.5	37.5
Important	0.176	0.566	0.018	100.0	0.0	22.7
Less important	0.106	0.461	0.034	0.0	0.0	8.5

*AV stands for autonomous vehicle

research; a cluster number less than 3 would not be able to classify the parameters properly. In addition, a cluster number of more than 6 would make it difficult to give the clusters a proper importance definition. The number of clusters was varied from 3 to 6, and the optimal value was chosen based on the assessment method introduced in Section 2.2.2.5.

2.3.2.4 Implementation process

The key steps to implement Ward's hierarchical clustering based on Gower's distance are as follows:

1) Calculate Gower's distance using the Python package Gower (Yan, 2019) based on extracted features with weights defined in section 2.2.2.2.
2) Apply Ward's hierarchical clustering in the Python package SciPy (SciPy, 2022) using the precomputed Gower's distance as the input.

The key steps to implement K-prototypes are as follows:

1) Extend original K-prototypes algorithms implemented in the original Python package KModes (Nelis J de Vos, 2022) to support the weight definition for features;
2) Apply the extended K-prototypes using the extracted features as the input.

2.3.2.5 Assessment of the clustering quality

To determine the best classification from the results obtained by combining different clustering methods and key parameter values, objective and subjective evaluations are combined. Subjective evaluation means that the results are examined by the authors to exclude abnormal and controversial results. The average silhouette width (ASW) was used to assess the quality of clustering objectively (Rousseeuw, 1987). Wegmann et al. (2021) denoted that the ASW works best for distance-based clustering. ASW ranges from −1 to 1. According to Sander and Lubbe (2018), ASW in different ranges can be interpreted as follows:

- [−1.000, 0.250]: No substantial structure was found.
- [0.251, 0.500]: A weak structure was found that could be artificial.
- [0.501, 0.700]: A reasonable structure was found.
- [0.701, 1.000]: A strong structure was found.

3 Results

In this section, the clustering results of the identified influence parameters were compared and examined to determine the best classification of the influence parameters. Then, the list of influence parameters including the identified influence parameters and the importance level of the parameters according to the best classification result is shown.

3.1 Result of clustering

As shown in Table 4, the best results (highest ASW) of both clustering methods were achieved when the number of clusters is 3. This suggests that it is reasonable to divide the influence parameters into three clusters. The ASW values of both methods with a defined cluster number of 3 (K-prototypes: 0.642, Ward: 0.677) also show that a reasonable structure was found according to the interpretations in section 2.2.2.5. The only difference between the results lies in three influence parameters (listed in Table 5), which are classified in the most important group by K-prototypes but in the less important group by Ward's hierarchical clustering. According to the features of the three parameters shown in Table 5, they are not supposed to be less important since features corresponding to standardized tests and online surveys are very high for all three parameters. These three parameters are not covered in the AV disengagement and accident reports. K-prototypes based on the method presented by Huang (1998) can adjust the weight of the cost associated with categorical features relative to the weight of the cost

TABLE 7 Influence parameter list with categorization and classification.

Layer	Class	Influence parameter	Sub-category
Layer 1—Road level	Important	Friction	Surface
		Road surface condition	
	Less important	Curvature	Road geometry
		Change of the curvature	
		Longitudinal slope	
		Change of the slope	
		Topology (layout)	Topology
		Road width	Road structure
		Lane width	
		Number of lanes	
		Structural separation (downtown)	
		Local change of the friction coefficient	Surface
		Heavy shadow	
		Frequent changes in the appearance of a road	
	Not classified	Intersection and the type of intersection	
		Merging lanes: junctions and crossings	
		Bank angle in a banked turn	
		Roadside (shoulder) and cross slope	
Layer 2—Traffic infrastructure	Important	Lane line clarity	Marking
		Lane line integrity	
		Structured or unstructured roads	
		Traffic light	Traffic sign
	Less important	General marking	Marking
		Lane line type	
		Lane line number	
		Lane line color	
		Speed limitation	Traffic sign
		Stop sign	
		Give way sign	
		Traffic sign visibility	
		Traffic sign position	
		Other traffic sign	
Layer 4—Objects	Most important	Visual obstruction	Stationary objects
		Longitudinal speed	eGO vehicle
		Initial position and alignment	
		Relative longitudinal distance with respect to the eGO car	Target moveable objects
		Lateral offset with respect to the eGO car	
		Relative speed with respect to the eGO car	

(Continued on following page)

TABLE 7 (*Continued*) Influence parameter list with categorization and classification.

Layer	Class	Influence parameter	Sub-category
		Relative moving direction with respect to the eGO car	
		Acceleration	
	Important	Obstacles on the road	Stationary objects
		Type	Target moveable objects
		Size	
		Type	Other moveable objects
		Size	
		Relative speed with respect to the eGO car	
		Relative longitudinal distance with respect to eGO car	
		Lateral offset with respect to the eGO car	
		Relative moving direction with respect to the eGO car	
		Acceleration	
	Less important	Roadside objects	Stationary objects
		Size	
		Position	
		Type	eGO vehicle
		Lateral speed	
		Departure direction	
		Initial departure angle	
		Acceleration	
		Turning radius	
	Not classified	Type of the stationary object	Stationary objects
		Obstacle shape	
		Is the object over-ridable or crushable?	
		Toys and sports equipment (segway, skateboard etc.)	Moveable objects
		Objects lost from other vehicles	
		Objects on the road transported by wind (bag etc.)	
		eGO/target yaw rate and the course angle	
		Did the object follow the rules or regular behavior?	
		Reflexion properties with respect to different sensors	
		Color of objects	
Layer 5—Environment	Important	Rain	Weather
		Fog	
		Snow/ice	
		Visibility	
		Sun	
		Sand, salt, or dust in the air	
	Less important	Cloudy	Weather

(Continued on following page)

TABLE 7 (*Continued*) Influence parameter list with categorization and classification.

Layer	Class	Influence parameter	Sub-category
		Temperature	
		Wind	
		Humidity	
		Streetlight	Lighting
		Position of the un and light	
		Brightness	
		Daytime	
		Light change	
		Site (urban, highway etc.)	Site
		Traffic flow density	Traffic
		Speed	
		Congestion	
		False-positive disturbance	Other disturbance
		Other radars	
		Infrared sources	
	Not classified	Rain droplet size	
		Snow intensity	
Layer 6—Digital information		GPS signal (e.g., tunnel)	

associated with numerical features. The costs associated with categorical features were lowered during clustering. This resulted in the different clustering result of the three parameters listed in Table 5. The clustering result obtained by applying K-prototypes with a cluster number of three was accepted.

According to the result of clustering, the influence parameters were divided into three different importance levels, namely, most important, important, and less important. These importance levels are relative concepts, and less important does not mean unimportant. The means of numerical features extracted from the literature, online survey, and the percentage of a value of 1 (true) of categorical features corresponding to autonomous vehicle disengagement and accident reports and accident analysis are shown in Table 6 for clusters with different importance levels. The difference in means and percentages between clusters with different importance levels proves the plausibility of the classification.

3.2 Influence parameter list

In total, 94 influence parameters were collected and are listed in Table 7. To be consistent with other researchers on the topic of "scenario description," the six-layer model presented in the German research project PEGASUS (PEGASUS METHOD, 2019) was used. The influence parameters were assigned to these layers (column "Layer" in Table 7) except for layer 3—temporal modification. Layer 3 describes only the temporal change of influence parameters included in layers 1 and 2. The column "Sub-cat" indicates a subcategory to which the parameter belongs, to allow deeper categorization and definition that are more precise. A total of 77 influence parameters were identified or summarized from the published literature, IGLAD codebook, and five standardized tests. In total, 17 parameters were supplemented by experts through the online surveys and are tagged as "not classified" in the column "Class." The column "Class" implies the importance of influence parameters for ADAS safety effectiveness evaluation based on the clustering result accepted in section 3.1. There are, in total, four different definitions in column "Class": "Most important," "Important," "Less important," and "not classified." In total, 77 of the 94 influence parameters were divided into the first three classes. In particular, eight parameters in the "most important" class and 22 parameters in the "important" class are of particular interest. The 17 parameters in the "not classified" class should also be noted as they were added by survey experts, indicating that they were kept in mind by the experts. It should be noted that the importance definition given for the influence parameters is a general definition where different ADAS are treated as a whole. In particular use cases, the characteristics of specific ADAS types (e.g., systems based on different sensors and systems designed for different purposes, etc.) and scenarios (e.g. highway scenarios, urban scenarios, etc.) should be considered in combination with the general importance definition.

4 Conclusion

4.1 Key findings

By combining information from different sources including the published literature, accident analysis knowledge, standardized tests, autonomous vehicle disengagement, and accident reports and expert knowledge from online surveys, an extensive list of 94 influence parameters has been collected and structured according to a six-layer scenario description model defined by PEGASUS (PEGASUS METHOD, 2019). In addition to the 17 influence parameters added by experts through the online survey, 77 of the 94 influence parameters were generally classified into three different levels of importance (most important, important, and less important) using K-prototype clustering based on weighted features extracted from various sources mentioned previously. Among them, the eight most important influence parameters (ego vehicle: longitudinal speed, initial position, and alignment; target moveable objects: relative longitudinal distance with respect to the eGO car, lateral offset with respect to the eGO car, relative speed with respect to the eGO car, relative moving direction with respect to the eGO car, and acceleration; and stationary objects: visual obstruction) and 22 important influence parameters (listed in Table 7) are especially worthy of attention. The list of influence parameters allows researchers and system developers to select influence parameters for the generation of scenarios in virtual scenario-based testing from a comprehensive point of view.

4.2 Limitations and outlooks

There are three main directions to improve the result of this paper.

- This paper focuses on ADAS features rather than autonomous driving features as ADAS features have a significantly higher market penetration than autonomous driving features. Adequate information on ADAS features can be obtained from all presented sources and will be analyzed comprehensively, e.g., standardized tests are currently only developed and performed for ADAS features. Autonomous driving features are expected to play a bigger role in the future of transportation. A similar methodology can be applied specially to autonomous driving features, which are likely to be more complex in terms of application scenarios, available functionality, and system architecture.
- The ADAS features are constantly being improved and expanded. The influence parameters should also be further supplemented and updated to match the development trend of ADAS for the completeness of the list of influence parameters. It should also be considered and discussed whether driver behavior should be included in the description of the scenarios and whether driver-related parameters should be included in the list of influencing parameters.
- In this paper, importance levels of influence parameters are determined by analyzing information synthesized from various sources in a general context. To obtain more specific and validated definitions of the importance level, the influence parameters can be examined for specific types of ADAS in specific types of scenarios using simulation in which the influence of the variation of influence parameters on the safety effectiveness of ADAS can be quantitatively observed and evaluated. It is important to note that the effects of variations of influence parameters should be accurately reflected in the used simulators.

Data availability statement

The raw data supporting the conclusion of this article will be made available by the authors, without undue reservation.

Author contributions

FG, AF, SK, WS, ET, HS, and JM contributed to the conception and design of the study and execution of the online survey. FG, JM, and ET contributed to the perfection and finalization of the influence parameter list. FG contributed to meta-analysis, cluster analysis. FG wrote the first draft of the manuscript. All authors contributed to manuscript revision and improvement, and read and approved the submitted version.

Funding

This work is supported by Virtual Vehicle Research GmbH under the project IMPACT. The authors would like to acknowledge the financial support within the COMET K2 Competence Centers for Excellent Technologies from the Austrian Federal Ministry for Climate Action (BMK), the Austrian Federal Ministry for Labour and Economy (BMAW), the Province of Styria (Dept. 12), and the Styrian Business Promotion Agency (SFG). The Austrian Research Promotion Agency (FFG) has been authorized for the program management. The publication fee is supported by the TU Graz Open Access Publishing Fund. The funders were not involved in the study design, collection, analysis, interpretation of data, the writing of this article, or the decision to submit it for publication.

Conflict of interest

Authors AF and SK are employed by Virtual Vehicle Research GmbH.

The remaining authors declare that the research was conducted in the absence of any commercial or financial relationships that could be construed as a potential conflict of interest.

Publisher's note

References

Antona-Makoshi, J., Uchida, N., Kitahara, E., Ozawa, K., and Taniguchi, S. (2019). "Development of A Safety assurance process for automated driving systems," in *26th ITS world congress* (Singapore, 21–25.

Ben Abdessalem, R., Nejati, S., Briand, L. C., and Stifter, T. (2016). "Testing advanced driver assistance systems using multi-objective search and neural networks," in *Proceedings of the 31st IEEE/ACM international conference on automated software engineering - ASE 2016. Singapore, Singapore* (New York, New York, USA: ACM Press), 63–74. 03.09.2016 - 07.09.2016. doi:10.1145/2970276.2970311

Boggs, A. M., Arvin, R., and Khattak, A. J. (2020). Exploring the who, what, when, where, and why of automated vehicle disengagements. *Accid. analysis Prev.* 136, 105406. doi:10.1016/j.aap.2019.105406

Buehler, O., and Wegener, J. (2005). Evolutionary functional testing of a vehicle brake assistant system. in *6th metaheuristics international conference* (Vienna, Austria).

California Department of Motor Vehicles (2022). *Autonomous vehicles*. [Online]. Available at: https://www.dmv.ca.gov/portal/vehicle-industry-services/autonomous-vehicles/ (Accessed May 2, 2022).

Chelbi, N. E., Gingras, D., and Sauvageau, C. (2019). "New field operational tests sampling strategy based on metropolis-hastings algorithm," in *Intelligent systems and applications*. Editors K. Arai, S. Kapoor, and R. Bhatia (Cham: Springer International Publishing), 1285–1302. doi:10.1007/978-3-030-01054-6_90

Chelbi, N. E., Gingras, D., and Sauvageau, C. (2018). Proposal of a new virtual evaluation approach of preventive safety applications and advanced driver assistance functions – application: AEB system. *IET Intell. Transp. Syst.* 12 (9), 1148–1156. doi:10.1049/iet-its.2018.5269

Chen, M., Andreas, K., Martin, P., and Klaus, D. (2018). *Taming functional deficiencies of automated driving systems: A methodology framework toward safety validation: 26-30*. Piscataway, NJ: IEEE. doi:10.1109/IVS.2018.8500679

Chen, Q., Chen, Y., Bostrom, O., Ma, Y., and Liu, E. (2014). *A comparison study of car-to-pedestrian and car-to-E-bike accidents: Data source: The China in-depth accident study (CIDAS)*. Warrendale, PA, United States: SAE International400 Commonwealth Drive. *SAE Technical Paper Series,* APR. 08, 2014. doi:10.4271/2014-01-0519

Chowdhury, S. (2021). *Learning feature weights for density-based clustering*. Dissertation, Hertfordshire, University of Hertfordshire.

Comparing different clustering algorithms on toy datasets (2022). *Comparing different clustering algorithms on toy datasets*. [Online]. Available at: https://scikit-learn.org/stable/auto_examples/cluster/plot_cluster_comparison.html (Accessed May 1, 2022).

Doric, I. (2017). *A generalised approach to active pedestrian safety testing*. Warwick: Doctoral dissertation, University of Warwick.

Duan, J., Gao, F., and He, Y. (2020). *Test scenario generation and optimization technology for intelligent driving systems*. IEEE Intelligent Transportation Systems Magazine, 1. doi:10.1109/MITS.2019.2926269

Eckstein, P., Götze, W., Hartl, F., Rönz, B., and Strohe, H. G. (1994). *Lexikon statistik*. Wiesbaden: Gabler Verlag. doi:10.1007/978-3-322-91144-5

Ester, M., Kriegel, H.-P., Sander, J., and Xu, X. (1996). *A density-based algorithm for discovering clusters in large spatial databases with noise*.

Euro, N. (2019). *Assessment protocol – vulnerable road user protection*.

Everitt, B. (2011). *Cluster analysis*. 5th edn. Chichester, West Sussex, U.K.: Wiley.

Favarò, F., Eurich, S., and Nader, N. (2018). Autonomous vehicles' disengagements: Trends, triggers, and regulatory limitations. *Accid. analysis Prev.* 110, 136–148. doi:10.1016/j.aap.2017.11.001

Favarò, F. M., Nader, N., Eurich, S. O., Tripp, M., and Varadaraju, N. (2017). Examining accident reports involving autonomous vehicles in California. *PloS one* 12 (9), e0184952. doi:10.1371/journal.pone.0184952

Goodin, C., Carruth, D., Doude, M., and Hudson, C. (2019). Predicting the influence of rain on LIDAR in ADAS. *Electronics* 8 (1), 89. doi:10.3390/electronics8010089

Google (2021). *Forms*. [Online]. Available at: https://www.google.com/forms/about/ (Accessed, 2021).

Gower, J. C. (1971). A general coefficient of similarity and some of its properties. *Biometrics* 27 (4), 857. doi:10.2307/2528823

Hartigan, J. A., and Wong, M. A. (1979). Algorithm as 136: A K-means clustering algorithm. *Appl. Stat.* 28 (1), 100. doi:10.2307/2346830

Hasirlioglu, S., Doric, I., Kamann, A., and Riener, A. (2017). *Reproducible fog simulation for testing automotive surround sensors'*, 2017 IEEE 85th vehicular technology conference (Sydney, NSW; VTC Spring). 04.06.2017 - 07.06.2017, IEEE, 1–7. doi:10.1109/VTCSpring.2017.8108566

Hasirlioglu, S., Doric, I., Lauerer, C., and Brandmeier, T. (2016). "Modeling and simulation of rain for the test of automotive sensor systems," in *2016 IEEE intelligent vehicles symposium (IV). Gotenburg* (Sweden: IEEE), 286–291. 19.06.2016 - 22.06.2016. doi:10.1109/IVS.2016.7535399

Huang, Z. (1998). Extensions to the k-means algorithm for clustering large data sets with categorical values. *Data Min. Knowl. Discov.* 2 (3), 283–304. doi:10.1023/A:1009769707641

IGLAD (2018). *Codebook: Member year 2018*.

Junietz, P., Bonakdar, F., Klamann, B., and Winner, H. (2018). "Criticality metric for the safety validation of automated driving using model predictive trajectory optimization," in *2018 21st international conference on intelligent transportation systems (ITSC)* (Maui, HI: IEEE), 60–65. 04.11.2018 - 07.11.2018. doi:10.1109/ITSC.2018.8569326

Kalra, N., and Paddock, S. M. (2016). Driving to safety: How many miles of driving would it take to demonstrate autonomous vehicle reliability? *'*, Transp. Res. Part A Policy Pract. 94 (4), 182–193. doi:10.1016/j.tra.2016.09.010

Kluck, F., Zimmermann, M., Wotawa, F., and Nica, M. (2019). "Genetic algorithm-based test parameter optimization for ADAS system testing," in *2019 IEEE 19th international conference 22.07.2019*, 418–425. doi:10.1109/QRS.2019.00058

Kolk, H., Tomasch, E., Haberl, M., and Fellenndorf, M. (2018). " crash-simulation," in *8th international conference on ESAR*. Hannover: Expert Symposium on Accident Research.

Koné, T. F., Bonjour, E., Levrat, E., Mayer, F., and Géronimi, S. (2020). "Safety demonstration of autonomous vehicles: A review and future research questions," in *Complex systems design & management*. Editors G. A. Boy, A. Guegan, D. Krob, and V. Vion (Cham: Springer International Publishing), 176–188. doi:10.1007/978-3-030-34843-4_15

Kurt, A., Özbilgin, G., Redmill, K. A., Sherony, R., and Özgüner, Ü. (2015). "Test scenarios, equipment and testing process for LDW LDP performance evaluation," in *SAE technical paper series* (Warrendale, PA, United States: SAE International400 Commonwealth Drive). doi:10.4271/2015-01-1404

Lakshmanan, S. (2019). *Data science: How, when, and why should you normalize/standardize/rescale your data?* [Online]. Available at: https://towardsai.net/p/data-science/how-when-and-why-should-you-normalize-standardize-rescale-your-data-3f083def38ff.

Mathworks (Editor) (2021). *k-Means Clustering*. [Online]. Available at: https://www.mathworks.com/help/stats/k-means-clustering.html.

Murtagh, F., and Legendre, P. (2014). Ward's hierarchical clustering method: Clustering criterion and agglomerative algorithm. *J. Classif.* 31 (3), 274–295. doi:10.1007/s00357-014-9161-z

Nalic, D., Tomislav, M., Maximilian, B., Matthias, L., Arno, E., and Stefan, B. (2020). *Scenario based testing of automated driving systems: A literature survey*. Prague: FISITA Web Congress.

J de Vos, Nelis (2022) *Kmodes 0.12.1* [Online]. Available at: https://pypi.org/project/kmodes/ (Accessed 1 May 2022).(2019) PEGASUS METHOD: An Overview.

Raffaëlli, L., Vallée, F., Fayolle, G., Souza, P. D., Rouah, X., Pfeiffer, M., et al. (2016). Facing ADAS validation complexity with usage oriented testing. *ERTS 2016*. [Online]. Available at: http://arxiv.org/pdf/1607.07849v1.

Rousseeuw, P. J. (1987). Silhouettes: A graphical aid to the interpretation and validation of cluster analysis. *J. Comput. Appl. Math.* 20, 53–65. doi:10.1016/0377-0427(87)90125-7

SAE On-Road Automated Vehicle Standards Committee (2014). *SAE Standard J 3016: Taxonomy and definitions for terms related to on-road motor vehicle automated driving systems*.

Sander, U., and Lubbe, N. (2018). The potential of clustering methods to define intersection test scenarios: Assessing real-life performance of AEB. *Accid. analysis Prev.* 113, 1–11. doi:10.1016/j.aap.2018.01.010

Sarkar, S., Melnykov, V., and Zheng, R. (2020). Gaussian mixture modeling and model-based clustering under measurement inconsistency. *Adv. Data Analysis Classif.* 14 (2), 379–413. doi:10.1007/s11634-020-00393-9

Schmidt, F., and Sax, E. (2009). *'Funktionaler Softwaretest für aktive Fahrerassistenzsysteme mittels parameterierter Szenario-Simulation'*, Informatik 2009–Im Focus das Leben.

SciPy (2022). *Fundamental algorithms for scientific computing in Python*. [Online]. Available at: https://scipy.org/ (Accessed May 1, 2022).

Seiniger, P., and Gail, J. (2015). *'A methodology to derive precision requirements for automatic emergency braking (AEB) test procedures'*, 24th International Technical Conference on the Enhanced Safety of Vehicles. Gottenburg: ESV.

Staender, P. (2010). Eine modellbasierte Methode zur Objektivierung der Risikoanalyse nach ISO 26262*, Doctoral dissertation*. Braunschweig: Technische Universität Braunschweig.

Sun, J., Zhang, H., Zhou, H., Yu, R., and Tian, Y. (2021). Scenario-based test automation for highly automated vehicles: A review and paving the way for systematic safety assurance. In *IEEE transactions on intelligent transportation systems*, 1–16. doi:10.1109/TITS.2021.3136353

TÜV SÜD (2021). Assessment of automated vehicles with scenario-based testing: Testing of critical scenarios in a controlled environment. [Online]. Available at: https://www.tuvsud.com/en/industries/mobility-and-automotive/automotive-and-oem/autonomous-driving/assessment-of-automated-vehicles-with-scenario-based-testing.

Wegmann, M., Domenique, Z., Jonas, H., and Jürgen, F. (2021). *A review of systematic selection of clustering algorithms and their evaluation*. *arXiv preprint*.

Weitzel, A., and Winner, H. (2013) 'Controllability assessment for unintended reactions of active safety systems', in *Proceedings of the 23rd international technical conference on the enhanced safety of vehicles*.

Weitzel, D. A. (2014) *Absicherungsstrategien für Fahrerassistenzsysteme mit Umfeldwahrnehmung: Bericht zum Forschungsprojekt FE 82.0546/2012* [Online], Bremen, Fachverl. NW. Available at: http://bast.opus.hbz-nrw.de/volltexte/2015/836/pdf/F98b.pdf.

Wimmer, P., Düring, M., Chajmowicz, H., Granum, F., King, J., Kolk, H., et al. (2019). Toward harmonizing prospective effectiveness assessment for road safety: Comparing tools in standard test case simulations. *Traffic Inj. Prev.* 20(1), S139–S145. doi:10.1080/15389588.2019.1616086

Wittmann, D., Lienkamp, M., and Wang, C. (2017). "Method for comprehensive and adaptive risk analysis for the development of automated driving," in *2017 IEEE 20th international conference on intelligent transportation systems (ITSC)* (Yokohama: IEEE), 1–7. 16.10.2017 - 19.10.2017. doi:10.1109/ITSC.2017.8317791

Wittmann, D., Wang, C., and Lienkamp, M. (2015). *Definition and identification of system boundaries of highly automated driving*. Munich: Tagung Fahrerassistenz, 7.

Xia, Q., Duan, J., Gao, F., Chen, T., and Yang, C. (2017). "Automatic generation method of test scenario for ADAS based on complexity," in *SAE technical paper series* (Warrendale, PA, United States: SAE International400 Commonwealth Drive). SEP. 26, 2017. doi:10.4271/2017-01-1992

Xia, Q., Duan, J., Gao, F., Hu, Q., and He, Y. (2018). Test scenario design for intelligent driving system ensuring coverage and effectiveness. *Int. J. Automot. Technol.* 19 (4), 751–758. doi:10.1007/s12239-018-0072-6

Yan, M. (2019). *Gower 0.0.5*. [Online]. Available at: https://pypi.org/project/gower/ (Accessed May 1, 2022).

Zhang, Q., Chen, D., Li, Y., and Li, K. (2015). "Research on performance test method of lane departure warning system with PreScan," in *Proceedings of SAE-China congress 2014: Selected papers* (Berlin, Heidelberg: Springer Berlin Heidelberg), 445–453. doi:10.1007/978-3-662-45043-7_45

Zhao, D., Lam, H., Peng, H., Bao, S., LeBlanc, D. J., Nobukawa, K., et al. (2017). "Accelerated evaluation of automated vehicles safety in lane-change scenarios based on importance sampling techniques," in *IEEE transactions on intelligent transportation systems* (a publication of the IEEE Intelligent Transportation Systems Council), 18, 595–607. doi:10.1109/TITS.2016.2582208

Zhou, J., and Re, L. d. (2017). Reduced complexity safety testing for ADAS & ADF. *IFAC-PapersOnLine* 50 (1), 5985–5990. doi:10.1016/j.ifacol.2017.08.1261

Frontiers in
Future Transportation

Innovations in travel, transportation and mobility systems

An innovative journal that explores technology that will transform the future of transportation and mobility systems in our highly-connected global society.

Discover the latest Research Topics

See more →

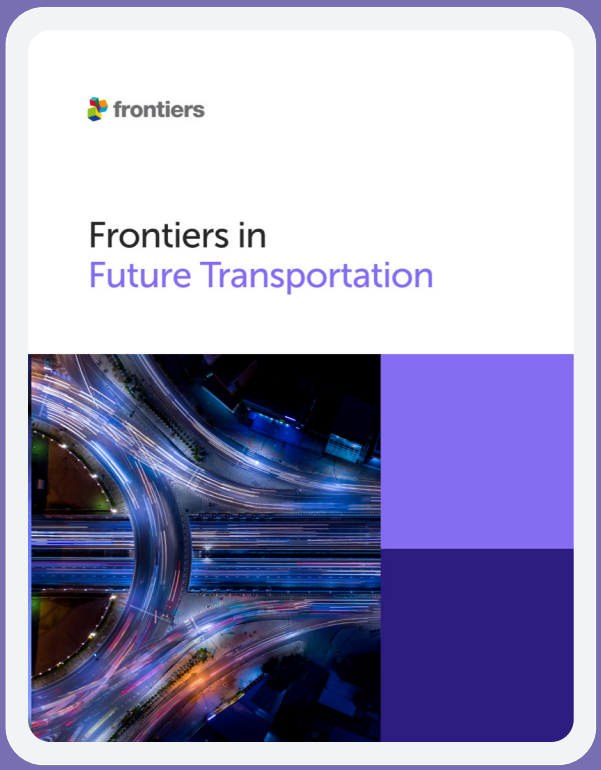

Frontiers

Avenue du Tribunal-Fédéral 34
1005 Lausanne, Switzerland
frontiersin.org

Contact us

+41 (0)21 510 17 00
frontiersin.org/about/contact